

## ABSTRACT

Title of Document: Study of real-time traffic state estimation and short-term prediction of signalized arterial network considering heterogeneous information sources

Yang Lu, Ph.D. Candidate, 2013

Directed By: Ali Haghani, Professor, Department of Civil Engineering, Department Chair

Compared with a freeway network, real-time traffic state estimation and prediction of a signalized arterial network is a challenging yet under-studied field. Starting from discussing the arterial traffic flow dynamics, this study proposes a novel framework for real-time traffic state estimation and short-term prediction for signalized corridors. Particle filter techniques are used to integrate field measurements from different sources to improve the accuracy and robustness of the model. Several comprehensive numerical studies based on both real world and simulated datasets showed that the proposed model can generate reliable estimation and short-term prediction of different traffic states including queue length, flow density, speed and travel time with a high degree of accuracy. The proposed model can serve as the key component in both ATIS (Advanced Traveler's Information System) and proactive traffic control systems.

STUDY OF REAL-TIME TRAFFIC STATE ESTIMATION AND SHORT-TERM  
PREDICTION OF SIGNALIZED ARTERIAL NETWORK CONSIDERING  
HETEROGENEOUS INFORMATION SOURCES

By

Yang Lu

Dissertation submitted to the Faculty of the Graduate School of the  
University of Maryland, College Park, in partial fulfillment  
of the requirements for the degree of

Doctor of Philosophy

2013

Advisory Committee:

Professor Haghani Ali (Committee chair)

Professor Paul Schonfeld

Associate Professor Lei Zhang

Associate Professor Cinzia Cirillo

Professor Christopher Davis

© Copyright by

Yang Lu

2013

## Acknowledgements

I would never have been able to finish my dissertation without the guidance of my advisor and committee members, and help and support from friends and my family.

First of all, I would like to express my deepest gratitude to my advisor, Dr. Haghani, not only for his patient and caring instructions and continuous financial support during my doctoral study, but also for enlightening me in the way of innovative thinking which is of the most importance for a prospective researcher. I also want to thank Drs. Christopher Davis, Paul Schonfeld, Lei Zhang, and Cinzia Cirillo for being my defense committee members and providing me precious feedback comments for my research.

I also would like to thank all lab members and colleagues especially Dr. Masoud Hamedi, Dr. Wenxin Qiao, Kaveh Farokhi, and Yanru Zhang for your help and excellent advice regarding my research. Furthermore, I would like to thank all dear friends of mine, Lei Feng, Xianfeng Yang, Chenfeng Xiong, Xiang He, and Karl Lu for your support and help during my Ph.D. course. Special gratitude goes to Dr. Shanjiang Zhu, who not only shared with me precious research experience but also gave me a lot of excellent advice as a senior research fellow.

Lastly I would like to express my sincere thanks to my parents for their understanding and continuous support and encouragement during my study. Your support is the biggest motivation for me to complete this dissertation.

# Table of Contents

Acknowledgements.....	ii
Table of Contents.....	iii
List of Tables .....	v
List of Figures .....	vi
1. Introduction.....	1
2. Literature Review.....	5
2.1. Traffic state estimation .....	5
2.2. Short-term traffic flow prediction.....	7
2.3. Macroscopic traffic flow model.....	9
2.4. Summary and research objective .....	10
3. The Shifting Boundary Cell Model: A New Type of Macroscopic Traffic Flow Model for Signalized Arterial Corridors.....	13
3.1. State definition and notations.....	13
3.2. Evolution of cell queue and density.....	17
3.3. Evolution of cell speed.....	25
3.4. Dynamic estimation of model parameters .....	28
3.5. Chapter Summary .....	29
4. Integrating Heterogeneous Detector Information with Particle Filtering.....	32
4.1. Fundamentals of Kalman Filter and Extend Kalman Filter .....	32
4.2. Fundamentals of Particle Filter (PF).....	36
4.3. Evaluate the probability of traffic state with fixed location detectors .....	39
4.4. Evaluate the probability of traffic state with probe vehicle data .....	42
4.4.1. Probe data and flow speed at moving area.....	43
4.4.2. Probe data and flow density and queue length.....	43
4.5. Computation procedure of PF algorithm .....	45
4.6. Chapter Summary .....	46
5. Estimation of Arterial Travel Time and Its Variability .....	48
5.1. Summary of previous studies.....	48
5.2. Trajectory Method for Arterial Travel Time Estimation .....	54
5.3. Chapter Summary .....	58
6. Short-term Traffic Flow Prediction Algorithm.....	59
6.1. Traffic state transition equation and short-term prediction.....	59
6.2. Description of SARIMA model.....	60
6.3. Real-time traffic state prediction procedure .....	62
6.4. Chapter Summary .....	65
7. Numerical Investigation Part I: Model Validation with Field Data.....	66
7.1. Introduction of NGSIM dataset .....	66
7.2. Calibration of speed-density-queue function using field data .....	69

7.3.	Validation of traffic state estimation.....	74
7.4.	Validation of traffic state prediction.....	83
7.5.	Comparison analysis using SMART signal data .....	99
7.6.	Chapter Summary .....	103
8.	Numerical Investigation Part II: Model Validation with Synthetic Data .....	105
8.1.	Network Description.....	105
8.2.	Calibration of speed-density-queue function using simulated data .....	109
8.3.	Validation of traffic state estimation.....	114
8.4.	Validation of Short-term Prediction Results.....	122
8.5.	Chapter Summary .....	132
9.	Conclusion and Future Research Direction .....	134
9.1.	Summary of the dissertation .....	134
9.2.	Conclusion .....	135
9.3.	Future research direction.....	139
10.	Appendix A: Computation Result of NGSIM Dataset .....	142
11.	Appendix B: Computation Results of Simulation Dataset .....	154
12.	References.....	167

## List of Tables

Table 1 Summary of previous studies regarding traffic state estimation.....	7
Table 2 The number of trajectory data samples contained in NGSIM dataset .....	66
Table 3 Summary of speed function fitted results in NGSIM dataset .....	73
Table 4 Summary of fitted parameter values in NGSIM dataset.....	73
Table 5 Summary of model performance indices of estimation results in NGSIM dataset .....	75
Table 6 Summary of model performance indices of travel time estimation in NGSIM dataset .....	76
Table 7 Summary of travel time prediction MAEB of different time periods in NGSIM dataset.....	84
Table 8 Summary of travel time prediction MAPEB of different time periods in NGSIM dataset.....	84
Table 9 Summary of average prediction MAEB of different cells and time periods in NGSIM dataset.....	85
Table 10 Summary of average prediction MAPEB of different cells and time periods in NGSIM dataset .....	86
Table 11 Link and turning bay length of the simulation network.....	106
Table 12 The demand volume ratio between OD pairs .....	107
Table 13 The total demand volume of different demand generating nodes (veh/hour) .....	107
Table 14 Summary of speed function fitted results .....	111
Table 15 Summary of fitted parameter values.....	111
Table 16 Summary of performance index of the model under simulation dataset ...	116
Table 17 Summary of average prediction MAEB of different traffic state variables of simulation dataset.....	123
Table 18 Summary of average prediction MAPE of different traffic state variables of simulation dataset.....	123
Table 19 Summary of prediction MAEB of individual cells of simulation dataset..	126
Table 20 Summary of prediction MAPEB of individual cells of simulated dataset.	127

## List of Figures

Figure 1 The cell representation of a hypothetical arterial corridor .....	13
Figure 2 Illustration of moving and queuing area within a cell .....	14
Figure 3 Traffic flow movements inside a cell (a) and traffic flow between two adjacent cells (b) .....	17
Figure 4 3-D plot of approximated sending flow rate.....	25
Figure 5 Illustration of traffic flow movements and their speeds.....	26
Figure 6 Computation step of KF .....	34
Figure 7 Probe vehicles in a cell.....	44
Figure 8 Relationship between traffic state, travel time and traffic surveillance data	50
Figure 9 Real-time traffic state estimation and short-term prediction flow chart.....	63
Figure 10 Map view of the Peachtree street.....	68
Figure 11 The sketch of geometric layout of the Peachtree arterial and corresponding cell network structure.....	68
Figure 12 Trajectory plot of Peachtree street between 12:45 to 1:00 northbound traffic .....	69
Figure 13 The speed density scatter plots of Peachtree street .....	70
Figure 14 (a) ~ (d) The speed-queue scatter plots of Peachtree street.....	71
Figure 15 (a) ~ (d) The speed-density-queue three dimensional scatter plots of Peachtree street .....	72
Figure 16 Estimated and ground truth travel time of PT street 12:45 to 1:00 northbound traffic .....	77
Figure 17 Estimated and ground truth travel time of PT street 12:45 to 1:00 southbound traffic .....	78
Figure 18 Estimated and ground truth travel time of PT street 4:00 to 4:15 northbound traffic.....	78
Figure 19 Estimated and ground truth travel time of PT street 4:00 to 4:15 southbound traffic.....	79
Figure 20 Estimated and ground truth queue length plot of selected cells in NGSIM dataset .....	80
Figure 21 Estimated and ground truth density plot of selected cells in NGSIM dataset .....	81
Figure 22 Estimated and ground truth speed plot of selected cells in NGSIM dataset .....	82
Figure 23 Plots of predicted travel time MAPEB over different prediction range using NGSIM data .....	87
Figure 24 Plots of predicted queue length MAPEB over different prediction range with NGSIM Peachtree data from 12:45 to 1:00 .....	88
Figure 25 Plots of predicted queue length MAPEB over different prediction range with NGSIM Peachtree data from 4:00 to 4:15 .....	88
Figure 26 Plots of predicted density MAPEB over different prediction range with NGSIM Peachtree data from 12:45 to 1:00 .....	89
Figure 27 Plots of predicted density MAPEB over different prediction range with NGSIM Peachtree data from 4:00 to 4:15 .....	89

Figure 28 Plots of predicted speed MAPEB over different prediction range with NGSIM Peachtree data from 12:45 to 1:00 .....	90
Figure 29 Plots of predicted speed MAPEB over different prediction range with NGSIM Peachtree data from 4:00 to 4:15 .....	90
Figure 30 Predicted and ground truth travel time of Peachtree street northbound 12:45 to 1:00 .....	92
Figure 31 Predicted and ground truth travel time of Peachtree street southbound 12:45 to 1:00 .....	93
Figure 32 Predicted and ground truth travel time of Peachtree street northbound 4:00 to 4:15 .....	93
Figure 33 Predicted and ground truth travel time of Peachtree street southbound 4:00 to 4:15 .....	94
Figure 34 Predicted and ground truth queue of Peachtree street 12:45 to 1:00 cell 1	94
Figure 35 Predicted and ground truth queue of Peachtree street 12:45 to 1:00 cell 5	95
Figure 36 Predicted and ground truth queue of Peachtree street 4:00 to 4:15 cell 5 ..	95
Figure 37 Predicted and ground truth queue of Peachtree street 4:00 to 4:15 cell 6 ..	96
Figure 38 Predicted and ground truth queue of Peachtree street 4:00 to 4:15 cell 5 ..	96
Figure 39 Predicted and ground truth queue of Peachtree street 12:45 to 1:00 cell 2	97
Figure 40 Predicted and ground truth speed of Peachtree street 12:45 to 1:00 cell 2.	97
Figure 41 Predicted and ground truth speed of Peachtree street 4:00 to 4:15 cell 3...	98
Figure 42 Predicted and ground truth speed of Peachtree street 4:00 to 4:15 cell 5...	98
Figure 43 The map of study area along TH 13, Minnesota .....	99
Figure 44 Geometric layout (a) and cell network structure (b) used in comparison study.....	100
Figure 45 Comparison of estimated queue length of cell 1 .....	101
Figure 46 Comparison of estimated queue length of cell 2 .....	101
Figure 47 Comparison of estimated queue length of cell 3 .....	102
Figure 48 Comparison of estimated queue length of cell 4 .....	102
Figure 49 Geometric layout of the hypothetical arterial corridor .....	105
Figure 50 Number of demand generation and sink nodes of the simulation network .....	106
Figure 51 Observed travel time of the corridor obtained from VISSIM .....	108
Figure 52 Observed speed and density plot of (a) Eastbound traffic (b) Westbound traffic of the simulated network .....	109
Figure 53 Observed speed and queue ratio plot of (a) Eastbound traffic (b) Westbound traffic of simulated network.....	110
Figure 54 Observed speed, density and queue ratio 3-D plot of (a) Eastbound traffic (b) Westbound traffic of simulated network.....	110
Figure 55 Plots of three dimensional curves fitted under linear-exponential and parabolic exponential .....	113
Figure 56 Estimated versus ground truth travel time plot of (a) Eastbound traffic (b) Westbound traffic of simulation dataset .....	117
Figure 57 Estimated versus ground truth queue length plot of (a) Cell 1 (b) Cell 3 (c) Cell 8 of simulation dataset.....	119
Figure 58 Estimated versus ground truth density plot of (a) Cell 1 (b) Cell 4 (c) Cell 6 of simulation dataset .....	120

Figure 59 Estimated versus ground truth density plot of (a) Cell 5 (b) Cell 6 (c) Cell 7 of simulation dataset .....	121
Figure 60 Line plot of average prediction MAEB of different traffic state variables of simulation dataset.....	123
Figure 61 Line plot of average prediction MAPEB of different traffic state variables of simulation dataset .....	124
Figure 62 Eastbound predicted versus ground truth travel time for 5, 15, 30 and 60 time step prediction of simulation dataset .....	128
Figure 63 Westbound predicted versus ground truth travel time for 5, 15, 30 and 60 time step prediction of simulation dataset .....	129
Figure 64 Predicted versus ground truth queue length of cell 8 of simulation dataset .....	129
Figure 65 Predicted versus ground truth queue length of cell 1 of simulation dataset .....	130
Figure 66 Predicted versus ground truth density of cell 2 of simulation dataset .....	130
Figure 67 Predicted versus ground truth density of cell 4 of simulation dataset .....	131
Figure 68 Predicted versus ground truth speed of cell 2 of simulation dataset .....	131
Figure 69 Predicted versus ground truth speed of cell 6 of simulation dataset .....	132

# 1. Introduction

With the rapid advance of information technology, ATIS (Advanced Traveler's Information System) has become a crucial part of modern traffic management system especially in urban regions where recurrent and non-recurrent traffic congestion has become a serious social problem. According to the *Urban Mobility Report (2012)*, congestion causes urban Americans to travel 5.5 billion hours more and to purchase an extra 2.9 billion gallons of fuel annually. One core task of an ATIS (Advanced Traveler's Information System) is to provide reliable real-time traffic information to both travelers and traffic management authorities to support advanced traffic management strategies such as dynamics traffic rerouting, real-time route guidance, and advanced traffic signal control.

Another trend in the field of intelligent transportation system is the proliferation and implementation of many advanced traffic sensing system, wireless communication and mobile computing technology. The development of these technologies can revolutionize the conventional transportation management modes. Imagine a mobile device which can upload individual's future trip plan onto the web server and in turn receive optimal departure time and routing based on predicted future traffic condition. Such traffic information service may not have been feasible a decade ago but is becoming more and more possible nowadays. The truth behind the phenomenon is that the speed by which information processing and communication technologies have advanced has exceeded most people's expectation. From traffic surveillance point of view, large amount of GPS probe vehicles can provide real-time traffic information within a much wider spatial range compared with conventional fixed point detectors. Wireless sensors such as Bluetooth sensors can identify vehicles traveling inside the network and report their experienced travel time. Vehicle-to-vehicle and vehicle-to-

station communication technology also allows each individual driver to communicate with information centers. From users' point of view, their smart phones and GPS route guidance systems can be used to receive or send traffic information. Hence the largest challenge of constructing a modern ITS system is how to effectively and smartly utilize huge amount of real time traffic information to alleviate congestion and improve the performance of the network.

In order to provide reliable real-time traffic information to both network users and traffic authorities, two types of information are of most concern: the traffic flow status of the network in both **present** and **future time**. Generally speaking, there are three categories of information regarding a transportation network: the first category is the traffic flow state within network such as link speed, volume and density; the second category is the travel time experienced by network users; and the third category is the drivers' characteristics, behavior and trip related information such as characteristics of driving population, OD demand volume, route and departure time choice and so on. This study focuses on the first two categories of data, namely the network traffic flow state and travel time experienced by drivers under different traffic conditions.

As an essential component of ITS system, a high performance traffic state estimation and prediction model should have the following properties:

1. Accuracy: The output of the model should be accurate enough for real world applications;
2. Robustness: The performance of the model should be stable under various traffic conditions;
3. Flexibility: The model should be able to take advantage of information source with different format and quality;

Therefore the primary motivation of this research is to develop a solid traffic state estimation framework for urban networks through which the real-time traffic information can be integrated and generalized both spatially and temporally. Based on the estimated current traffic state, the near future traffic flow states can be predicted.

Although many research activities have been reported in the field of traffic state estimation, travel time prediction and data fusion, many unresolved issues still exist when one tries to construct a system that estimates and predicts the traffic condition of a signalized arterial network. First of all, compared with freeways, the traffic state estimation and prediction methodology for arterial network is insufficient. Due to the huge difference between freeways and arterial roads in terms of capacity, control mechanism and network topology, it is difficult to implement existing traffic flow models directly to arterial traffic state estimation problem. Many ITS related studies focus on one particular type of the detector and network structure, and as a result, the model becomes not applicable when the external conditions are changed even slightly. The second challenge we face in this area is that the integration of data sources with different quality and resolution is extremely difficult from a general perspective since each model needs to be developed based on particular form of data input. In viewing those issues, this study is dedicated to develop a well-structured arterial traffic state estimation framework considering heterogeneous information sources. Starting from the formulation of arterial traffic flow dynamics, the main part of this study emphasizes on establishing a robust yet flexible data fusion algorithm which can take full advantage of modern traffic surveillance system.

The organization of this dissertation is as follows: Chapter 2 provides a complete summary of previous studies related to traffic state estimation and traffic flow theory, and

short-term prediction methods. Based on the literature review, the objective of the study is also given in Chapter 2. In Chapter 3, a new type of arterial traffic flow model named “shifting boundary queue model” is developed. Chapter 4 discusses the data fusion algorithm for integrating multiple field measurements during the estimation process. Chapter 5 discusses the relationship between traffic state and travel time and Chapter 6 presents the development of short-term traffic flow prediction algorithm. Then Chapter 7 and 8 demonstrate the results of several comprehensive numerical studies in order to support the model validation. Finally the conclusion and future works are given in Chapter 9.

## 2. Literature Review

Previous studies regarding real-time traffic state estimation and short-term prediction generally follows three avenues: traffic state estimation, short-term traffic flow prediction and traffic flow modeling. In this section, the major research findings of previous literature are summarized.

### 2.1. Traffic state estimation

The main focus of real-time traffic state estimation is how to scientifically utilize field measurements to assess the actual traffic flow condition of a transportation network. The real-time field measurements (such as flow, occupancy and speed) are the foundations of traffic state estimation. There are generally three crucial problems associated with the traffic surveillance device: measurement errors, limited spatial coverage and heterogeneity in data format and temporal resolution. Therefore the real-time traffic state estimation problem is usually formulated as a recursive stochastic estimation model where the transition of traffic state is described by some analytical traffic flow model and field measurements are used to adjust the prior estimation result. Since the emergence of Kalman filter technique in 1960s, the method was soon recognized by many transportation professionals and subsequent research efforts were reported in seeking its application in the field of traffic state estimation. *Gazis and Knapp* (1971) proposed a recursive estimator of freeway speed and density based on time-series flow and speed measurements of detectors. *Szeto and Gazis* (1972) first introduced extended Kalman filtering framework into recursive traffic state estimation applications and proposed a flow density and speed estimation model for freeway segments. Similar issue was also discussed by *Nahi and Trivedi* (1973) where the impact of downstream density is

explicitly considered when computing the upstream flow. Based on some of the previous works, *Wang and Papageorgiou* (2005, 2007) proposed a comprehensive freeway traffic state estimation model based on EKF technique. Additionally, *Boel and Mihaylova* (2006) and *Mihaylova et al.* (2007) developed a freeway traffic state estimation algorithm using particle filter technique.

In recent years, traffic state estimation of signalized arterial network has received increasing attention. However difficulties arise when one attempts to apply KF framework in arterial applications due primarily to three reasons: 1) traffic flows moving inside the arterial network are periodically interrupted by signal lights at intersections and the periodical accumulation and dissipation of the queue have predominant impact on the evolution of other traffic flow parameters including density, speed and travel time; 2) there is a huge difference between the accessibility of freeway and arterial. Freeway network can be considered as a perfect closed system whose inflows and outflows are controlled by on-ramps and off-ramps. In other words, the traffic that enters or exits the system can be monitored by ramp detectors, however arterial network is an open system with many middle link demand generation and extinction. Such condition will significantly increase the estimation error for any type of traffic flow models; 3) last but not least, the amount of traffic surveillance information available is usually insufficient in arterial applications due to the more complex traffic flow movements and limited detector coverage. Therefore existing literature regarding arterial traffic state estimation is sparse compared with freeway studies. *Di et al.* (2010) proposed an arterial traffic density estimation model based on Markov compartment model and used large population approximation to convert the system dynamics equations into a differentiable form. The accuracy of their estimation result depends heavily on the penetration rate of GPS

probe vehicle data which is the primary information source of the study. *Chris et al. (2007)* integrated CTM (cell transmission model) into the EKF traffic state estimation framework using implicit switching technique. *Kwong et al. (2009)* proposed a travel time estimation model based on vehicle re-identification technique. *Liu and Ma (2009)*, *Liu et al. (2009)*, *Wu and Liu (2011)* and *Ban et al. (2009)* developed their own queue and travel time estimation model using high resolution signal and detector data. Recently, the integration of multiple data sources became a major trend. A series of studies are conducted to investigate the performance of mobile sensing and smart phone data on traffic state estimation (see *Hofleitner et al. 2012*, *Herrera and Bayen 2010*, and *Work et al. 2008*). Table 1 summarizes the abovementioned studies in this field.

Table 1 Summary of previous studies regarding traffic state estimation

<i>Authors</i>	<i>Year</i>	<i>Network</i>	<i>Research Content</i>
Gazis	1971	Freeway	Density and speed, loop detector data, EKF
Szeto and Gazis	1972	Freeway	Density and speed, loop detector data, EKF
Nahi and Trivedi	1973	Freeway	Density and speed, loop detector data, EKF
Boel, R., and Mihaylova, L.	2006	Freeway	Density and speed, loop detector data, PF
Wang and Papageorgiou	2007	Freeway	Density and speed, loop detector data, EKF
Chris et al.	2007	Freeway	Density and speed, loop detector data, CTM model with implicit Mode Switching
Kwong et al.	2009	Freeway	Travel time, vehicle re-identification
Liu and Ma	2009	Arterial	Queue and travel time, smart signal data
Di, Liu, and Davis	2010	Arterial	Density and speed, GPS probe vehicle, EHKF (extended hybrid Kalman filter) with Markov compartment model
Herrera and Bayen	2010	Freeway	Density, Cell phone data/GPs probe data, Newtonian relaxation
Hofleitner et al.	2012	Arterial	Travel time, density and speed, smart phone data

## 2.2. Short-term traffic flow prediction

The short-term traffic flow prediction technique received extensive amount of attention during the last three decades as a core component of most ITS systems. It focuses on forecasting future traffic flow conditions based on historical information collected by traffic surveillance devices. The majority of literature in this field concentrated on predicting traffic flow variables (volume, speed, density) of one particular location using various statistical

methods. The underlying rationale of statistical methods belongs to either of the following two concepts: 1) the future value of traffic state is some function of past values; 2) the future traffic condition can be determined by finding the historical traffic conditions which are most similar to the current one. The former is basis of regression methods and the latter is the foundation of pattern matching techniques.

The literature on short-term traffic flow prediction started to flourish from 1980s. The proposed methods ranged from time series models including linear and non-linear regression, ARIMA (autoregressive integrated moving average), dynamic generalized linear models (see *Cetin and Comert 2006, Fei et al. 2011, Hamed et al. 1995, Kamarianakis and Prastacos 2003, Min and Wynter 2011, Vlahogianni et al. 2004, 2005, Williams and Hoel 2003, Zhang et al. 2011*), Kalman filtering method (*Okutani and Stephanedes, 1984*), non-parametric statistical methods (*Davis and Nihan 1991, Smith et al. 2002*), spectral analysis methods (*Stathopoulos and Karlaftis 2003*), artificial neural network methods (*Chen et al. 2001, Dia 2001, Jiang and Adeli 2005, Park and Rilett 1998, Park et al. 1999*), K-nearest neighbor methods (*Qiao et al. 2012*), sequential learning methods (*Chen and Grant-Muller 2001*), to cusp catastrophe theory method (*Pushkar et al. 1995*).

Compared with local traffic state prediction models, the traffic flow theory based short-term prediction performs forecast on a system level. The statistical methods usually do not consider the traffic flow property behind the detector data and treat each measurement source as independent data stream, meanwhile an alternative solution is to use macroscopic traffic flow model to approximate the future traffic flow condition based on 1) the estimated current traffic state and 2) the predicted inflows and other boundary conditions of the network.

Previous research along this direction is very sparse. *Szeto et al.* (2009) reported a prediction model based on SARIMA and cell transmission model.

### 2.3. Macroscopic traffic flow model

The majority of literatures in this area focus on the development of mathematical formulations that are capable of replicating the traffic flow evolution in freeway or arterial networks. Starting from the earliest first order traffic fluid models developed by *Lighthill and Whitham* (1955) and *Richards* (1956), many subsequent research efforts have reported to either enhance the computational aspects of the model (*Daganzo* 1994 and *Daganzo* 1995) or incorporate stochastic property into the traffic flow models (see *Davis and Kang* 1994, *Geroliminis and Sun* 2011 and *Sumalee et al.* 2011). Recently, there is an increasing concern on the development of arterial traffic flow models that can accommodate the unique nature of interrupted flows under the impact of signal controls. Several relevant studies include the shockwave theory while estimating the arterial queue and delays (see *Geroliminis and Skabardonis*, 2005, *Wu and Liu* 2011) and empirical study of arterial fundamental diagram was also reported in literature (*Wu et al.* 2011).

One the other hand, traffic flow theory in signalized network is developed revolving the queue evolution of signalized intersections. Many traffic problems arise when a signalized road network is loaded with high demand volume due to the accumulation of queues. As a result, the primary concern of studies of arterial traffic flow is how to effectively estimate the queue length at signalized intersection.

Many early studies in off-line queue estimation focused on evaluating the queue length at isolated intersection with fixed cycle traffic-light using stochastic queuing theory. Important early works in this field include *Webster* (1958), *McNeil* (1968), *Newell* (1965), *Darroch* (1964)

and Ohno (1978). Later the queue computation was expanded into dynamic context by switching from equilibrium queue length to time-dependent queue length. Relevant works ranged from Kimber and Hollis (1979), Akcelik (1980), Akcelik (1988), Akcelik and Roupail (1994) to Viti and Zuylan (2010). However these offline queue models are only applicable for intersection design and evaluation purpose while most ITS system demands for real-time queue estimation technique that can take advantage of different detector data. The most widely used dynamic queue estimation model is called cumulative count method or input-output method. Sharma et al (2007) proposed an on-line queue estimation method using this classical method. In cumulative count method, the queue length is obtained by computing the vertical distance between the cumulative arrival and departure curve at the intersection. The cumulative arrival curve is usually obtained through the traffic volume measurement of upstream detectors and the cumulative departure curve is usually obtained by either installing downstream detectors or by computation based on signal parameters. More relevant works include Bhaskar et al. (2009), Geroliminis and Skabardonis (2005), Liu et al. (2009), Comert and Cetin (2009) and Mehran et al. (2012). Unlike freeway traffic flow models, various arterial queue models share less common theoretical foundation and each researcher tends to develop their own methodology based on the available input and desired output of the application.

#### 2.4. Summary and research objective

Through literature survey, one can find that there is a missing link between macroscopic traffic flow formulation and the short-term traffic flow prediction of arterial networks. Once applied to short-term prediction, the traffic flow theory based model will demonstrate the following unique advantages:

- The forecast of traffic flow states is conducted on a network level, therefore the model inherently considers the complex correlations between traffic flow measurements obtained from different locations;
- The model does not require a large historical database for parameter calibration purpose;
- The model is highly robust and flexible, therefore easy to incorporate heterogeneous data sources;
- The model not only predicts traffic state variables that are directly observable from field detectors (flow, density, speed) but also is capable of predicting unobservable traffic flow variables such as queue length or turning ratios.
- With the help of traffic flow model, the proposed prediction model can essentially perform what-if analysis given different traffic control strategies. Hence the model can also apply to signal control optimization problems.

The objective of this research is to seek theoretical advance of real-time traffic state estimation and short-term prediction in the following aspects:

- Propose an innovative real-time traffic state estimation framework for arterial network considering the technical challenges discussed in the earlier part of this chapter. The proposed framework should be accurate, flexible and applicable.
- Discuss the mathematical formulation of traffic flow dynamics of arterial road network considering the impact of signal control devices. Develop appropriate expressions for system dynamics under different type of traffic control strategies.
- Develop a data fusion algorithm under the proposed framework to accommodate heterogeneous data sources to increase the overall accuracy and flexibility of the model

- Discuss the relationship between arterial traffic state and travel time and establish a reliable travel time estimation mechanism.
- Discuss the application of the proposed arterial traffic state estimation model in short term traffic state prediction and its accuracy.
- Through extensive numerical studies, quantitatively evaluate the performance of the proposed model under different degrees of congestion.

### 3. The Shifting Boundary Cell Model: A New Type of Macroscopic Traffic Flow Model for Signalized Arterial Corridors

#### 3.1. State definition and notations

Consider a hypothetical arterial corridor consisting of  $m$  consecutive links. Signal control devices are installed at the end of each link to control the right-of-way of through traffic streams. Each link of the arterial corridor is modeled as an independent unit referred to as a *cell*. The spatial boundary of each cell is aligned with the start and end point of the link in the longitudinal direction; and is aligned with the outer rim of the through lanes in the lateral direction. Figure 1 illustrates the geometric layout of the hypothetical arterial corridor with four links and corresponding cell network representations.

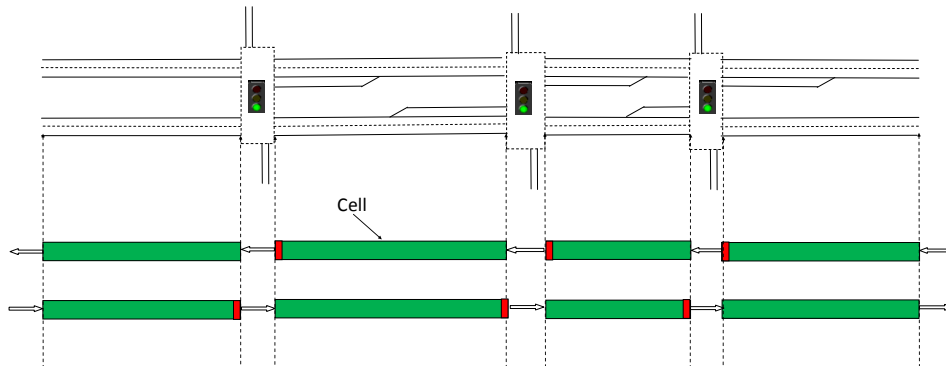


Figure 1 The cell representation of a hypothetical arterial corridor

Assuming there are no bottlenecks other than signalized intersection, each link can be divided into two distinct areas with different traffic flow characteristics: one is the “queuing area” which is in front of the signal stop line where vehicles either stop completely during the red phase or move at very low speed during the queue discharge period of the green phase; and the remaining part of the link can be viewed as the “moving area” where vehicles travel at a certain speed determined typically by the

macroscopic speed-density relationship of the link. Therefore the traffic state of cell  $i$  can be described by a triple variable set: the number of queued vehicles in “queuing area”, denoted by  $q_i(t)$ ; the average travel speed of vehicles in “moving area” denoted by  $v_i(t)$  and the number of vehicles contained in the “moving area” denoted by  $n_i(t)$ . Alternatively, the queuing and moving area can be viewed as two sub cells of its mother cell and the boundary between them is shifting constantly as the size of the queue changes.

Figure 2 presents the above idea through graphic illustration.

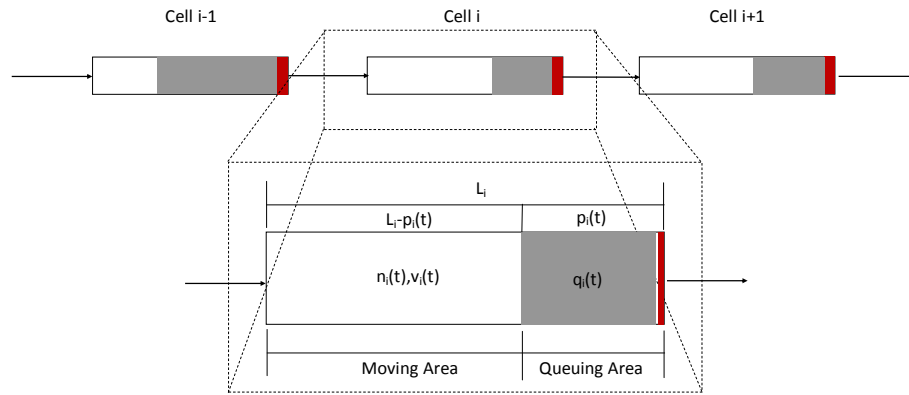


Figure 2 Illustration of moving and queuing area within a cell

To facilitate the model presentation, key notations used in the state definition are summarized as follows:

$q_i(t)$  is the number of queued vehicle in front of the stop line of cell  $i$  at time step  $t$ ,  $q_i(t)$

is also referred to as the queue mass of cell  $i$ ;

$n_i(t)$  is the number of vehicles contained in the moving area of cell  $i$ ;

$v_i(t)$  is the average traffic flow speed of vehicles traveling in the moving area of cell  $i$ ;

$k_i(t)$  is the traffic flow density of the moving area of cell  $i$ ;

$p_i(t)$  is the physical length of the queue within cell  $i$ ;

$w_i$  is the number of lanes contained in cell  $i$ ;

$l_i$  is the length of cell  $i$ ;

$h$  is the average vehicle length;

$\Delta$  is the computation time interval;

Since all traffic flow states are time-dependent,  $t$  represents time index in all above definitions.

At each time step, the traffic flow state of signalized corridor consisting of  $m$  cells can be quantified by the following  $3m$  dimensional vector,  $X(t)$ :

$$X(t) = [q_1(t), n_1(t), v_1(t), q_2(t), n_2(t), v_2(t), \dots, q_m(t), n_m(t), v_m(t)] \quad (3-1)$$

We define such vector  $X$  as the state variable of the arterial network.

Although in reality the traffic flow state changes continuously with respect to time, one still needs to approximate it with appropriate discrete form for computational purpose, namely the temporal discretization of the traffic state. Now imagine the continuous time axis is divided into small time intervals with uniform length  $\Delta$ , then  $X(t) \ t \in Z^+$  actually represents the traffic flow state at the beginning of time interval  $[t\Delta, (t+1)\Delta]$ . And instead of  $t$ , notation  $u$  is used to represent the continuous time variable in the remaining part of this paper. The continuous form of each traffic state variable is represented by adding a cap above their original notations. For instance,  $q_i(t), t \in Z^+$  represents the queue mass of cell  $i$  at the beginning of interval  $t$  while  $\hat{q}_i(u) \ u \in R^+$  represents the queue mass of cell  $i$  at time  $u$ .

The following relations are directly obtainable from the definition.

$$p_i(t) = \frac{q_i(t)h}{w_i} \quad \forall t \quad (3-2)$$

$$k_i(t) = \frac{n_i(t)}{w_i[l_i - p_i(t)]} \quad \forall t \quad (3-3)$$

The derivation of Equation (3-2) and (3-3) is straightforward.

One primary purpose of this study is to formulate a set of stochastic equations to replicate the transition of arterial traffic states between two consecutive time intervals, namely

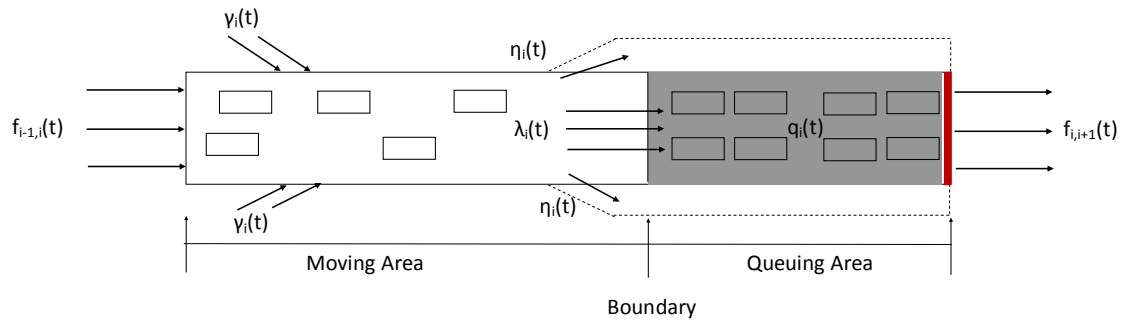
$$X(t + 1) = f(X(t), t), t \in Z^+ \quad (3-4)$$

Here  $f(X(t), t)$  is usually referred to as the system dynamics equations.

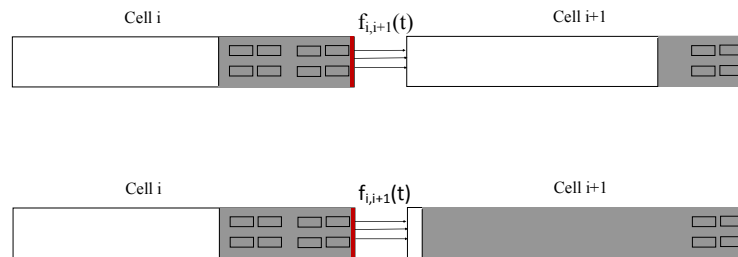
Compared with the freeway traffic state estimation models, this study treats the number of queued vehicles at each link as an explicit state variable. The underlying rationale is that the evolution of traffic flow states on arterials is governed by two different mechanisms. Within queuing areas, the formation and dissipation of queues are mainly determined by the signal control changes, while in moving areas, the evolution of traffic flow density and speed is mainly governed by the fundamental diagram. There are at least two advantages in doing so. First of all, queue lengths are important traffic state variables in arterial applications such as travel time estimation or signal optimization. Those applications will certainly benefit a lot from the estimated queue lengths of the proposed model. Second, such state definition allows us to model the traffic condition on arterial roads with less number of state variables. If the freeway modeling paradigm were used for signalized arterial, then one needs to divide each arterial links into a large number of small cells in order to capture the evolution of queues. The dilemma here is that while cell model always adopts homogeneous assumption within each cell, the traffic density distribution around the boundary between the queuing and moving area is not homogeneous. Also, replicating arterial traffic flow with large number of cells will put huge computational burden for online applications in any real scale network.

### 3.2. Evolution of cell queue and density

The change of  $n_i(t)$  and  $q_i(t)$  involves four types of traffic flow movements within a cell: 1) The incoming traffic flow from external network to cell  $i$  during interval  $t$  denoted by  $\gamma_i(t)$ ; 2) The traffic flow moving from cell  $i$  to cell  $i+1$  during interval  $t$  denoted by  $f_{i,i+1}(t)$ ; 3) The traffic flow exiting the network from cell  $i$  during interval  $t$  denoted by  $\eta_i(t)$ ; and 4) The traffic flow passing the boundary between the moving area and the queuing area denoted by  $\lambda_i(t)$ . The relationship between these four types of movements is illustrated by Figure 3 (a).



(a)



(b)

Figure 3 Traffic flow movements inside a cell (a) and traffic flow between two adjacent cells (b)

By applying vehicle conservation law to each area, one can write  $n_i(t + 1)$  and  $q_i(t + 1)$  as a function of  $f_{i-1,i}(t)$ ,  $f_{i,i+1}(t)$ ,  $\gamma_i(t)$ ,  $\eta_i(t)$  and  $\lambda_i(t)$ .

$$n_i(t + 1) = n_i(t) + f_{i-1,i}(t) + \gamma_i(t) - \eta_i(t) - \lambda_i(t) \quad (3-5)$$

$$q_i(t + 1) = q_i(t) + \lambda_i(t) - f_{i,i+1}(t) \quad (3-6)$$

The main concern here is to write  $\lambda_i(t)$  and  $f_{i,i+1}(t)$  as some explicit functions of  $n_i(t)$ ,  $q_i(t)$  and other state variables.

First of all, consider the number of vehicles crossing the boundary between moving and queuing area during interval  $t$ . The computation of  $\lambda_i(t)$  depends on the current queuing condition. If no vehicle is waiting before the intersection, namely if  $q_i(t) = 0$ , then the probability of an arbitrary vehicle inside the moving area to pass the boundary of the cell during current interval is  $\frac{v_i(t)\Delta[1-\varphi_i(t)]}{l_i}$ . Here  $\varphi_i(t)$  is the probability of vehicles to exit network from cell  $i$  during interval  $t$ . Since there are  $n_i(t)$  vehicles inside the moving area at the beginning of interval  $t$ , the total number of vehicles reaching the end of the cell follows a binomial distribution with successful rate  $\frac{v_i(t)\Delta[1-\varphi_i(t)]}{l_i}$ . Hence,

$$\lambda_i(t) = w_i k_i(t) v_i(t) [1 - \varphi_i(t)] \Delta + \xi_1(t) \quad (3-7)$$

Where  $\xi_1(t)$  is the random error term associated with  $\lambda_i(t)$ .

To derive Equation (3-7), one only needs to take the expectation of  $\lambda_i(t)$ .

$$E(\lambda_i(t)) = n_i(t) \frac{v_i(t)\Delta[1 - \varphi_i(t)]}{l_i} = w_i k_i(t) v_i(t) [1 - \varphi_i(t)] \Delta \quad (3-8)$$

On the other hand, if  $q_i(t)$  is greater than zero, then the boundary between the moving and queuing area will move toward upstream direction at a speed which can be determined by the LWR shockwave theory given by the following equation,

$$\vartheta_i(t) = \frac{\Omega(k_i(t), q_i(t)) - \Omega(k_{jam}, q_i(t))}{k_m - k_i(t)} \quad (3-9)$$

Where

$\vartheta_i(t)$  is the backward shockwave speed of the boundary between the moving and queuing area;

$\Omega(k_i(t), q_i(t))$  is the flow capacity given density and queue mass, namely the fundamental flow-density diagram; and  $k_m$  is the jam density;

The fundamental diagram  $\Omega$  typically represents the quantitative relationship between the flow rate and density. In this study, we formulate the fundamental diagram  $\Omega$  as a two-dimensional function of both density  $k_i(t)$  and queue mass  $q_i(t)$ . The modeling of the fundamental diagram will be elaborated in the next section. For now, let's simply assume that for any given queue mass  $q_i(t)$ , the flow rate is a continuous and differentiable function of density  $k_i(t)$ . Based on condition (3-9), the maximum number of vehicles joining the end of the queue during the interval is  $\vartheta_i(t)\Delta k_m w_i$ , however, considering possibility of vehicles exiting the network, the actual number of vehicles joining the queue follows a binomial distribution given by Equation (3-10),

$$\lambda_i(t) = \vartheta_i(t)\Delta k_m w_i [1 - \varphi_i(t)] + \xi_2(t) \quad (3-10)$$

Where,  $\xi_2(t)$  is the random error associated with  $\lambda_i(t)$  and  $\vartheta_i(t)$  is the shockwave speed given by (3-9).

To summarize,  $\lambda_i(t)$  can be obtained by combing expression (3-7) and (3-10).

$$\lambda_i(t) = \begin{cases} w_i k_i(t) v_i(t) [1 - \varphi_i(t)] \Delta + \xi_1(t) & \text{if } q_i(t) = 0 \\ \vartheta_i(t) \Delta k_m w_i [1 - \varphi_i(t)] + \xi_2(t) & \text{if } q_i(t) > 0 \end{cases} \quad (3-11)$$

Note that  $\varphi_i(t)$ ,  $i = 1, 2, \dots, m$  are time-varying model parameters representing the exit flow rates from cells. The estimation of  $\varphi_i(t)$  is discussed in later sections.

So far, we have emphasized the computation of the number of arrivals observed at the end of queue. Now let's move on to the modeling of flows between adjacent cells. The traffic flow that connects neighboring cells,  $f_{i,i+1}(t)$ , is more sophisticated due to several reasons. First,  $f_{i,i+1}(t)$  should not exceed the maximum number of vehicles that can be accommodated by the downstream cell; second,  $f_{i,i+1}(t)$  is affected by the signal light status during time interval  $t$ ; furthermore,  $f_{i,i+1}(t)$  also depends on both the queuing condition at the beginning of the interval and the arrival rate during the interval.

The analysis of  $f_{i,i+1}(t)$  begins with defining two additional variables, the number of vehicles sending flow from cell  $i$  denoted by  $s_i(t)$  and the maximum number of vehicle receivable by cell  $i+1$  denoted by  $r_{i+1}(t)$ . These two variables are usually referred to as the sending flow function and the receiving flow function in most literature.  $f_{i,i+1}(k)$  can then be written into the minimum value between  $s_i(t)$  and  $r_{i+1}(t)$ ,

$$f_{i,i+1}(t) = \min(s_i(t), r_{i+1}(t)) \quad (3-12)$$

$r_{i+1}(t)$  depends on the remaining capacity of cell  $i+1$  which can be computed using the following equation,

$$r_{i+1}(t) = k_m l_{i+1} w_{i+1} - q_{i+1}(t) - n_{i+1}(t) \quad (3-13)$$

Equation (3-12) considers both maximum number of sending flow of upstream cell and the maximum number of vehicle receivable by the downstream link. When downstream is not congested, then the shockwave propagates forward and the flow between two adjacent cells equals to the sending flow; contrarily, when the downstream is congested,

the shockwave will propagate backward toward upstream, therefore the flow between cells equals to the maximum number of vehicle accommodated by the downstream cell. The minimum operator of Equation (3-12) reflects such concept. Figure 3 (b) illustrated these two possible scenarios.

In order to derive  $s_i(t)$ , the following assumptions are introduced.

*Assumption 1* The traffic signal phasing of each cell remains unchanged during one time interval.

*Assumption 2* The number of arrivals observed at the end of the queue spreads evenly within each time interval, namely  $\hat{\lambda}_i(u) = \frac{\lambda_i(t)}{\Delta}$ ,  $u \in [t\Delta, (t+1)\Delta]$ .

*Assumption 3* The maximum discharge rate during the effective green time of the intersection is greater than arrival rate for any cell at any time.

The complexity of  $s_i(t)$  originates from the fact that the discharge flow rate from cell  $i$  depends on queuing condition. Let  $\acute{s}_i(u)$  be the sending flow rate at time  $u$ , then  $\acute{s}_i(u)$  is a step-wise function of  $\acute{q}_i(u)$  given by the following equation,

$$\acute{s}_i(u) = \Lambda(\acute{q}_i(u))\mu_i(t) + [1 - \Lambda(\acute{q}_i(u))]\hat{\lambda}_i(u) \quad t\Delta \leq u \leq (t+1)\Delta \quad (3-14)$$

$$\Lambda(x) = \begin{cases} 1 & x > 0 \\ 0 & x \leq 0 \end{cases} \quad (3-15)$$

Where

$\mu_i(u)$  is the maximum discharge rate of queue at time  $u$ ; and,

$\hat{\lambda}_i(u)$  is the arrival flow rate observed at the end of the queue at time  $u$ .

$\mu_i(t)$  is also known as the saturation flow rate and is determined by signal control status during interval  $t$ . Given  $t$ ,  $\mu_i(t)$  is a constant due to Assumption 1. Equation (3-14) and (3-15) modeled sending flow rate  $\acute{s}_i(u)$  as a stepwise linear function of  $\acute{q}_i(u)$  and  $\hat{\lambda}_i(u)$ :

when  $\hat{q}_i(u)$  is positive,  $\hat{s}_i(u)$  is equal to the saturation flow rate which is the maximum number of vehicle discharged from the queue per unit time; while when  $\hat{q}_i(u)$  becomes zero,  $\hat{s}_i(u)$  is equal to the arrival flow rate  $\hat{\lambda}_i(u)$ . And  $s_i(t)$  is the integral form of  $\hat{s}_i(u)$  over time, namely,

$$s_i(t) = \int_{t\Delta}^{(t+1)\Delta} \hat{s}_i(u) du \quad (3-16)$$

$$= \int_{t\Delta}^{(t+1)\Delta} \{\Lambda(\hat{q}_i(u))\mu_i(t) + [1 - \Lambda(\hat{q}_i(u))]\hat{\lambda}_i(u)\} du$$

The closed form of integral (3-16) cannot be obtained directly since piecewise linear function  $\Lambda(x)$  is not continuous. However computing the integration with numerical method will not only generate huge computational burden to the algorithm but also prevents one from exploring the mathematical property of the model. To overcome this issue, the following proposition is stated to provide a numerical approximation of integral (3-16).

*Proposition 1*

$$s_i(t) \approx \frac{1}{\alpha} \log \left( \frac{e^{-\alpha[q_i(t)-\beta]} + 1}{e^{-\alpha[q_i(t)+\lambda_i(t)-d_i(t)-\beta]} + 1} \right) + d_i(t) \quad (3-17)$$

Where,

$d_i(t)$  is the maximum number of discharge during current time interval,  $d_i(t) =$

$w_i\mu_i(t)\Delta$ ; and,

$\alpha, \beta$  are model parameters, by default one can take  $\alpha = 4, \beta = 0.5$ .

Proof.

First, create an artificial variable  $\tilde{q}_i(u)$  to represent the change of queue mass over time within the current interval,

$$\tilde{q}_i(u) = q_i(t) + (u - t\Delta)[\hat{\lambda}_i(u) - \mu_i(t)], t\Delta \leq u \leq (t+1)\Delta \quad (3-18)$$

Equation (3-18) establishes a reversible (one-to-one) mapping between  $\tilde{q}_i(u)$  and time  $u$ . Note that  $\tilde{q}_i(u)$  may take negative value if the queue vanishes completely at certain time point in the middle of the interval if  $q_i(t) + \Delta\hat{\lambda}_i(u) < \Delta\mu_i(t)$ . In reality the value of queue mass  $\hat{q}_i(u)$  never drops below zero, however, by allowing the artificial variable  $\tilde{q}_i(u)$  to take negative value, we are trying to approximate the sending flow with the following continuous function given by condition (3-19).

$$\hat{s}_i(u) \approx \frac{\mu_i(t)}{1 + e^{-\alpha[\tilde{q}_i(u) - \beta]}} + \frac{\hat{\lambda}_i(u)e^{-\alpha[\tilde{q}_i(u) - \beta]}}{1 + e^{-\alpha[\tilde{q}_i(u) - \beta]}} , t\Delta \leq u \leq (t+1)\Delta \quad (3-19)$$

Consequently, the integral (16) can be computed analytically as follows,

$$s_i(t) = \int_{t\Delta}^{(t+1)\Delta} \hat{s}_i(u) du \quad (3-20)$$

$$= \int_{t\Delta}^{(t+1)\Delta} \left\{ \frac{\mu_i(t)}{1 + e^{-\alpha[\tilde{q}_i(u) - \beta]}} + \frac{\hat{\lambda}_i(u)e^{-\alpha[\tilde{q}_i(u) - \beta]}}{1 + e^{-\alpha[\tilde{q}_i(u) - \beta]}} \right\} du \quad (3-21)$$

$$= \frac{1}{[\hat{\lambda}_i(u) - \mu_i(t)]} \int_{q_i(t) - \beta}^{q_i(t) + \Delta[\hat{\lambda}_i(u) - \mu_i(t)] - \beta} \left\{ \frac{\mu_i(t)}{1 + e^{-\alpha z}} + \frac{\hat{\lambda}_i(u)e^{-\alpha z}}{1 + e^{-\alpha z}} \right\} dz \quad (3-22)$$

$$= \frac{1}{[\hat{\lambda}_i(u) - \mu_i(t)]} \left\{ \frac{1}{\alpha} \log(e^{-\alpha(z-\beta)} + 1) [\mu_i(t) - \hat{\lambda}_i(u)] \right. \quad (3-23)$$

$$\left. + \mu_i(t)z \right\} \Big|_{q_i(t) - \beta}^{q_i(t) + \Delta[\hat{\lambda}_i(u) - \mu_i(t)] - \beta}$$

$$= \frac{1}{\alpha} \log \left( \frac{e^{-\alpha[q_i(t) - \beta]} + 1}{e^{-\alpha[q_i(t) + \hat{\lambda}_i(u)\Delta - \mu_i(t)\Delta - \beta]} + 1} \right) + \mu_i(t)\Delta \quad (3-24)$$

Note that from Equation (3-21) to (3-22), we changed the variable of the integral from  $u$  to  $\tilde{q}_i(u) - \beta$  using condition (3-18) and replaced  $\tilde{q}_i(u) - \beta$  with  $z$  for simplicity purpose,

$$z = \tilde{q}_i(u) - \beta = q_i(t) + (u - t\Delta)[\lambda_i(u) - \mu_i(t)] - \beta \quad (3-25)$$

$$du = \frac{dz}{[\lambda_i(u) - \mu_i(t)]} \quad (3-26)$$

Therefore the corresponding upper and lower bound of the integral changed from  $[t\Delta, (t + 1)\Delta]$  to  $[q_i(t) - \beta, q_i(t) + \Delta[\lambda_i(u) - \mu_i(t)] - \beta]$  accordingly. The proof is finished by replacing  $\bar{\lambda}_i(u)\Delta$  and  $\mu_i(t)\Delta$  with  $\lambda_i(t)$  and  $d_i(t)$  respectively.

In order to help readers better understand the output of equation (3-17), Figure 4 plots  $s_i(t)$  as a function of arrival rate  $\lambda_i(t)$  and initial queue  $q_i(t)$  given  $\mu_i(t) = 0.5$  and  $\Delta = 10$ .

By inserting Equation (3-13) and (3-17) into condition (3-12), the flow between adjacent cells  $f_{i,i+1}(t)$  can now be written as the following explicit form:

$$f_{i,i+1}(t) = \min \left( \frac{1}{\alpha} \log \left( \frac{e^{-\alpha[q_i(t) - \beta]} + 1}{e^{-\alpha[q_i(t) + \lambda_i(t) - d_i(t) - \beta]} + 1} \right) + d_i(t), k_m l_{i+1} w_{i+1} - q_{i+1}(t) - n_{i+1}(t) \right) \quad (3-27)$$

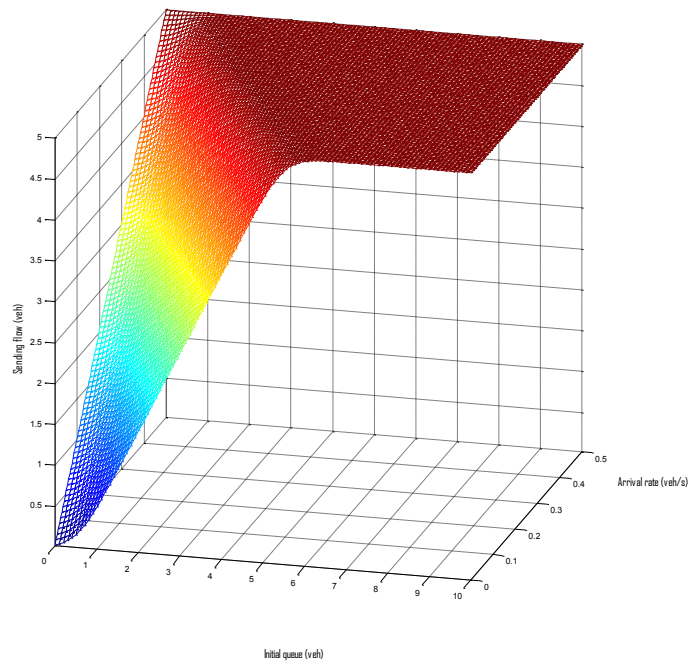


Figure 4 3-D plot of approximated sending flow rate

### 3.3. Evolution of cell speed

In the moving area of each cell, the change of traffic flow speed is induced by two primary causes: first, traffic flow speed is changed for the mixture between the incoming flow from both upstream cell and external demand sources and the existing vehicles within the moving area; second, the speed of vehicles also adapts dynamically to the local traffic conditions based on the macroscopic speed-density relationship. Again, consider the traffic flow movements within a cell shown in Figure 5.

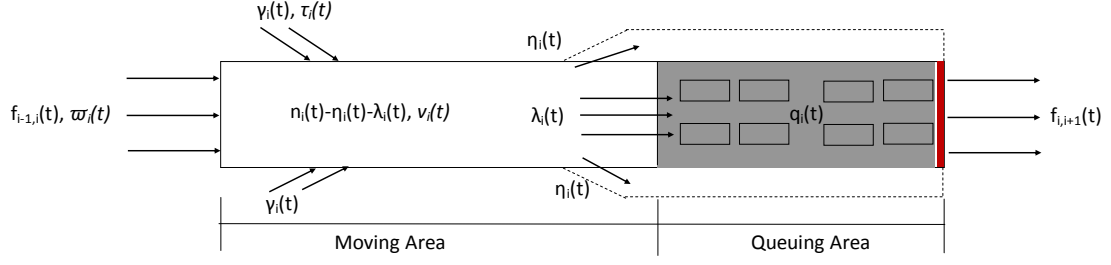


Figure 5 Illustration of traffic flow movements and their speeds

During interval  $t$ , the composition of the traffic flow in the moving area will change due to the traffic flows moving inbound and outbound. At the beginning of interval  $t + 1$ , the moving area contains three groups of vehicles. The first group is the vehicles remaining in the area from previous time step  $n_i(t) - \eta_i(t) - \lambda_i(t)$ , the second group is the inflow vehicles from upstream cell  $f_{i-1,i}(t)$  and the third group is the inflow vehicles from outside of the network  $\gamma_i(t)$ . Let  $\varpi_i(t)$  and  $\tau_i(t)$  denote the average flow speed of the latter two groups, then the average speed of the mixed traffic at the beginning of interval  $t + 1$  is computed as,

$$\tilde{v}_i(t + 1) = \frac{[n_i(t) - \eta_i(t) - \lambda_i(t)]v_i(t) + f_{i-1,i}(t)\varpi_i(t) + \gamma_i(t)\tau_i(t)}{n_i(t) + f_{i-1,i}(t) + \gamma_i(t) - \eta_i(t) - \lambda_i(t)} \quad (3-28)$$

In the above formulation,  $\tilde{v}_i(t + 1)$  is the anticipated flow speed only considering the blending effect of different movements. Meanwhile, vehicles tend to adjust their speed to adapt to the local traffic condition, and such behavior is usually described mathematically by the fundamental diagram. A majority of the literature formulated the speed as some decreasing function of density. While such macroscopic speed-density function is well-accepted in general, another important relevant concept is the anticipated traffic density of drivers. The idea is that drivers adjust their speed not only according to the local density surrounding them but also the predicted traffic flow condition of downstream link. Several studies have discussed this issue from both theoretical and empirical

prospective (see *Wang and Papageorgiou 2005, 2006* and *Boel and Mihaylova 2006*). On arterial links, drivers tend to reduce their speed when they see a red signal or queue accumulation. Hence the target traffic flow speed in the moving area is modeled as a function of both density and queue mass. The speed adjustment process is modeled with the following equation,

$$v_i(t + 1) = \theta(t)\tilde{v}_i(t + 1) + [1 - \theta(t)]V(k_i(t), q_i(t)) \quad (3-29)$$

Where,

$V(k_i(t), q_i(t))$  is the macroscopic speed-density-queue relationship for the moving area of arterial cells; and,

$\theta(t)$  is a model parameter representing the adapting rate of traffic flow speed,  $0 \leq \theta(t) \leq 1$ .

Equation (3-29) computes  $v_i(t + 1)$  as a linear combination of  $\tilde{v}_i(t + 1)$  and the theoretical speed  $V(k_i(t), q_i(t))$ . And the changing rate of speed is controlled by a time-dependent parameter  $\theta(t)$ . The specific form of speed function  $V$  is given by Equation (3-30).

$$V(k_i(t), q_i(t)) = v_f \left(1 - \frac{k_i(t)}{k_m}\right) e^{-\gamma \frac{q_i(t)}{c_i}} \quad (3-30)$$

Where,

$v_f$  is the free flow speed of the cell;

$k_m$  is the jam density;

$c_i$  is the storage capacity of link  $i$  measured by the maximum number of vehicles contained on the link as shown in equation (3-31);

$$c_i = w_i l_i k_m \quad (3-31)$$

and,

$\gamma$  is a model parameter representing the rate of speed decay as the queue ratio increases; The speed function given by (3-30) is a two dimensional convex function of  $k_i(t)$  and  $q_i(t)$  in which the cell speed decreases linearly with normalized density (the ratio between  $k_i(t)$  and  $k_m$ ) and exponentially with normalized queue length (the ratio between  $q_i(t)$  and  $c_i$ ). There are many alternative forms of Equation (3-30), such macroscopic correlation between the speed, density and queue within an arterial link should be determined and calibrated using field data available. The calibration of Equation (3-30) will be further discussed in numerical investigation sections.

#### 3.4. Dynamic estimation of model parameters

So far we have accomplished two important tasks. First, the traffic flow state of an arterial corridor is defined as the collection of its link density, speed and queue length. Then based on such traffic state definition, we have formulated the transition equations for system state variables including  $q_i(t)$ ,  $n_i(t)$  and  $v_i(t)$ . However without careful calibration of the model parameters that determines the property of system transition equations, the estimation result may quickly diverge from the actual situation. Model parameters defined in this study can be generally categorized into two groups: parameters describing the route choice behavior of the drivers such as turning fractions at each intersection  $\varphi_i(t)$ , and parameters that describe the driving behavior such as speed adaption rate  $\theta(t)$ . Generally, the change of those model parameters over time is not dominated by any type of traffic flow model. And those model parameters need to be dynamically estimated because of their time-dependent nature. Such dynamic calibration of the model is realized by state augmentation technique.

To begin with, the original system state variable is expanded to incorporate additional model parameters. Let  $\tilde{X}(t)$  be the system state variable after the state augmentation.

$$\tilde{X}(t) = [X(t), \varphi_1(t), \varphi_2(t), \dots, \varphi_m(t), \theta(t)] \quad (3-32)$$

Here  $X(t)$  is original traffic state variable defined previously and  $\varphi_1(t), \varphi_2(t), \dots, \varphi_m(t), \theta(t)$  are additional model parameters to be estimated. The new system state variable  $\tilde{X}(t)$  not only contains all the traffic flow variables but also those unknown model parameters associated with the transition process.

Then the change of non-traffic flow related part of  $\tilde{X}(t)$  is then modeled as following random walk process,

$$\begin{cases} \varphi_1(t+1) = \varphi_1(t) + \Delta\xi \\ \varphi_2(t+1) = \varphi_2(t) + \Delta\xi \\ \vdots \\ \varphi_m(t+1) = \varphi_m(t) + \Delta\xi \\ \theta(t+1) = \theta(t) + \Delta\xi \end{cases} \quad (3-33)$$

Where  $\xi$  is the random walk step with zero mean and unit variance.

We have thus far formulated the transition of system state along with all its time-varying parameters into the state-space form given by condition (3-11), (3-13), (3-15) (3-27), (3-29) and (3-33).

### 3.5. Chapter Summary

In this chapter, an innovative macroscopic traffic flow model is developed to describe the arterial traffic flow dynamics under given signal timing parameters. In later parts of the dissertation, the traffic flow model developed in this chapter will serve as the theoretical foundation for the real time traffic state estimation and short-term prediction. Such analytical traffic flow model can become very powerful tool once combined with other recursive stochastic estimation methods such as Kalman filter or particle filter.

Compared with existing traffic flow models such as CTM, the proposed model emphasizes on the modeling of queue formation and dissipation along signalized arterial corridor. The traffic flow models discussed in this section attempts to explain the high non-linearity and stochastic nature of arterial traffic flow dynamics based on rigorous mathematical derivation. The proposed model decomposed each arterial link into two distinct areas (moving and queuing area) and formulated the transition of flow density, speed and queue length using a set of stochastic equations. Such model is capable of predicting the movement of the boundary between the moving and queuing area without dividing the entire link into many tiny cells. From a theoretical point of view, the proposed model attempts to overcome the *homogeneity assumption* adopted by most freeway traffic flow models. The homogeneity condition always assume that the vehicles are uniformly distributed within each cell and their speeds are identical within each time period, therefore appropriate size of the cell needs to be selected in order to validly replicate the propagation of shockwave along freeway. However the traffic flow condition in arterial corridor is considerably different from that of freeway mainly because shockwaves form regularly within each link due to the signal, hence each arterial link needs to be represented by a large number of small cells in order to implement conventional freeway traffic flow model. However such approach is not only computationally expensive but also to some extent clumsy. To contend with such issue, the proposed model referred as *shifting boundary queue model*, intended to adapt conventional traffic flow model to arterial networks and offer a more straightforward and computationally efficient modeling framework.

The second contribution of this study is that it proposed the existence of some macroscopic relationship between traffic flow speed, density and queue within an arterial link. In freeway traffic flow studies, the correlation between speed and density is a fundamental concept usually referred to as speed-concentration curve or speed-density curve. In this study, we first proposed the three dimensional speed-density-queue function as an extension of the conventional speed-density curve on arterial links. The three dimensional speed-density-queue diagram describes the speed of a link as a function of both density and the ratio between queue length and link length, therefore it explicitly considers drivers' reaction to the queue in front of a signal. In later chapters, extensive numerical studies are conducted to fit the three dimensional speed-density-queue curve using field dataset.

The last noticeable contribution of the proposed model is the formulation of queue evolution in an analytical form considering the signal impact. Usually in stochastic estimation problems, the property of transition equations determines both the applicability and performance of the model. In this chapter, the transition of queue length or the boundary between queuing and moving area is a primary challenge in the modeling process. By using numerical approximation technique, we derived analytical transition expression for the queue length considering the non-continuous change of signal and discharging process. A further extension of the proposed model is capable of predicting the queue over multiple time steps during which the signal status changes according to some pre-fixed timing plan. Therefore the formulation obtained in this chapter is not only meaningful for traffic state estimation but also in other traffic control applications such as signal optimization.

## 4. Integrating Heterogeneous Detector Information with Particle Filtering

### 4.1. Fundamentals of Kalman Filter and Extend Kalman Filter

Many dynamic systems can be modeled with state-space formulations. In such formulation, the “state” of the system at a particular time  $t$  is represented by a vector, denoted by  $X(t)$ . Each component of  $X(t)$  represents the value of variable that characterizes certain aspect of the system. Thus,

$$X(t) = [x_1(t), x_2(t), \dots, x_N(t)]^T \quad (4-1)$$

$X(t)$  is mathematical representation of the system state at time  $t$ . Consequently the change of system state with respect to time can be described by a set of partial differential equations, which is known as the fundamental dynamics equation of the system. The arterial traffic flow model proposed in previous section is a specific example of a dynamic system. If the stochastic system dynamics equation is linear then the state estimation can be done by using Discrete Kalman filter. Mathematically,

$$X_k = AX_{k-1} + Bu_k + w_{k-1} \quad (4-2)$$

Here the continuous time  $t$  is rewritten with discrete time step  $k$ ,  $u_k$  is the control variables of the system at time step  $k$  and  $w_k$  is the noise of system dynamics. And the system is also associated with the following measurement equations, thus

$$Z_k = HX_k + v_{k-1} \quad (4-3)$$

Where  $Z_k$  is the field measurements obtained at time  $k$  and  $v_k$  is the noise of the measurement.

If both  $w_k$  and  $v_k$  are white noises following Gaussian distribution, the optimal estimation of system state can be computed recursively using Kalman filter. At each time step, the following two expressions are used to compute the prior and posterior estimation of  $X_k$ .

$$\tilde{X}_k = A\hat{X}_{k-1} + Bu_k \quad (4-4)$$

$$\hat{X}_k = \tilde{X}_k + K_k(Z_k - HX_k) \quad (4-5)$$

Where

$\tilde{X}_k$  is the prior estimation of  $X_k$  without considering the measurement at time  $k$ ;

$\hat{X}_k$  is the posterior or adjusted estimation of  $X_k$ ;

$K_k$  is Kalman gain at time step  $k$ ;

The weighting factor between prior estimation and the “measurement residual” between the actual observation and estimated measurements is called Kalman gain. The Kalman gain represents statistically optimal weighting factor between the estimation and observation values:

$$K_k = \frac{P_k^- H^T}{HP_k^- H^T + R} \quad (4-6)$$

$$P_k^- = AP_{k-1}A^T + Q \quad (4-7)$$

Where  $P_k$  and  $Q$  are error covariance matrix of state variable  $X_k$  and system noise  $w_k$ .

When applying Kalman filter, one needs to follow a two-step computation procedure: time update and measurement update. The former projects the estimated system state at previous time step to current time step, and the latter adjusts the prior estimation using Kalman gain. The general procedure of discrete time Kalman filter is illustrated in Figure 6.

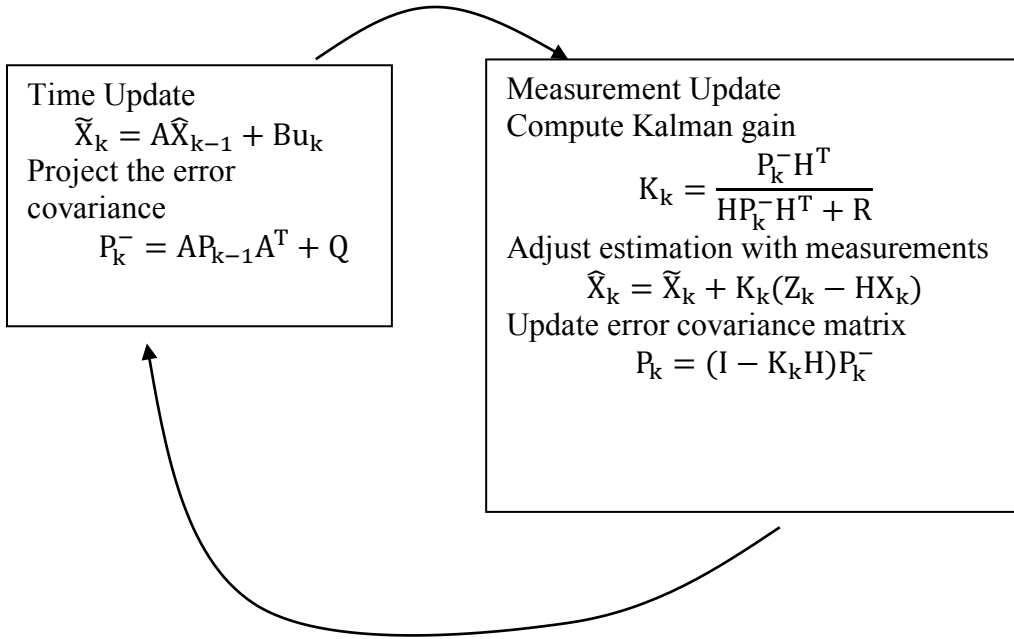


Figure 6 Computation step of KF

The original linear KF can be used to solve the estimation problem of a dynamic system governed by **linear stochastic differential equations**. However when the system dynamics equation is non-linear, the EKF technique can be implemented to handle the non-linear transition equations. Mathematically, the system governed by non-linear stochastic partial differential equation can be expressed as follows,

$$X_k = f(X_{k-1}, u_k, w_{k-1}) \quad (4-8)$$

$$Z_k = h(X_k, v_k) \quad (4-9)$$

All notations appearing in above equations have the same definitions as in the previous section. The non-linear function  $f$  and  $h$  are the fundamental system dynamics equation and measurement equation.

For non-linear system, one can still use Eq. (4-10) to perform the time update, thus,

$$\tilde{X}_k = f(\hat{X}_{k-1}, u_k, 0) \quad (4-10)$$

And compute the predicted measurement using Eq. (4-11)

$$\tilde{z}_k = h(\tilde{X}_k, 0) \quad (4-11)$$

However in order to compute Kalman gain using Eq. (4-6) ~ (4-7), the non-linear system dynamics equation and measurement equation need to be linearized first using Taylor expansion technique. The system transition and measurement are approximated by the following set of linear equations,

$$X_k \approx \bar{X}_k + A(X_k - \hat{X}_{k-1}) + Ww_{k-1} \quad (4-12)$$

$$Z_k \approx \bar{Z}_k + H(X_k - \hat{X}_{k-1}) + Vv_k \quad (4-13)$$

Where

$X_k$  and  $Z_k$  are the system state and measurement variables at time  $k$ ;

$\hat{X}_k$  is the posterior estimation of system state at time  $k$ ;

$\bar{X}_k$  is the approximated state obtained from Eq.(4-10);

$w_k$  and  $v_k$  are process and measurement noise;

$A$ ,  $W$ ,  $H$  and  $V$  are determined by the Jacobian matrices of  $f$  and  $h$ ; more specifically,

$$A = [a_{i,j}] = \frac{\partial f_i(X_k, u_k, 0)}{\partial x_{j,k}} \quad (4-14)$$

$$A = [h_{i,j}] = \frac{\partial h_i(X_k, v_k)}{\partial x_{j,k}} \quad (4-15)$$

$$W = [w_{i,j}] = \frac{\partial f_i(X_k, u_k, 0)}{\partial w_{j,k}} \quad (4-16)$$

$$V = [v_{i,j}] = \frac{\partial h_i(X_k, v_k)}{\partial v_{j,k}} \quad (4-17)$$

All the remaining computation procedures of EKF are the same as that of KF. There are several noticeable points regarding the application of EKF:

- In order to compute the linear approximation of the system, the dynamics equation  $f$  must be continuous and differentiable;

- The change of system should at least be locally linear so that the approximation result of (4-12) do not deviate too far from the actual state;
- After non-linear transformation, the distribution of process and measurement noise  $w_k$  and  $v_k$  became no longer normal. However when computing Kalman gain with EKF technique, such distortion effect on the error term distributions are not considered.

These can be regarded as the constraints of EKF. For more detail information of KF and EKF, readers can refer to other publications such as *Paul and Howard (2005)*.

#### 4.2. Fundamentals of Particle Filter (PF)

Particle filter is a type of recursive Bayesian filter designed to estimate the state of stochastic dynamics system with high non-linearity. The algorithm was first proposed by *Gordon et al. (1993)* and later studied and improved by many other researchers. Particle filter uses a large number of particles to represent the distribution of system state and compute the probability of each particle using the measurement function. Again let  $f(X_k, w_k)$  be the non-linear system dynamic equations,

$$X_{k+1} = f(X_k, w_k) \quad (4-18)$$

where  $w_k$  is the noise term of system transition. And at each time step, the measurement values are related to the state vector via the observation equation,

$$Z_k = h(X_k, v_k) \quad (4-19)$$

where  $v_k$  is the white noise of observation equation. PF uses a set of particles  $X_{k,1}, X_{k,2}, \dots, X_{k,m}$  to represent the system state at each time step and a weight is associated with each particle to represent its probability,  $w_{k,1}, w_{k,2}, \dots, w_{k,m}$ , thus

$$P(X_k = X_{k,i}) = w_{k,i} \quad (4-20)$$

Then using the system model it is possible to obtain the prior PDF of system state at each time step  $k$ ,

$$P(X_k|D_{k-1}) = \int P(X_k|X_{k-1})P(X_{k-1}|D_{k-1})dX_{k-1} \quad (4-21)$$

Where  $D_k = [Z_1, Z_2, \dots, Z_k]$

Since the probabilistic model of the state evolution  $P(X_k|X_{k-1})$  is described by  $f(X_{k-1}, w_{k-1})$  where  $w_{k-1}$  is a Markov model with known distribution, therefore,

$$P(X_k|X_{k-1}) = \int \Lambda(X_k - f(X_{k-1}, w_{k-1}))P(w_{k-1})dw_{k-1} \quad (4-22)$$

where  $\Lambda(x)$  is the Dirac delta function, since the delta function arise when both  $X_{k-1}$  and  $w_{k-1}$  are known, then  $X_k$  is computed based on a pure deterministic relationship.

According to Bayes rule,

$$P(X_k|D_k) = \frac{P(X_k|Z_k)P(X_k|D_{k-1})}{P(Z_k|D_{k-1})} \quad (4-23)$$

The above equation can be used to update the probability of each particle at every time step  $k$ . At each iteration in PF, first the prediction of system state is done by using system transition function to each particle; and then the weight of each particle is updated using measurement  $Z_k$ . The prediction and update algorithm in PF is summarized below:

Prediction: For each particle in the set, compute its predicted value using system transition function,

$$X_{k+1,i} = f(X_{k,i}, \xi_{k,i}) \quad i = 1, 2, \dots, m$$

Where  $\xi_i$  is the random error drawn from the distribution of  $w_{k,i}$ .

Update weight: update the weight of each particle,

$$w_{k,i} = w_{k-1,i} P(X_{k+1,i} | Z_{k+1})$$

For more detailed information on PF, readers can refer to articles by *Gordon (1993)*, *Chen and Liu (1996)*, and *Carpenter et al. (1999)*. The primary advantage of PF includes two points. First, it does not require the computation of Jacobian matrix of the transition function therefore it can handle dynamic system with high non-linearity. In the arterial traffic flow formulation, the first order derivative of system dynamic equation is not continuous. As a result, it is very difficult to implement EKF using the proposed traffic flow model. However introducing PF technique can solve this problem. Second, in a non-linear system, the distribution of error term in transition function will become non-normal after non-linear transformation, however the computation of Kalman gain is based on the assumption of normally distributed error term. Therefore applying EKF on a highly non-linear system will yield considerable amount of estimation error. To overcome this problem, PF uses a large number of particles to approximate the distribution of system state so that the algorithm remains effective even when the distribution of system state is not normal. That is the performance of PF is superior compared with EKF when the system transition is highly non-linear.

In this study, we use PF as a mathematical tool to incorporate detector measurements.

#### 4.3. Evaluate the probability of traffic state with fixed location detectors

Fixed location detectors are one of the most widely deployed detectors worldwide. The family of fixed detectors includes inductive loops, magnetic loops, laser detectors and so on. Although different types of detectors are made based on different technologies and have their respective accuracy and resolution, one common feature of fixed location detectors is that they can provide measurements of traffic flow speed, volume and occupancy around a particular point of the roadway.

Traffic volume count is the most basic measurement of detectors and represents the number of vehicles observed during each time interval. The traffic flow occupancy readings represent the proportion of time that the detector is occupied by the traffic and the speed reading of detector represents the average speed of passing vehicle.

In reality, the measurement of detectors is always subject to some degree of random error. The random error stems from two sources. First is the measurement error where due to some technical or non-technical reasons the detector readings deviate from the actual value. Second is the sampling error. Sampling error can be defined as the discrepancy between average traffic state of sampled vehicle set and the average traffic state of the entire traffic population on a link. More specifically, suppose  $m$  vehicle samples are observed by the detector during one time interval, and each of their observed speed is  $z_i$ , then the measurement vector of the link can be written as:

$$Z_t = [z_1, z_2, \dots, z_m]$$

We are interested in the conditional probability of link traffic speed  $v$  given above observation. Let  $v_j$  be the actual speed of vehicle  $j$  within the cell and the total number of vehicle at time  $t$  is  $n$ . Then the random error between measured and actual cell state can be computed as follows:

$$\frac{1}{m} \sum_{i=1}^m (z_i + \xi_i) - \frac{1}{n} \sum_{j=1}^n v_j \quad (4-24)$$

Where,

$z_i$  is the speed of  $i$ th vehicle captured by fixed detector, each  $z_i$  is a sampling of traffic speed of the cell;

$\xi_i$  is the random error associated with  $i$ th observation;

The first term of Eq.(4-24) represents the observed average traffic flow speed and the second term of Eq. (4-24) represents actual average traffic flow speed. By taking the expectation and variance at both sides of above equation, we can obtain,

$$\begin{aligned} E \left( \frac{1}{m} \sum_{i=1}^m (z_i + \xi_i) - \frac{1}{n} \sum_{j=1}^n v_j \right) &= \frac{1}{m} \sum_{i=1}^m \frac{1}{n} \sum_{j=1}^n v_j - \frac{1}{n_t} \sum_{j=1}^{n_t} v_j \\ &= 0 \end{aligned} \quad (4-25)$$

$$\begin{aligned} \text{Var} \left( \frac{1}{m} \sum_{i=1}^m (z_i + \xi_i) - \frac{1}{n} \sum_{j=1}^n v_j \right) &= \frac{1}{m^2} \text{Var} \left( \sum_{i=1}^m (z_i + \xi_i) \right) \\ &= \frac{1}{m} [\text{Var}(z_i) + \text{Var}(\xi_i)] \end{aligned} \quad (4-26)$$

Note that  $\xi_i$  is assumed to be I.I.D. following normal distribution with zero mean and fixed variance, thus,

$$\text{Var}(\xi_i) = \delta, E(\xi_i) = 0 \quad (4-27)$$

The variance of  $z_i$  is determined by the distribution of current system state,

$$\text{Var}(z_i) = \sum_{i=1}^{n_t} \left[ v_j - \frac{1}{n_t} \sum_{j=1}^{n_t} v_j \right]^2 \quad (4-28)$$

However since the true speed of each individual vehicle is unknown during the estimation process, we need to approximate it with the estimated speed variance during the PF method.

$$\text{Var}(z_i) \approx \sum_{i=1}^N \left[ \tilde{s}_i - \sum_{j=1}^N w_j \tilde{s}_j \right]^2 \quad (4-29)$$

Where

$\tilde{s}_i$  is the estimated speed of cell by particle  $i$ ;

$w_i$  is the weight of particle  $i$ ;

$N$  is the total number of particle;

The variance computed from Eq. (4-26) is influenced by three factors: 1) the number of observations,  $m$ ; 2) the variance of measurement error  $\delta$  and 3) the variance of the cell speed. Therefore distance between estimated cell speed  $v$  and observed traffic speed follows a normal distribution with zero mean and variance given by Eq.(4-30).

$$v - \frac{1}{m} \sum_{i=1}^m (z_i + \xi_i) \sim N \left( 0, \frac{1}{m} \left\{ \sum_{i=1}^N \left[ \tilde{s}_i - \sum_{j=1}^N w_j \tilde{s}_j \right]^2 + \delta \right\} \right) \quad (4-30)$$

Note that when  $m=0$ , the variance tends to be infinity and the conditional probability of any estimation will become identical. This make sense because under some rare condition, when no observation is obtained or the detector is occupied by one single vehicle, then no useful information can be obtained from the detector. Therefore the conditional probability of any given state should be equal to each other under such circumstance.

#### 4.4. Evaluate the probability of traffic state with probe vehicle data

Probe vehicle technique is receiving increasing attention from many transportation professionals due to its unique advantages. By installing GPS and wireless communication devices in probe vehicles, they can report their speed and location in a real-time manner to any information processing units around the world. And the high mobility of probe vehicles allow them to cover a wide range of the area in the network, another merit of probe vehicles is that they don't require installation which may interrupt the normal operation of the network.

This section focuses on the formulations of conditional probability of traffic state given speed and location information of probe vehicles. We will show that under the proposed framework, it is very easy to incorporate different types of traffic information into the process.

First of all, according to the location of each probe vehicle and network topology, one can map each probe vehicle into its corresponding cell. This work should be done before the state estimation. Within cell, suppose the location and speed of  $m$  probe vehicles are reported. Suppose their location and speed are represented by the following vectors,

$$[p_1, p_2, \dots, p_m]$$

$$[\tau_1, \tau_2, \dots, \tau_m]$$

Secondly, according to each of their speed, we can divide probe vehicles within the cell into two groups. The first group contains vehicles traveling at normal speed (higher than particular threshold), and vehicles assigned to the first group are considered as moving vehicles. The second group contains vehicles traveling at very low speed or those that are completely stopped, and vehicles in the second group are considered as in queuing condition.

Assume that there are  $m_1$  vehicle in group one and  $m_2$  vehicles in group two, and their respective speed and location are denoted as follows:

$$[p_{v1}, p_{v2}, \dots, p_{vm_1}] \text{ and } [\tau_{v1}, \tau_{v2}, \dots, \tau_{vm_1}] \text{ for group 1 and;} \\ [p_{q1}, p_{q2}, \dots, p_{qm_2}] \text{ and } [\tau_{q1}, \tau_{q2}, \dots, \tau_{qm_2}] \text{ for group 2}$$

#### 4.4.1. Probe data and flow speed at moving area

The average flow speed of moving area should be correlated only with the observed vehicle speed in the first group. Since each reported probe speed can be treated as a sampling process of the entire traffic population, the variance computed from Eq. (4-26) is also applicable to probe vehicle case. Thus,

$$\text{Var} \left( \frac{1}{m_1} \sum_{i=1}^{m_1} (\tau_{vi} + \xi_i) - \frac{1}{n} \sum_{j=1}^n v_j \right) = \frac{1}{m_1} [\text{Var}(\tau_{vi}) + \text{Var}(\xi_i)] \quad (4-31)$$

Therefore the conditional probability of each speed state given  $[\tau_{v1}, \tau_{v2}, \dots, \tau_{vm_1}]$  can be computed using condition (4-31).

#### 4.4.2. Probe data and flow density and queue length

In order to discuss the conditional probability between number of probes observed at each group and the cell density and queue length, the concept of penetration rate of probe vehicles needs to be introduced. The penetration rate of probe vehicle represents the proportion of probe vehicle to the total number of vehicles traveling within the network. Hence probe penetration rate is a probability value between 0 and 1. If one randomly picks

a vehicle from the entire population, then the probability that the selected vehicle is a probe vehicle is  $p$ .

Figure 6 illustrates a typical scenario of probe distribution within a cell. There are  $m_1$  probes in moving area and  $m_2$  probes in queuing area. Meanwhile, the estimated density and queue are  $k(t)$  and  $q(t)$  respectively, then given the probe penetration rate  $p$ , the conditional probability of the estimation can be computed with the following expression:

$$p(k(t), q(t) | m_1, m_2, p) \quad (4-32)$$

$$= C_{n(t)}^{m_1} p^{m_1} (1 - p)^{n(t) - m_1} C_{wq(t)}^{m_2} p^{m_2} (1 - p)^{wq(t) - m_2}$$

Where,

$w$  is the number of lanes of the cell;

$n(t)$  is estimated number of vehicles in moving area,  $n(t) = k(t)[1 - p(t)]w$ ;

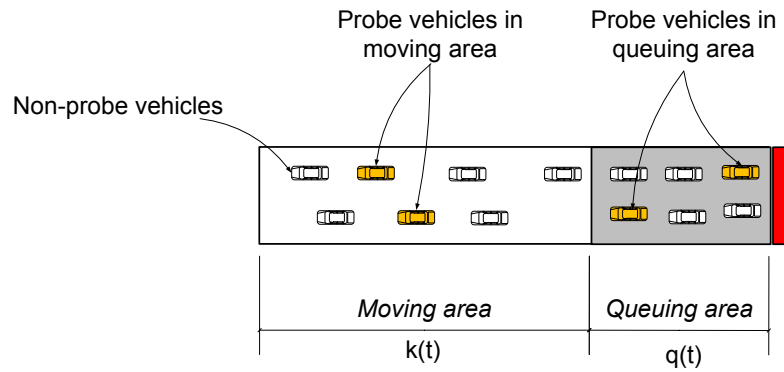


Figure 7 Probe vehicles in a cell

Conditional probability expression (4-32) is quite self-explanatory, since given the probe penetration rate, the probability of observing  $m_1$  probe vehicles among  $n(t)$  total vehicles follows binomial distribution. And such condition is the same in queuing area. Therefore a necessary condition for Eq.(4-32) to be valid is that  $m_1 \leq n(t)$ ,  $m_2 \leq wq(t)$ ,

otherwise the conditional probability should be zero since the total number of vehicle within each zone cannot be less than the actual observed number of probe vehicles.

#### 4.5. Computation procedure of PF algorithm

This section provides a detailed summary of the computational procedure of PF applied in this study. The notations used in this section are first summarized as follows:

$M$ - total number of particles contained in the estimation set;

$X_i(t)$  - the  $i$ th estimation particle at time step  $t$ ;

$S(t)$  - the particle set at time step  $t$ ,  $S(t) = [X_1(t), X_2(t), \dots, X_M(t)]$

$w_i(t)$ - the weight associated with particle  $i$  at time step  $t$ ;

$Y(t)$  – the field measurements obtained from traffic sensors at time  $t$ ;

$f_t(X, \delta_t)$  – the system dynamics equation or system transition equation at time  $t$ ;

$g_t(X_i(t), Y(t))$  –the conditional probability computation function at time  $t$ ;

The computation procedure of PF given above notations is summarized by Procedure 1.

### Procedure 1 Computation procedure of particle filter

1) Initialization: According to particle set size  $M$ , set  $S_0 = [X_1(0), X_2(0), \dots, X_M(0)]$  and repeat step 2) ~ 4) until the estimation process is finished;

2) Forward State Projection: For each particle, compute its projected state at next time step using  $f_t(X, \delta_t)$ .

$$X_i(t + 1) = f_t(X_i(t), \delta_t), i = 1, 2, \dots, M$$

3) Update weights: For each particle, first evaluate its conditional probability given measurements  $Y(t + 1)$ , and update its weight.

$$w_i(t + 1) = w_i(t) g_{t+1}(X_i(t + 1), Y(t + 1)), i = 1, 2, \dots, M$$

4) Re-sampling: Compute the number of effective samples according to the following condition,

$$N_{\text{eff}} = \frac{1}{\sum_{i=1}^M w_i^2(t + 1)}$$

Then perform re-sampling if the number drops below particular threshold. In re-sampling process, a new particle set is created with the following condition,

$$\tilde{S}(t + 1) = [\tilde{X}_1(t + 1), \tilde{X}_2(t + 1), \dots, \tilde{X}_M(t + 1)]$$

Where,

$$P(\tilde{X}_j(t + 1) = X_i(t + 1)) = w_i(t + 1)$$

#### 4.6. Chapter Summary

In this chapter, we emphasized the integration of estimation results from traffic flow models with the field observations considering the possible errors at both sides. As a mathematical tool, PF is selected as the primary filter algorithm in this study due to its unique advantages over other filtering algorithms. The simple yet flexible computation procedure provided by PF allows us to incorporate high non-linear and non-continuous

system dynamics equations. Also the estimation result of PF can provide us the entire distribution of traffic flow state over its mean value and by multiplying conditional probability obtained from multiple information sources, the framework can accommodate heterogeneous data sources and take full advantage of the additional information provided by multiple dataset.

The applications of two types of traffic sensing technologies were discussed in this chapter: the fixed location detectors and probe vehicles. The correlation between the real-time measurements from those two types of sensors and the estimated traffic state was analyzed. In the following chapters, a more detailed numerical investigation will be performed using a real world data set, and the performance of the model will be discussed in more detail.

## 5. Estimation of Arterial Travel Time and Its Variability

### *5.1. Summary of previous studies*

Travel time estimation (TTE) techniques are designed to evaluate the current or historical travel time of a path based on all external information provided by traffic sensors. Generally speaking, there is an intimate connection between TTE and travel time prediction (TTP) since TTP focuses on predicting the future travel time value based on historical information while TTE emphasizes on computing the present or past travel time values. Although these two are closely related concepts, they are still quite different in many ways. First of all, as a commonly used performance indicator of transportation network, the travel time is not a simple state variable of the network rather it is a complex function of many network states including traffic flow speed and density, queue length, signal timings and so on. The essential part of a TTE algorithm is to develop an effective method to link those traffic states with the travel time. On the other hand, TTP emphasizes more on the prediction side of the problem, namely how to compute the future travel time value effectively based on existing traffic information. Also, prediction can be done with or without estimation process, and we can categorize TTP studies into two groups, direct and indirect travel time prediction models, according to whether the prediction is performed based on an embedded TTE algorithm or not.

In a direct TTP, future travel time is often treated as a function of historical travel times and statistical methods are employed to describe the quantitative relation between the historical and future values. This family of algorithm includes regression methods and time series methods (*Fei et al. 2011, Yang et al. 2004*), KNN methods (*Qiao et al. 2012*), ANN methods (*Kwon and Petty 2005, Park and Rilett 1998, Stathopoulos and Karlaftis 2003*),

Kalman filter methods (*Liu et al. 2005*) and fuzzy regression methods (*Dimitriou et al. 2008*). All direct TTP relies on large amount of observed travel times in order to obtain stable parameter set for statistical models, and historical travel time data of a link or path can easily be obtained from various vehicle matching sensors including Bluetooth sensors, vehicle plate recognition cameras, magnetic sensors and video cameras. In summary, direct TTP methods are usually data driven models that require extensive data manipulation without considering the underlying traffic condition of the network.

Contrary to direct TTP methods, indirect travel time prediction models take an alternative approach in terms of how to obtain the travel time value. As mentioned previously, the indirect TTP methods attempt to quantify the complex relationship between travel time and underlying traffic flow state variables. Hence in indirect TTP, future network traffic states are predicted first, as an intermediate step, in order to compute future travel times. The relationship between network infrastructure, traffic flow state, travel time and traffic surveillance system is illustrated in Figure8.

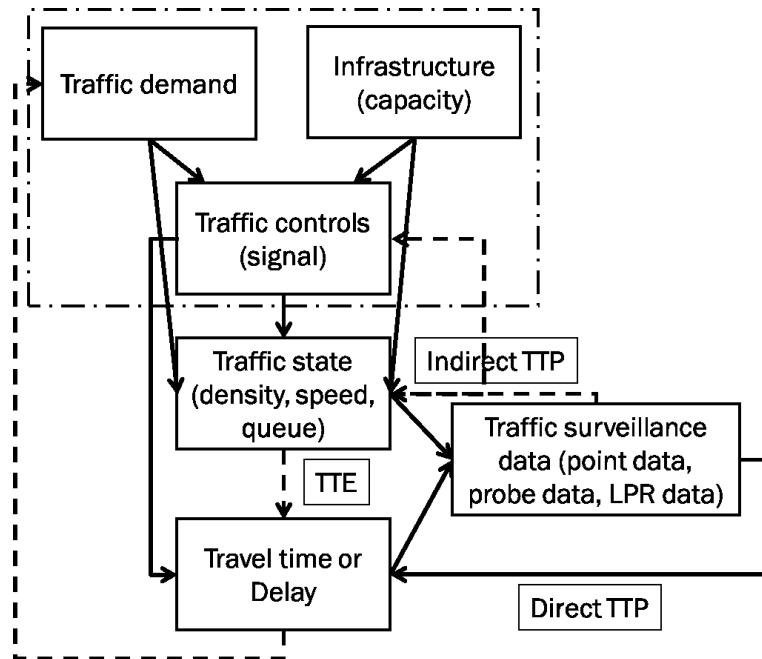


Figure 8 Relationship between traffic state, travel time and traffic surveillance data

The traffic flow condition of an arterial network is influenced by three major factors: the user demand, the network capacity and traffic control strategies employed. The interaction between these three factors determines the density, speed and queue distribution of the network. According to different network status, drivers may experience different travel times, however it is usually very difficult to write down analytical expression of travel time as a function of traffic state especially in arterial case. Hence TTE often serves as a numerical procedure to obtain real-time travel time. On the other hand, both traffic state and travel time can be measured by traffic surveillance system.

TTE is an essential component in indirect TTP method, and that's why the terminology TTE and TTP are sometimes used interchangeably. There are several advantages in developing an indirect TTP algorithm. First of all, indirect TTP does not rely on the direct observation of actual travel times from vehicle matching sensors since travel time in this

case is computed from estimated traffic states (link speed and density). Direct observation of field travel time is very difficult if not impossible under certain scenarios even without considering the availability of the vehicle matching devices, for example, the number of observations decreases significantly as congestion level increases and statistical models cannot achieve stability without sufficient data samples. Also in a complex network where the travel times between multiple OD pairs are concerned, it is very challenging to monitor the historical travel time between every OD pair. The indirect TTP, on the other hand, is able to take advantage of multiple data sources and does not rely on measurement of real-time travel time hence it can tackle the above problems with additional modeling effort.

Among the research that deals with TTE, trajectory method is one of the most famous and widely used algorithms. The core concept of trajectory method is to reconstruct the trajectory of a virtual probe vehicle based on estimated traffic states of the network. Trajectory method can be used for both freeways and arterials. *Coifman (2002)* first proposed a trajectory estimation method for freeway segments using densely deployed detector data. In his study, the local speed of traffic flow measured by loop detectors was expanded to the entire freeway segment based on kinematic shockwave theory from which the vehicle trajectory line was computed. Later, similar trajectory methods for arterial roads were discussed by several researchers including *Bhaskar et al. (2009)*, *Liu and Ma (2009)*, *Liu et al. (2009)*, *Sharma et al. (2007)* and *Geroliminis and Skabardonis (2005)*. Compared with freeway trajectory methods, the arterial trajectory methods focus more on the estimation of queue length and delay experienced by drivers at each intersection. More specifically, *Geroliminis and Skabardonis (2005)* proposed an arterial queue model considering the shockwave propagation from upstream to downstream intersection based

on which the average delay traveling along the arterial corridor is estimated. *Sharma et al. (2007)* proposed a real-time queue estimation method using detector counts. Similar approach was also considered by *Bhaskar et al. (2009)* who employed both upstream and downstream vehicle counters to determine the number of queued vehicles before the intersection. *Liu and Ma (2009)* and *Liu et al. (2009)* proposed a queue estimation method considering the occupancy change of loop detector during the accumulation and dissipation of the queue in front of a signal. Based on their proposed dynamic queue method, a virtual probe method was developed to estimate the arterial travel time in which the trajectory of an imaginary probe vehicle traveling along the road is computed according to the estimated queue length. *Bhaskar et al. (2009)* computed arterial queue length based on detector and probe vehicle data explicitly considering the demand generation and extinction at mid-link points. In general, trajectory methods are widely used in arterials due to their capacity of accurately regenerating the full trajectory and travel time of vehicle. And the core part of arterial trajectory method is a highly effective queue estimation model since it is proved in multiple studies that the travel time estimated from trajectory methods are very reliable as long as the underlying traffic states are computed correctly. Readers can see numerical results provided in the literature.

Due to the proliferation of probe vehicle technology, many recent studies focused on estimating the travel time with probe data. *Sethi et al. (1995)* proposed an incident detection system based on travel time measured from probe vehicle data. *Cetin et al. (2005)*, and *Chen and Chien (2000)* discussed the determination of the number of probes for freeway travel time estimation problems. *Chaudhuri (2011)* discussed the accuracy of the probe vehicle in speed estimation. *Comert and Cetin (2009)* proposed a probabilistic model to estimate the

arterial queue distribution according to probe data. Hellinga and Fu (2002) discussed the method of reducing the bias of speed estimation from probe vehicle data. More recently *Mehran et al.* (2012) proposed a trajectory reconstruction method based on probe data and fixed location sensors using kinematic wave theory. In general, research on probe vehicle technology is very versatile and each study has its own objective and methodology.

Another research direction in TTE is the computation of travel time variability over its mean value. Since travel time can be view as a complex function of the congestion level and other external factors such as road condition, signal control parameters and weather conditions, it is highly stochastic in nature especially under congested traffic condition. The range of travel time, not only its mean value, can affect the decision making process of individual drivers since depending on the expected mean value and potential range of the travel time, users may consider the tradeoff between the mean travel time and its reliability.

The reliability of travel time is usually measured by its variance over the mean value. However due to the dynamic and high stochastic nature of the travel time, computing travel time reliability through mathematical derivation is a challenging task. Hence most existing literatures usually seek alternative approaches. We can largely categorize the research in this field into two groups: statistical models and simulation-based models. Statistical models work on large amount of historical travel time dataset and describe the distribution of link travel time with particular statistical models. On the other hand, simulation based models try to investigate the stochastic property of travel time via microscopic simulation programs. Recently, the emergence of advanced vehicle matching techniques such as Bluetooth sensors has created more opportunity for researches to collect massive amount of actual travel time data (see *Haghani et al.* 2010, *Aliari and Haghani* 2012). *Fei et al.* (2011)

propose a Bayesian inference-based dynamic linear model for predicting route travel time by combining an a priori known initial distribution and real-time traffic information. They predict the posteriori route travel time distribution in terms of the variation of travel time around its historical median. *Hollander and Liu (2008)* analyzed the travel time distribution of a network using repeated simulation. Both *Sun et al. (2003)* and *Kwong et al. (2009)* studied the distribution of travel time based on the actual path travel time measured by vehicle matching technique. *Hollander and Liu (2007)* investigated the travel time distribution using data generated from repeated simulation. More recently, *Du et al. (2012)* proposed a data fusion model to combine the historical travel time distribution with real-time measurement data to obtain a more reliable short term link travel time distribution. In summary, compared with the estimation of mean travel time, study on the short term travel time reliability is sparse due to huge amount of travel time information required by such studies and most existing literature use artificial methods such as microscopic simulation to generate travel time data.

In this chapter, the fundamentals of trajectory method are first explained. Then an arterial travel time estimation algorithm is proposed combining the conventional trajectory methods with the traffic state estimation framework proposed in this study.

## 5.2. Trajectory Method for Arterial Travel Time Estimation

As it has been mentioned earlier, the idea of trajectory method is very straightforward. The estimation of travel time is performed by replicating the trajectory of a virtual probe vehicle traveling along the designated path. Consider a vehicle traveling along a freeway corridor. The freeway is divided into  $M$  segments. The average traffic flow speed within

segment  $i$  at time  $t$  is  $v_i(t)$  (this value could be obtained from traffic state estimation models or through direct observation), then the travel time of the vehicle to travel through the corridor can be approximated by the following expression,

$$Y(t) = \sum_{i=1}^M \frac{L_i}{v_i(t)} \quad (5-1)$$

Where

$Y(t)$  is the estimated travel time at time  $t$ ;

$L_i$  is the length of segment  $i$ ;

The trajectory of this hypothetical probe vehicle can be described by the following set of points in the space-time diagram.

$$\left[0, \frac{L_1}{v_1}, \frac{L_1}{v_1} + \frac{L_2}{v_2}, \dots, \sum_{i=1}^M \frac{L_i}{v_i(t)}\right] \quad (5-2)$$

$$\left[0, L_1, L_1 + L_2, \dots, \sum_{i=1}^M L_i\right] \quad (5-3)$$

Similar algorithm was employed by *Coifman* (2002), and he demonstrated the effectiveness of this type of simple trajectory method. (In his paper, the primary challenge was to obtain the traffic flow speed of the entire freeway segment using point measurements; the computation of travel time is only a small part of his study.)

However when the problem comes down to arterial travel time, the situation turns out to be much more complicated. Because the travel time estimator (5-1) is no longer valid due to the fact that vehicles will experience additional delays at intersection if they are caught by red signal. Hence in arterial roads, the travel time is composed of travel time on

the link and waiting time before the intersection. More sophisticated trajectory method is required for arterial case. Liu and Ma (2009) proposed a trajectory method for arterial corridors where the maneuver of a virtual probe vehicle is computed based on estimated queue length at each time step. The model is built on another dynamic queue model which uses high resolution signal and detector data.

Now suppose the time-dependent traffic flow state during the entire period of analysis is obtained by applying the traffic state estimation model proposed in the previous chapters. Then the network traffic state during the period of analysis can be represented by the following two matrices:

$$Q = \begin{bmatrix} Q_{1,1} & \cdots & Q_{1,T} \\ \vdots & \ddots & \vdots \\ Q_{N,1} & \cdots & Q_{N,T} \end{bmatrix}_{N \times T} \quad (5-4)$$

$$V = \begin{bmatrix} V_{1,1} & \cdots & V_{1,T} \\ \vdots & \ddots & \vdots \\ V_{N,1} & \cdots & V_{N,T} \end{bmatrix}_{N \times T} \quad (5-5)$$

Matrices Q and V contain N\*T elements where N is the number of cells and T is the period of analysis. Now again suppose each element of Q and V follows normal distribution with estimated mean and variance.

$$\begin{aligned} E(V_{i,j}) = v_{i,j}, \text{Var}(V_{i,j}) = \delta_{i,j}, E(Q_{i,j}) = q_{i,j}, \text{Var}(Q_{i,j}) = \vartheta_{i,j} \\ i = 1,2 \dots N, j = 1,2, \dots T \end{aligned} \quad (5-6)$$

Note that above traffic states are outputs of our arterial traffic state estimation model.

Now consider a virtual probe vehicle moving along the arterial path, the objective of trajectory method is to reconstruct the trajectory of this imaginary vehicle based on the traffic state matrix  $Q$  and  $V$ .

The trajectory of an imaginary vehicle can be computed using the procedure described by Procedure 2.

#### Procedure 2 Description of arterial trajectory method computation procedure

Step 1: initialization, set time  $t=0$ , simulation time step  $\Delta t = h$ , set the initial state of the vehicle to traveling, the current location of vehicle  $p(0)=0$ . At each time step, repeat the following computation steps.

Step 2: determine the current status of the vehicle. If the vehicle is at traveling mode then go to step 3), otherwise go to step 4).

Step 3: update the location and status of vehicle under traveling mode. First determine the traffic flow speed according to current time  $t$  and current location  $p(t)$ . Then the position at next time slot would be

$$p(t + h) = p(t) + \tilde{v}_{i,t}h$$

Obtain current queue length of the link,  $q_{i,j}(t)$ , compare the location of vehicle and the length of moving area of the link. If the vehicle is caught by the queue, then set the vehicle status to waiting mode and  $w_t = q_{i,t}$  and go to step 5), otherwise go to step 5) directly.

Step 4: update the location and status of vehicle under waiting mode. Compute the number of vehicles departed from the queue within the current time slot from estimated traffic states.  $d_t = q_{i,t+1} - q_{i,t}$ . Update the number of vehicles that remain before the virtual probe vehicle at the end of current time slot,

$$w_{t+1} = w_t - d_t$$

If  $w_{t+1} > 0$ , then the vehicle is still in the waiting mode after time slot

t; otherwise if  $w_{t+1} \leq 0$ , then it indicates that the vehicle is advancing to the next link, set  $i=i+1$  and  $p(t+h) = \sum_{j=1}^i L_j$  where  $L_j$  is the length of link  $j$ .

Step 5: advance to the next time step. Set  $t=t+1$  and check if the probe vehicle has finished the travel based on the current location and the length of the path, if yes then set  $j=j+1$  and return to step 1), otherwise go to step 2).

Note that above trajectory method can be applied multiple times to form a travel time distribution.

### 5.3. Chapter Summary

In this chapter, a new type of travel time estimation algorithm is proposed to evaluate the reliability of travel time along a signalized arterial road. By combining the real time traffic state estimation and trajectory method, the advantage of the proposed TTE algorithm is two-fold. First, the model can estimate the approximate distribution of travel time based on the traffic state estimation model discussed in the earlier chapters. Compared with other analytical models, the proposed method is very simple and easily understandable. Also the utilization of the model does not rely on particular traffic state estimation model. Second, compared with other simulation based models, the proposed method is computationally more efficient since it does not involve any microscopic simulation and obtaining the travel time distribution by repeatedly simulating the network which is a very time consuming task.

## 6. Short-term Traffic Flow Prediction Algorithm

### 6.1. Traffic state transition equation and short-term prediction

Recall the arterial traffic state definition given by (3-1),

$$X(t) = [q_1(t), \dots, q_m(t), n_1(t), \dots, n_m(t), v_1(t), \dots, v_m(t)] \quad (6-1)$$

The vector  $X(t)$  represents the traffic states of the corridor at time  $t$ , later such state vector  $X(t)$  is expanded to include additional turning ratio variables. The enhanced traffic state variable  $\tilde{X}(t)$  was defined by condition (3-33). And the transition of  $X(t)$  is described by the system transition equations developed in Chapter 3 which is summarized as follows,

$$n_i(t+1) = (1 - \varphi_i(t))n_i(t) + f_{i-1,i}(t) + \gamma_i(t) - \lambda_i(t) + \xi$$

$$q_i(t+1) = q_i(t) + \lambda_i(t) - f_{i,i+1}(t)$$

$$\lambda_i(t) = \begin{cases} w_i k_i(t) v_i(t) [1 - \varphi_i(t)] \Delta + \xi & \text{if } q_i(t) = 0 \\ \theta_i(t) \Delta k_m w_i [1 - \varphi_i(t)] + \xi & \text{if } q_i(t) > 0 \end{cases}$$

(6-2)

$$f_{i,i+1}(t) = \min \left( \frac{1}{\alpha} \log \left( \frac{e^{-\alpha[q_i(t) - \beta]} + 1}{e^{-\alpha[q_i(t) + \lambda_i(t) - d_i(t) - \beta]} + 1} \right) + d_i(t), k_m l_{i+1} w_{i+1} - q_{i+1}(t) - n_{i+1}(t) \right)$$

$$v_i(t+1) = \theta_i(t) \frac{[n_i(t) - \eta_i(t) - \lambda_i(t)]v_i(t) + f_{i-1,i}(t)\varpi_i(t) + \gamma_i(t)\tau_i(t)}{n_i(t) + f_{i-1,i}(t) + \gamma_i(t) - \eta_i(t) - \lambda_i(t)} + [1 - \theta_i(t)]V(k_i(t), q_i(t))$$

The forecasted system state  $\tilde{X}(t+1), \tilde{X}(t+2), \dots, \tilde{X}(t+K)$  can be obtained by repeatedly applying the above system transition equations to the estimated current system state,  $\tilde{X}(t)$ , given the following two types of additional information:

- 1) The predicted inflows at all demand generating nodes from  $t$  to  $t+k$ ,  $\gamma_i(t+k)$ ,  $k = 1, 2, \dots, K$ ;
- 2) The predicted turning ratio of each cell from  $t$  to  $t+k$ ,  $\varphi_i(t+k)$ ,  $k = 1, 2, \dots, K$ ;

Here  $K$  is the prediction time range defined as the maximum number of time steps to be predicted from the current time  $t$ .

The above two pieces of information are both essential because they represent two crucial aspects of the arterial network:  $\gamma_i(t)$  represents the boundary condition of the network, namely the number of vehicles that will enter the network in the near future; on the other hand,  $\varphi_i(t)$  represents the route choice behavior of drivers within the network and will determine the proportion of traffic flow volume at diverging points. A common feature shared by these two variables is that both of their transition cannot be described by traffic flow models, hence statistical methods need to be employed.

In this study, the SARIMA (Seasonal Autoregressive Integrated Moving Average) time series technique is applied to conduct the prediction of  $\gamma_i(t)$  and  $\varphi_i(t)$ .

## 6.2. *Description of SARIMA model*

The SARIMA is an enhanced ARIMA model considering the effect of seasonal change of the time series. Let  $\{Z_t\}$  be a seasonal time series with period  $S$  then if the series  $Y_t = (1 - B)^d(1 - S)^D Z_t$  is a stationary autoregressive moving average process (ARMA), then the original time series  $\{Z_t\}$  is a SARIMA process whose stochastic property can be described by the Equation (6-3) and (6-4).

$$Y_t = (1 - B)^d(1 - S)^D Z_t \quad (6-3)$$

$$\omega(B)\Omega(B^S)Y_t = \psi(B)\Psi(B^S)e_t \quad (6-4)$$

where,

B is the backshift operator defined by  $B^a Z_t = Z_{t-a}$ ;

$$\omega(X) = 1 - \omega_1 X - \omega_2 X^2 - \dots - \omega_p X^p;$$

$$\Omega(X) = 1 - \Omega_1 X - \Omega_2 X^2 - \dots - \Omega_P X^P;$$

$$\psi(B) = 1 - \psi_1 X - \psi_2 X^2 - \dots - \psi_q X^q;$$

$$\Psi(B^S) = 1 - \Psi_1 X - \Psi_2 X^2 - \dots - \Psi_Q X^Q;$$

$e_t$  is the white noise error with zero mean and fixed variance,  $E(e_t) = 0$  and  $D(e_t) = \sigma^2$

and  $\text{cov}(e_t, e_{t-k}) = 0$  for any  $k$ ;

The model parameters  $p$  and  $P$  represent the non-seasonal and seasonal autoregressive polynomial order and  $q$  and  $Q$  represent the non-seasonal and seasonal moving average polynomial order respectively. And  $d$  and  $D$  are the order of differencing for non-seasonal and seasonal part of the time series.

Equation (6-3) and (6-4) established a linear correlation between  $Z_{t+1}$  and its prior values  $Z_t, Z_{t-1}, \dots$ , thus both the single step or multiple step prediction of  $\{Z_t\}$  can be realized. In order to implement SARIMA model, the following four-step procedure is required,

- 1) Model identification: Determine the structure of SARIMA( $p,d,q$ )( $P,D,Q$ ) based on historical data.
- 2) Parameter estimation: Estimated the unknown parameter in (6-4).
- 3) Diagnostic checking: Compute the goodness of fit performance measurements.

- 4) Model optimization: Select optimal model from several alternative candidates according to diagnosis result.

In our model, the model identification is conducted offline using historical database. The inflow demand rate  $\gamma_i(t)$  is observed by detectors deployed at the demand generating links and turning ratio  $\varphi_i(t)$  is computed from the estimation model developed in chapter 3. Therefore the historical database is composed of both field observation and estimated results.

### 6.3. Real-time traffic state prediction procedure

Figure 9 illustrates the overall prediction procedure based on existing traffic state estimation steps. In the figure,  $N$  represents the total number of particles contained by the filtering algorithm and  $S$  represents the seasonal period of the prediction.  $X_i(t)$  represents the  $i$ th particle at time  $t$  and  $\tilde{X}_i(t)$  and  $\hat{X}_i(t)$  are the prior and posterior estimation of  $X_i(t)$ .  $\check{X}_i(t)$  is the predicted traffic state at time  $t$ . The system transition equation at time  $t$  is denoted by  $f(X_i(t), t)$  and the system measurement equation is denoted by  $g(X_i(t), Y(t))$  where  $Y(t)$  represents the measurement vector at time  $t$ . The lower circle represents the real-time traffic state estimation process and the upper circle illustrates the short-term prediction.  $\psi$  represents the SARIMA prediction function.

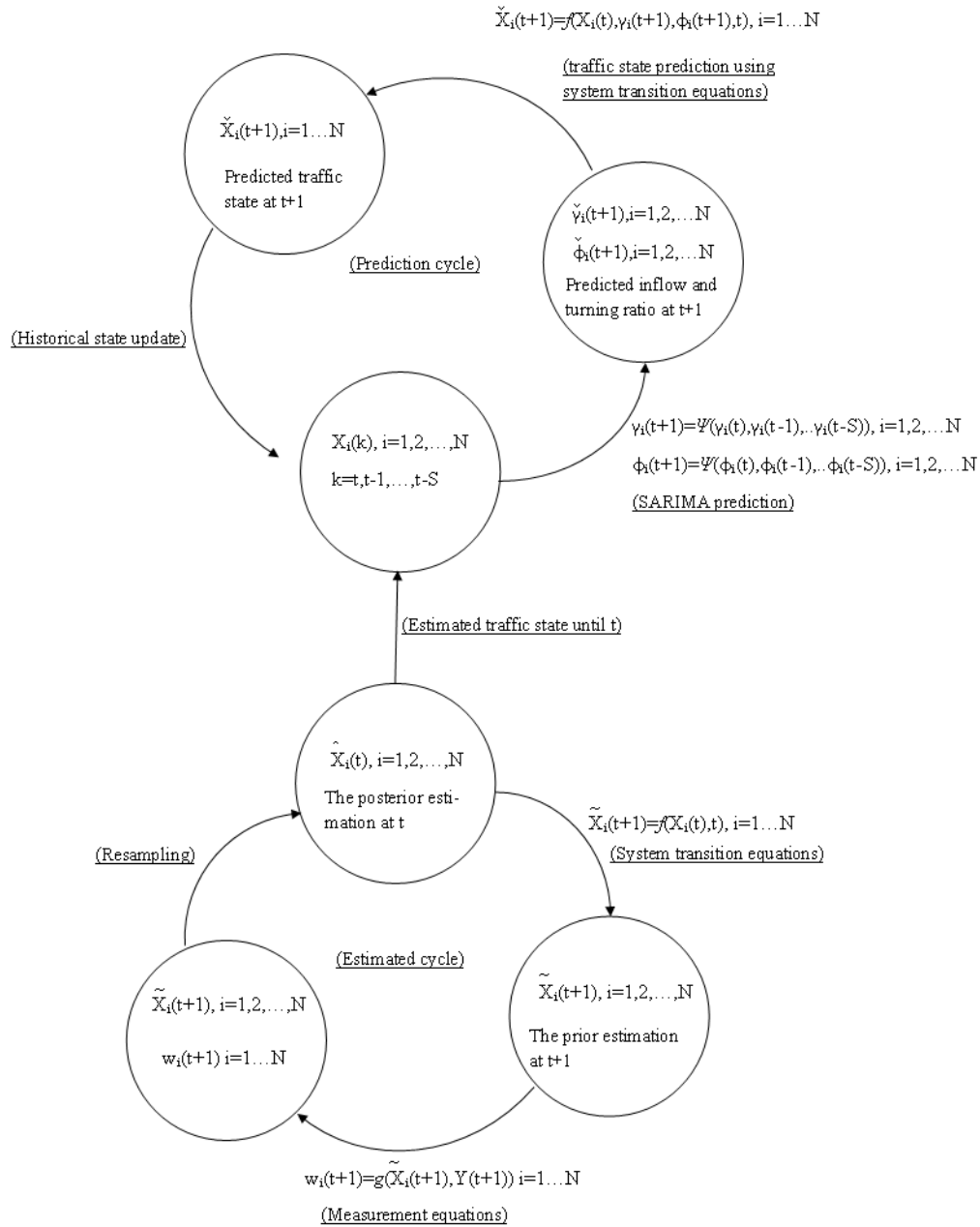


Figure 9 Real-time traffic state estimation and short-term prediction flow chart

Figure 9 presented the overall computation procedure of the proposed model. The estimation cycle contains three crucial procedures which are respectively state projection, state adjustment and resampling; on the other hand the prediction cycle also includes three key steps which are prediction of boundary conditions, state projection and state update.

The detailed computation procedure corresponding to Figure 9 is summarized by Procedure 3.

Procedure 3 Computation procedure of short-term traffic state prediction

- 1) State projection (for estimation): For each particle  $X_i(t)$ , compute the prior estimation of the particle at  $t+1$  using transition equation.  $\tilde{X}_i(t+1) = f(X_i(t), t)$ ;
- 2) State adjustment: Using field measurement collected at time  $t+1$ , compute the conditional probability of each particle,  $w_i(t+1) = w_i(t)g(\tilde{X}_i(t+1), Y(t))$ ;
- 3) Resampling: According to the update weights at  $t+1$ , resample the particle set to compute the distribution of traffic state at time  $t+1$ ;
- 4) Prediction of boundary conditions: For prediction, the algorithm stores recent system state up to  $S$  previous time step,  $X_i(t-1), X_i(t-2), \dots, X_i(t-S)$ . Using the SARIMA model, predict the future inflows and turning ratio,  $\gamma_i(t+1)$  and  $\varphi_i(t+1)$ .

$$\gamma_i(t+1) = \Psi(\gamma_i(t), \gamma_i(t-1), \dots, \gamma_i(t-S))$$

$$\varphi_i(t+1) = \Phi(\varphi_i(t), \varphi_i(t-1), \dots, \varphi_i(t-S))$$

where  $\Psi$  represents the SARIMA model determined through offline calibration process.

- 5) State projection (for prediction): Compute the predicted traffic state at  $t+1$  based on system transition equation and  $\gamma_i(t+1)$  and  $\varphi_i(t+1)$ .

$$X_i(t+1) = f(X_i(t), \gamma_i(t+1), \varphi_i(t+1), t)$$

- 6) State projection (for prediction): Compute the predicted traffic state at  $t+1$  based on system transition equation and  $\gamma_i(t+1)$  and  $\varphi_i(t+1)$ .

Note that the predicting cycle needs to be repeated  $K$  times where  $K$  is the prediction time range.

#### 6.4. Chapter Summary

This chapter discussed the development of short-term traffic flow prediction method within the proposed model framework. Key points of this chapter is summarized as follows,

- Grounded on the real-time traffic state estimation results, the future traffic condition is predicted by repeatedly applying the system transition equation to each particle;
- A well accepted time series model, SARIMA model, is applied in order to obtain the future boundary condition of the network. Future boundary condition is an extended concept which includes incoming demand flow rate and turning fractions of each cell;
- The prediction model also inherited the particle set and weight system, therefore the future traffic flow state is predicted as distributions instead of mean values;
- Based on the predicted traffic flow state, the future travel time can also be predicted using trajectory method.

## 7. Numerical Investigation Part I: Model Validation with Field Data

### 7.1. *Introduction of NGSIM dataset*

The NGSIM program is initiated by Federal Highway Administration (FHWA) and the main objective of the program is to validate the next generation simulation program using reliable field data. The NGSIM dataset contains high-resolution vehicle trajectory data which is collected through video devices. In this research, NGSIM data collected from two arterial segments are used for model validation purpose. The overall situation of arterial database used in this chapter is summarized in Table 2:

Table 2 The number of trajectory data samples contained in NGSIM dataset

<i>Dataset</i>	<i>Location</i>	<i>Time</i>	<i>Observed Number of Trajectory</i>
1	Peachtree Street, Atlanta, Georgia	12:45 to 1:00 PM	1114
2	Peachtree Street Atlanta, Georgia	4:00 to 4:15 PM	1222

The study area contains four signalized intersections which are respectively the intersection between Peachtree Street and 10<sup>th</sup> St. NE, 11<sup>th</sup> St. NE, 12<sup>th</sup> St. NE and 14<sup>th</sup> St. NE. The arterial road is divided into three segments by those four intersections; hence we use six cells to represent the structure of the network of the study area.

Vehicle trajectory data contained in above two dataset is collected from video devices deployed at high storage building within the study area. The location of each vehicle is extracted from the video files at an interval of 0.1 second, and all vehicle speed and acceleration information is obtained by parsing the vehicle trajectories. Ground truth traffic flow state including average flow speed, flow density and queue length in front of each

stop line is extracted from trajectory data using the program code developed by the author. For more detailed information regarding the data collection process, readers can refer to the original study report published by FWHA Peachtree Data Report (2007).

The NGSIM dataset contains vehicle trajectory data of two periods, 12:45 pm to 1:00 pm and 4:00 pm to 4:15 pm on November 8, 2006. Figure 10 shows the satellite map view of the target region and Figure 11 provides detailed geometric layout of the arterial corridor and the cell network used. The target arterial segment is modeled with a cell network composed of six cells which are marked by C1 ~ C6 in Figure 11 (b). In order to study the model performance under different types of sensors, the model is tested under two different scenarios (A1, A2). In scenario A1, six virtual detectors are installed in the middle of each cell (marked with P1 ~ P6 in Figure 11 (a)) to provide traffic flow speed and occupancy readings every five seconds; and in scenario A2, 15% of the vehicles is randomly selected as probe vehicles and their positions and speeds are reported for each time interval. Both the ground truth link traffic states (queue, density and speed) and virtual detector readings are generated by analyzing the high resolution trajectory data. A trajectory plot sample is given by Figure 12 which contains the northbound vehicle trajectory between 12:45 to 1:00 pm.

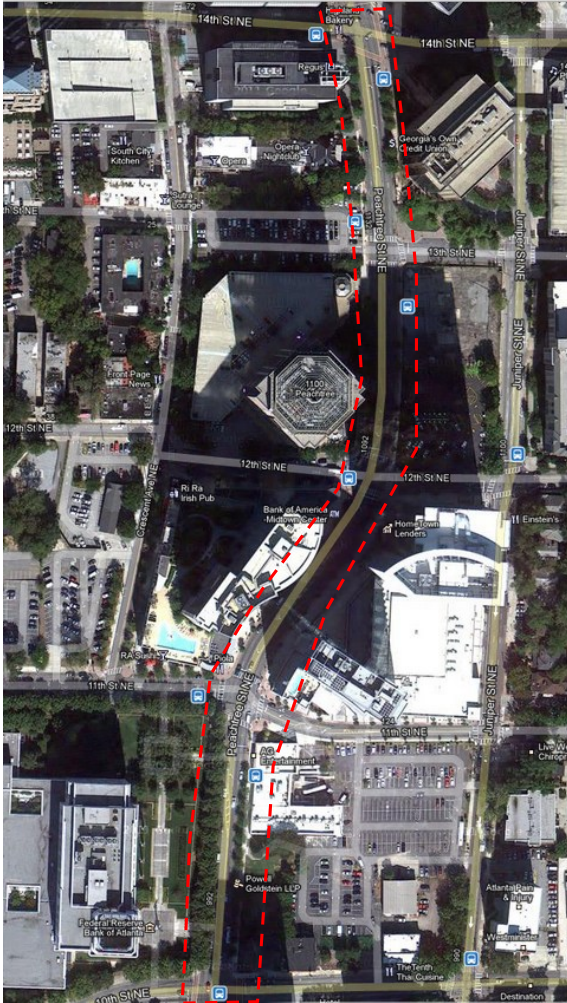


Figure 10 Map view of the Peachtree street

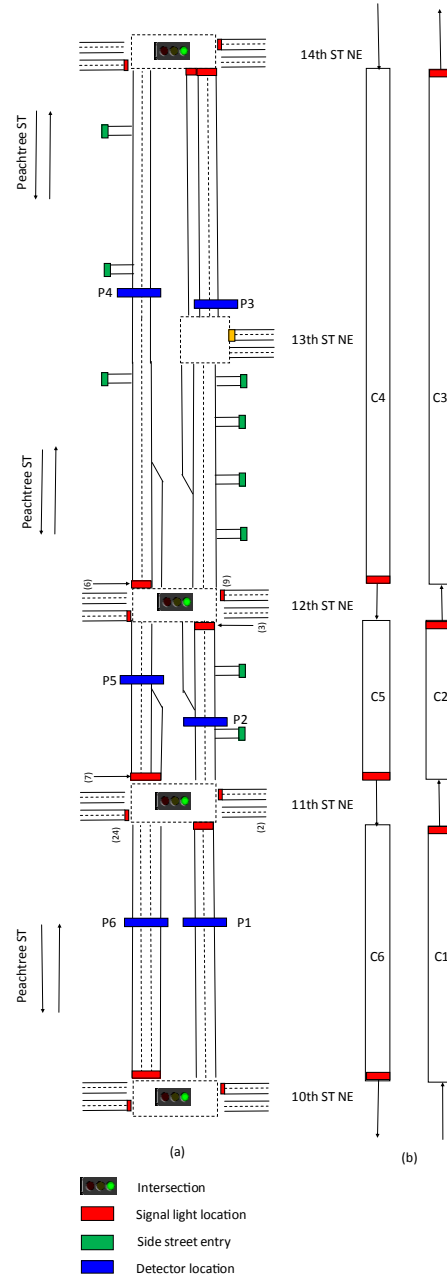


Figure 11 The sketch of geometric layout of the Peachtree arterial and corresponding cell network structure

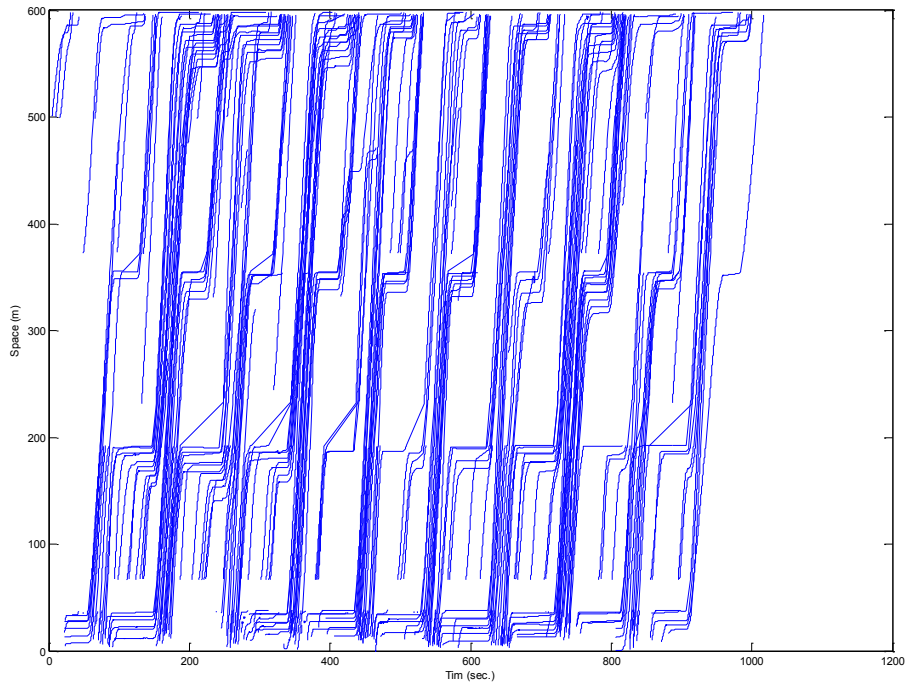
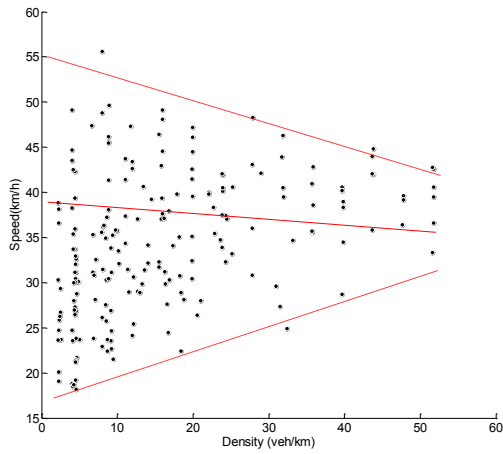


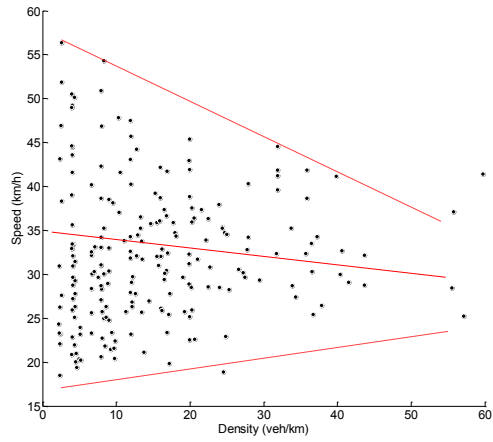
Figure 12 Trajectory plot of Peachtree street between 12:45 to 1:00 northbound traffic

### 7.2. Calibration of speed-density-queue function using field data

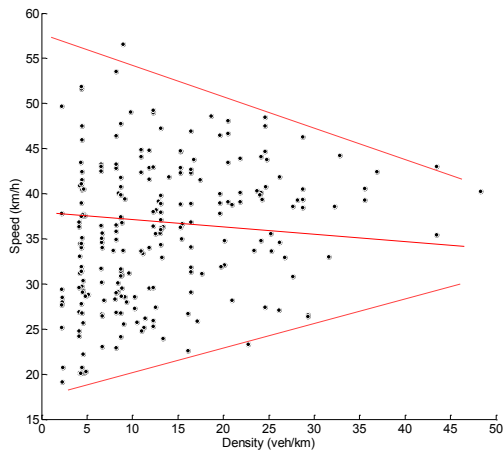
In order to implement the proposed framework, the fundamental speed-density-queue relationship needs to be calibrated based on observed trajectory data. The speed, density and queue length (queue length ratio) are extracted from the high resolution trajectory data provided by NGSIM database. The following two set of figures show the relationship between traffic flow density, queue length ratio (ratio between physical queue length and link length) and traffic flow speed in the form of scatter plots organized by direction and time period. Figure 13 displays the correlation between density and speed; Figure 14 displays the correlation between queue and speed; and Figure 15 demonstrates the correlation between density, queue and speed in three dimensional scatter plots.



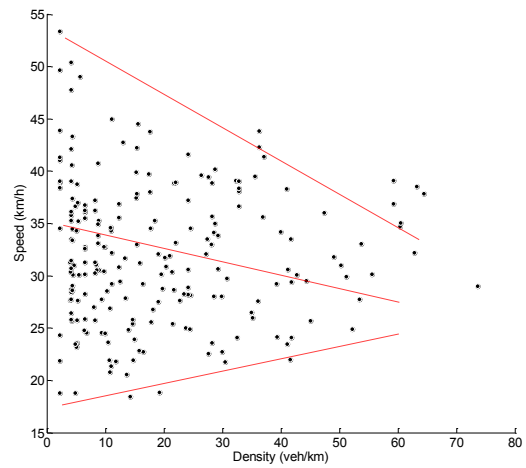
(a)



(b)



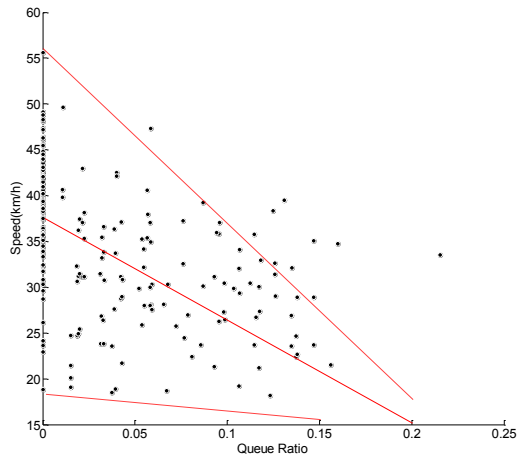
(c)



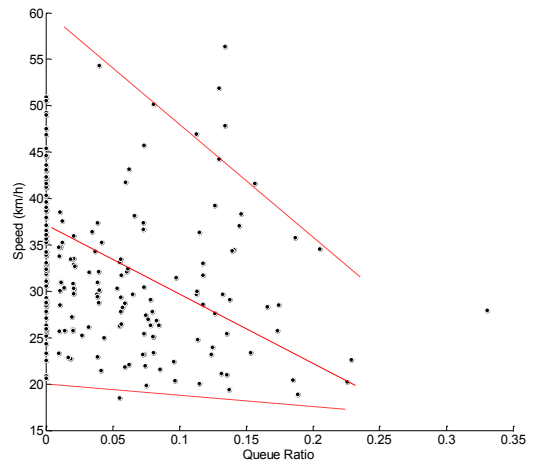
(d)

Figure 13 The speed density scatter plots of Peachtree street

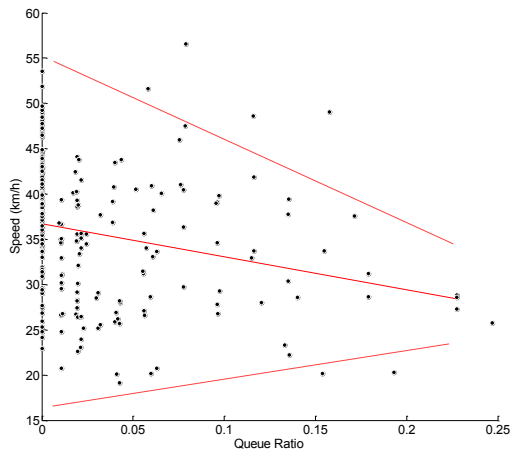
(a) 12:45 ~ 1:00 Northbound traffic; (b) 12:45 ~ 1:00 Southbound traffic; (c) 4:00 ~ 4:15 Northbound traffic; (d) 4:00 ~ 4:15 Southbound traffic;



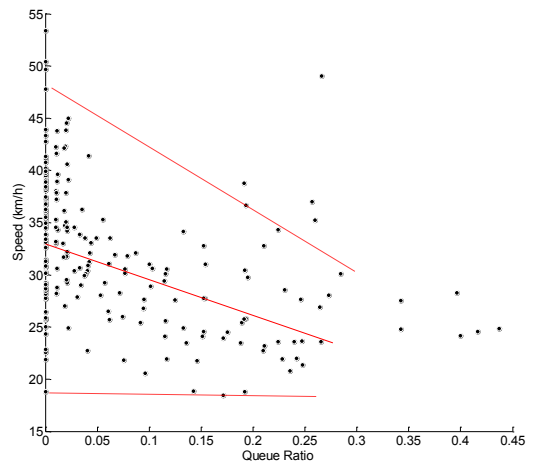
(a)



(b)



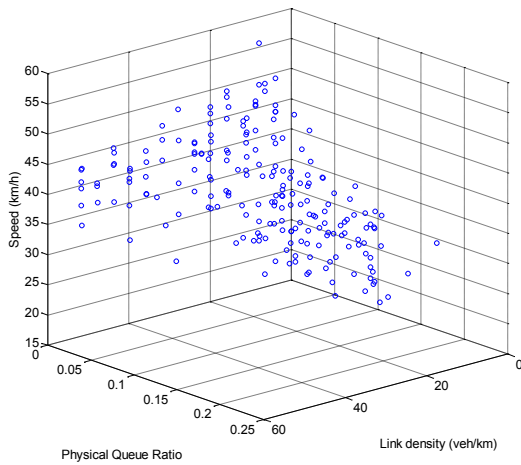
(c)



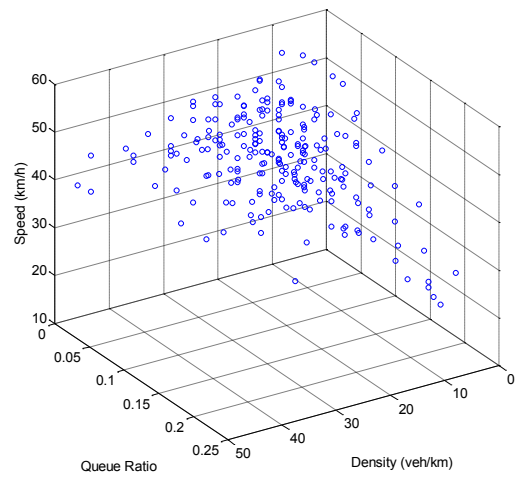
(d)

Figure 14 (a) ~ (d) The speed-queue scatter plots of Peachtree street

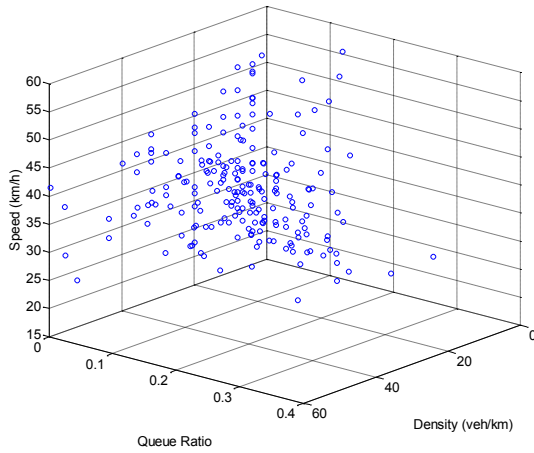
(a) 12:45 ~ 1:00 Northbound traffic; (b) 12:45 ~ 1:00 Southbound traffic; (c) 4:00 ~ 4:15 Northbound traffic; (d) 4:00 ~ 4:15 Southbound traffic;



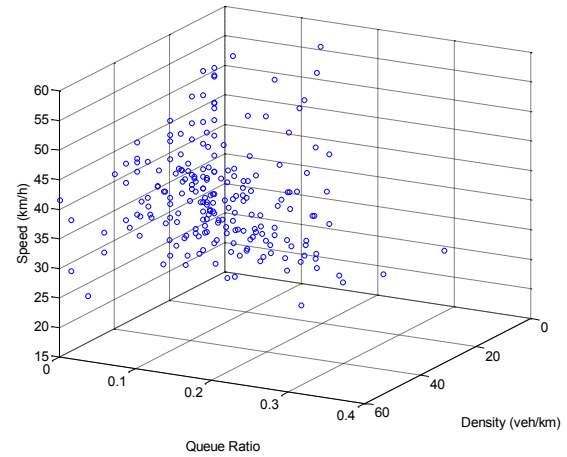
(a)



(b)



(c)



(d)

Figure 15 (a) ~ (d) The speed-density-queue three dimensional scatter plots of Peachtree street

(a) 12:45 ~ 1:00 Northbound traffic; (b) 12:45 ~ 1:00 Southbound traffic; (c) 4:00 ~ 4:15 Northbound traffic; (d) 4:00 ~ 4:15 Southbound traffic;

According to observed traffic flow data, the following functional form is selected as the fundamental speed-density-queue correlation:

$$V(k, q) = v_f \left(1 - \frac{k}{k_m}\right) e^{-\gamma q} \quad (7-1)$$

Equation 7-1 is referred to as linear-exponential speed-density-queue function where,

$k$  is the traffic flow density of the moving area;

$q$  is the queue length ratio defined as the ratio between physical queue length and link length;

$v_f$  can be interpreted as free flow speed;

$k_m$  is the jam density;

$\gamma$  is the speed decay factor;

$v_f$  and  $\gamma$  are model parameters to be calibrated and the curve fitting is performed using non-linear least square method with trust region algorithm. All the curve fitting process is done with Matlab curve fitting toolbox. Tables 3 and 4 summarized the fitted R square and parameter values.

Table 3 Summary of speed function fitted results in NGSIM dataset

Arterial Speed Model	Direction and time period	R-Square	Adjusted R-Square	RMSE
Linear-Exponential model	12:45 to 1:00 northbound traffic	0.158	0.147	7.608
	12:45 to 1:00 southbound traffic	0.21	0.203	7.82
	4:00 to 4:15 northbound traffic	0.18	0.178	7.8
	4:00 to 4:15 southbound traffic	0.198	0.192	6.3
	Average	0.186	0.18	7.382

Table 4 Summary of fitted parameter values in NGSIM dataset

Arterial Speed Model	Direction and time period	Free flow speed (m/s)	Speed decay factor
Linear-Exponential model	12:45 to 1:00 northbound traffic	14.42	3.109
	12:45 to 1:00 southbound traffic	13.87	1.27
	4:00 to 4:15 northbound traffic	14.10	1.11
	4:00 to 4:15 southbound traffic	13.36	1.087
	Average	13.93	1.64

Based on Tables 3 and 4, the following functional form is used for both traffic state estimation and prediction in this numerical example.

$$V(k, q) = 13.93 \left( 1 - \frac{k}{0.167} \right) e^{-1.64q} \quad (7-2)$$

### 7.3. Validation of traffic state estimation

First of all, we want to demonstrate the model performance in estimating the real-time traffic flow condition of the arterial using detector data as field observation source. Three quantitative performance measures including MAEB, MAPEB and CIE are computed in order to assess the accuracy of the model. In all definitions, the ground truth values are represented by  $Z = [z_1, z_2, \dots, z_T]$  and the estimated mean, upper and lower boundaries are represented by  $X = [x_1, x_2, \dots, x_T]$  and  $\bar{X} = [\bar{x}_1, \bar{x}_2, \dots, \bar{x}_T]$ ,  $\underline{X} = [\underline{x}_1, \underline{x}_2, \dots, \underline{x}_T]$  respectively.  $T$  is the analysis period. The upper and lower bound of the traffic state is computed by taking 15 and 75 percentile of the estimated distribution.

Mean Absolute Error comparing with the boundary (MAEB) is computed as:

$$\text{MAEB} = \frac{1}{T} \sum_{t=1}^T [\Lambda(z_t - \bar{x}_t) |z_t - \bar{x}_t| + \Lambda(\underline{x}_t - z_t) |z_t - \underline{x}_t|] \quad (7-3)$$

Mean Absolute Percentage Error comparing with the boundary (MAPEB) is computed as:

$$\text{MAPEB} = \frac{1}{T} \sum_{t=1}^T \left[ \Lambda(z_t - \bar{x}_t) \frac{|z_t - \bar{x}_t|}{z_t} + \Lambda(\underline{x}_t - z_t) \frac{|z_t - \underline{x}_t|}{z_t} \right] \quad (7-4)$$

Confidence interval of the estimation (CIE) is computed as:

$$\text{CIE} = \frac{1}{T} \sum_{t=1}^T |\bar{x}_t - \underline{x}_t| \quad (7-5)$$

where  $\Lambda(x)$  is the step-wise linear function defined as follows.

$$\Lambda(x) = \begin{cases} 1 & x \geq 0 \\ 0 & x < 0 \end{cases}$$

Table 5 provides an overview of performance measures computed based on the model outputs. For each type of traffic state variable estimated (queue length, density and speed), the MAEB, MAPEB and CIE indices are displayed for each individual cell. The performance indices are organized according to the type of traffic state, detector scenario and performance index types. Table 6 demonstrates similar content regarding the travel time estimation. The units for queue, density and speed are meter, veh/km and m/s respectively.

Table 5 Summary of model performance indices of estimation results in NGSIM dataset

<i>Traffic state variables</i>	<i>Scenario</i>	<i>Performance index</i>	<i>Cell Number (Link)</i>						<i>Total average</i>
			<i>C1</i>	<i>C2</i>	<i>C3</i>	<i>C4</i>	<i>C5</i>	<i>C6</i>	
<b>Queue length</b>	A1	MAEB (m)	1.97	1.38	4.16	1.36	2.46	2.23	2.26
		MAPEB (%)	21.8%	10.0%	27.5%	17.6%	21.1%	13.0%	18.5%
		CIE (m)	4.53	2.99	7.50	2.98	3.81	5.55	4.56
	A2	MAEB (m)	3.62	1.98	4.68	1.79	2.56	3.47	3.02
		MAPEB (%)	40.7%	14.5%	30.3%	24.5%	20.7%	23.6%	25.7%
		CIE (m)	2.12	1.70	3.54	1.54	2.39	2.77	2.34
<b>Traffic flow density</b>	A1	MAEB (veh/km)	1.17	1.64	2.95	0.89	2.67	3.03	2.06
		MAPEB (%)	7.7%	9.6%	28.7%	9.1%	16.7%	17.7%	14.9%
		CIE (veh/km)	6.13	7.84	7.17	4.61	9.29	7.16	7.04
	A2	MAEB (veh/km)	1.61	2.06	2.24	1.04	1.81	2.01	1.80
		MAPEB (%)	10.7%	12.1%	21.8%	10.4%	12.6%	12.1%	13.3%
		CIE (veh/km)	4.32	4.68	3.54	3.21	6.67	5.06	4.58
<b>Traffic flow speed</b>	A1	MAEB (m/s)	0.92	0.45	0.84	1.70	0.60	0.62	0.85
		MAPEB (%)	10.3%	4.5%	9.2%	17.3%	6.3%	7.0%	9.1%
		CIE (m/s)	1.21	1.63	1.39	0.73	1.51	1.69	1.36
	A2	MAEB (m/s)	1.01	0.56	1.17	1.68	0.63	0.61	0.94
		MAPEB (%)	11.3%	5.5%	12.7%	17.1%	6.6%	6.8%	10.0%
		CIE (m/s)	0.80	1.12	0.84	0.50	1.04	1.24	0.92

As we can see from Table 5, the proposed model has excellent performance under all three types of traffic flow states. In scenario A1, the MAEB of queue length, cell density and cell speed are respectively 2.26 (m), 2.06 (veh/km) and 0.85 (m/s) with confidence interval 4.56 (m), 7.04 (veh/km) and 1.36 (m/s), these numbers remain similar in scenario A2. Considering

another primary performance index MAPEB, among three types of traffic states, the model performed better in estimating the traffic flow density and speed compared with queue length. In A1, the relative error of density and speed estimation are 14.9% and 9.1% respectively, while the relative error of queue estimation is 18.5%; in A2, the relative error of density and speed estimation are 13.3% and 10.0% respectively, while the relative error of queue estimation is 25.7%. Two possible reasons that caused comparatively large error in queue estimation are:

Table 6 Summary of model performance indices of travel time estimation in NGSIM dataset

<i>Scenario</i>	<i>Time period and direction</i>	<i>MAEB</i>	<i>MAPEB</i>	<i>CIE</i>
A1 (Detector)	1245 to 100 Northbound	8.25	8.5%	0.55
	1245 to 100 Southbound	6.56	9.1%	3.19
	415 to 430 Northbound	7.08	6.7%	3.74
	415 to 430 Southbound	9.36	8.9%	9.47
	Average	7.81	8.3%	4.23
A2 (Probe vehicle data)	1245 to 100 Northbound	7.85	8.1%	0.49
	1245 to 100 Southbound	6.98	9.6%	2.10
	415 to 430 Northbound	6.30	6.0%	2.18
	415 to 430 Southbound	9.11	8.6%	6.26
	Average	7.56	8.1%	2.76

1) For queue estimation, there are no field measurements which can be used for state adjustments. Therefore the estimation error will accumulate as the analysis period becomes longer.

2) The proposed model assumes all queued vehicles are evenly distributed among all lanes, which may not be true in reality due to various reasons.

The overall estimation accuracy in scenario A1 is higher than that of A2 indicating that although two types of traffic sensors are complementary to each other, the model attains higher degree of accuracy when receiving inputs from fixed location detectors in this dataset. Compared with fixed location detectors such as inductive loops, probe vehicle data does not provide continuous observations of traffic flows therefore the penetration rate of probe

vehicle is a crucial factor affecting the estimation reliability. The traffic volume along Peachtree street during the observation period is quite low, hence in our example, the 15% penetration rate only provided sparse data points for the estimation.

To further demonstrate the model outputs versus ground truth traffic state values, the estimation results of individual cells are selectively displayed in Figures 20 through 22. For each type of traffic state variable, the estimation results of three cells are selected and plotted against the ground truth values. And for comparison purpose, the estimation results under both scenarios (detector and probe vehicle data) are presented together. The estimated and ground truth travel time data is plotted for each direction in Figure 16 through Figure 19. For a complete list of estimated traffic states, readers can refer to Appendix A.

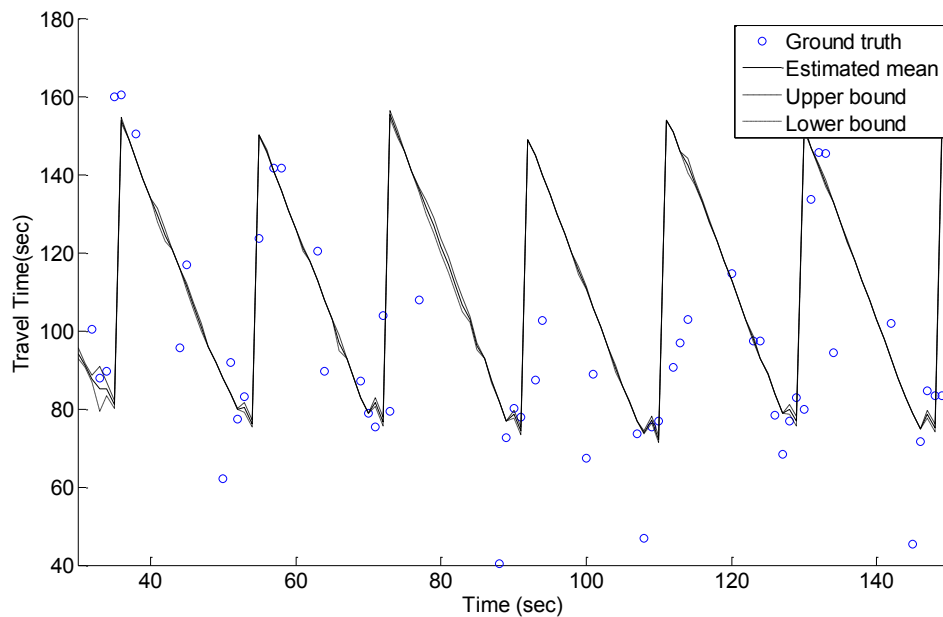


Figure 16 Estimated and ground truth travel time of PT street 12:45 to 1:00 northbound traffic

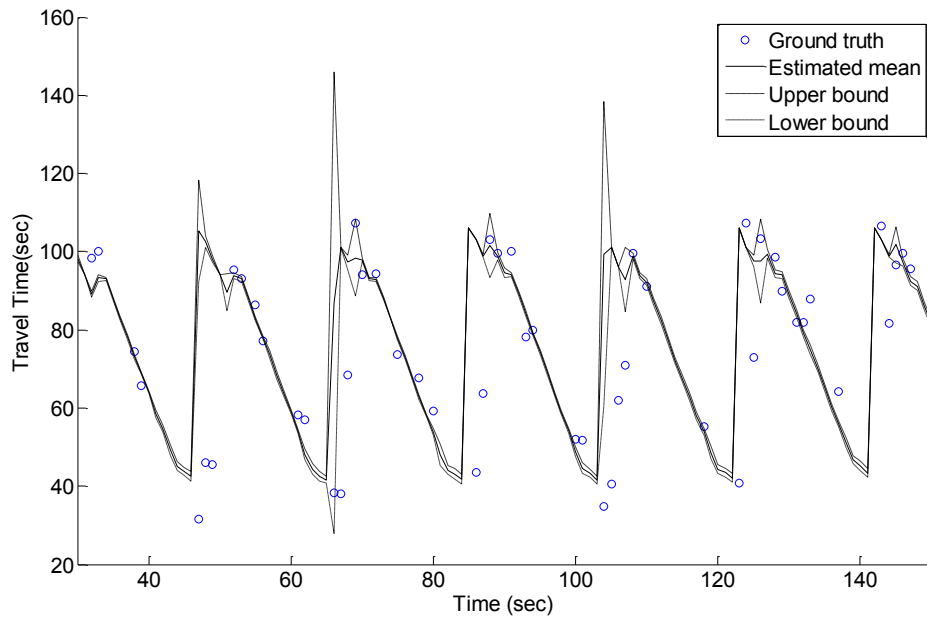


Figure 17 Estimated and ground truth travel time of PT street 12:45 to 1:00 southbound traffic

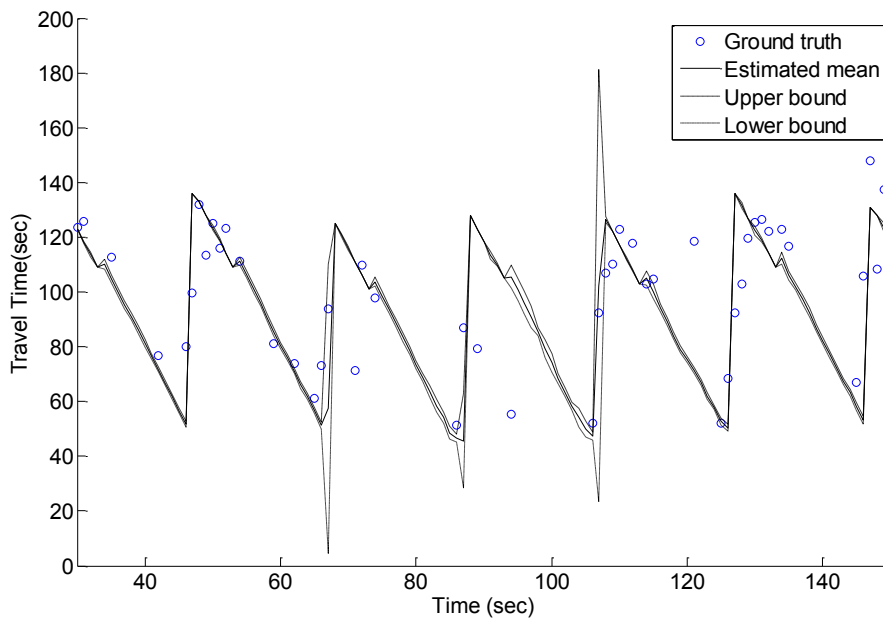


Figure 18 Estimated and ground truth travel time of PT street 4:00 to 4:15 northbound traffic

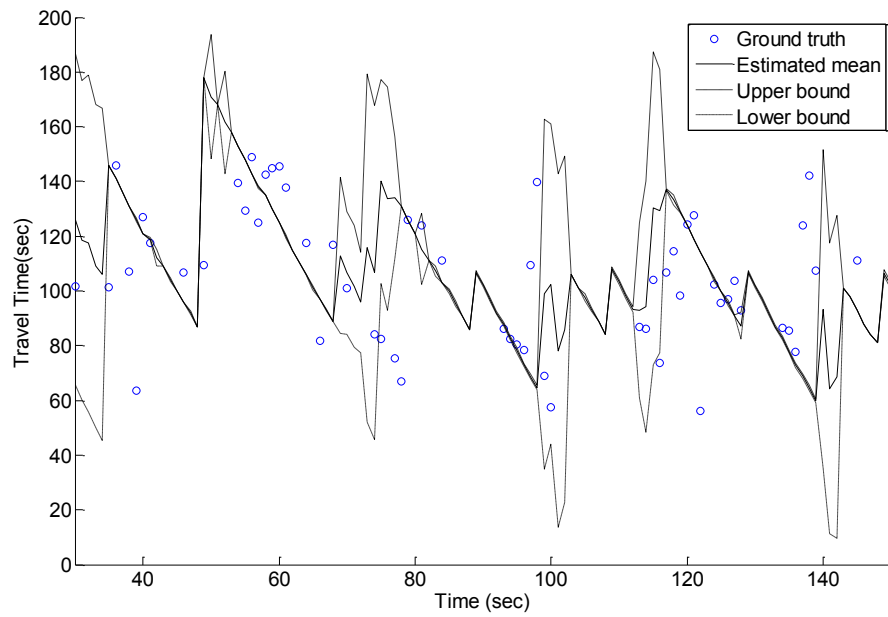
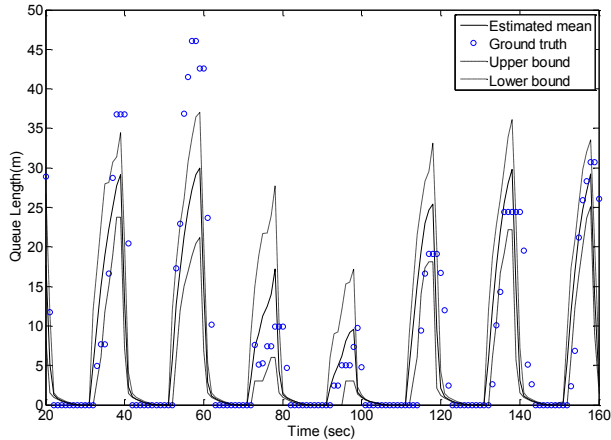


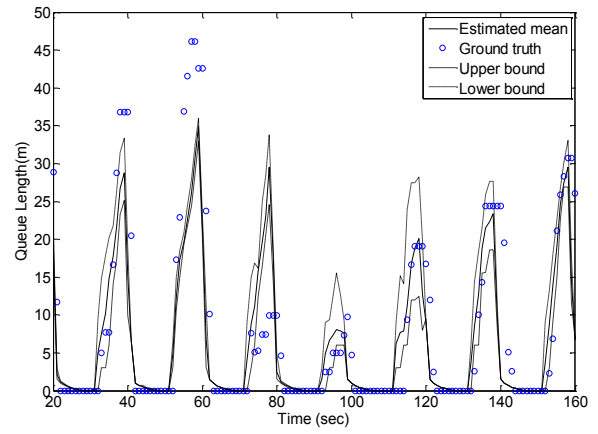
Figure 19 Estimated and ground truth travel time of PT street 4:00 to 4:15 southbound traffic

Scenario A1 (using detector information)

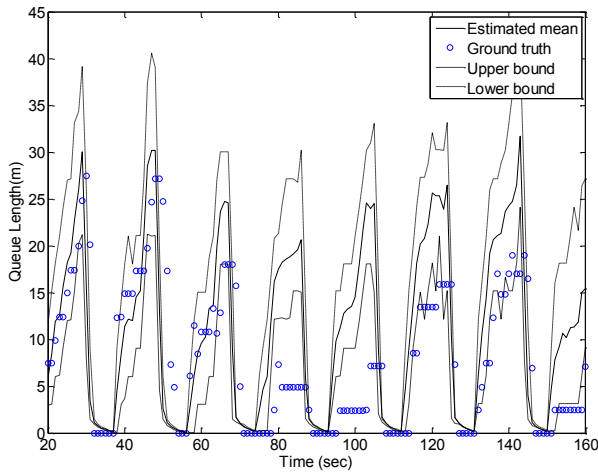


(a) MAPEB= 9.9%

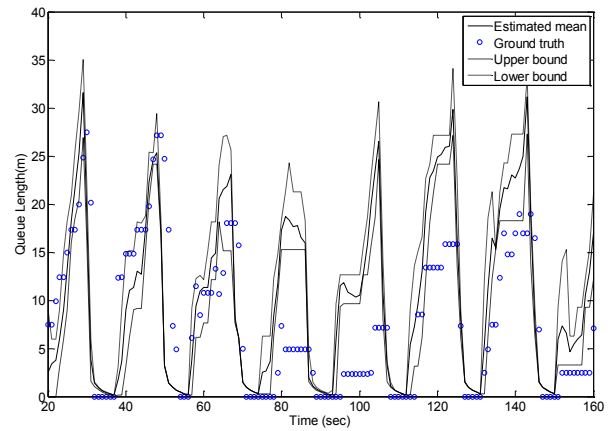
Scenario A2 (using probe information)



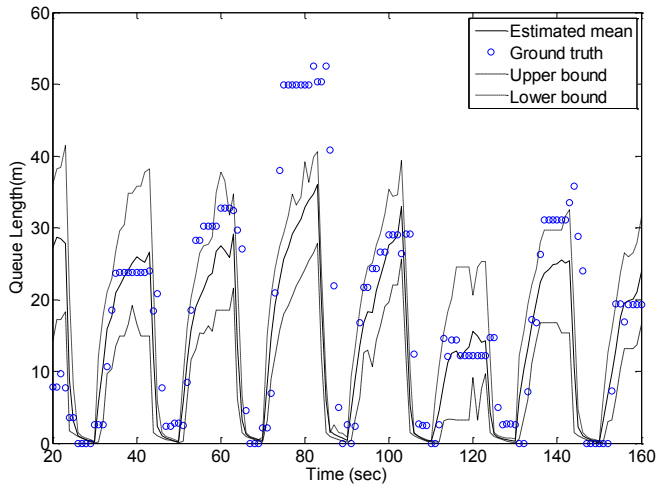
(b) MAPEB= 13.4%



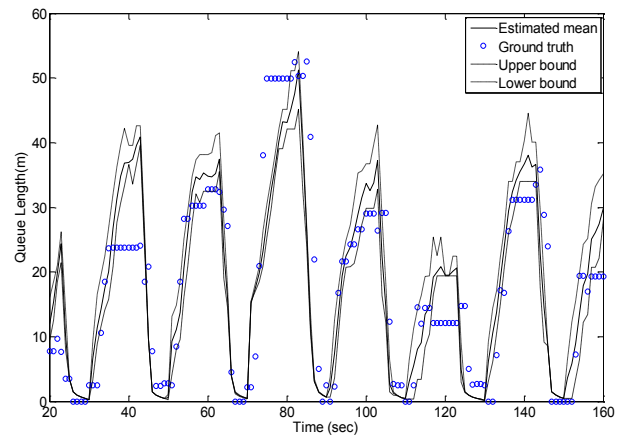
(c) MAPEB=20.2%



(d) MAPEB=31.2%



(e) MAPEB=17.9%



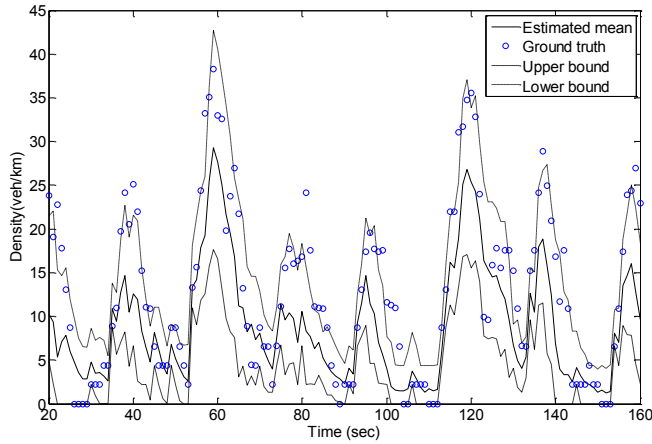
(f) MAPEB=17.2%

Figure 20 Estimated and ground truth queue length plot of selected cells in NGSIM dataset

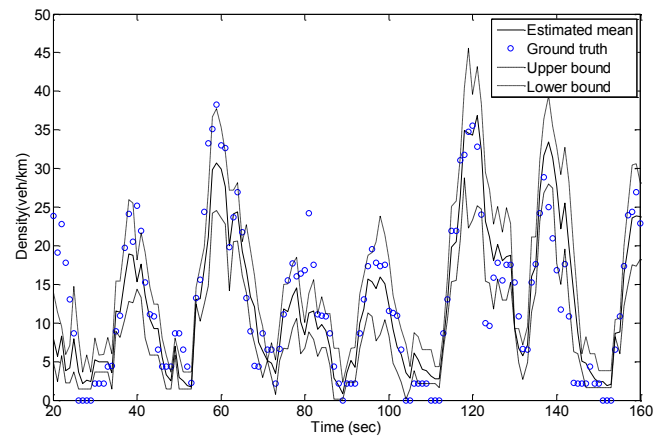
(a) and (b) Queue of C2, 400 to 415 NB; (c) and (d) Queue of C1, 1245 to 100 NB; (e) and (f) Queue of C3, 400 to 415 SB

Scenario A1 (using detector information)

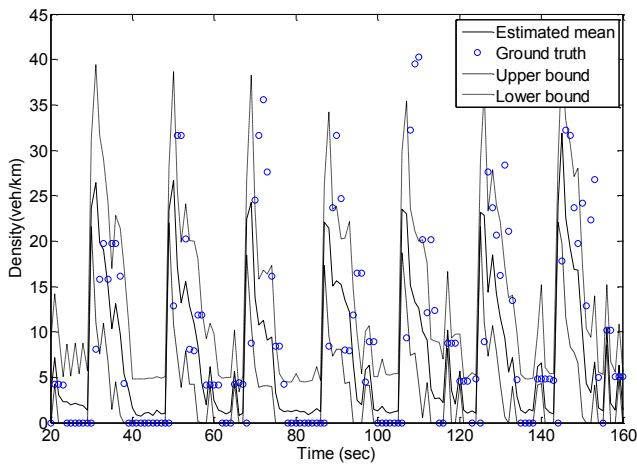
Scenario A2 (using probe information)



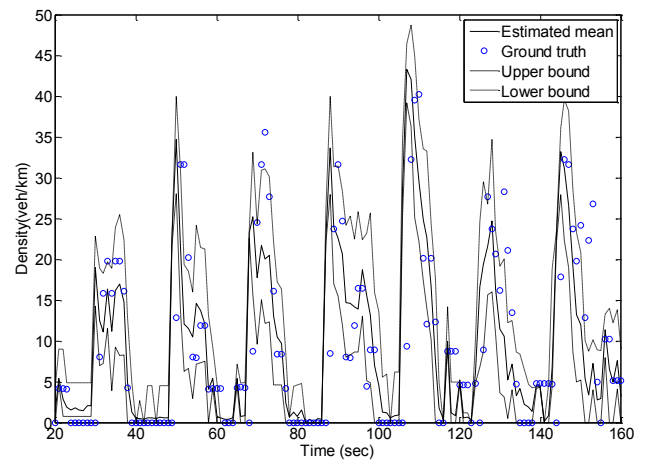
(a) MAPEB= 5.46%



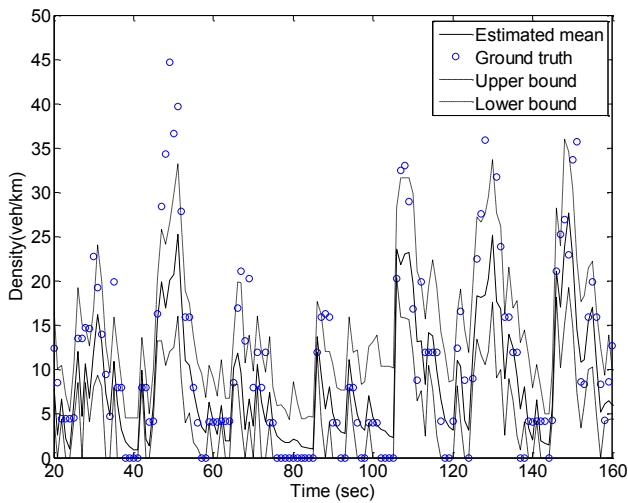
(b) MAPEB= 7.25



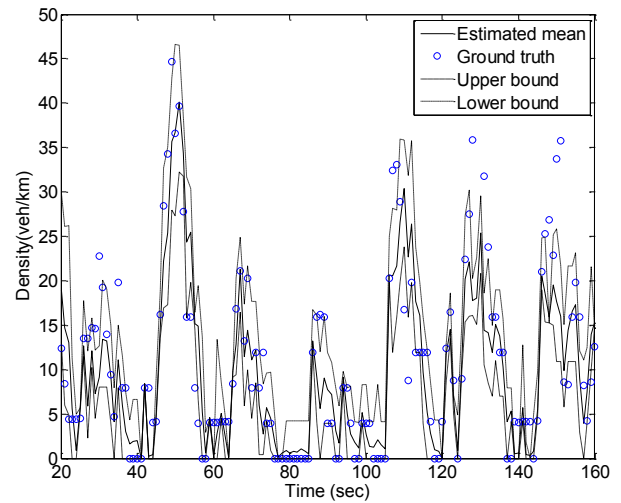
(c) MAPEB=11.3%



(d) MAPEB=9.98



(e) MAPEB=6.52%

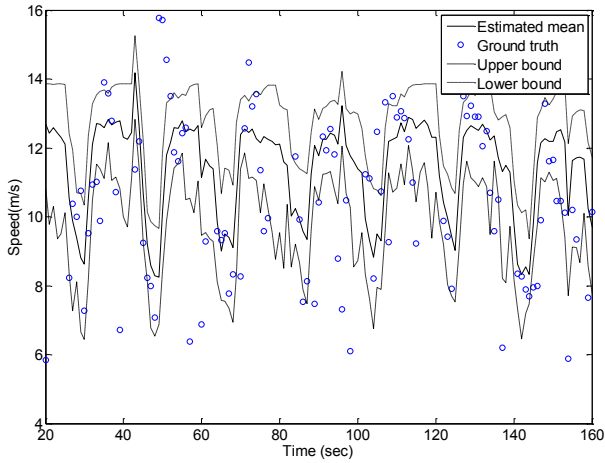


(f) MAPEB=10.8%

Figure 21 Estimated and ground truth density plot of selected cells in NGSIM dataset

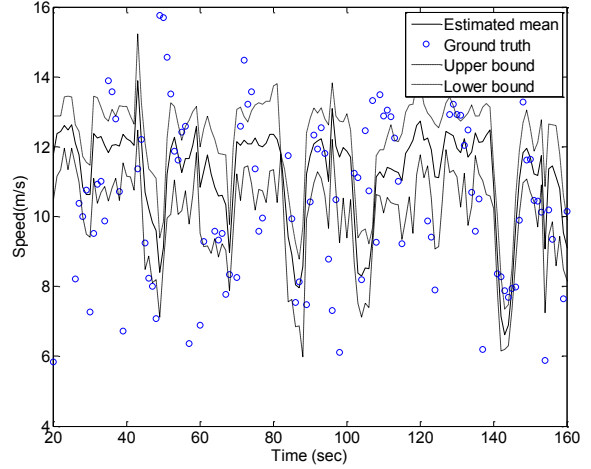
(a) and (b) Density of C1, 400 to 415 SB; (c) and (d) Density of C3, 1245 to 100 SB; (e) and (f) Density of C1, 400 to 415 NB

Scenario A1 (using detector information)

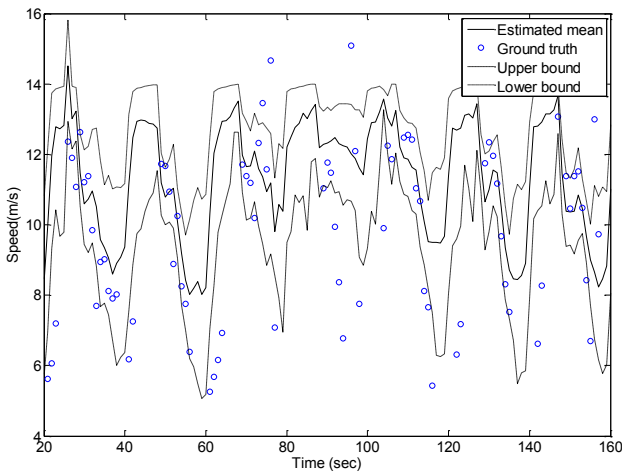


(a) MAPEB= 5.0% A1

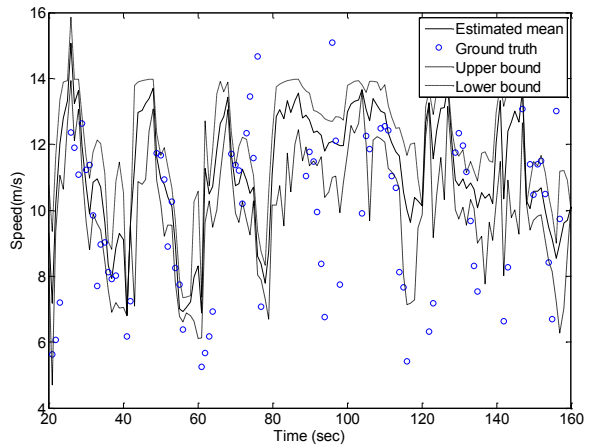
Scenario A2 (using probe information)



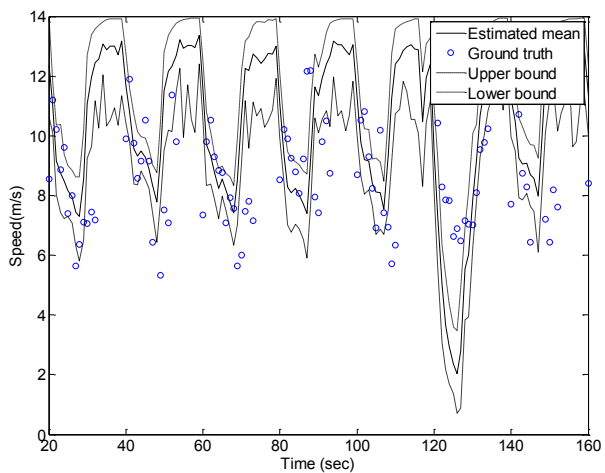
(b) MAPEB= 6.4%



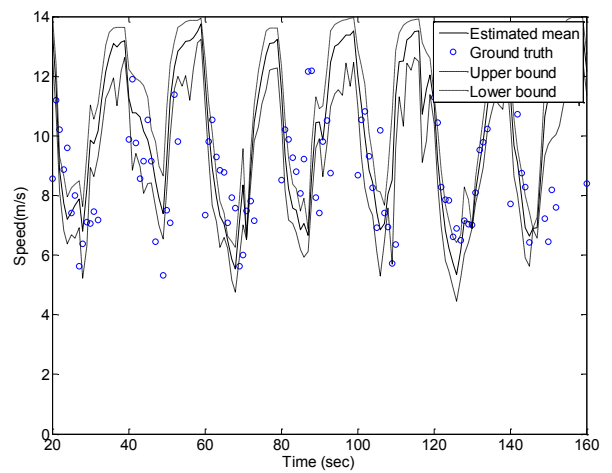
(c) MAPEB=4.5%



(d) MAPEB=6.3%



(e) MAPEB=7.6



(f) MAPEB=6.7%

Figure 22 Estimated and ground truth speed plot of selected cells in NGSIM dataset

(a) and (b) speed of C2, 1245 to 100 SB; (c) and (d) Speed of C2, 400 to 415 NB; (e) and (f) speed of C2, 400 to 415 SB

#### *7.4. Validation of traffic state prediction*

This section examines the accuracy of prediction results offered by the proposed model. There are two important aspects of model performance we want to investigate through this section: 1) the overall prediction accuracy of different type of traffic state (queue length, density, speed and travel time) based on the proposed prediction method; 2) the change of prediction accuracy w.r.t. prediction range. The prediction range is usually measured by the number of time steps over which the traffic state variables are predicted. It is one of the most important measurements of effectiveness of a particular prediction model because longer prediction range implies obtaining the future information in a more advanced manner. In this part of the study, the MAEB and MAPEB indices are computed from 1 to 30 time step prediction. Since each time step represents a duration of 5 seconds in this numerical study, 30 time steps prediction represents a two and half minutes ahead prediction of traffic flow conditions.

The measurement criteria of the prediction accuracy are slightly different from that of the estimation since the variance (uncertainty) of predicted values always becomes larger as the prediction range increases. Therefore fixed error tolerance boundaries are employed when evaluating the quality of the model outputs. The error tolerance value depends on the type of the traffic flow variable to be predicted, in this study, the error tolerance of queue, density, speed and travel time are selected as 10 (meters), 10 (veh/km), 2.5 (m/s) and 10 (seconds) respectively.

Tables 7 and 8 presented the summary of prediction error of travel time and Tables 9 and 10 summarized the prediction error of queue, density and speed. The contents of tables

are organized vertically based on individual cells and horizontally according to different prediction time steps.

Table 7 Summary of travel time prediction MAEB of different time periods in NGSIM dataset

	<i>Direction and time-period</i>	<i>1-5</i>	<i>5-10</i>	<i>10-15</i>	<i>15-20</i>	<i>20-25</i>	<i>25-30</i>
Travel time (sec.)	1245 to 100 Northbound	5.53	5.71	5.75	5.18	5.15	5.25
	1245 to 100 Southbound	5.86	6.57	5.57	5.25	5.43	5.34
	400 to 415 Northbound	3.67	3.85	4.56	4.76	4.76	4.51
	415 to 430 Southbound	7.48	7.11	6.08	5.60	5.98	5.55
	Average	5.63	5.81	5.49	5.20	5.33	5.16

Table 8 Summary of travel time prediction MAPEB of different time periods in NGSIM dataset

	<i>Direction and time-period</i>	<i>1-5</i>	<i>5-10</i>	<i>10-15</i>	<i>15-20</i>	<i>20-25</i>	<i>25-30</i>
Travel time	1245 to 100 Northbound	5.7%	5.9%	6.0%	5.4%	5.3%	5.4%
	1245 to 100 Southbound	8.1%	9.1%	7.7%	7.2%	7.5%	7.4%
	400 to 415 Northbound	3.5%	3.6%	4.3%	4.5%	4.5%	4.3%
	415 to 430 Southbound	7.1%	6.7%	5.8%	5.3%	5.7%	5.3%
	Average	6.1%	6.3%	5.9%	5.6%	5.7%	5.6%

Table 9 Summary of average prediction MAEB of different cells and time periods in NGSIM dataset

<i>MAEB of Prediction</i>									
Traffic State Variable	Direction	Cell	Prediction Time Step (One step = 5 seconds)						
			1-5	5-10	10-15	15-20	20-25	25-30	
Queue Length (m)	1245 to 100 Northbound	Cell 1	2.40	3.43	1.99	2.64	4.04	3.12	
		Cell 2	0.78	1.10	0.80	0.41	0.86	0.93	
		Cell 3	5.44	4.59	3.09	4.42	5.16	4.03	
	1245 to 100 Southbound	Cell 4	0.17	0.12	0.16	0.35	0.24	0.13	
		Cell 5	1.07	1.13	1.02	1.14	1.27	0.53	
		Cell 6	1.38	2.76	2.17	1.20	2.16	2.76	
	415 to 430 Northbound	Cell 1	1.66	1.54	0.86	1.94	2.08	1.11	
		Cell 2	2.71	3.69	3.03	1.20	2.80	3.17	
		Cell 3	6.70	7.68	4.66	4.13	7.04	7.24	
		Cell 4	1.66	1.54	0.95	1.03	1.83	1.26	
		415 to 430 Southbound	Cell 5	4.04	4.07	2.31	0.91	3.80	3.62
			Cell 6	4.70	8.53	6.93	2.88	4.53	8.39
Density (veh/km)	1245 to 100 Northbound	Cell 1	1.88	2.15	1.80	2.32	2.58	2.30	
		Cell 2	3.24	4.23	3.02	1.94	4.00	4.28	
		Cell 3	1.86	1.32	1.14	0.90	1.04	0.87	
	1245 to 100 Southbound	Cell 4	0.13	0.32	0.47	0.33	0.27	0.44	
		Cell 5	2.34	2.05	2.40	2.69	2.72	2.64	
		Cell 6	2.63	3.71	3.17	1.32	2.82	3.68	
	415 to 430 Northbound	Cell 1	1.19	1.55	1.64	1.54	1.80	1.94	
		Cell 2	2.16	3.19	3.12	1.34	2.26	3.04	
		Cell 3	1.32	0.74	1.39	0.52	1.18	0.62	
	415 to 430 Southbound	Cell 4	1.07	1.26	1.55	2.17	2.16	1.74	
		Cell 5	5.47	0.01	0.01	2.79	3.07	3.68	
		Cell 6	5.57	0.01	0.01	2.96	3.77	5.31	
Speed (m/s)	1245 to 100 Northbound	Cell 1	0.39	0.57	0.80	0.47	0.39	0.57	
		Cell 2	0.36	0.48	0.35	0.49	0.37	0.52	
		Cell 3	0.54	0.60	0.57	0.36	0.47	0.59	
	1245 to 100 Southbound	Cell 4	1.14	1.19	1.13	0.99	1.00	1.07	
		Cell 5	0.61	0.76	1.16	0.77	0.60	0.72	
		Cell 6	0.33	0.31	0.36	0.28	0.20	0.17	
	415 to 430 Northbound	Cell 1	0.74	0.77	0.74	0.60	0.70	0.75	
		Cell 2	0.57	0.80	0.63	0.40	0.52	0.71	
		Cell 3	0.93	0.63	0.73	0.87	0.88	0.57	
	415 to 430 Southbound	Cell 4	0.89	0.89	0.82	0.74	0.80	0.76	
		Cell 5	0.99	1.13	0.75	0.37	0.84	0.93	
		Cell 6	0.57	0.41	0.47	0.31	0.43	0.33	

Table 10 Summary of average prediction MAPEB of different cells and time periods in NGSIM dataset

<i>MAPEB of Prediction</i>										
Traffic State Variable	Direction	Cell	Prediction Time Step (One step = 5 seconds)							
			1-5	5-10	10-15	15-20	20-25	25-30		
Queue Length (m)	1245 to 100 Northbound	Cell 1	23.9%	34.1%	19.7%	26.2%	40.2%	31.0%		
		Cell 2	7.3%	10.3%	7.5%	3.8%	8.0%	8.7%		
		Cell 3	40.7%	34.3%	23.1%	33.0%	38.6%	30.1%		
		Cell 4	3.4%	2.3%	3.1%	6.8%	4.6%	2.5%		
		1245 to 100 Southbound	Cell 5	18.1%	19.2%	17.3%	19.3%	21.6%	9.1%	
			Cell 6	11.7%	23.3%	18.3%	10.1%	18.3%	23.3%	
	415 to 430 Northbound	Cell 1	20.3%	18.8%	10.5%	23.7%	25.4%	13.6%		
		Cell 2	16.1%	21.9%	18.0%	7.2%	16.7%	18.9%		
		Cell 3	40.0%	45.8%	27.8%	24.6%	42.0%	43.2%		
		Cell 4	18.6%	17.2%	10.7%	11.5%	20.5%	14.2%		
		415 to 430 Southbound	Cell 5	21.7%	21.9%	12.5%	4.9%	20.5%	19.5%	
			Cell 6	24.0%	43.5%	35.4%	14.7%	23.1%	42.8%	
	Density (veh/km)	1245 to 100 Northbound	Cell 1	11.4%	13.1%	10.9%	14.1%	15.7%	13.9%	
			Cell 2	18.7%	24.4%	17.4%	11.2%	23.1%	24.7%	
			Cell 3	18.6%	13.1%	11.4%	9.0%	10.4%	8.6%	
			Cell 4	1.6%	3.9%	5.7%	4.0%	3.2%	5.3%	
			1245 to 100 Southbound	Cell 5	20.5%	18.0%	21.0%	23.6%	23.9%	23.2%
				Cell 6	19.2%	27.2%	23.2%	9.6%	20.6%	26.9%
415 to 430 Northbound		Cell 1	8.7%	11.3%	12.0%	11.3%	13.2%	14.2%		
		Cell 2	12.9%	19.1%	18.6%	8.0%	13.5%	18.2%		
		Cell 3	12.6%	7.0%	13.3%	5.0%	11.3%	5.9%		
		Cell 4	8.0%	9.4%	11.6%	16.3%	16.2%	13.0%		
		415 to 430 Southbound	Cell 5	29.1%	27.5%	27.1%	14.8%	16.3%	19.5%	
			Cell 6	29.7%	33.9%	34.8%	15.8%	20.1%	28.3%	
Speed (m/s)		1245 to 100 Northbound	Cell 1	4.3%	6.2%	8.7%	5.2%	4.2%	6.3%	
			Cell 2	3.4%	4.6%	3.3%	4.7%	3.5%	4.9%	
			Cell 3	5.6%	6.3%	6.0%	3.7%	4.9%	6.2%	
			Cell 4	11.5%	12.0%	11.4%	10.0%	10.1%	10.8%	
			1245 to 100 Southbound	Cell 5	5.9%	7.4%	11.2%	7.4%	5.8%	6.9%
				Cell 6	3.5%	3.2%	3.8%	2.9%	2.0%	1.8%
	415 to 430 Northbound	Cell 1	8.4%	8.7%	8.4%	6.8%	7.9%	8.5%		
		Cell 2	5.8%	8.2%	6.4%	4.1%	5.3%	7.2%		
		Cell 3	10.4%	7.0%	8.1%	9.7%	9.8%	6.4%		
		Cell 4	9.1%	9.2%	8.4%	7.6%	8.3%	7.8%		
		415 to 430 Southbound	Cell 5	11.3%	12.9%	8.5%	4.2%	9.6%	10.6%	
			Cell 6	6.8%	4.9%	5.6%	3.6%	5.1%	3.9%	

In the following set of figures, the change of prediction accuracy of all traffic state variables is plotted. The change of MAPEB versus prediction time step is the best representation of model performance over time. Figure 23 is the predicted MAPEB of travel times over time; Figures 24 and 25 are the predicted MAPEB of queue length over time; Figures 26 and 27 present the predicted MAPEB of density over time; and Figures 28 and 29 present the predicted MAPEB of speed over time.

Figures 23 to 29 are simply the graphic representation of Table 7 ~ 10, therefore readers can refer to the tables for detailed performance statistics.

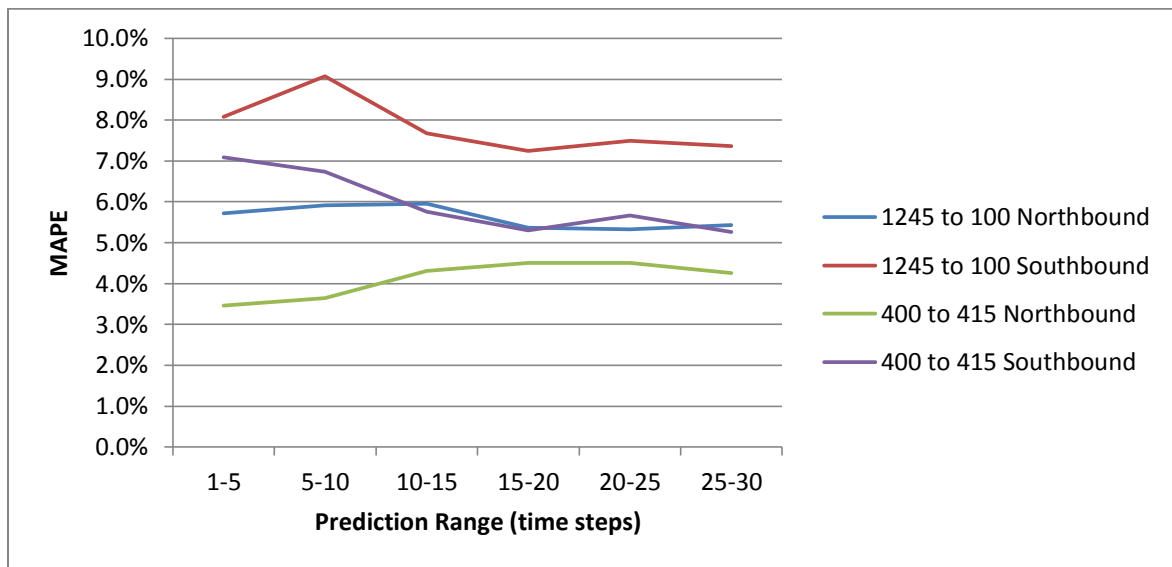


Figure 23 Plots of predicted travel time MAPEB over different prediction range using NGSIM data

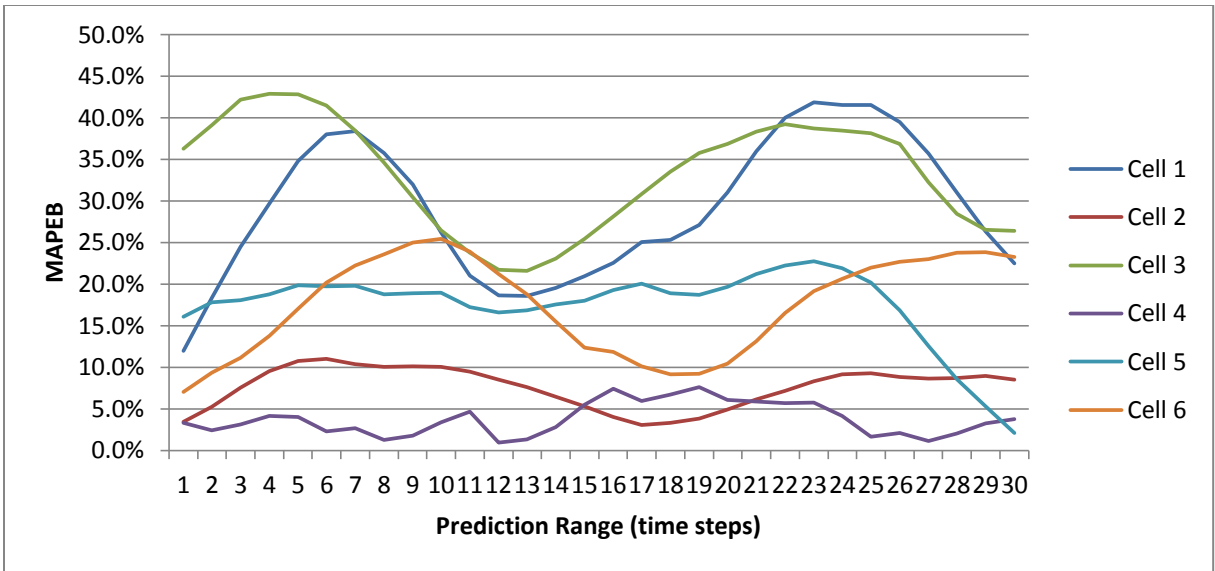


Figure 24 Plots of predicted queue length MAPEB over different prediction range with NGSIM Peachtree data from 12:45 to 1:00

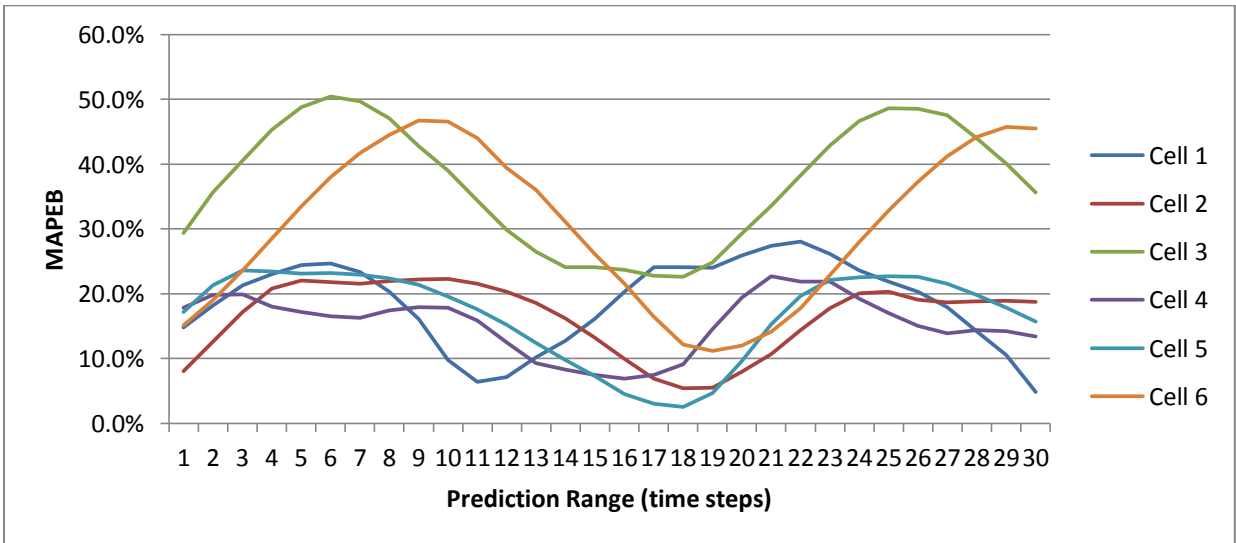


Figure 25 Plots of predicted queue length MAPEB over different prediction range with NGSIM Peachtree data from 4:00 to 4:15

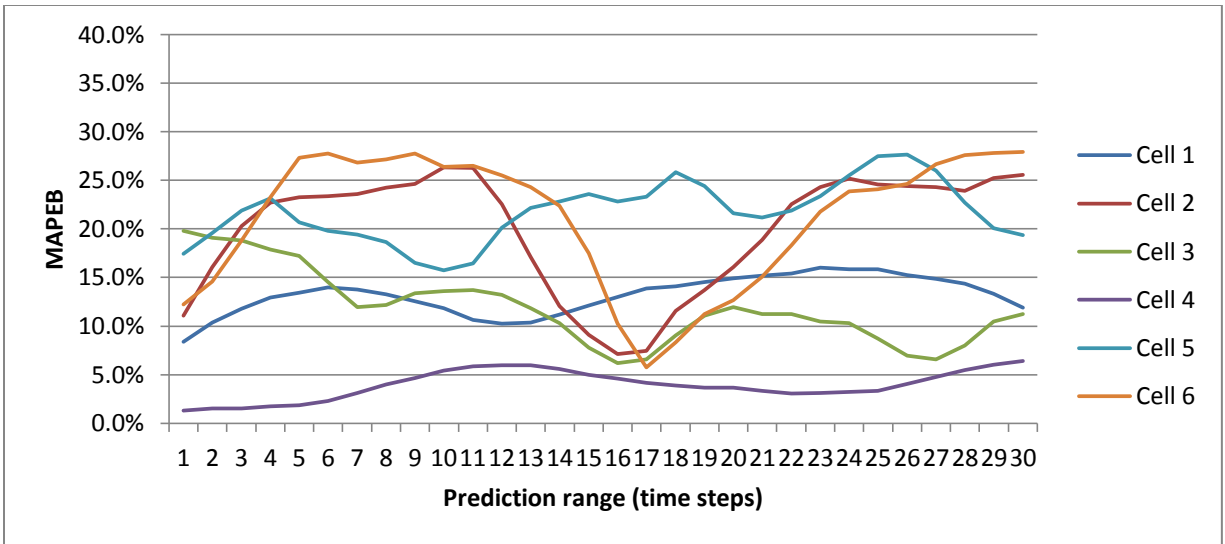


Figure 26 Plots of predicted density MAPEB over different prediction range with NGSIM Peachtree data from 12:45 to 1:00

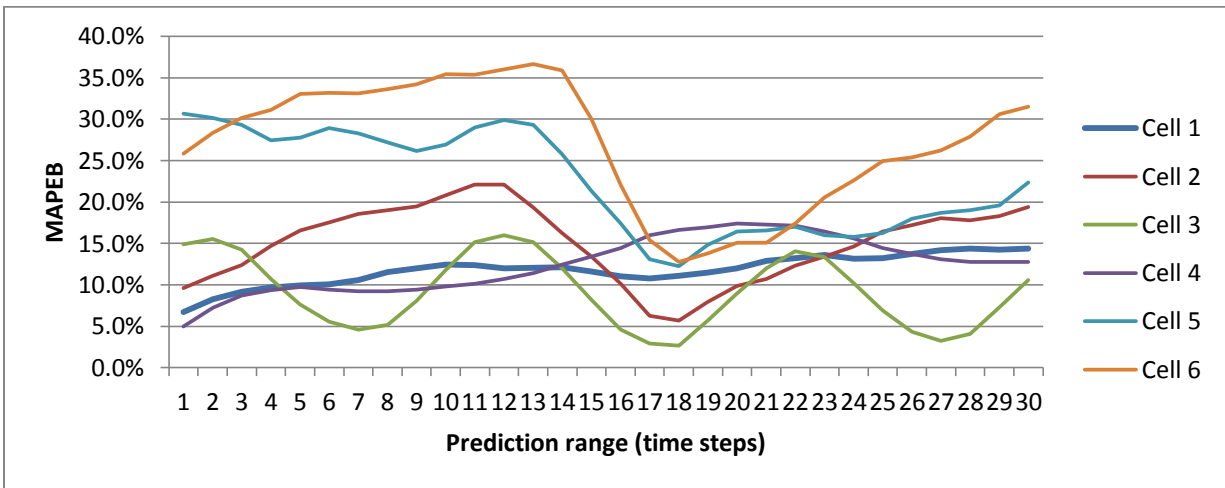


Figure 27 Plots of predicted density MAPEB over different prediction range with NGSIM Peachtree data from 4:00 to 4:15

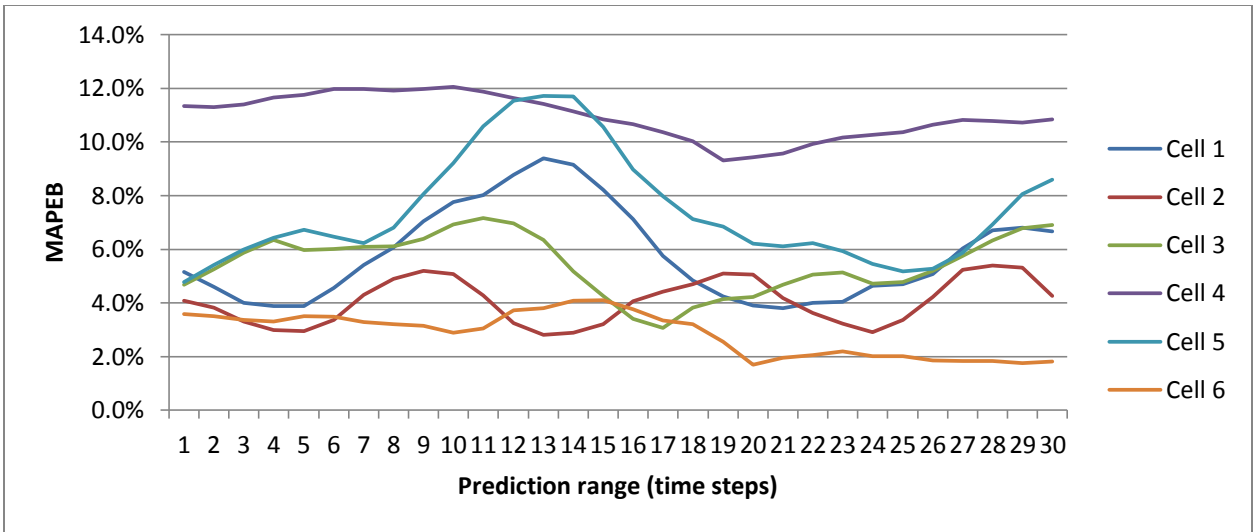


Figure 28 Plots of predicted speed MAPEB over different prediction range with NGSIM Peachtree data from 12:45 to 1:00

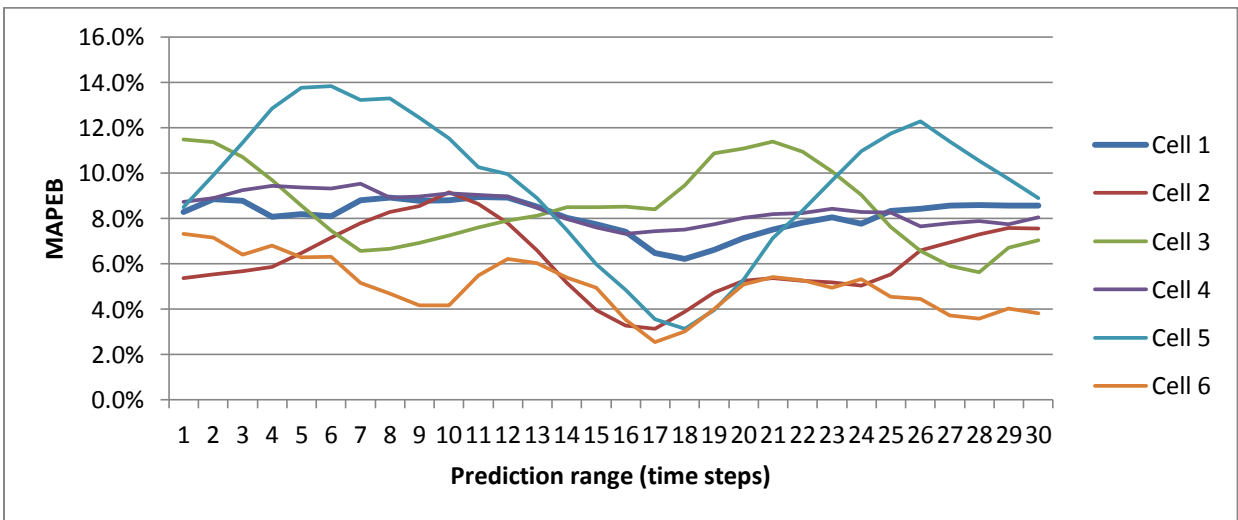


Figure 29 Plots of predicted speed MAPEB over different prediction range with NGSIM Peachtree data from 4:00 to 4:15

There are several conclusions obtainable from above figures and tables which deserve our special attention:

- 1) First of all, the change of MAPE depends on both the type of traffic state and geometric and signal configuration of the arterial link. Generally speaking, the trend of MAPEB curve can be divided into five categories: monotonic increase, stable, monotonic

decrease, periodic and non-periodic. The former three types of change are quite self-explanatory, and the latter two types of trend curve refer to curves without monotonic increase or decrease property and with multiple local peaks and valleys. The periodic curve demonstrates repeated patterns at fixed intervals while in non-periodic curves no periodicity is observed. In prediction problems, one would expect that the accuracy of the prediction decays as the number of time steps increases however here that is not the case based on the observation from Figures 23 to 29. The trend of prediction curves of different traffic flow variables are summarized as follows:

Travel time: stable

Queue length: mostly periodic, some are stable

Density: mostly non-periodic, some are stable

Speed: mostly stable, some are periodic or non-periodic

Therefore, the mean prediction error of the proposed model does not increase w.r.t. the prediction time range. This is a very important property because it implies that the performance of the prediction does not deteriorate quickly as we increase the number of time steps to be predicted. On the other hand, the prediction of queue, density and speed demonstrate different degree of periodicity in their MAPEB plots indicating that the model is very sensitive to the signal timing configurations. Such phenomenon is particular obvious in queue prediction. One reasonable explanation is that since the proposed model relies on traffic flow model in order to perform prediction, the primary error source comes from the discrepancy between the actual traffic flow dynamics and its mathematical approximation. The periodicity of density and speed prediction is much weaker compared with that of queue, however readers can still observe such periodicity on the prediction of some cells.

2) The order of prediction accuracy of different traffic state variable is: travel time > speed > density > queue. However since the statistics of different state variables are computed based on different error tolerance rates, such comparison is not very rigorous and serves only for future reference purpose.

To help readers further understand outputs of prediction model, the prediction curves of selected individual cells are presented together with corresponding ground truth values. Due to the space constraint of the dissertation, only the prediction result of part of the cells is listed here (three cells for each type of traffic state variable). Figures 30 ~ 33 are predicted travel time plots and Figures 34~ 36 are queue prediction plots, Figures 37 ~ 39 are density prediction plots and Figure 40 ~ 42 are speed prediction plots. For a complete list of predicted traffic states, readers can refer to Appendix A.

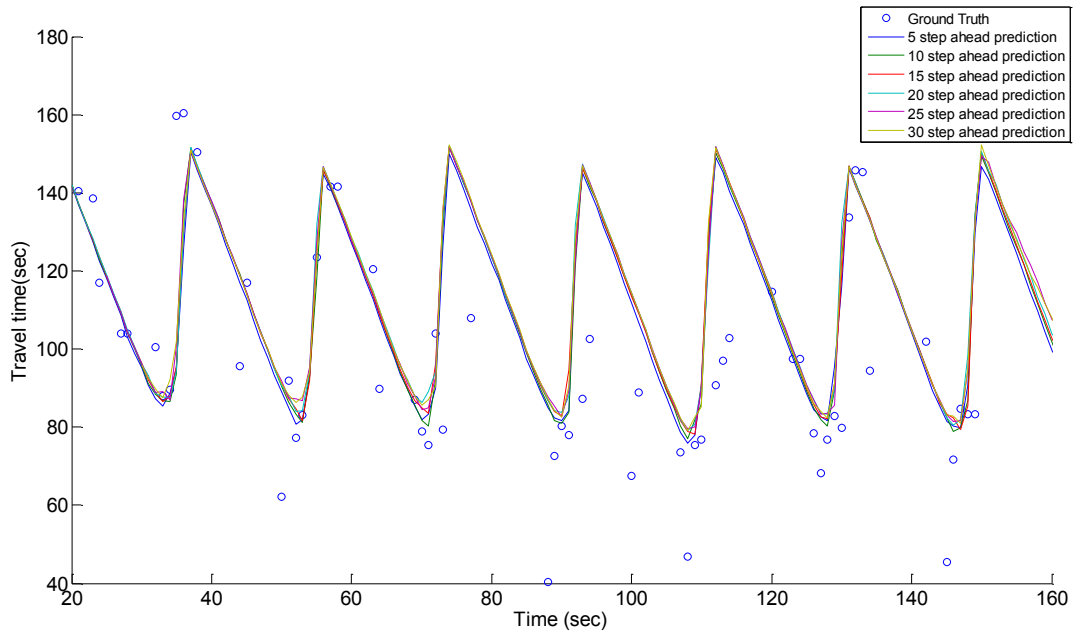


Figure 30 Predicted and ground truth travel time of Peachtree street northbound 12:45 to 1:00

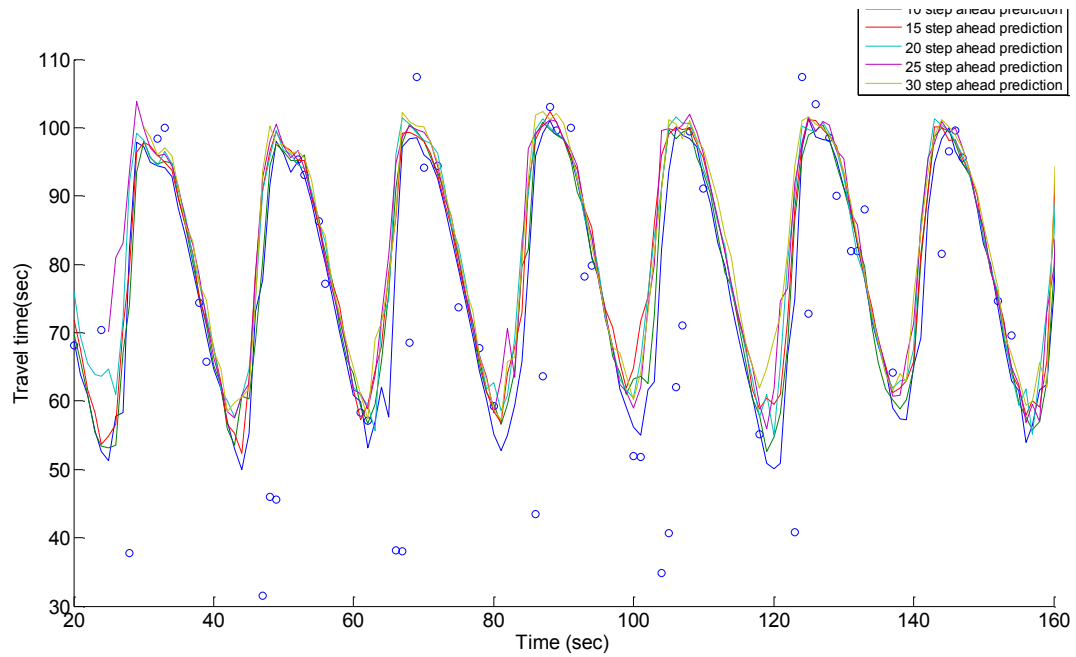


Figure 31 Predicted and ground truth travel time of Peachtree street southbound 12:45 to 1:00

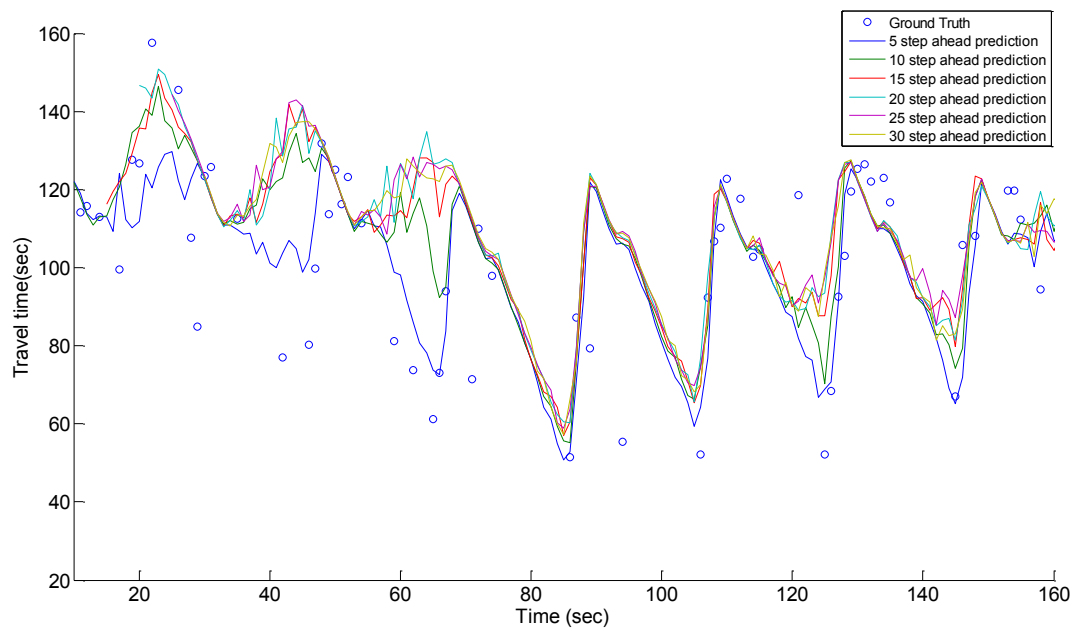


Figure 32 Predicted and ground truth travel time of Peachtree street northbound 4:00 to 4:15

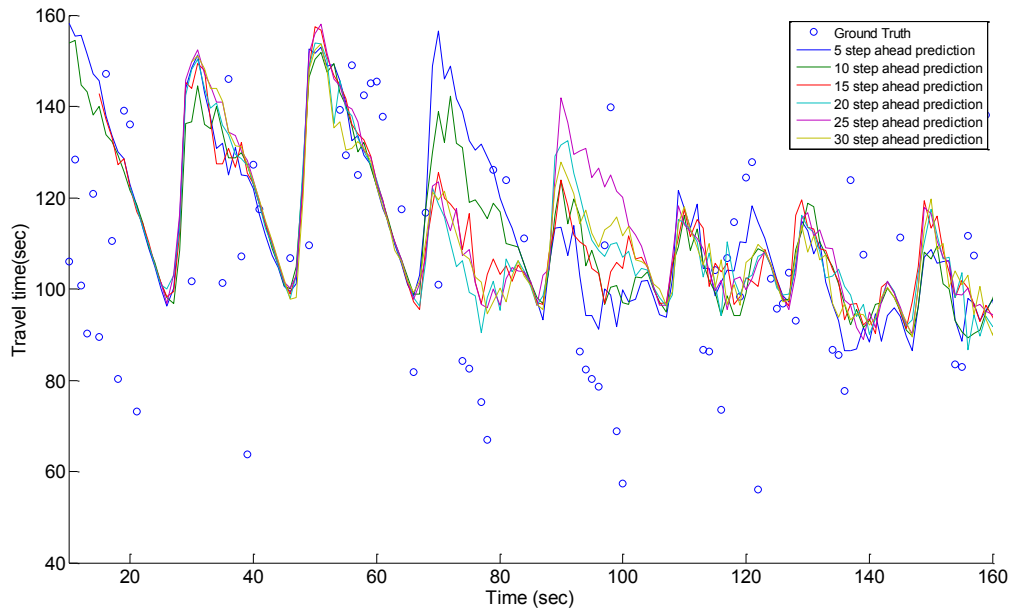


Figure 33 Predicted and ground truth travel time of Peachtree street southbound 4:00 to 4:15

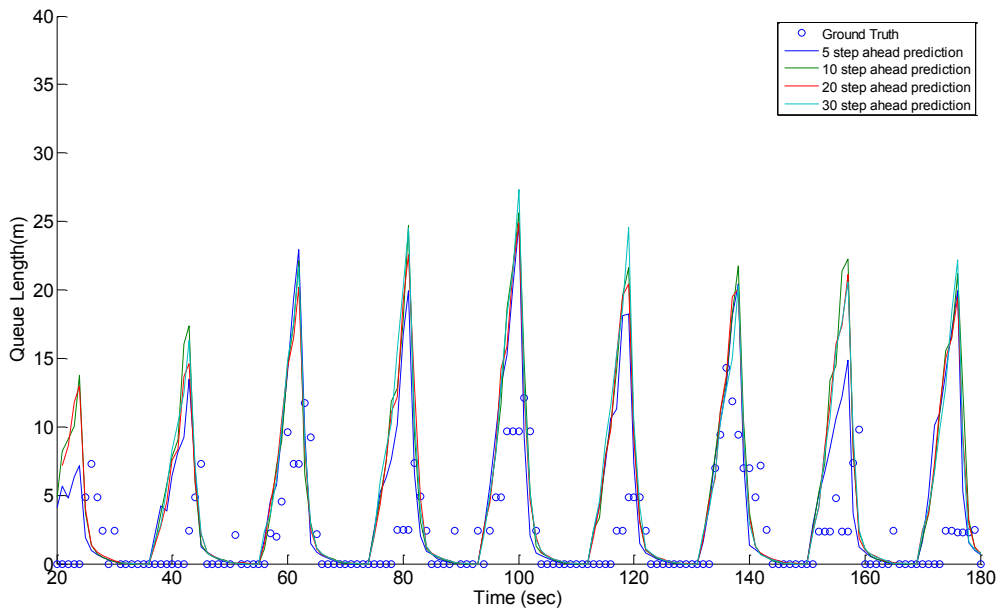


Figure 34 Predicted and ground truth queue of Peachtree street 12:45 to 1:00 cell 1

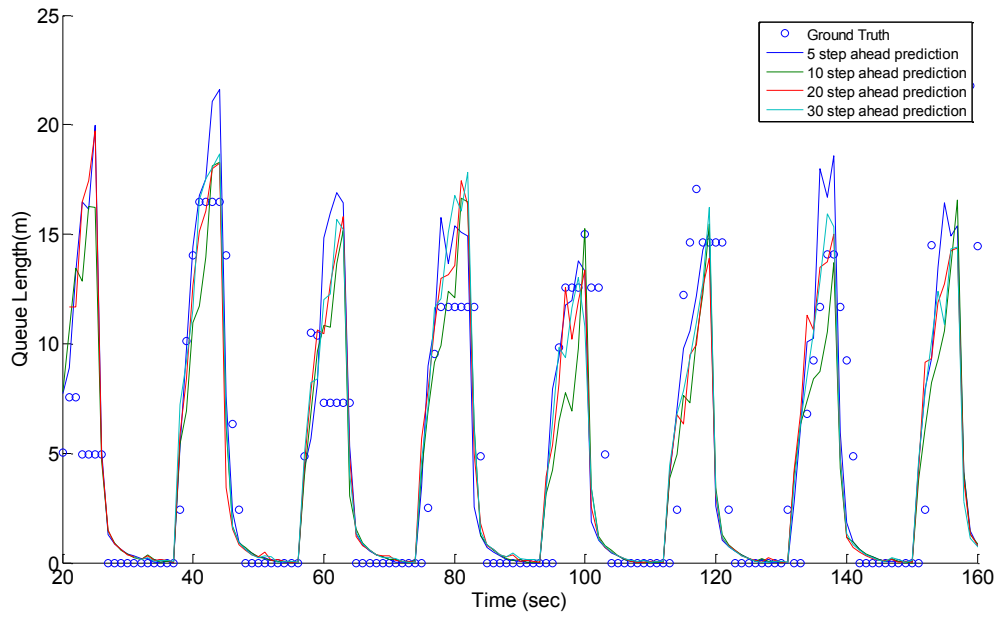


Figure 35 Predicted and ground truth queue of Peachtree street 12:45 to 1:00 cell 5

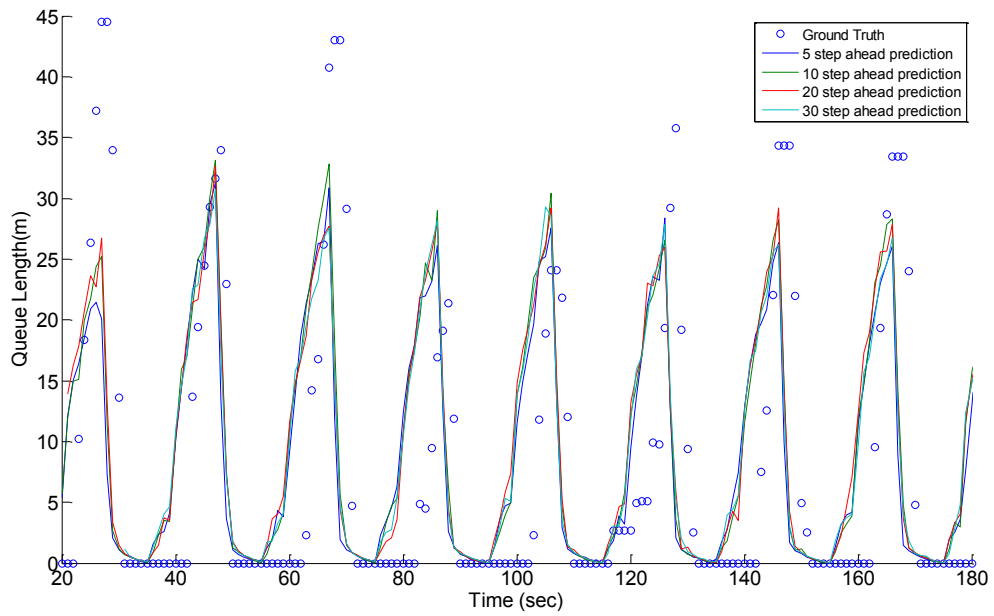


Figure 36 Predicted and ground truth queue of Peachtree street 4:00 to 4:15 cell 5

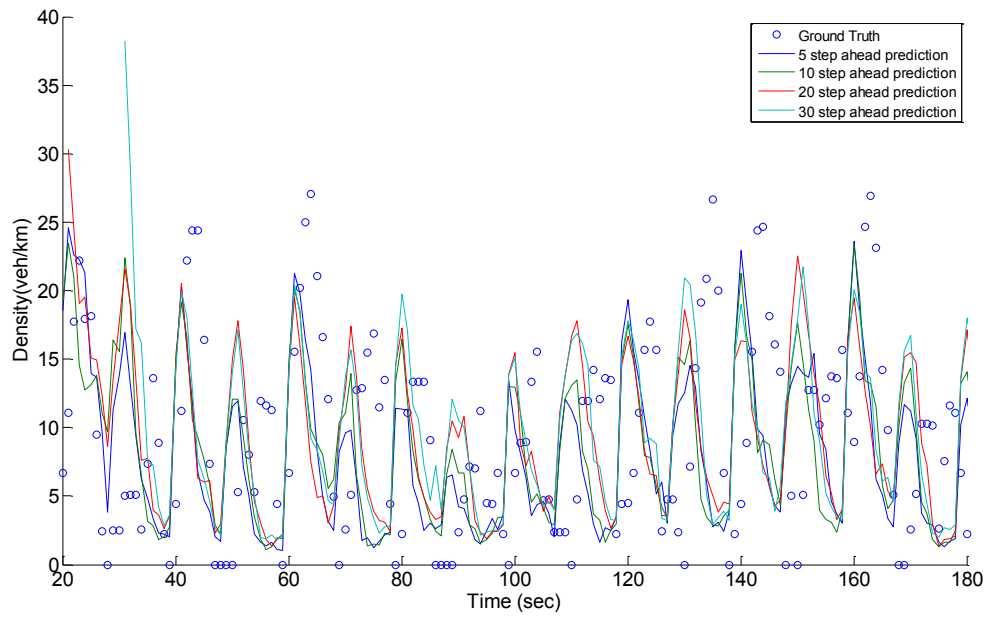


Figure 37 Predicted and ground truth queue of Peachtree street 4:00 to 4:15 cell 6

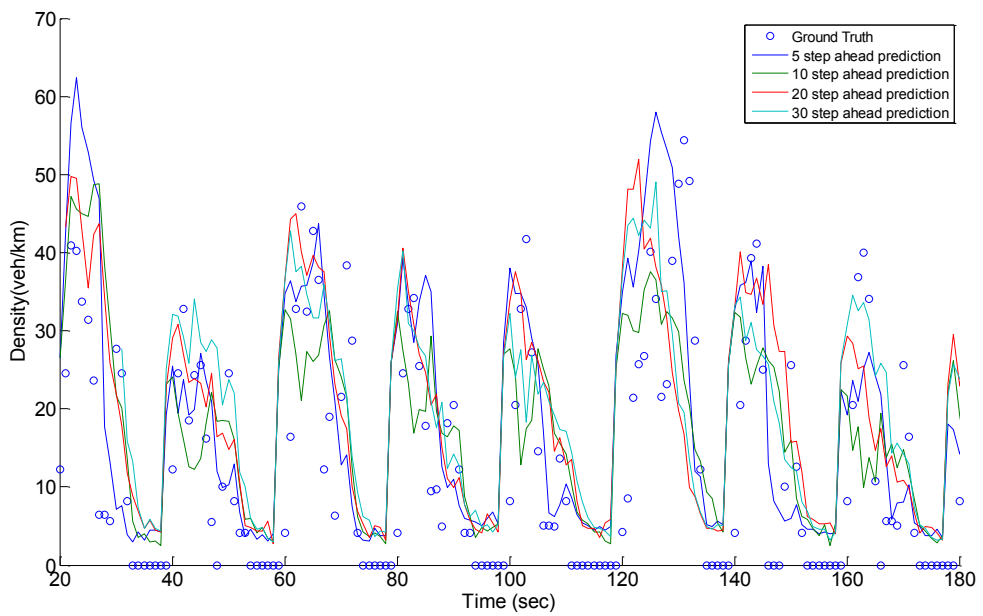


Figure 38 Predicted and ground truth queue of Peachtree street 4:00 to 4:15 cell 5

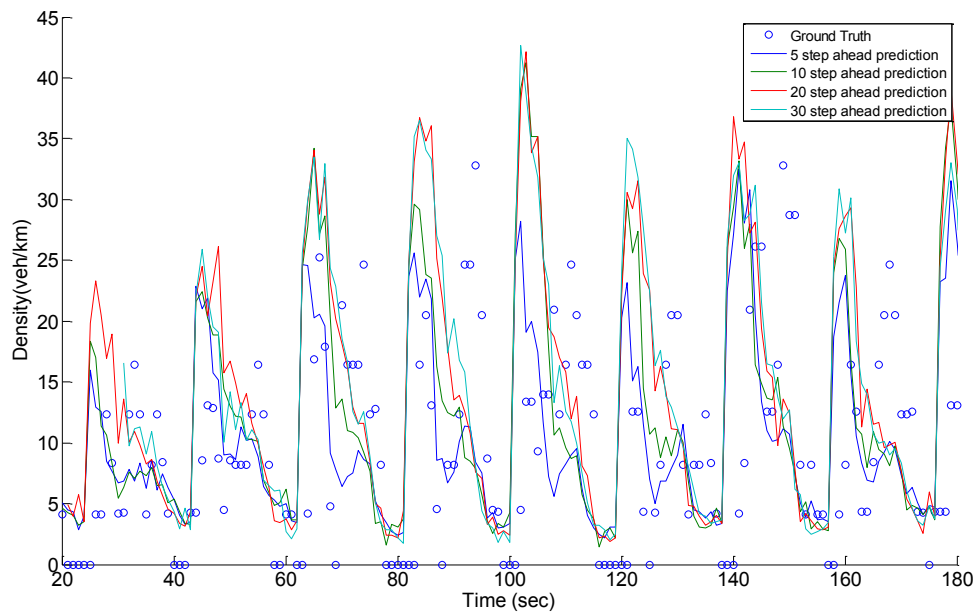


Figure 39 Predicted and ground truth queue of Peachtree street 12:45 to 1:00 cell 2

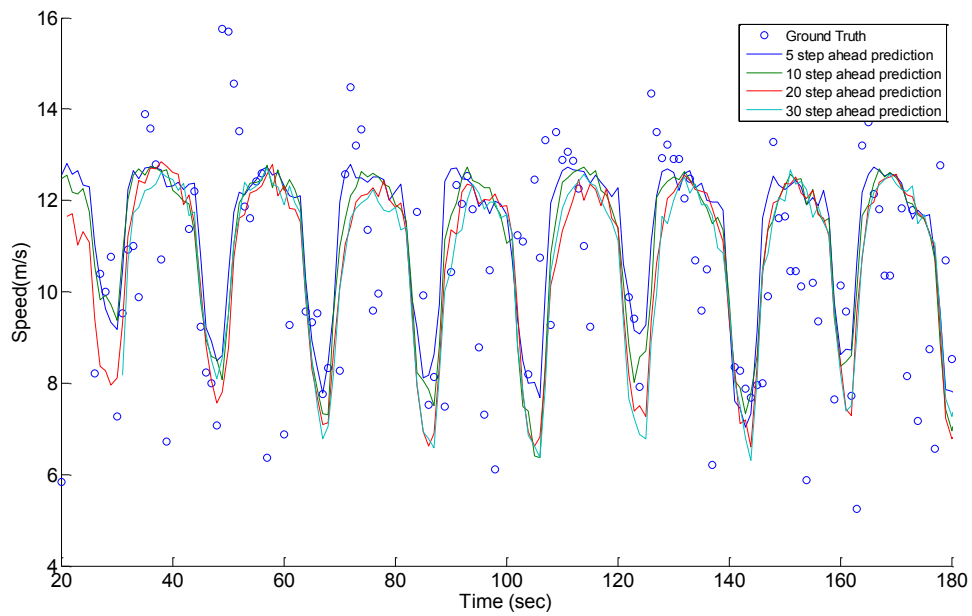


Figure 40 Predicted and ground truth speed of Peachtree street 12:45 to 1:00 cell 2

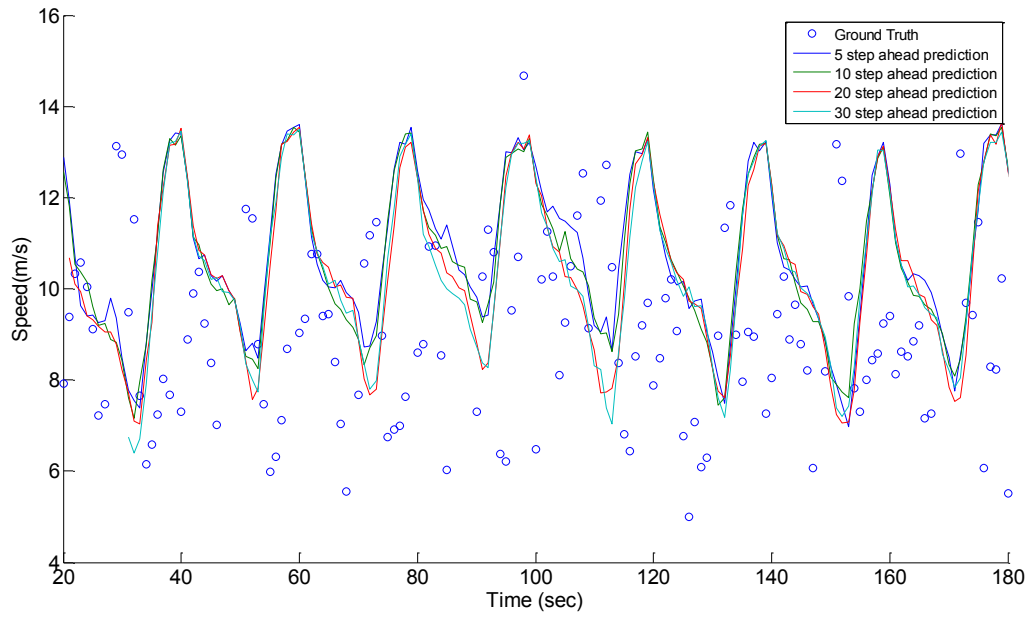


Figure 41 Predicted and ground truth speed of Peachtree street 4:00 to 4:15 cell 3

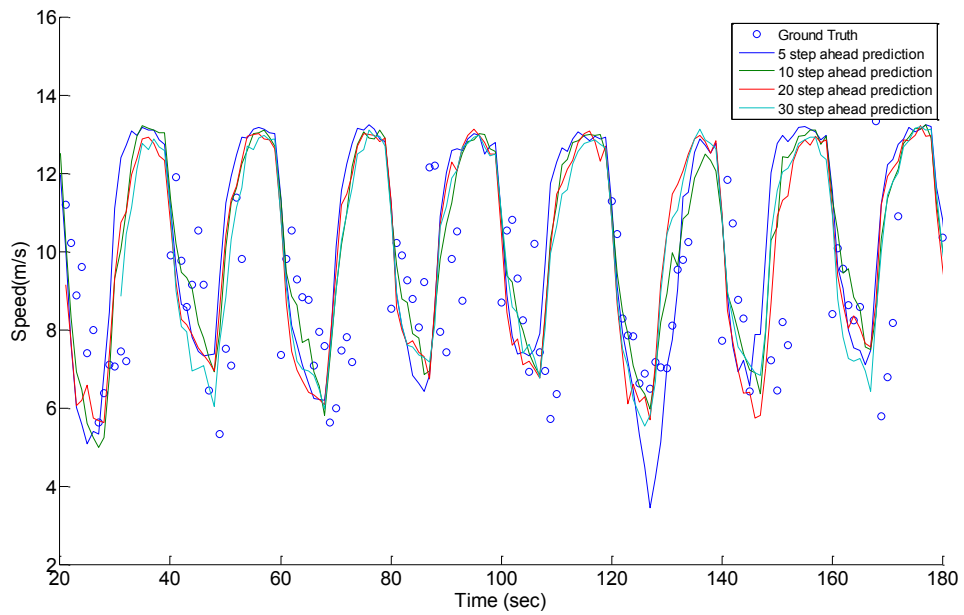


Figure 42 Predicted and ground truth speed of Peachtree street 4:00 to 4:15 cell 5

7.5. Comparison analysis using SMART signal data

In order to vertically compare the result of the proposed model with other state of art methods, the SMART signal data is used for further analysis and comparison purpose. Henry Liu et al. (2009) proposed a real-time queue estimation method based on high resolution signal and detector data. In this section, a comparison study is performed for queue estimation between the proposed model and Liu et al.'s model.

The study site is selected at TH-13 highway between Lynn Ave and Co-Rd 5 in state of Minnesota where the SMART signal system is installed.



Figure 43 The map of study area along TH 13, Minnesota

Figure 44 (a) and (b) presents respectively the detail geometric layout and the corresponding cell network structure applied in this example.

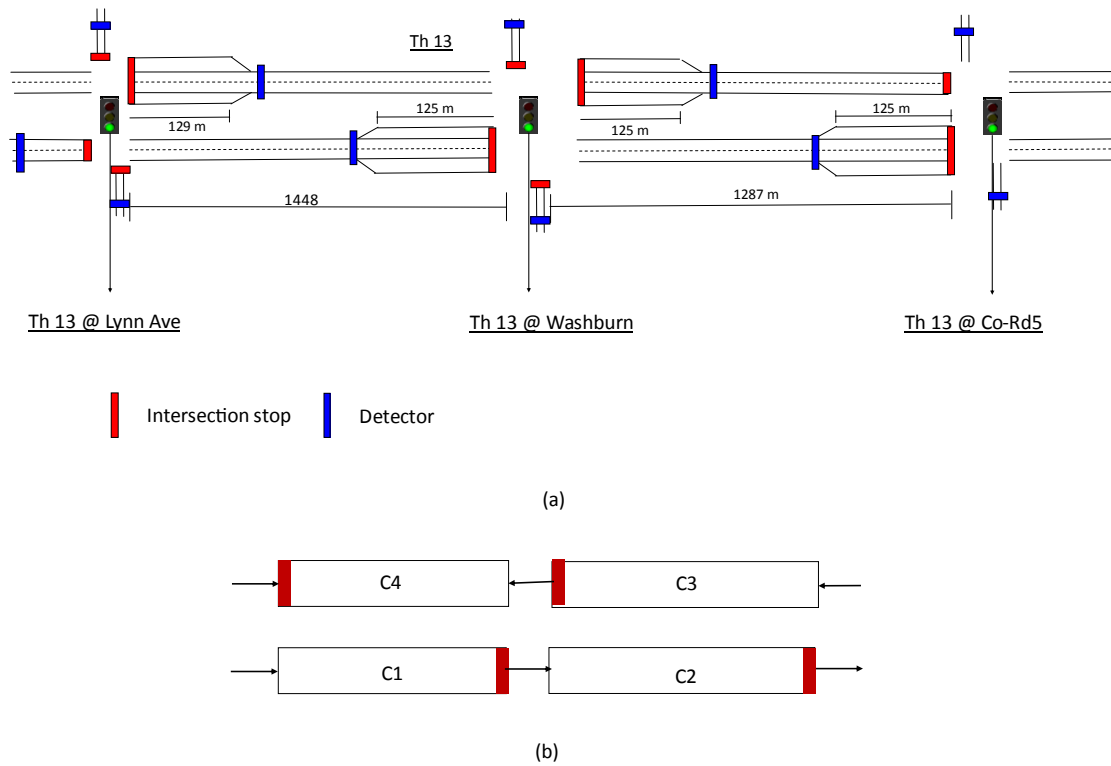


Figure 44 Geometric layout (a) and cell network structure (b) used in comparison study

The queue length along with other traffic flow state of C1 ~ C4 (in Figure 44 (b)) is estimated using the proposed model. Both measured link traffic states and signal data is extracted from the high resolution SMART signal event based dataset. The estimated queue length of Liu et al.'s model is obtained through an active web application of their project. The test time period is selected between 7:00 and 8:00 AM on November 14<sup>th</sup>, 2012. The computation time step is 10 seconds.

Figures 45 ~ 48 demonstrate the estimated queue length from the proposed model and Liu et al.'s model.

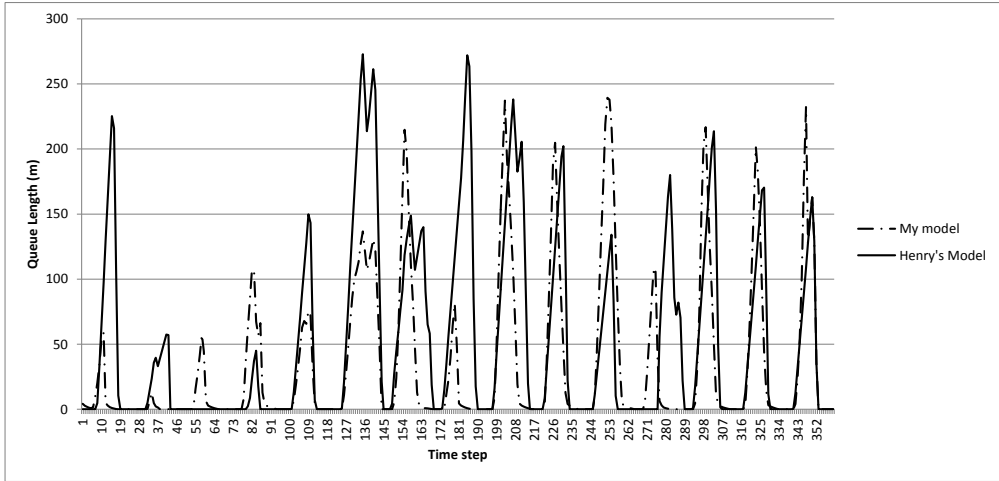


Figure 45 Comparison of estimated queue length of cell 1

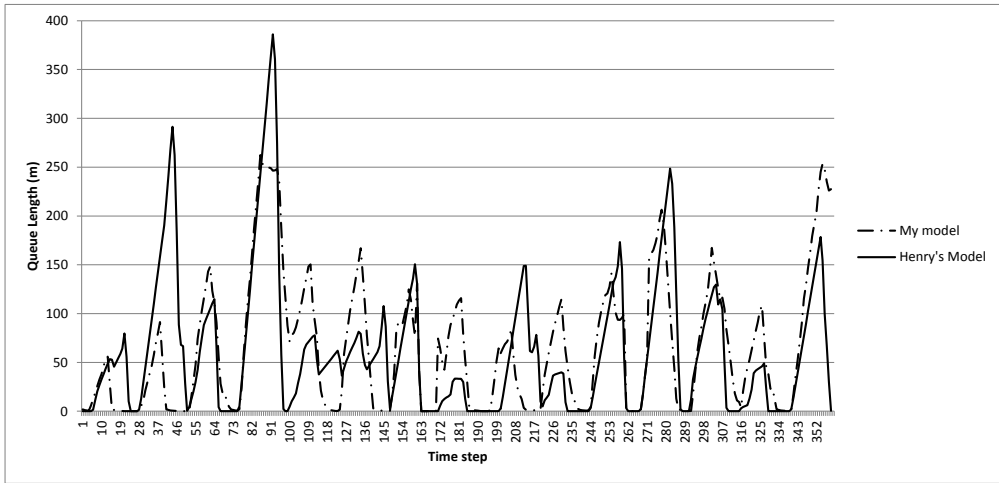


Figure 46 Comparison of estimated queue length of cell 2

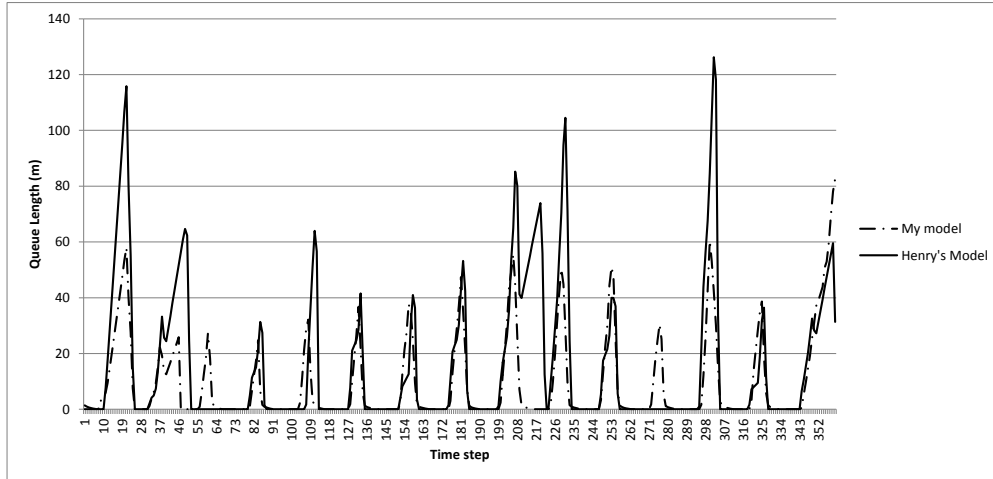


Figure 47 Comparison of estimated queue length of cell 3

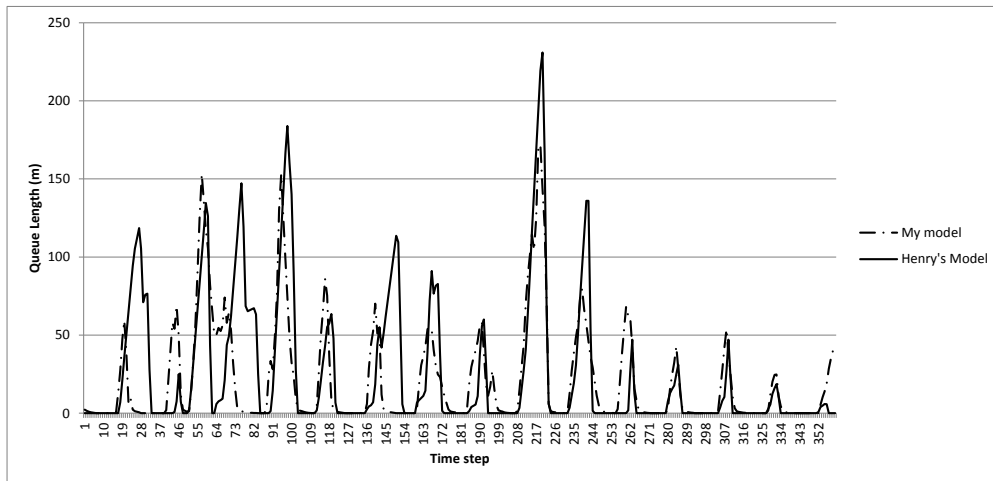


Figure 48 Comparison of estimated queue length of cell 4

As we can observe from above figures, the estimation result from the proposed model coincides with Liu et al.'s model under most situations with slight under estimation. The overall difference between the two models in this example is less than 15%. The maximum queue length is under-estimated sometimes by the proposed model due at least to two reasons:

- 1) First of all, the physical queue length is always larger than the theoretical queue length which is computed as the product between number of queued vehicles and

average queue length due to the propagation of backward shockwave during the beginning period of the green phase.

- 2) The model always assumes that vehicles are evenly distributed among all the lanes. Such assumption may easily be violated in reality.

Developing an extended traffic flow model in order to overcome above issues is left for future work.

### 7.6. *Chapter Summary*

This chapter reported the results of a first round of numerical investigation regarding the proposed shifting boundary cell queue model. The validation is conducted using the high resolution trajectory data contained in NGSIM dataset. Key findings of this chapter are summarized as follows:

- 1) The linear exponential speed-density-queue function is adopted in this numerical study and the parameters of speed function is calibrated using link speed, density and queue data extracted from trajectory data;
- 2) The Peachtree arterial dataset represents light traffic condition with stable traffic flow dynamics, such fact is observed from travel time plots;
- 3) The real-time estimation model is capable of reproducing the arterial corridor traffic flow condition accurately with multiple type of data source including detector and probe vehicle data;
- 4) The change of prediction accuracy over time measured by MAPEB is stable for travel time and changing periodically for queue;

- 5) The change of prediction accuracy of density and speed over time is sometimes periodic but sometimes non-periodic;
- 6) The prediction error of the proposed model is always constrained even if the prediction range increases and no lagging effect is observed from the prediction curves.
- 7) The queue estimation results are also compared against Liu et al.'s model using SMART signal dataset.

In the next chapter, another set of numerical investigation is done to explore the performance of the model under heavy traffic condition where temporary cycle failure and queue spillback may occur.

## 8. Numerical Investigation Part II: Model Validation with Synthetic

### Data

#### 8.1. Network Description

In this chapter, we want to further examine the model's performance under congested traffic conditions. Due to the lack of field data, a simulated traffic flow data on a hypothetical arterial is employed. The simulation was conducted using VISSIM, a well-established microscopic simulation software, on a two-directional arterial road network consisting four signalized intersections. The geometric layout of the arterial network is presented in Figure 49.

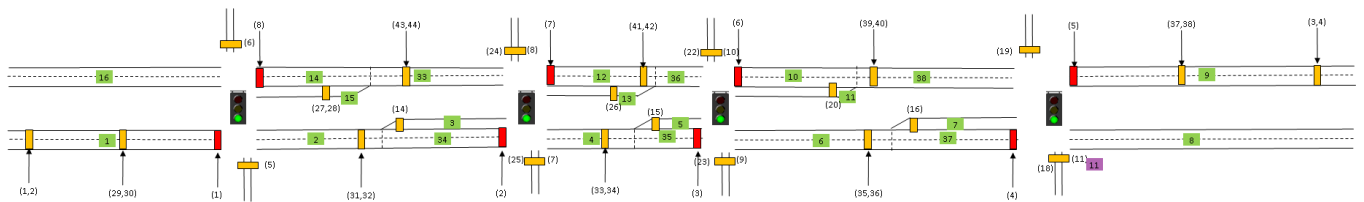


Figure 49 Geometric layout of the hypothetical arterial corridor

The arterial is divided into five links along each direction by signals which give us eight non-sink links. The links are numbered according to their location with regard to the most upstream link, eastbound links are numbered from 1 to 4 and westbound links are numbered from 5 to 8. The link numbers are also presented in Figure 50. The length and number of lane of each link and the size of turning bay associated with each link are summarized in Table 11.

Table 11 Link and turning bay length of the simulation network

Eastbound links				
Number	1	2	3	4
Link length (m)	303	397	196	304
Left-turn bay(m)	N/A	150	95	130
Westbound links				
Number	5	6	7	8
Link length(m)	794	304	196	397
Left-turn bay(m)	N/A	100	110	166

The simulation experiment is designed to replicate the arterial traffic status under time-varying demand volume and temporary over-saturated traffic condition. The performance of proposed traffic flow estimation and prediction model is then tested and validated using the trajectory data extracted from the simulator. Figure 50 presents the location of all demand generation nodes and Tables 12 and 13 summarize the OD ratio table and incoming traffic flow rate of each demand generating node within the simulation period respectively. The simulation time period is one hour and the computation is done every 10 seconds.

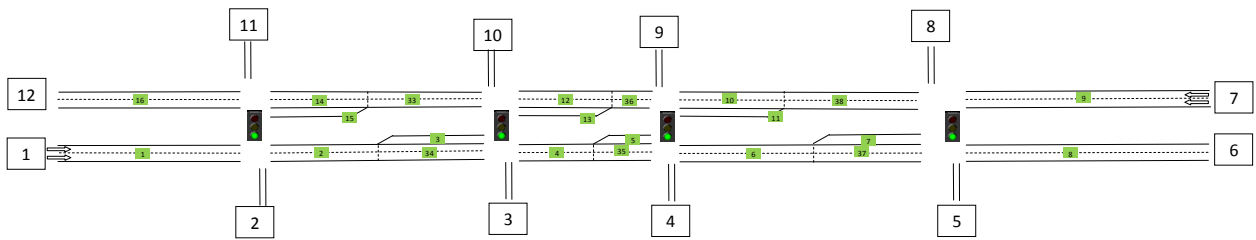


Figure 50 Number of demand generation and sink nodes of the simulation network

Table 12 The demand volume ratio between OD pairs

Origin/Dest	1	2	3	4	5	6	7	8	9	10	11	12
1	0.0%	7.7%	7.7%	7.7%	7.7%	38.5%	0.0%	7.7%	7.7%	7.7%	0.0%	7.7%
2	0.0%	0.0%	14.3%	14.3%	14.3%	14.3%	0.0%	14.3%	14.3%	14.3%	0.0%	0.0%
3	0.0%	16.7%	0.0%	16.7%	16.7%	16.7%	0.0%	0.0%	0.0%	0.0%	16.7%	16.7%
4	0.0%	14.3%	14.3%	0.0%	14.3%	14.3%	0.0%	0.0%	0.0%	14.3%	14.3%	14.3%
5	0.0%	14.3%	14.3%	14.3%	0.0%	0.0%	0.0%	0.0%	14.3%	14.3%	14.3%	14.3%
7	0.0%	15.4%	7.7%	7.7%	7.7%	0.0%	0.0%	7.7%	7.7%	7.7%	7.7%	30.8%
8	0.0%	14.3%	14.3%	14.3%	0.0%	0.0%	0.0%	0.0%	14.3%	14.3%	14.3%	14.3%
9	0.0%	0.0%	0.0%	0.0%	20.0%	0.0%	0.0%	20.0%	0.0%	20.0%	20.0%	20.0%
10	0.0%	0.0%	0.0%	14.3%	14.3%	14.3%	0.0%	14.3%	14.3%	0.0%	14.3%	14.3%
11	0.0%	0.0%	14.3%	14.3%	14.3%	14.3%	0.0%	14.3%	14.3%	14.3%	0.0%	0.0%

Table 13 The total demand volume of different demand generating nodes (veh/hour)

Demand Generation Node/Time Period	0-600	600-1200	1200-1800	1800-2400	2400-3000	3000-3600
1	1000	1400	1800	1800	1400	800
7	1600	1800	2200	1000	1000	1000
2	150	200	250	250	200	150
3	150	200	250	250	200	150
4	150	200	250	250	200	150
5	150	200	250	250	200	150
6	150	200	250	250	200	150
8	150	200	250	250	200	150
9	150	200	250	250	200	150
10	150	200	250	250	200	150

\*Time in seconds and volume in veh/hour

In this simulation example, we try to predict the traffic flow statistics including traffic density, queue and speed together with travel time along each direction of the road. The following figure plots the observed travel time points (captured by VISSIM) during the simulation period, the solid line represents the travel time along eastbound and the dash line represents the travel time along westbound road. As observable from the Figure 51, the travel time demonstrates high variability for both directions. The average free flow travel time under normal traffic condition is around 130 seconds according to the simulation results, however the highest travel time of westbound direction reached 290 seconds

approximately at 1970 seconds time mark due to the congestion; on the other hand, the eastbound traffic also experienced additional delay (but not as high as westbound traffic).

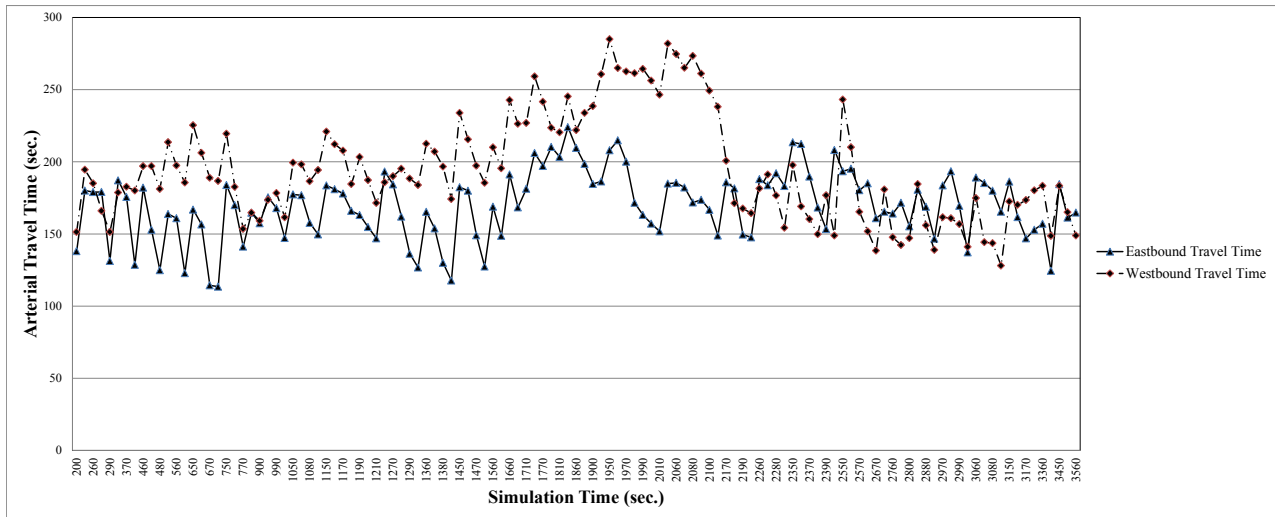


Figure 51 Observed travel time of the corridor obtained from VISSIM

## 8.2. Calibration of speed-density-queue function using simulated data

In order to implement the proposed framework, the fundamental speed-density-queue relationship needs to be calibrated based on simulated data. The speed, density and queue length (queue length ratio) are extracted from the trajectory data collected from the simulator. Figure 52 displays the correlation between density and speed. Figure 53 displays the correlation between queue and speed; and Figure 54 demonstrates the correlation between density, queue and speed in three dimensional scatter plots.

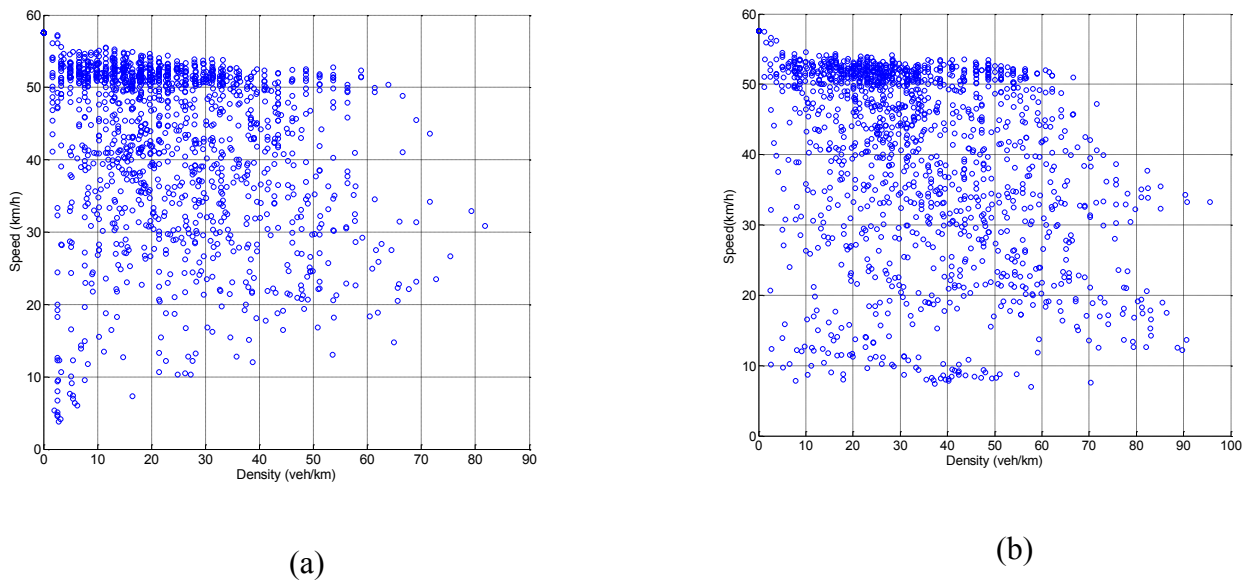


Figure 52 Observed speed and density plot of (a) Eastbound traffic (b) Westbound traffic of the simulated network

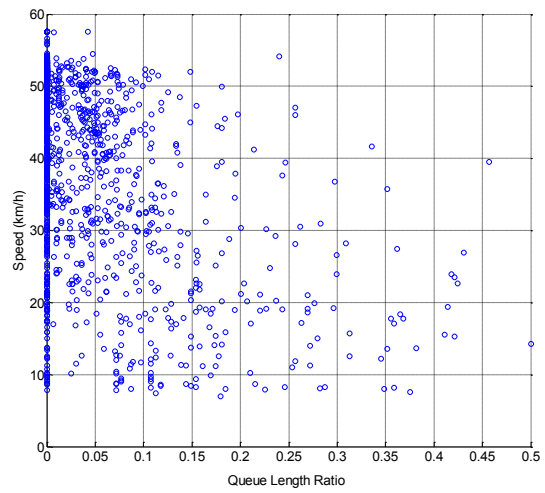
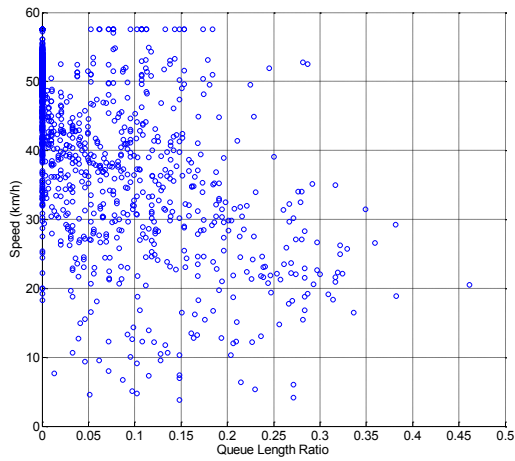


Figure 53 Observed speed and queue ratio plot of (a) Eastbound traffic (b) Westbound traffic of simulated network

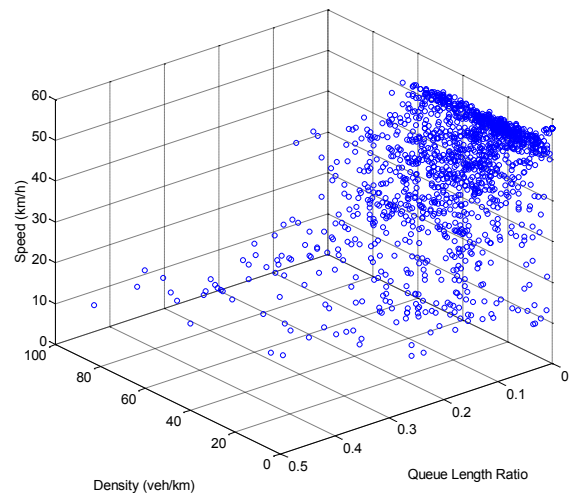
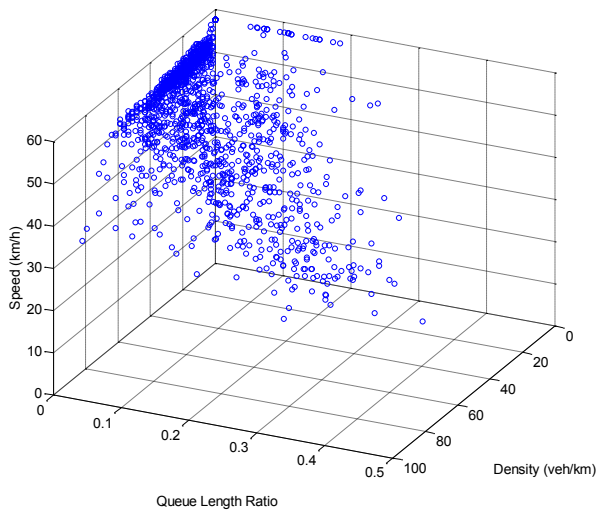


Figure 54 Observed speed, density and queue ratio 3-D plot of (a) Eastbound traffic (b) Westbound traffic of simulated network

According to observed traffic flow data, the following two functional forms are selected as the candidate speed-density-queue function:

$$V(k, q) = v_f \left(1 - \frac{k}{k_m}\right) e^{-\gamma q} \quad (8-1)$$

$$V(k, q) = \sqrt{\left[1 - \left(\frac{k}{k_m}\right)^2\right]} v_f e^{-\gamma q} \quad (8-2)$$

In Equation (8-1) and (8-2),  $V$  is the macroscopic speed-density-queue relationship;  $k$  is the traffic density of the moving area;  $q$  is the queue length ratio of the cell defined as the ratio between physical queue length and the link length; The parameters to be calibrated include free flow speed  $v_f$ , jam density  $k_m$  and speed decay factor  $\gamma$ . The curve fitting is performed using non-linear least square method with trust region algorithm and all the curve fitting process is done with Matlab curve fitting toolbox. Tables 14 and 15 display the results of curve fitting procedure.

Table 14 Summary of speed function fitted results

Speed-Density Queue Function	Direction	R-Square	Adjusted R-Square	RMSE
Linear-Exponential function (Equation 8-1)	Eastbound traffic	0.39	0.389	9.07
	Westbound traffic	0.36	0.359	10.53
	Average	0.375	0.374	9.8
Parabolic-Exponential model (Equation 8-2)	Eastbound traffic	0.403	0.402	8.975
	Westbound traffic	0.359	0.359	10.54
	Average	0.381	0.38	9.75

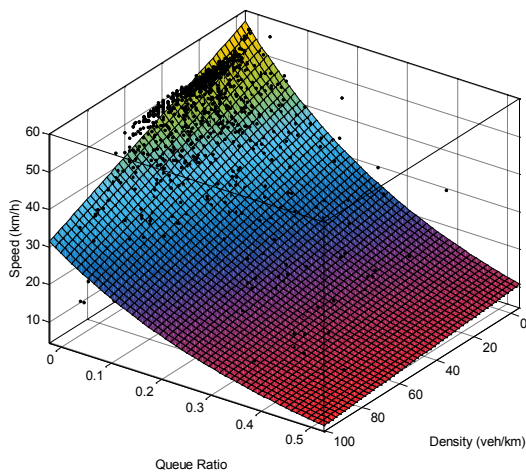
Table 15 Summary of fitted parameter values

Speed-Density Queue Function	Direction	Free flow speed	Jam density	Speed decay factor
Linear-Exponential function (Equation 8-1)	Eastbound traffic	52.36	250 (max)	2.572
	Westbound traffic	51.98	229	3.05
	Average	52.17	239.5	2.811
Parabolic-Exponential model (Equation 8-2)	Eastbound traffic	48.56	160.3	2.674
	Westbound traffic	47.54	111.8	3.118
	Average	48.05	136.05	2.896

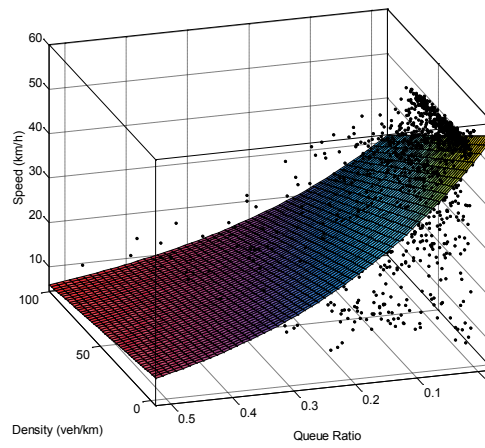
Figure 55 shows the three dimensional plot of fitted curve under different speed function form.

Comparing the R-square of Equation (8-1) and (8-2), we can conclude that the parabolic-exponential speed function slightly over-performs linear-exponential speed function along both directions. Therefore the parabolic exponential speed-density-queue function is selected in this numerical example.

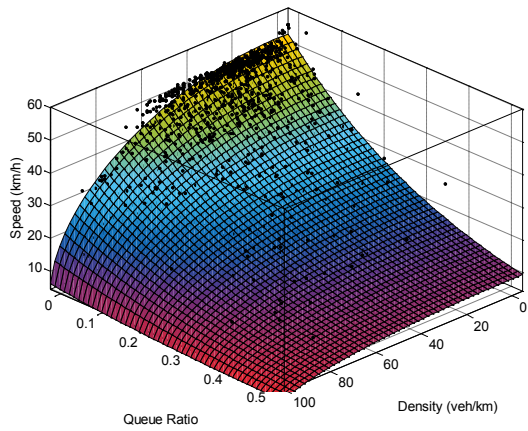
$$V(k, q) = 13.48 \sqrt{\left[1 - \left(\frac{k}{136.05}\right)^2\right]} e^{-2.896q} \quad (8-3)$$



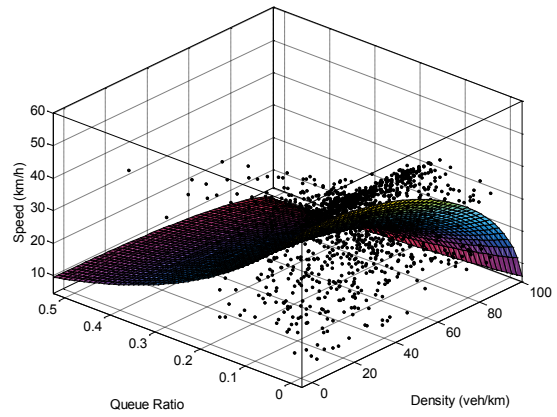
(a)



(b)



(c)



(d)

Figure 55 Plots of three dimensional curves fitted under linear-exponential and parabolic exponential

speed function. (a) and (b) Linear exponential function; (c) and (d) Parabolic exponential function

### 8.3. *Validation of traffic state estimation*

First of all, we want to demonstrate the model performance in estimating the real-time traffic flow condition of the arterial using detector data as field observation source. Three quantitative performance measures including MAEB, MAPEB and CIE are computed in order to assess the accuracy of the model. In all definitions, the ground truth values are represented by  $Z = [z_1, z_2, \dots, z_T]$  and the estimated mean, upper and lower boundaries are represented by  $X = [x_1, x_2, \dots, x_T]$  and  $\bar{X} = [\bar{x}_1, \bar{x}_2, \dots, \bar{x}_T]$ ,  $\underline{X} = [\underline{x}_1, \underline{x}_2, \dots, \underline{x}_T]$  respectively.  $T$  is the analysis period. The upper and lower bound of the traffic state is computed by taking 15 and 75 percentile of the estimated distribution.

Mean Absolute Error comparing with the boundary (MAEB) is computed as:

$$\text{MAEB} = \frac{1}{T} \sum_{t=1}^T [\Lambda(z_t - \bar{x}_t) |z_t - \bar{x}_t| + \Lambda(\underline{x}_t - z_t) |z_t - \underline{x}_t|] \quad (8-4)$$

Mean Absolute Percentage Error comparing with the boundary (MAPEB) is computed as:

$$\begin{aligned} \text{MAPEB} = \frac{1}{T} \sum_{t=1}^T \left[ \Lambda(z_t - \bar{x}_t) \frac{|z_t - \bar{x}_t|}{z_t} \right. \\ \left. + \Lambda(\underline{x}_t - z_t) \frac{|z_t - \underline{x}_t|}{z_t} \right] \end{aligned} \quad (8-5)$$

Confidence interval of the estimation (CIE) is computed as:

$$\text{CIE} = \frac{1}{T} \sum_{t=1}^T |\bar{x}_t - \underline{x}_t| \quad (8-6)$$

where  $\Lambda(x)$  is the step-wise linear function defined by condition (8-7).

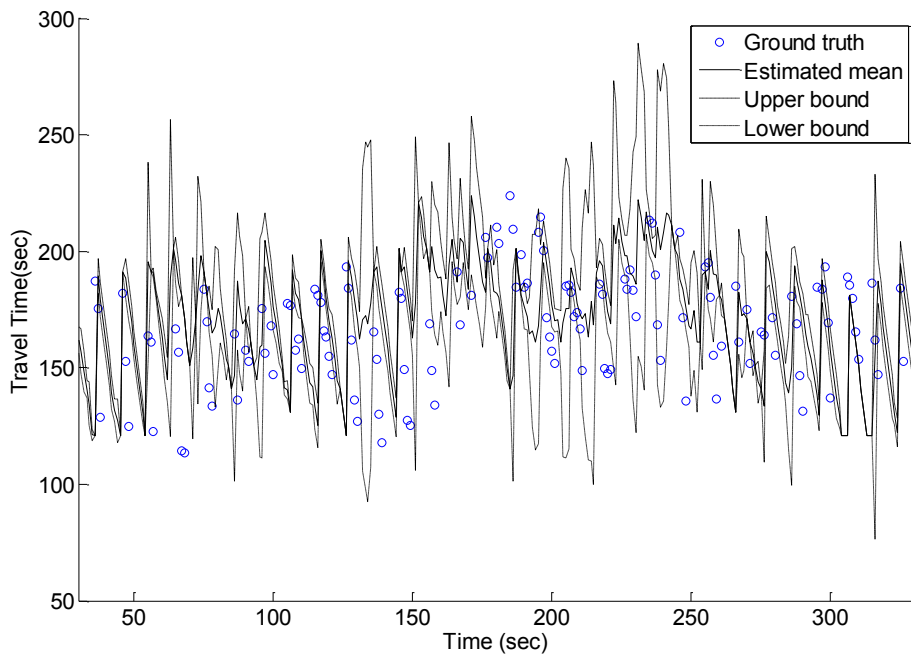
$$\Lambda(x) = \begin{cases} 1 & x \geq 0 \\ 0 & x < 0 \end{cases} \quad (8-7)$$

Table 16 provides an overview of performance measures computed based on the model outputs. For each type of traffic state variable estimated (queue length, density and speed), the MAEB, MAPEB and CIE indices are displayed for each individual cell. The performance indices are organized according to the type of traffic state, detector scenario and performance index types. The units for queue, density and speed are meter, veh/km and m/s respectively.

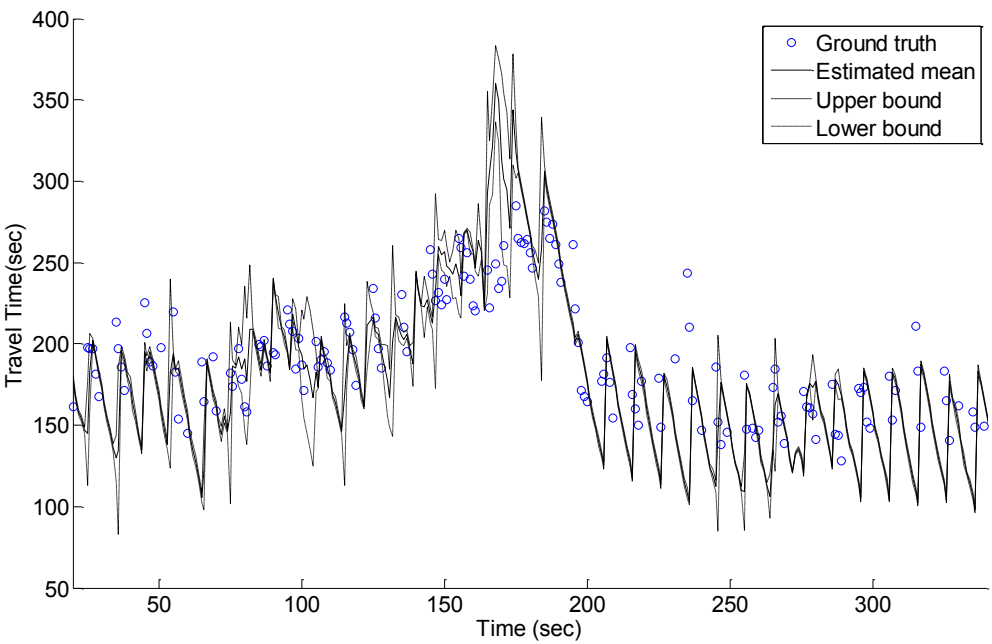
Table 16 Summary of performance index of the model under simulation dataset

Traffic State Variable	Direction	Performance index	C1	C2	C3	C4	Average
Queue Length	Eastbound	MAEB (m)	3.78	9.38	1.71	4.58	4.86
		MAPEB (%)	8.9%	21.8%	9.2%	22.8%	15.7%
		CIE (m)	3.58	5.84	2.66	4.05	4.03
	Westbound	MAEB (m)	6.77	12.62	2.45	5.55	6.85
		MAPEB (%)	16.0%	29.3%	13.2%	27.6%	21.6%
		CIE (m)	3.79	4.95	2.99	4.88	4.15
Density	Eastbound	MAEB (m)	5.40	6.20	6.50	6.40	6.125
		MAPEB (%)	24.3%	26.7%	23.7%	40.2%	28.7%
		CIE (m)	2.40	6.40	6.70	5.00	5.125
	Westbound	MAEB (m)	15.90	7.20	7.00	5.20	8.825
		MAPEB (%)	40.3%	25.1%	22.7%	27.8%	29.0%
		CIE (m)	2.50	6.30	8.40	3.90	5.275
Speed	Eastbound	MAEB (m/s)	0.51	0.92	1.68	0.95	1.01
		MAPEB (%)	4.0%	7.4%	12.5%	7.2%	7.8%
		CIE (m/s)	0.43	0.51	0.57	0.53	0.51
	Westbound	MAEB (m/s)	0.50	1.06	2.12	0.86	1.14
		MAPEB (%)	3.8%	9.6%	17.4%	6.4%	9.3%
		CIE (m/s)	0.44	0.58	0.64	0.47	0.53
Travel Time	Eastbound	MAEB (sec.)			7.89		
		MAPEB (%)			4.73%		
		CIE (sec.)			13.78		
	Westbound	MAEB (sec.)			12.57		
		MAPEB (%)			6.53%		
		CIE (sec.)			12.98		

The estimated and observed travel time is presented in Figure 56. To further demonstrate the model outputs versus ground truth traffic state values, the estimation results of individual cells are selectively displayed from Figures 57 through Figure 59. For each type of traffic state variable, the estimation results of three cells are selected and plotted against the ground truth values. For a complete list of estimated traffic states of each individual cell, readers can refer Appendix B.



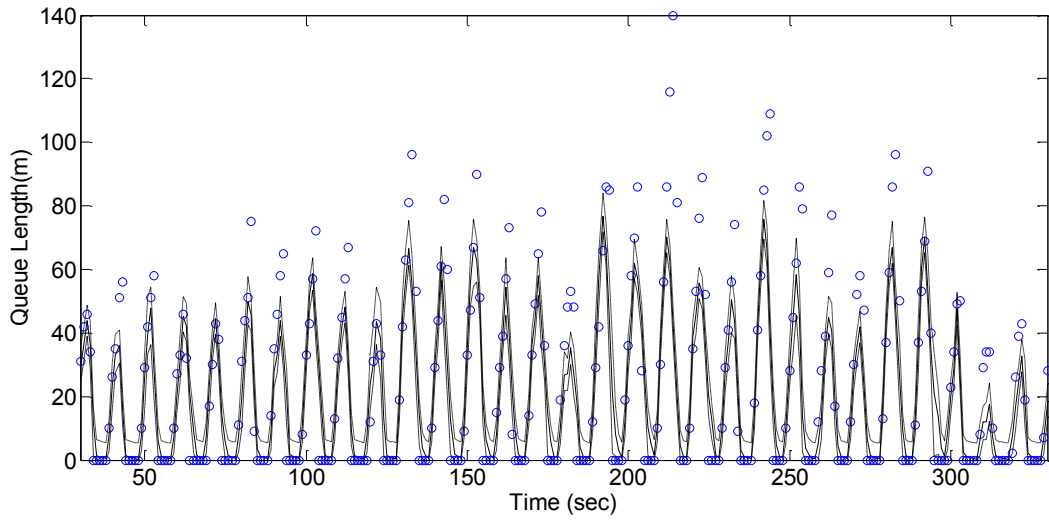
(a)



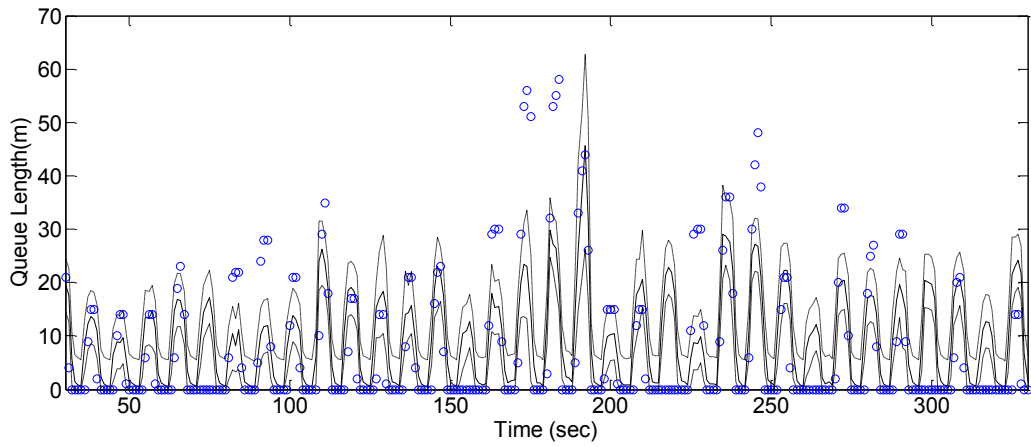
(b)

Figure 56 Estimated versus ground truth travel time plot of (a) Eastbound traffic (b) Westbound traffic of simulation dataset

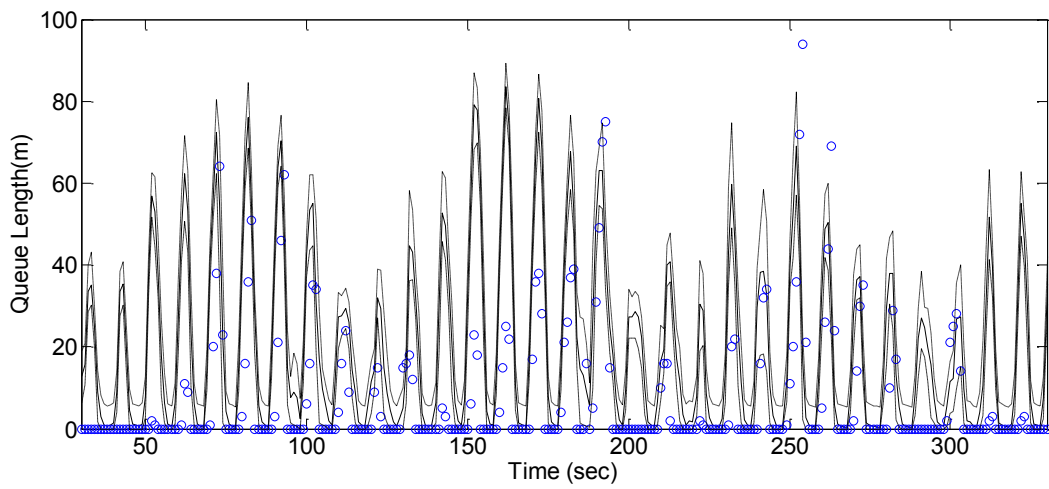
As one piece of very important information, the estimated travel time result is displayed in Figure 56. As observable from the figure, the travel time is estimated accurately for both direction of the arterial, the average error in percentage is around 5% considering both directions. Such statistics implies that the proposed model can offer very reliable travel time information even under congested situation.



(a)



(b)



(c)

Figure 57 Estimated versus ground truth queue length plot of (a) Cell 1 (b) Cell 3 (c) Cell 8 of simulation dataset

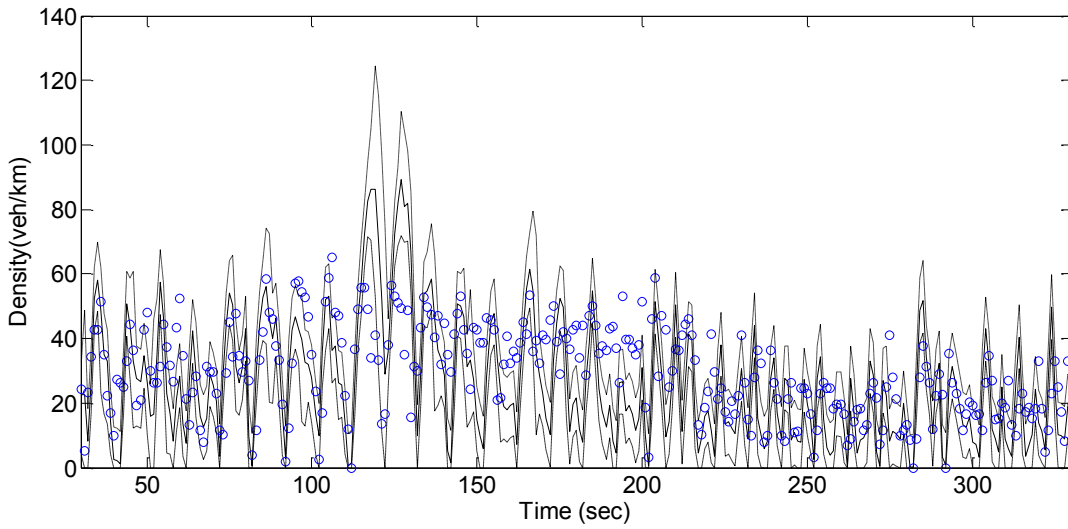
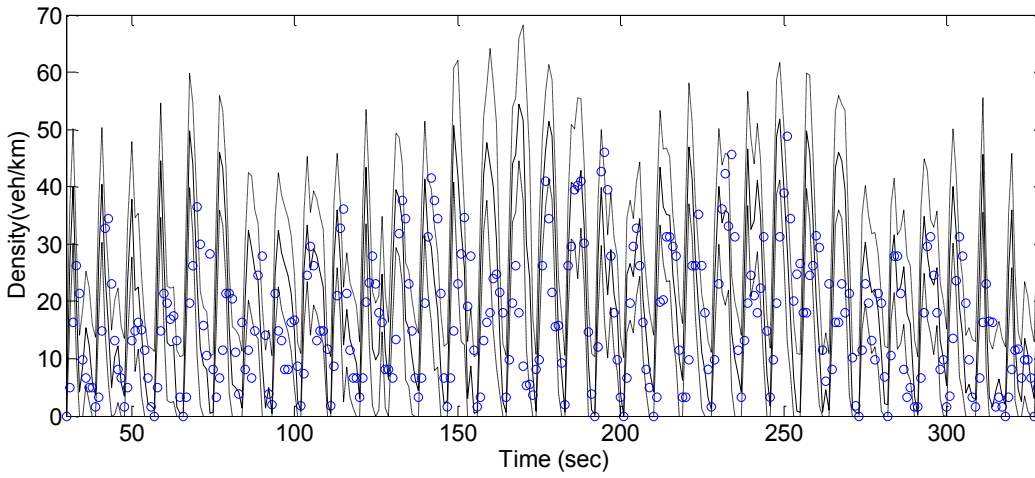
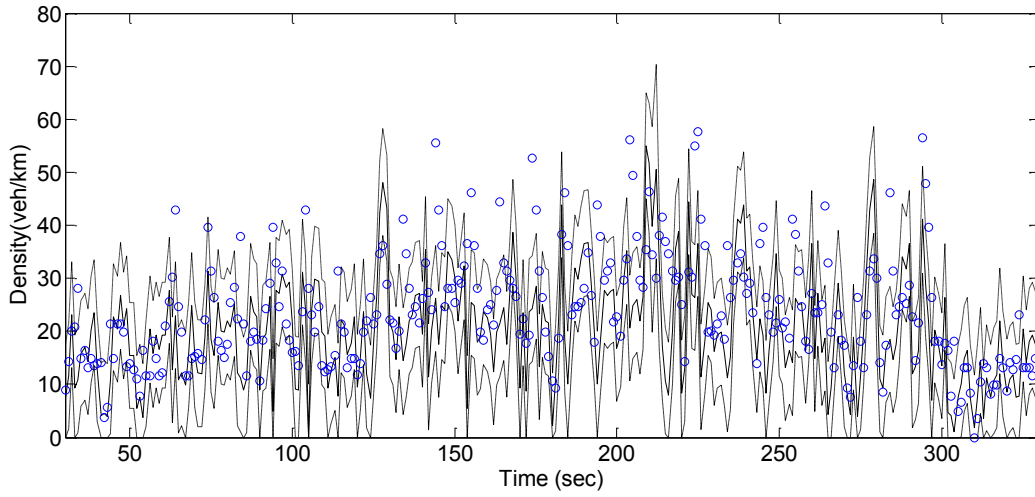


Figure 58 Estimated versus ground truth density plot of (a) Cell 1 (b) Cell 4 (c) Cell 6 of simulation dataset

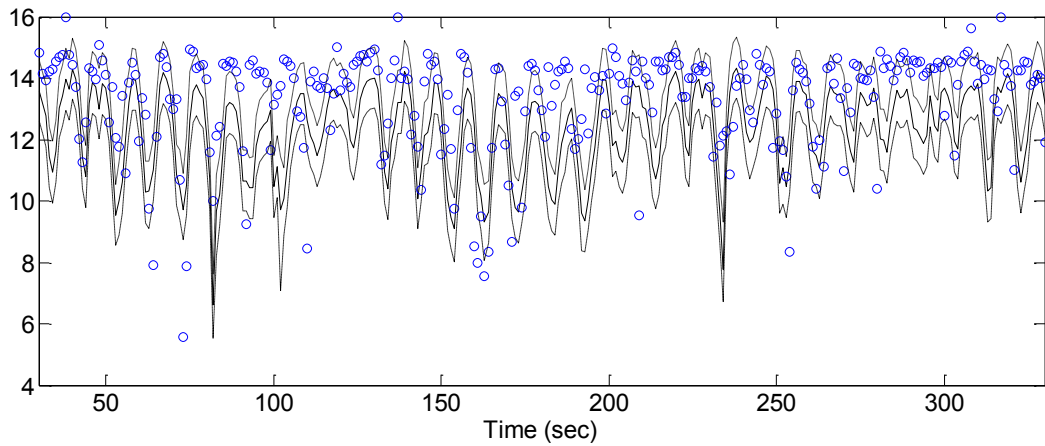
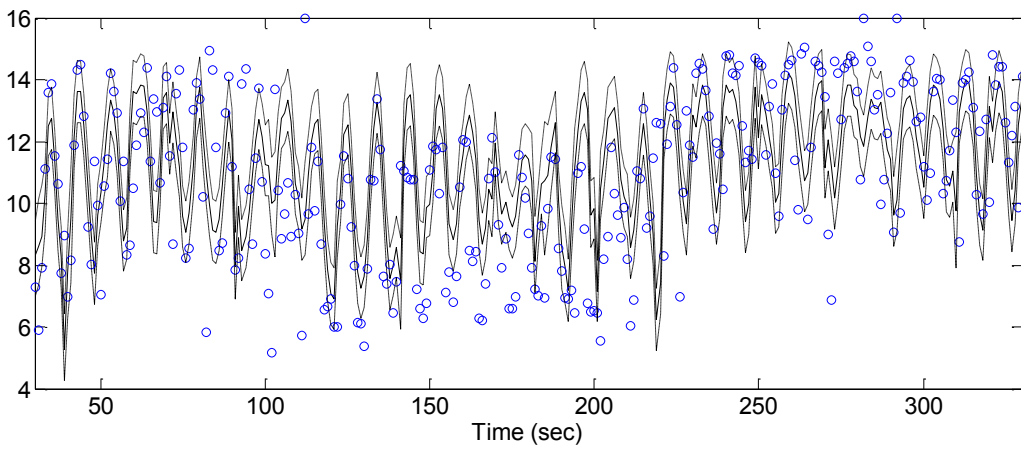
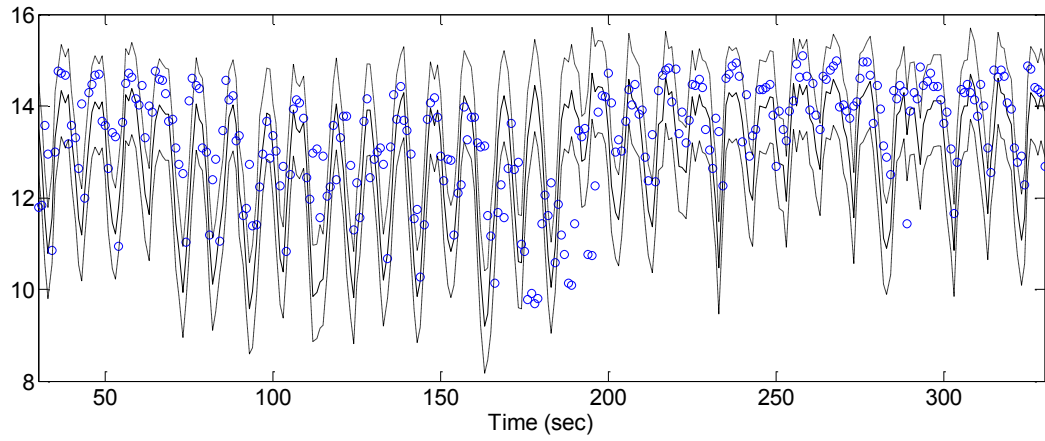


Figure 59 Estimated versus ground truth density plot of (a) Cell 5 (b) Cell 6 (c) Cell 7 of simulation dataset

#### *8.4. Validation of Short-term Prediction Results*

This section examines the accuracy of prediction results offered by the proposed model using simulated traffic state as ground truth values. There are two important aspects of model performance we want to investigate in this section: 1) the overall prediction accuracy of different types of traffic states (queue length, density, speed and travel time); 2) the change of prediction accuracy w.r.t. the prediction range. The prediction range, usually measured by the number of time steps over which the traffic state variables are predicted, plays a very important role when investigating the potential effectiveness of particular prediction model. In this numerical example, the MAEB and MAPE indices are computed from 1 to 60 time step prediction for each individual traffic state variable. Since each time step represents a duration of 10 seconds, 60 time steps prediction represents a 10 minutes ahead prediction of the traffic flow condition.

Tables 17 and 18 present the summary of average prediction error for each type of traffic state including queue, density, speed and travel time at different prediction ranges. Figures 60 and 61 are graphical presentation of Tables 17 and 18.

Table 17 Summary of average prediction MAEB of different traffic state variables of simulation dataset

Prediction Time Step (one step=10 seconds)

	5	10	15	20	25	30	35	40	45	50	55	60
Queue (m)	9.62	6.41	8.66	7.30	7.83	7.70	7.33	7.34	7.58	6.88	8.23	6.35
Density (veh/km)	11.19	7.35	10.21	8.77	8.34	9.74	6.88	10.30	7.12	9.87	7.85	8.85
Speed (m/s)	0.928	0.59	0.951	0.599	0.934	0.621	0.906	0.631	0.857	0.671	0.813	0.661
Travel time (s)	10.59	10.17	10.11	10.41	10.46	9.75	9.96	9.58	9.77	9.07	8.83	8.89

Table 18 Summary of average prediction MAPE of different traffic state variables of simulation dataset

Prediction Time Step (one step=10 seconds)

	5	10	15	20	25	30	35	40	45	50	55	60
Queue	27.4%	20.1%	24.7%	22.6%	22.4%	23.7%	20.9%	22.5%	21.4%	21.0%	22.9%	19.4%
Density	44.3%	29.0%	39.8%	35.3%	32.1%	39.5%	26.2%	41.5%	27.5%	39.1%	30.8%	34.6%
Speed	7.4%	4.7%	7.5%	4.7%	7.4%	4.9%	7.1%	5.0%	6.7%	5.4%	6.4%	5.3%
Travel time	5.8%	5.6%	5.6%	5.7%	5.8%	5.4%	5.5%	5.3%	5.4%	5.0%	4.9%	4.9%

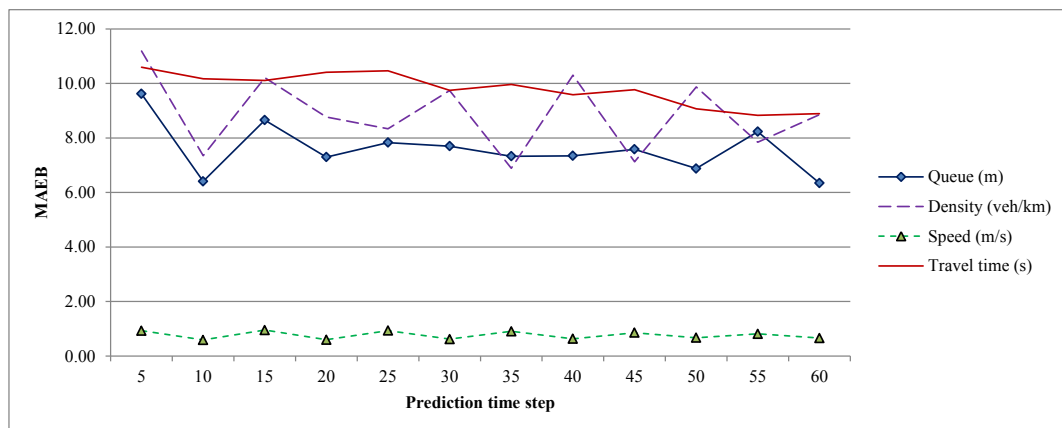


Figure 60 Line plot of average prediction MAEB of different traffic state variables of simulation dataset

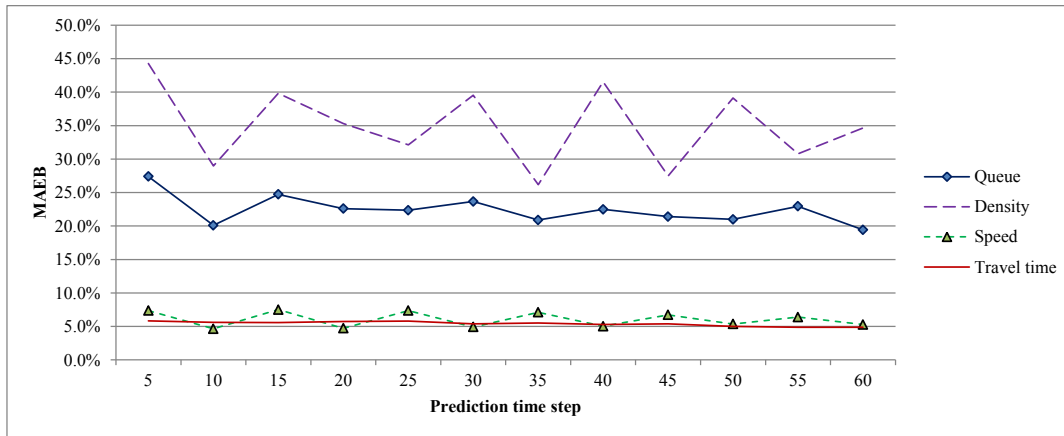


Figure 61 Line plot of average prediction MAPEB of different traffic state variables of simulation dataset

There are several noticeable points regarding Tables 17 and 18. First of all, the prediction accuracy of travel time, queue length and speed remains relatively stable as the prediction time step increases; as for the density prediction, the MAPEB curve demonstrates periodic changing pattern. Secondly, the average prediction accuracy (since the MAPEB of travel time, queue and speed are stable, checking the average error is meaningful) of travel time, queue length and speed are respectively 5%, 18% and 5.5% within 60 time step prediction range. Such performance measure indicates that the proposed model can offer very reliable prediction of those three traffic state variables within comparatively long prediction time range. Compared with the remaining three variables, the density prediction is comparatively low and demonstrates high periodical fluctuation in this numerical study. The average prediction MAPEB of density fluctuates between 30% and 45% with the prediction range. This implies that predicting the future density of each cell using the proposed model may yield large biased results. However if one just concentrates on the queue and speed values then such model weakness will not cause much trouble because travel time or delay along signalized arterial is primary

dominated by the link speed and queue length. Tables 19 and 20 provide more detailed information about the change of MAEB and MAPEB of each cell.

Table 19 Summary of prediction MAEB of individual cells of simulation dataset

Traffic State Variable	Direction	Link	Prediction Time Step											
			5	10	15	20	25	30	35	40	45	50	55	60
Queue Length (m)	Eastbound	Cell 1	15.48	3.32	15.16	3.61	15.00	3.86	14.73	3.95	14.45	4.28	14.07	4.41
		Cell 2	15.85	13.29	12.75	16.20	9.93	17.67	8.21	16.64	9.48	14.98	12.94	13.27
		Cell 3	3.27	1.04	2.77	1.91	2.03	2.75	1.45	3.12	1.24	3.09	1.31	2.71
		Cell 4	3.69	5.79	3.54	5.63	3.60	4.94	3.63	4.06	3.74	3.39	3.87	3.29
	Westbound	Cell 5	15.55	5.27	15.24	5.32	15.16	5.31	14.92	5.59	14.69	6.07	14.29	6.18
		Cell 6	16.36	14.20	13.57	17.05	11.17	18.43	10.14	17.38	11.58	15.76	13.93	13.86
		Cell 7	3.20	1.32	2.89	2.19	2.34	2.88	1.98	3.11	1.71	3.11	1.56	2.84
		Cell 8	3.54	7.04	3.32	6.47	3.41	5.76	3.59	4.90	3.78	4.34	3.88	4.22
Density (veh/km)	Eastbound	Cell 1	0.85	1.90	1.18	2.05	1.36	2.16	1.39	2.21	1.57	2.37	1.51	2.31
		Cell 2	8.35	4.79	8.07	4.84	8.27	4.68	8.41	4.46	8.27	4.45	7.87	4.23
		Cell 3	19.46	9.36	18.81	12.92	13.80	16.17	8.10	18.40	8.70	17.89	9.54	16.97
		Cell 4	10.76	7.83	8.98	10.21	6.70	11.50	5.10	11.56	6.26	10.02	7.67	8.32
	Westbound	Cell 5	9.16	9.71	9.54	9.85	9.36	9.33	8.84	9.04	8.77	9.07	8.95	9.30
		Cell 6	11.75	7.19	11.63	6.55	11.55	6.66	11.89	7.48	11.72	7.73	11.93	7.78
		Cell 7	21.41	12.83	17.84	16.32	12.05	18.59	9.31	20.37	9.45	20.05	11.32	16.13
		Cell 8	7.76	5.17	5.65	7.43	3.63	8.83	2.04	8.90	2.26	7.36	3.96	5.78
Speed (m/s)	Eastbound	Cell 1	1.176	0.36	1.194	0.377	1.177	0.382	1.182	0.372	1.124	0.381	1.091	0.365
		Cell 2	0.686	0.316	0.668	0.355	0.552	0.442	0.457	0.544	0.405	0.647	0.408	0.622
		Cell 3	0.665	0.857	0.742	0.869	0.783	0.73	0.881	0.622	0.913	0.649	0.845	0.725
		Cell 4	1.017	0.524	1.089	0.662	1.067	0.738	0.986	0.674	0.927	0.62	0.948	0.57
	Westbound	Cell 5	1.01	0.68	1.01	0.62	0.99	0.63	0.98	0.65	0.93	0.63	0.89	0.59
		Cell 6	1.29	0.59	1.11	0.71	0.88	0.93	0.70	1.07	0.67	1.11	0.75	1.05
		Cell 7	0.80	1.00	0.99	0.75	1.25	0.60	1.34	0.60	1.20	0.82	0.91	0.91
		Cell 8	0.79	0.39	0.80	0.44	0.77	0.51	0.73	0.52	0.68	0.51	0.66	0.46
Travel Time (s)	Eastbound		8.42	8.37	8.25	8.51	8.87	8.02	8.24	7.92	8.10	7.38	7.18	6.86
	Westbound		12.77	11.97	11.97	12.30	12.05	11.48	11.68	11.24	11.43	10.75	10.48	10.92

\*\*One time step represents 10 seconds

Table 20 Summary of prediction MAPEB of individual cells of simulated dataset

Traffic State Variable	Direction	Link	Prediction Time Step											
			5	10	15	20	25	30	35	40	45	50	55	60
Queue Length	Eastbound	Cell 1	36.6%	7.9%	35.9%	8.5%	35.5%	9.1%	34.8%	9.3%	34.2%	10.1%	33.3%	10.4%
		Cell 2	36.8%	30.9%	29.6%	37.6%	23.1%	41.1%	19.1%	38.7%	22.0%	34.8%	30.1%	30.8%
		Cell 3	17.6%	5.6%	15.0%	10.3%	11.0%	14.8%	7.8%	16.8%	6.7%	16.7%	7.1%	14.6%
		Cell 4	18.4%	28.8%	17.6%	28.0%	17.9%	24.6%	18.1%	20.2%	18.6%	16.9%	19.3%	16.4%
	Westbound	Cell 5	36.8%	12.5%	36.1%	12.6%	35.9%	12.6%	35.3%	13.2%	34.7%	14.4%	33.8%	14.6%
		Cell 6	38.0%	33.0%	31.5%	39.6%	25.9%	42.8%	23.5%	40.4%	26.9%	36.6%	32.4%	32.2%
		Cell 7	17.2%	7.1%	15.6%	11.8%	12.6%	15.5%	10.7%	16.8%	9.2%	16.8%	8.4%	15.3%
		Cell 8	17.6%	35.1%	16.5%	32.3%	17.0%	28.7%	17.9%	24.4%	18.8%	21.6%	19.3%	21.0%
Density	Eastbound	Cell 1	3.8%	8.6%	5.3%	9.3%	6.1%	9.8%	6.3%	10.0%	7.1%	10.7%	6.8%	10.4%
		Cell 2	36.2%	20.8%	35.0%	21.0%	35.8%	20.3%	36.4%	19.3%	35.8%	19.3%	34.1%	18.3%
		Cell 3	71.2%	34.3%	68.8%	47.3%	50.5%	59.2%	29.7%	67.4%	31.8%	65.5%	34.9%	62.1%
		Cell 4	67.7%	49.2%	56.5%	64.2%	42.2%	72.3%	32.1%	72.7%	39.4%	63.0%	48.3%	52.3%
	Westbound	Cell 5	23.2%	24.6%	24.2%	25.0%	23.7%	23.7%	22.4%	22.9%	22.2%	23.0%	22.7%	23.6%
		Cell 6	40.8%	24.9%	40.4%	22.7%	40.1%	23.1%	41.2%	25.9%	40.7%	26.8%	41.4%	27.0%
		Cell 7	69.9%	41.8%	58.2%	53.2%	39.3%	60.6%	30.4%	66.5%	30.8%	65.4%	36.9%	52.6%
		Cell 8	41.4%	27.6%	30.2%	39.7%	19.4%	47.2%	10.9%	47.5%	12.0%	39.3%	21.1%	30.8%
Speed	Eastbound	Cell 1	9.3%	2.8%	9.4%	3.0%	9.3%	3.0%	9.3%	2.9%	8.9%	3.0%	8.6%	2.9%
		Cell 2	5.5%	2.5%	5.4%	2.9%	4.4%	3.6%	3.7%	4.4%	3.3%	5.2%	3.3%	5.0%
		Cell 3	4.9%	6.4%	5.5%	6.5%	5.8%	5.4%	6.6%	4.6%	6.8%	4.8%	6.3%	5.4%
		Cell 4	7.7%	4.0%	8.2%	5.0%	8.1%	5.6%	7.5%	5.1%	7.0%	4.7%	7.2%	4.3%
	Westbound	Cell 5	7.5%	5.1%	7.5%	4.6%	7.4%	4.7%	7.3%	4.9%	7.0%	4.7%	6.6%	4.4%
		Cell 6	11.6%	5.3%	10.0%	6.4%	7.9%	8.4%	6.3%	9.7%	6.0%	10.0%	6.8%	9.4%
		Cell 7	6.5%	8.2%	8.1%	6.2%	10.3%	4.9%	11.0%	4.9%	9.8%	6.7%	7.5%	7.5%
		Cell 8	5.8%	2.9%	6.0%	3.3%	5.7%	3.8%	5.4%	3.9%	5.1%	3.8%	4.9%	3.4%
Travel Time	Eastbound		5.0%	5.0%	4.9%	5.1%	5.3%	4.8%	4.9%	4.7%	4.9%	4.4%	4.3%	4.1%
	Westbound		6.6%	6.2%	6.2%	6.4%	6.3%	6.0%	6.1%	5.8%	5.9%	5.6%	5.4%	5.7%

\*\*One time step represents 10 seconds

To help readers further understand outputs of prediction model, the prediction curves of selected individual cells are presented together with corresponding ground truth values. Due to the space constraint of the dissertation, only the prediction result of part of the cells is listed here (two cells for each type of traffic state variable). Figures 62 and 63 are predicted travel time plots and Figures 64 and 65 are queue prediction plots. Figures 66 and 67 are

density prediction plots and Figures 68 and 69 are speed prediction plots. For a complete list of predicted traffic states of each individual cell, readers can refer Appendix B.

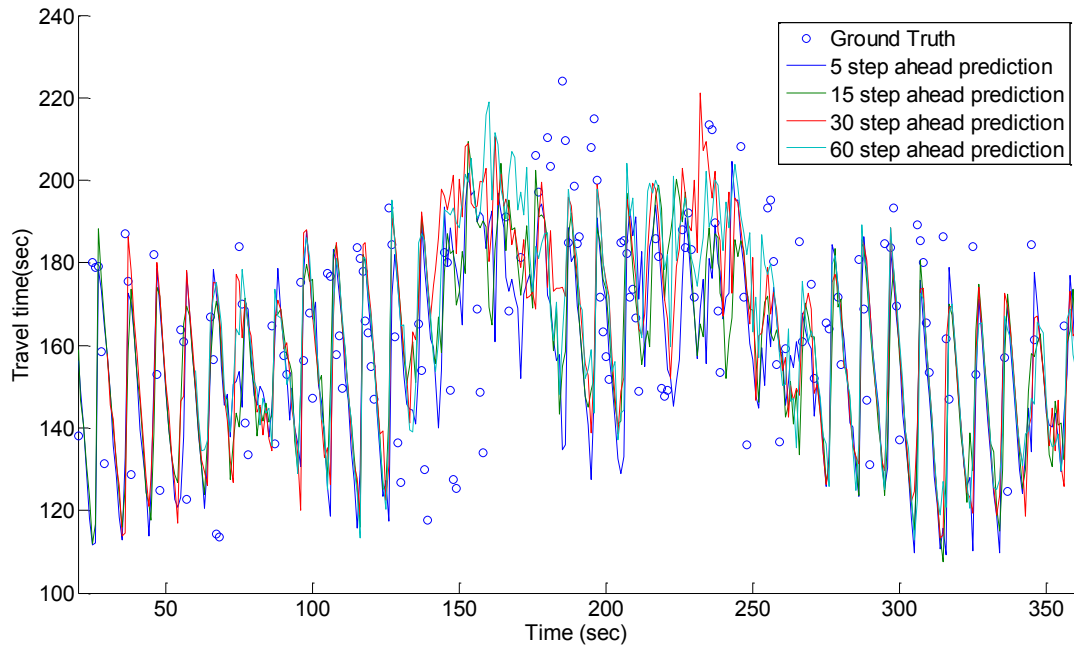


Figure 62 Eastbound predicted versus ground truth travel time for 5, 15, 30 and 60 time step prediction of simulation dataset

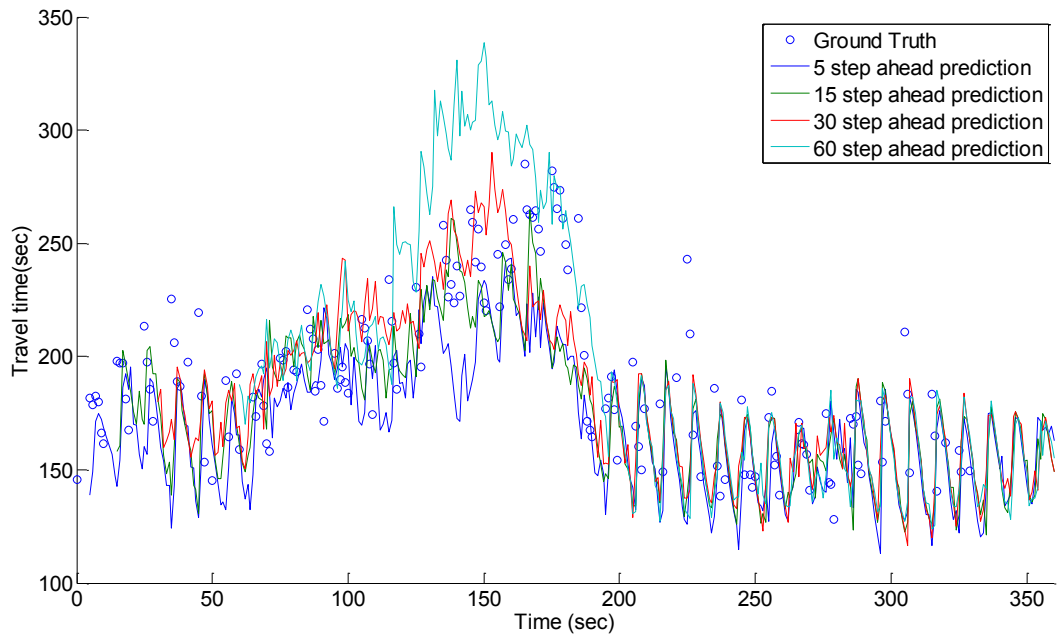


Figure 63 Westbound predicted versus ground truth travel time for 5, 15, 30 and 60 time step prediction of simulation dataset

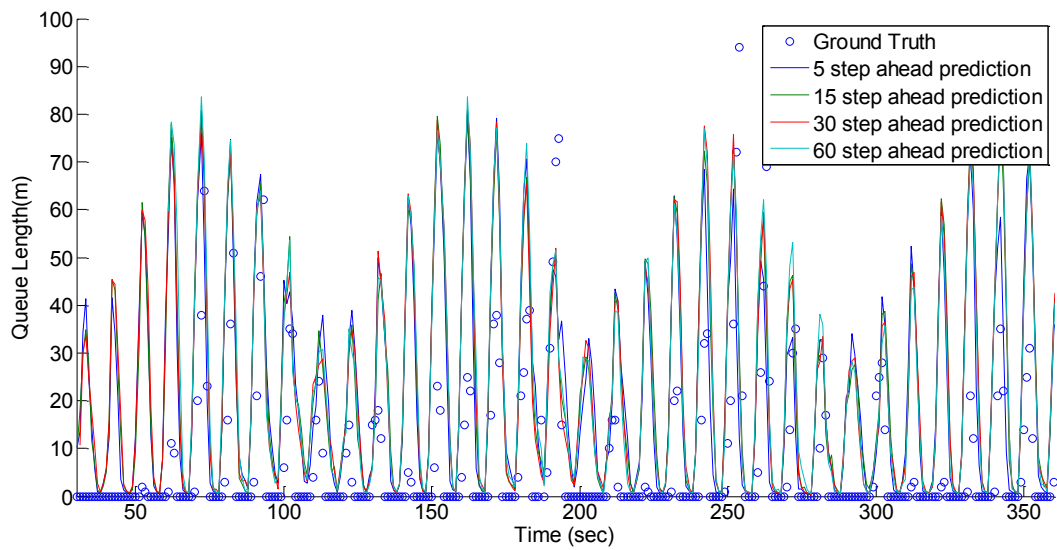


Figure 64 Predicted versus ground truth queue length of cell 8 of simulation dataset

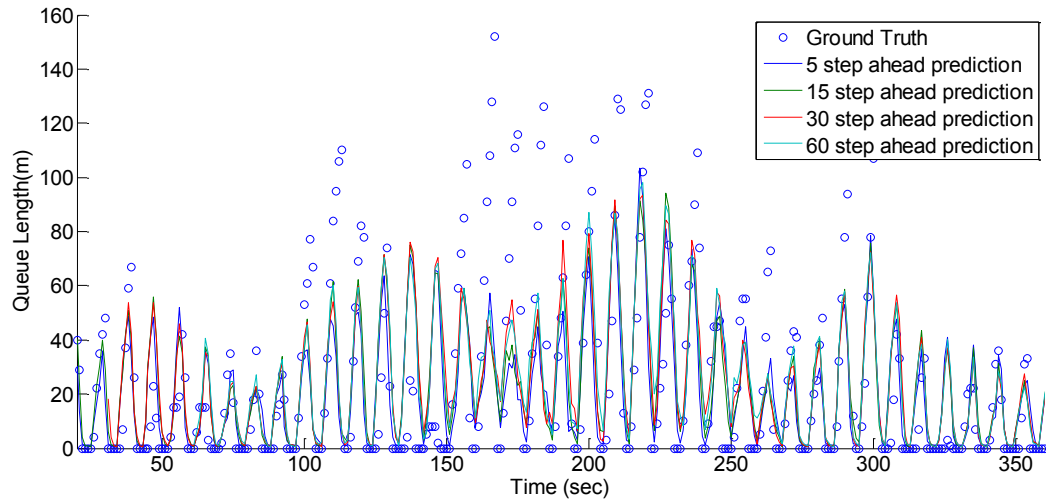


Figure 65 Predicted versus ground truth queue length of cell 1 of simulation dataset

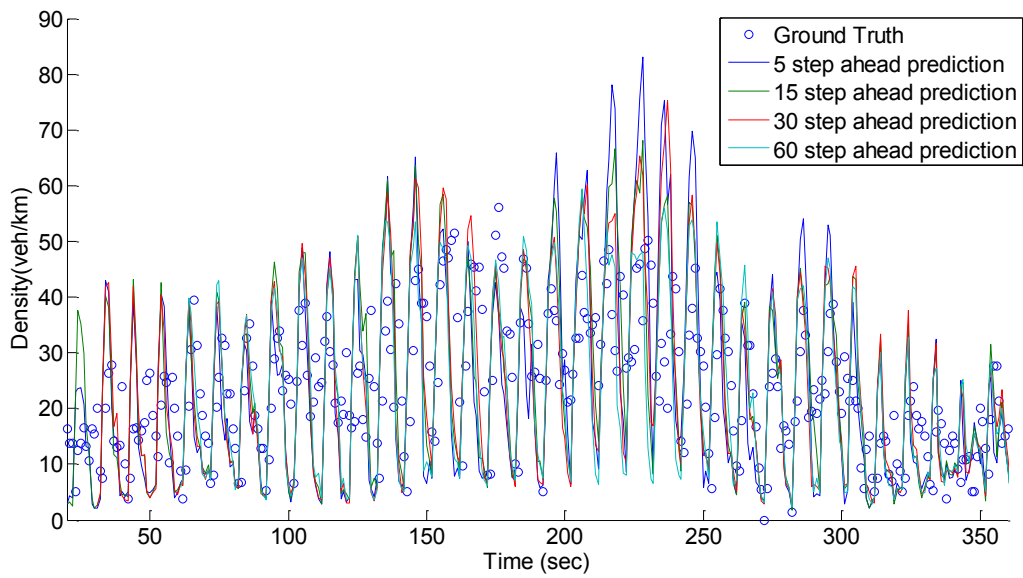


Figure 66 Predicted versus ground truth density of cell 2 of simulation dataset

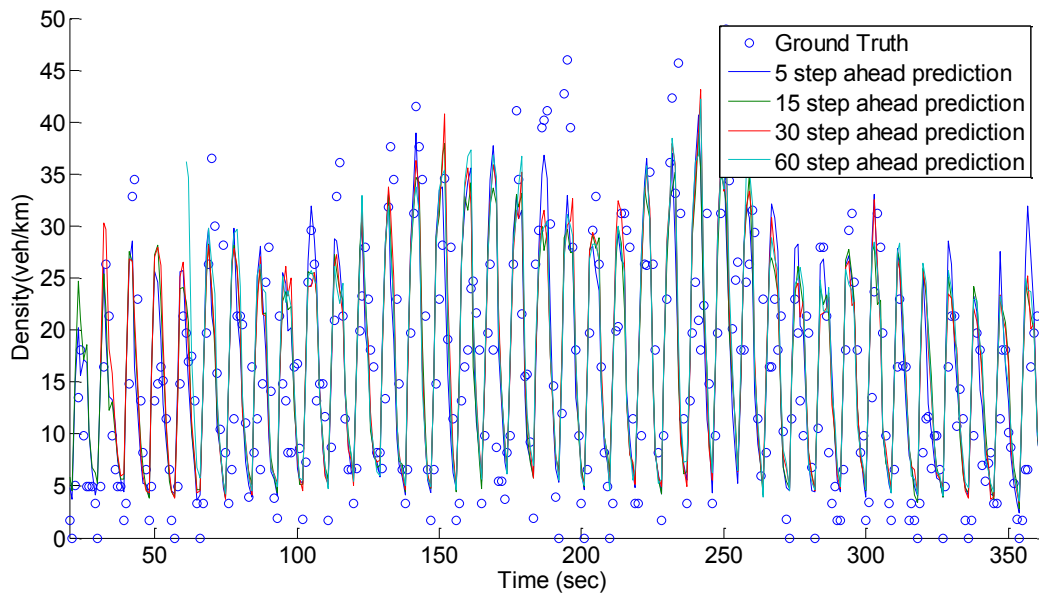


Figure 67 Predicted versus ground truth density of cell 4 of simulation dataset

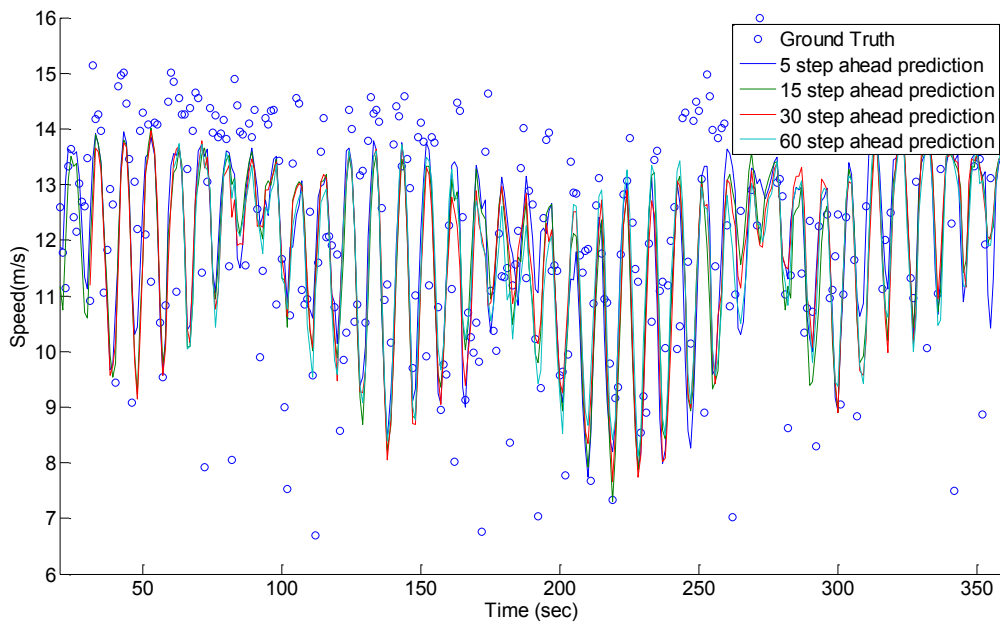


Figure 68 Predicted versus ground truth speed of cell 2 of simulation dataset

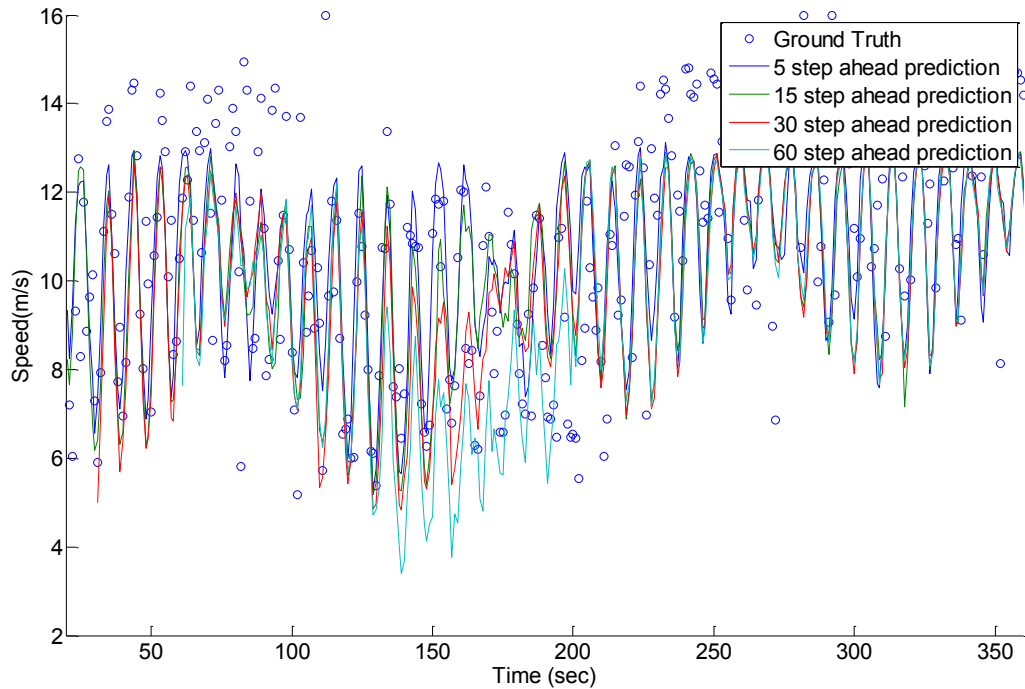


Figure 69 Predicted versus ground truth speed of cell 6 of simulation dataset

### 8.5. Chapter Summary

This chapter performed model validation using simulated arterial traffic flow data. Key findings of this chapter are summarized as follows:

- 1) The parabolic-exponential speed-density-queue function is applied in this numerical study and the parameters of speed function are calibrated using link speed, density and queue data extracted from the simulated trajectory data;
- 2) The simulation dataset represents the traffic flow dynamics of congested (near capacity) traffic flow condition which is observed from the travel time plots given by Figure 51
- 3) The change of prediction accuracy over time measured by MAPEB is stable for travel time, queue length and speed. On the other hand, the prediction error of traffic flow density demonstrates high fluctuation and periodicity property;

4) The model can offer reliable prediction for queue length, speed and travel time under long prediction time range (>60 time steps). The average MAPEB of predicted queue, speed and travel time are 5%, 18% and 5.5% respectively.

5) Predicting the future traffic flow density with the proposed model will generate considerable amount of prediction errors (30% ~ 40%);

## 9. Conclusion and Future Research Direction

### *9.1. Summary of the dissertation*

This study proposed an innovative traffic state estimation and short-term prediction framework for signalized arterial network using an integrated solution consisting of macroscopic traffic flow model, particle filtering and time series method. The proposed method is composed of two modules: the real-time estimation module and short-term prediction module. The former takes traffic detector information as input and provides estimated current traffic flow status while the latter forecasts near future traffic flow conditions. The main contributions of this research are summarized as follows,

- In the proposed model, queue length before the intersection stop lines is modeled as one state variable in the estimation process. Such approach not only highlighted the major characteristic of signalized arterial, but also significantly reduced the computational load of the model by avoiding segmenting links into a large number of small cells;
- A set of system state transition equations are developed based on traffic flow and queuing theory. The transition equations are mathematical representation of traffic flow dynamics of arterial cells under the proposed state definition;
- The study first proposed the fundamental relationship between speed, density and queue length of arterial links. Such concept is a natural expansion of freeway fundamental diagram considering drivers' reaction toward signal change and queue formation;
- This study established a real-time traffic state adjustment and feedback estimation mechanism for arterial roads using particle filtering technique. And using the flexibility provided by PF, this study discussed the data fusion approach to integrate real-time traffic information from different sources;

- The study proposed a short-term traffic flow prediction method for arterials through a combination of traffic flow model and time series method (SARIMA). The SARIMA model is employed to predict the future boundary conditions of the network and other traffic flow states are predicted by iteratively applying the flow transition model;
- The study conducted a series of numerical investigation regarding the performance of the proposed model under different traffic conditions. Both real-world and synthetic data were used. The validation result showed that the proposed model can yield accurate queue, density and speed estimation using both detector and probe vehicle data; as for the prediction, the model can predict queue and speed with high degree of accuracy which does not deteriorate w.r.t. prediction interval;
- Using trajectory method of imaginary vehicle, the travel time is estimated from the traffic states of links. Through numerical examples, the model performed excellently in estimating and predicting arterial travel time. Also the accuracy of travel time prediction remains almost constant within the entire prediction range;

## 9.2. Conclusion

Following the findings of existing literatures, the study developed a short-term traffic state prediction framework for signalized arterial corridor based on macroscopic traffic flow model, time-series method and stochastic estimation theory. The primary contribution of the study is to propose an arterial queue model called shifting boundary cell model to describe the periodical shockwave propagation before each intersection. Then the transition of arterial traffic flow state is quantified by a set of continuous system dynamic equations. Based on the traffic flow model developed in this study, the real-time traffic state

estimation and short-term prediction are conducted by combining particle filtering and SARIMA technique.

Compared with most existing short-term prediction methods, the proposed approach opened a new avenue to the field of short-term traffic state prediction by combining the advantage of traffic flow theory and other statistical methods. Given the boundary conditions, the model can perform reliable prediction of near future queue, density, speed which can be used for various traffic control purposes including short-term travel time prediction and signal timing optimization. We can argue the primary feature of the proposed model from several prospective:

First of all, instead of large amount of historical data, the proposed model relies more on the traffic flow model to perform the short-term prediction of traffic flow state. Thereafter, the proposed method requires neither massive amount of historical traffic flow data nor long computation time for model specification and calibration purpose. Through state augmentation method, all the parameters associated with the shifting boundary cell model are automatically calibrated during the real-time traffic state estimation process. Meanwhile, another merit of the proposed model is that traffic flow measurements obtained from different types of detectors can be integrated using particle filtering framework with relatively less modeling effort. In the numerical example where the NGSIM dataset is used to examine the accuracy of the real-time estimation result, the proposed model demonstrated similar degree of accuracy under fixed location detector and probe vehicle data indicating different types of detector measurements can be integrated to yield reliable estimation result through the proposed approach.

Secondly, the proposed traffic state estimation model has its unique state definition and state transition equations which are developed particularly for signalized corridors. The computational performance of the model is significantly higher than that of other existing macroscopic traffic flow models such as CTM. Also, by dividing each link into two distinct regimes (queuing area and moving area), the model traces the movement of the end of queue based on detector information. By doing so, the proposed method can offer real-time queue estimation without dividing the link into a large number of smaller cells. Piece-wise continuous system state transition equations are derived for signalized cells. Thus, the proposed model is both analytically traceable and computationally efficient.

Thirdly, the study revealed the important correlation between traffic flow speed, density and the queue length within an arterial cell. The study found that the average flow speed within the moving regime of each cell is significantly affected by both the traffic flow density of the moving area and the ratio between physical queue length and the cell length. Therefore traffic flow speed is then modeled as some convex function of density and queue length which can be viewed as arterial fundamental diagram. In this study, two types of arterial speed-density-queue relationship are fitted and employed: the linear-exponential speed function and linear-parabolic speed function. In either case, predicted traffic flow speed decreases linearly w.r.t. flow density and non-linearly w.r.t. physical queue ratio. Compared with freeway cells where speed is usually depicted as a univariable function of density, this study explained the complex nature of speed transition of arterial links.

Lastly, the system transition equation developed is also used for short-term prediction purpose. The boundary conditions (input flows on the boundary links of the network) is predicted by applying SARIMA algorithm. And based on the real-time estimation results,

all traffic state variables are predicted by iteratively applying the system transition equations developed in this study. The result of numerical study showed that the proposed framework can be considered as an excellent multiple step prediction algorithm. The change of prediction error of density and queue demonstrated periodical pattern, meanwhile that of speed and travel time demonstrated stable nature as the prediction range is increased. Compared with other statistical prediction methods such as time-series model or KNN model, the accuracy of the proposed model deteriorates very slowly when increase the prediction range.

The proposed model can have numerous applications including real-time travel time prediction, dynamics route guidance and signal control optimization. The real-time travel time prediction of urban streets is beneficial to both traffic management authority and network user because travel time, as a very important network performance indicator, is one essential piece of information regarding the near future traffic condition of the network. Traffic control center can monitor the current traffic flow condition of the network and identify all congested areas using the proposed model. Similarly drivers can also change their pre-planned route if bottlenecks are identified through the model. The dynamic route guidance is an extension of real-time travel time prediction. Based on the future travel time information provided by the algorithm, a dynamic route guidance system can provide recommended optimal path for road users. Combined with in-vehicle navigation system, the dynamic route guidance can balance the flow distribution of the network and mitigate the congestion level at bottleneck locations. The real-time signal optimization is another major application of the model. In arterial networks, the traffic flow is controlled by signal system and signal optimization is one of the most effective ways to improve the network

performance. Based on the proposed traffic state prediction model, one can perform signal timing optimization in a real-time manner.

Overall, the study successfully developed a reliable and robust traffic flow prediction model for arterial network considering heterogenous data sources.

### 9.3. Future research direction

The real-time traffic state estimation and short term prediction of arterial network is a very challenging field of research. The following issues remain to be explored during future research:

- Traffic state prediction under actuated and adaptive signal control

So far only the traffic flow dynamics of arterial road under pre-timed signal control strategy is discussed. For actuated and adaptive signal controls, the signal timing plan cannot be obtained in advance. Therefore the model needs to estimate (predict) signal timing parameters simultaneously with other traffic flow states;

- Investigate the model accuracy given precise future demand information

In this study, we proposed a traffic state prediction model consisting of real-time traffic state estimation and short-term prediction modules. The future boundary conditions of the network are predicted with SARIMA technique. One important numerical study is to study the model performance given the precise future demand information. The purpose of such study is to isolate the demand prediction from the proposed framework and examine the prediction power of the traffic flow theory.

- Study the impact of link length on the model output

The length of arterial link is a crucial factor that affects the traffic flow dynamics due to the existence of platoon dispersion. It is therefore very important to study the impact of

link/bay length on the final output of the model. The proposed shifting boundary cell model approximates the traffic flow state of each arterial link with a queuing area and a moving area where vehicles are assumed to be uniformly distributed. Hence if the link is so short that vehicles departed from upstream link move as a platoon before reaching the downstream intersection, then the model performance will be affected. In the future study, we want to perform various sensitivity analyses regarding the impact of link length on the model performance.

- Quantitatively investigate the benefit of integration of multiple data sources

One unique advantage of the proposed model is that it can utilize measurements from different types of traffic surveillance devices and combine them to increase the estimation/prediction accuracy. Two types of traffic flow detectors (loop detector and probe vehicle) are discussed in the numerical example. In the future work, we need to quantitatively evaluate the effect the integrating multiple data sources.

- Development of network flow model

The current traffic flow model only emphasizes on the traffic flow dynamics along one corridor, however in reality, the arterial road is a two-dimensional network where each link can have more than one upstream and downstream links. Hence the traffic flow of a link is not only affected by the signal but also the traffic flow status of all adjacent links. In a network context, both flow merging, diverging, queue blockage and spillback from turning pockets need to be considered;

- Numerical comparison with other prediction methods

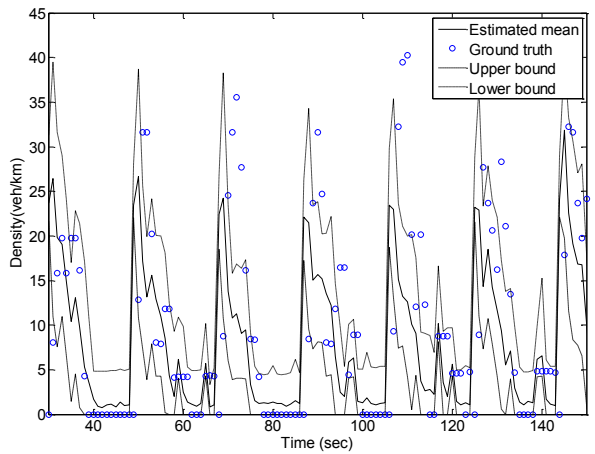
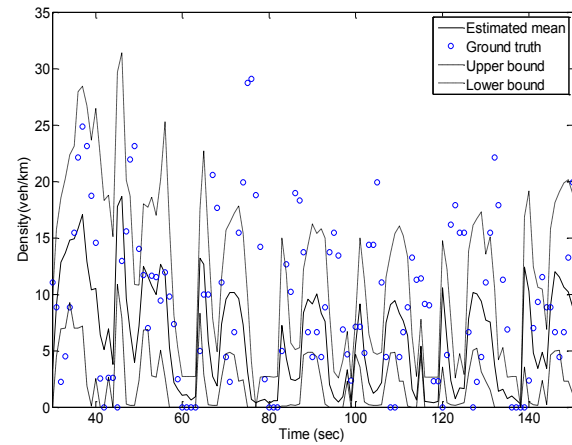
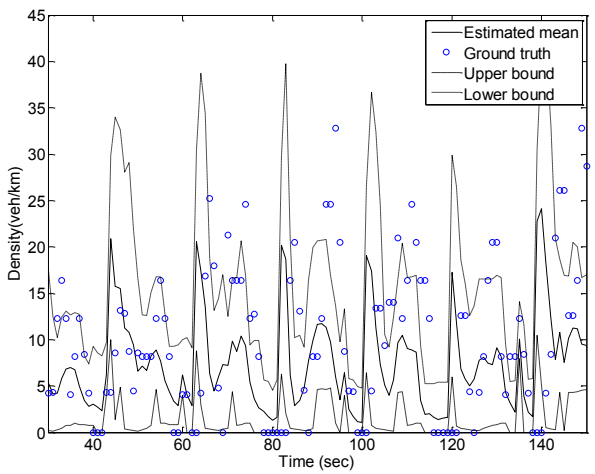
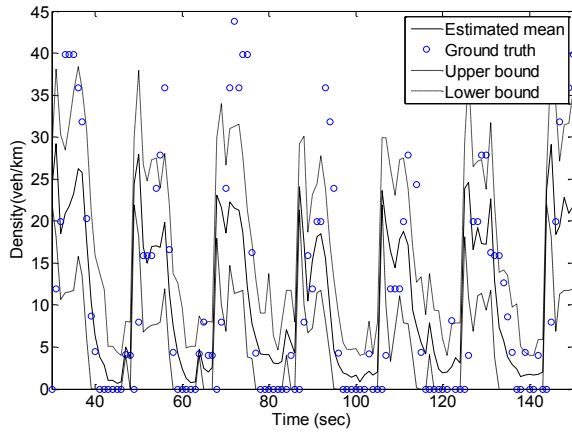
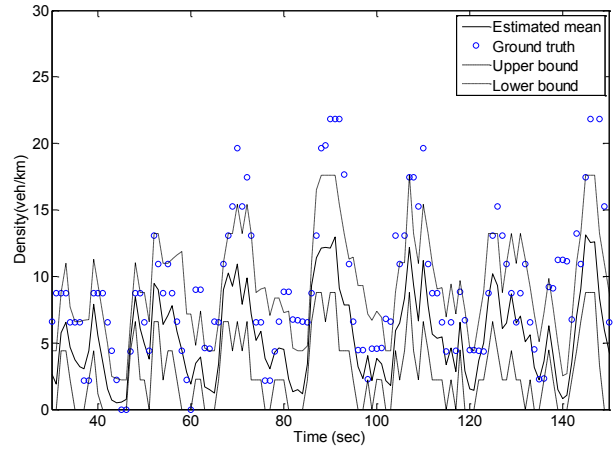
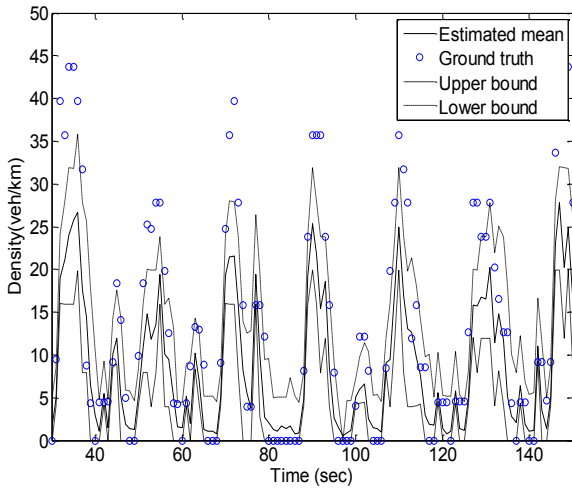
The short-term traffic flow prediction is very hot topic. Many statistical methods are proposed in literatures including time-series model, ANN model, KNN model, spectral

analysis method. The comparison between proposed model and other statistical model is a very interesting research topic.

# 10. Appendix A: Computation Result of NGSIM Dataset

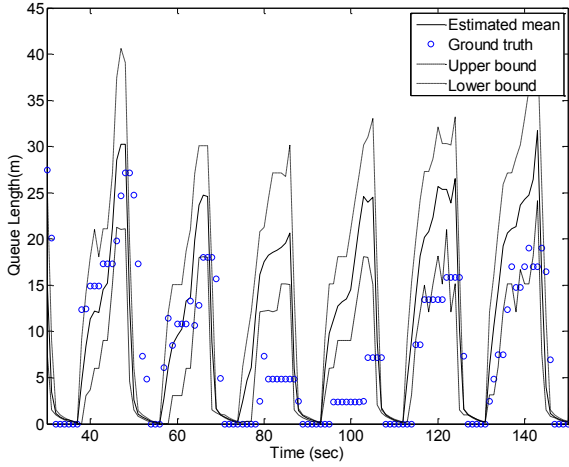
## Northbound

## Southbound

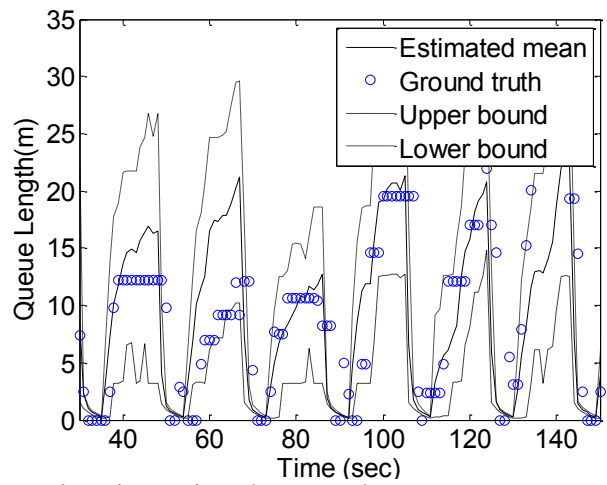
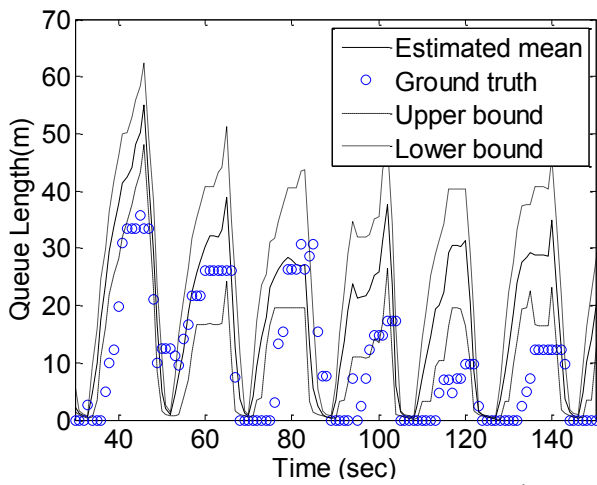
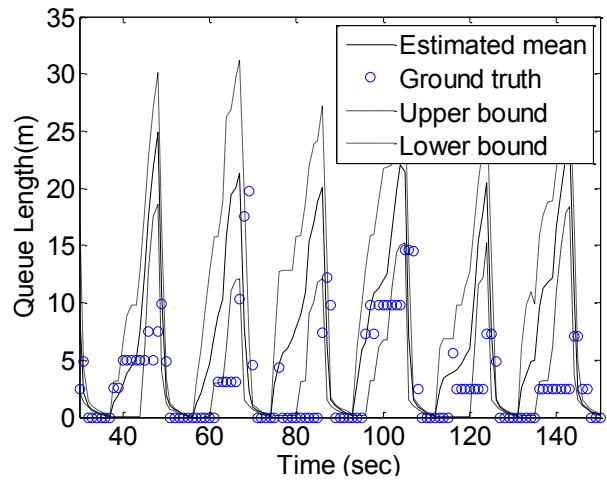
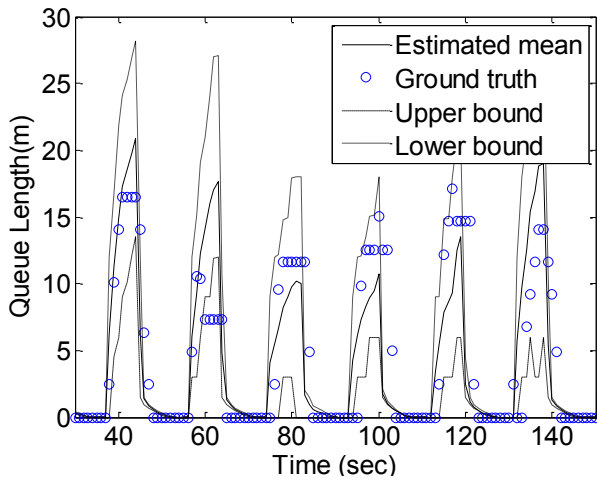
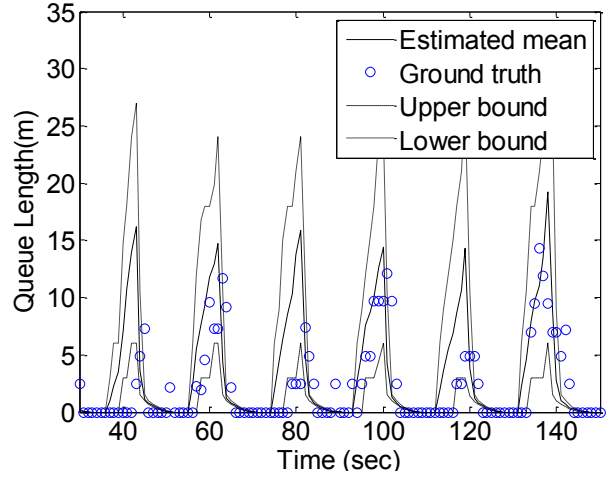


12:45 to 1:00 Peachtree street density estimation using detector data

Northbound

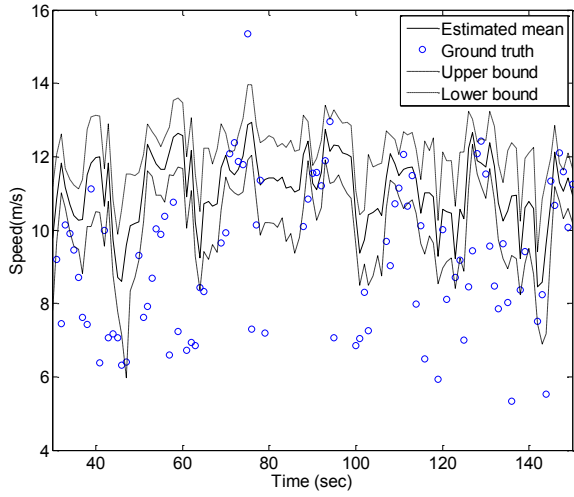


Southbound

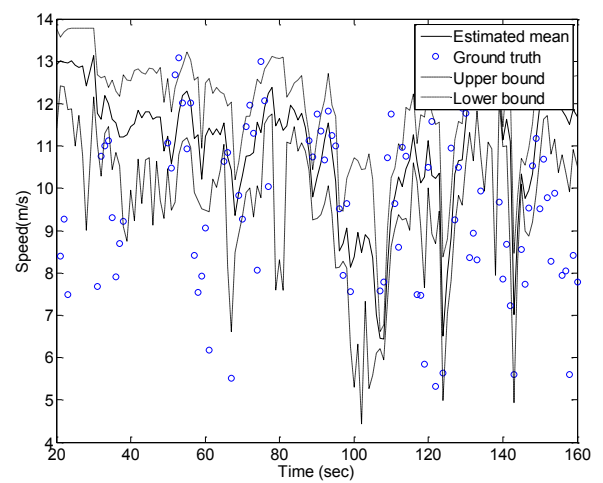
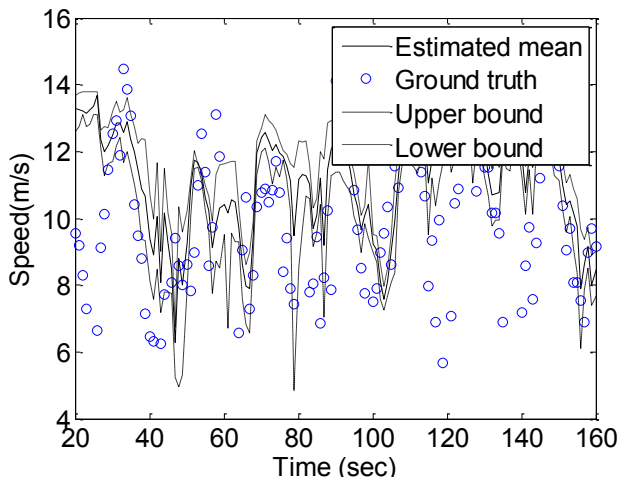
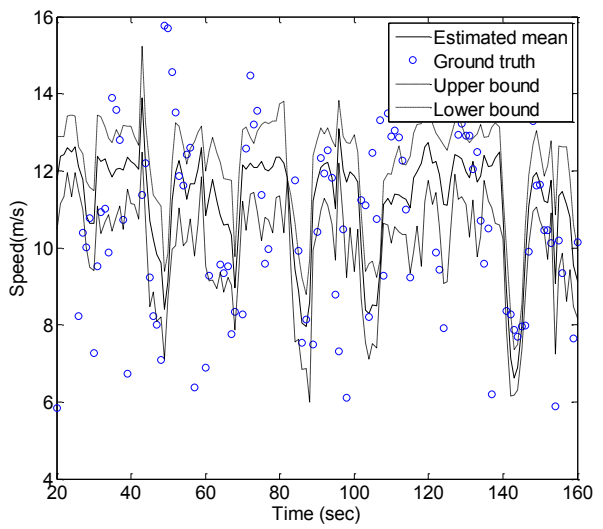
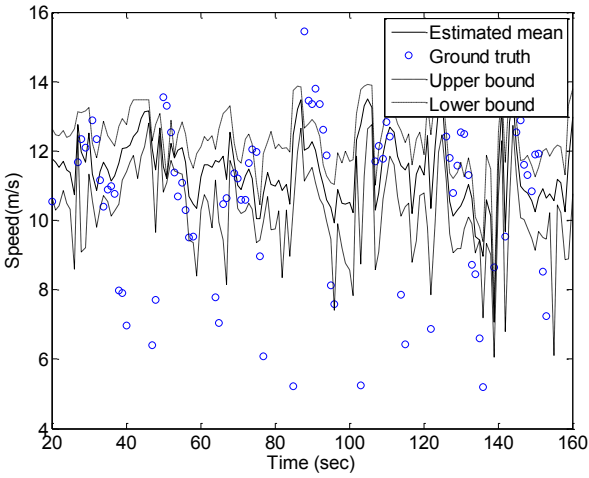
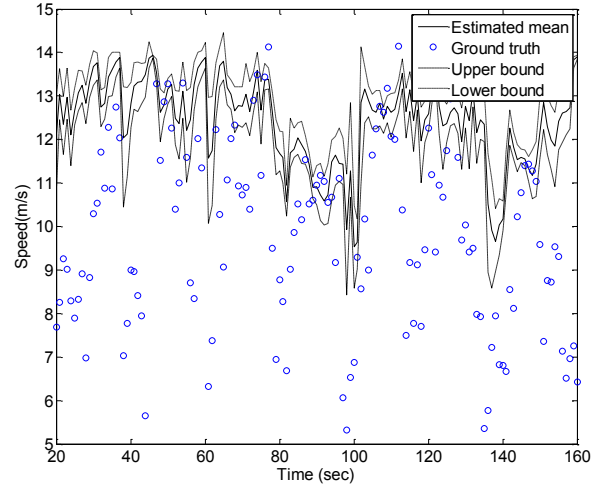


12:45 to 1:00 Peachtree street queue estimation using detector data

Northbound

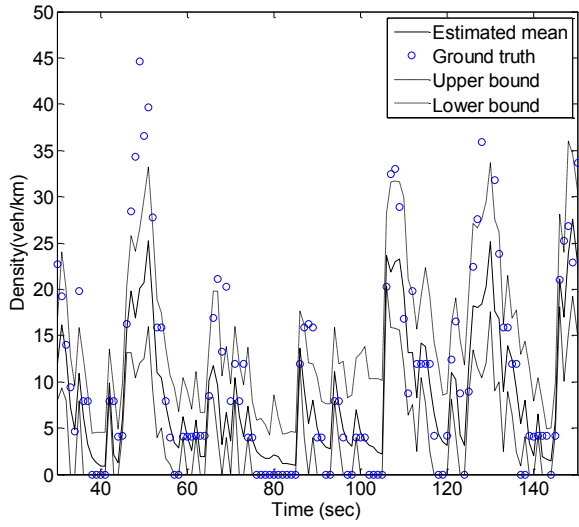


Southbound

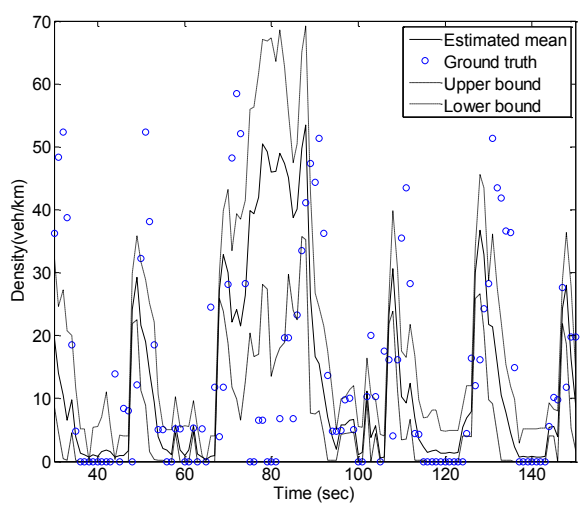
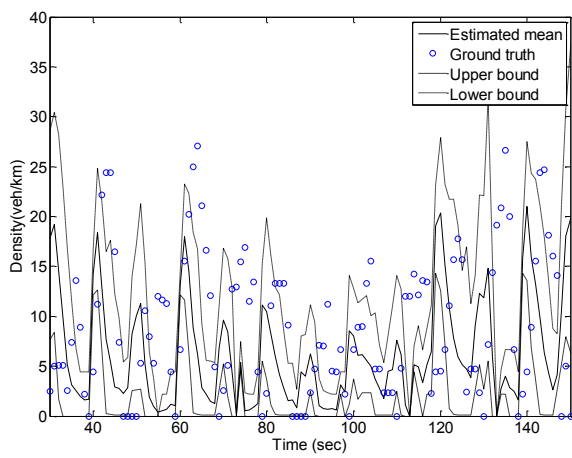
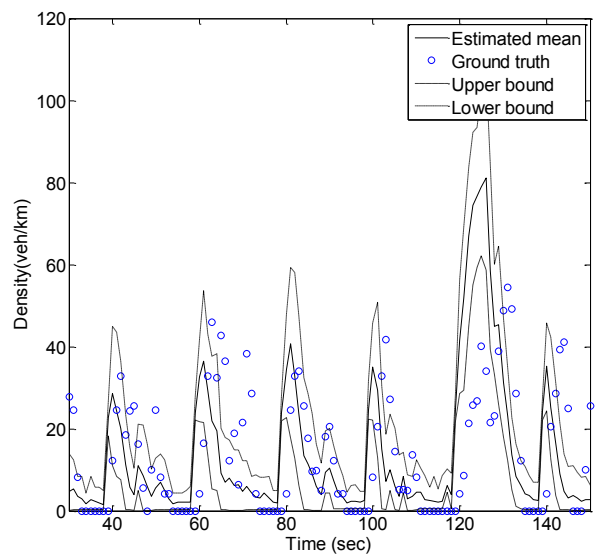
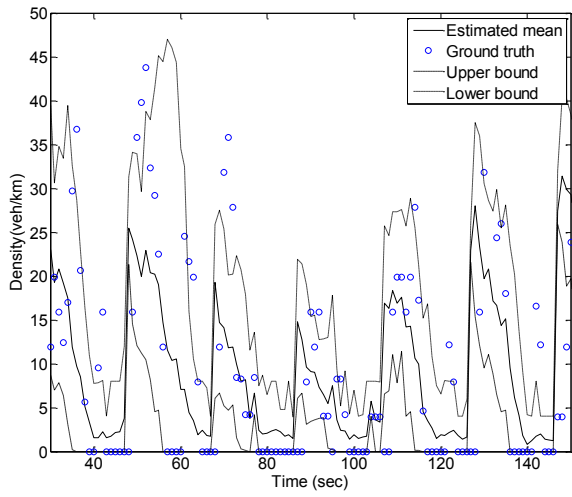
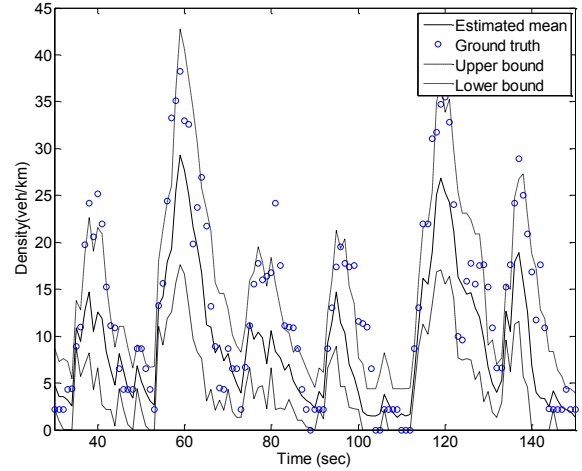


12:45 to 1:00 Peachtree street speed estimation using detector data

Northbound

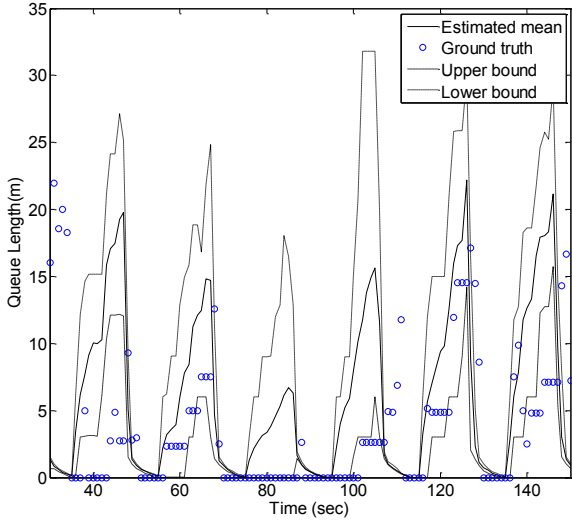


Southbound

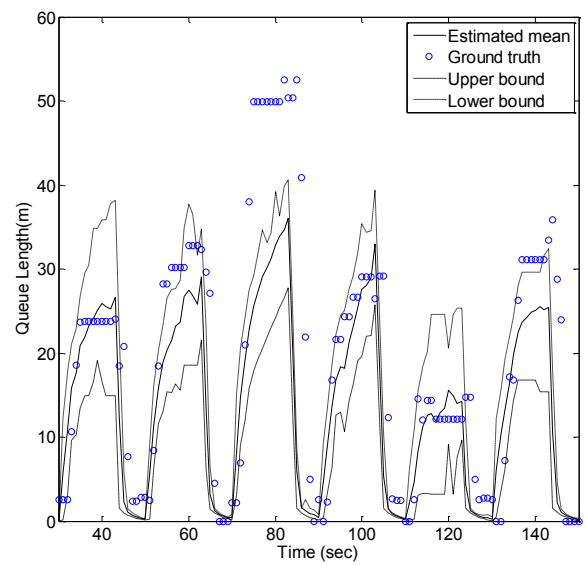
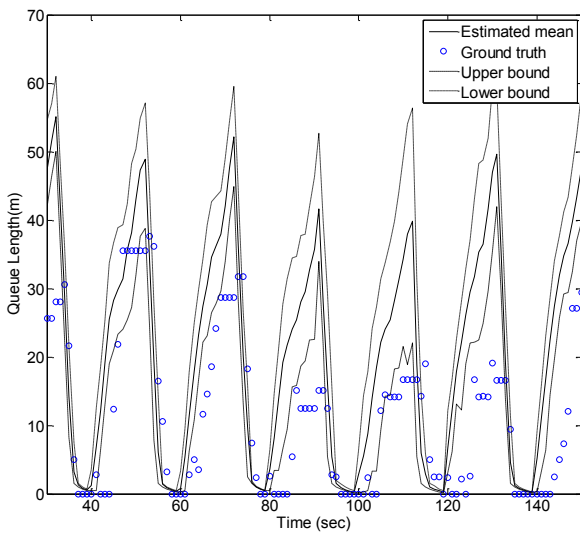
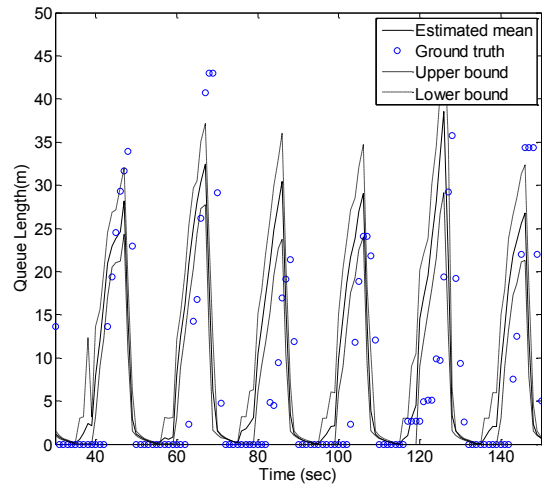
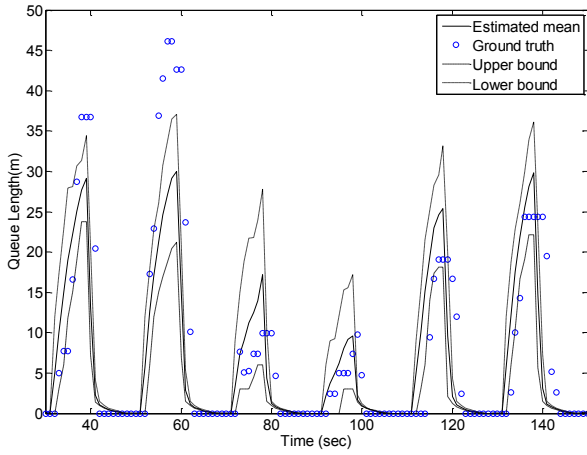
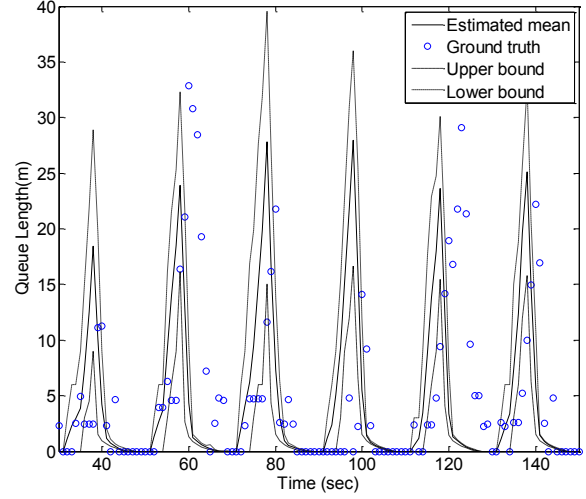


4:00 to 4:15 Peachtree street density estimation using detector data

Northbound

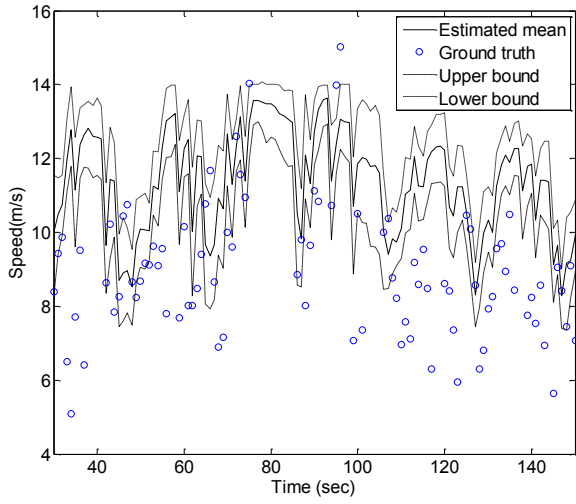


Southbound

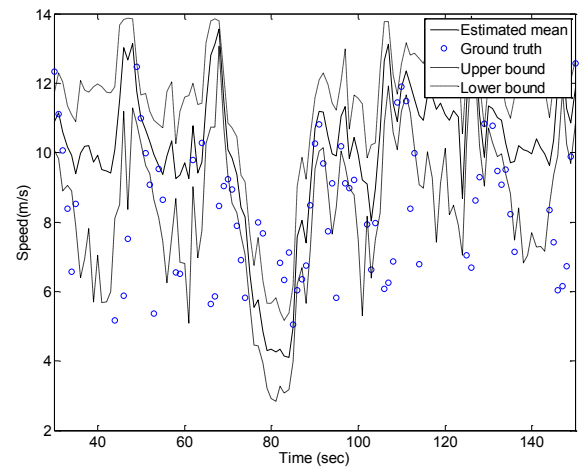
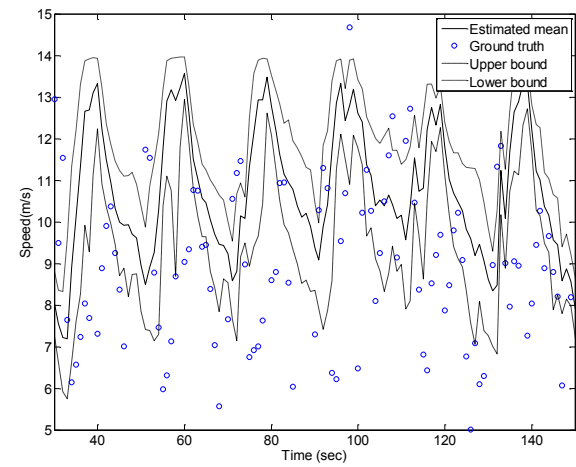
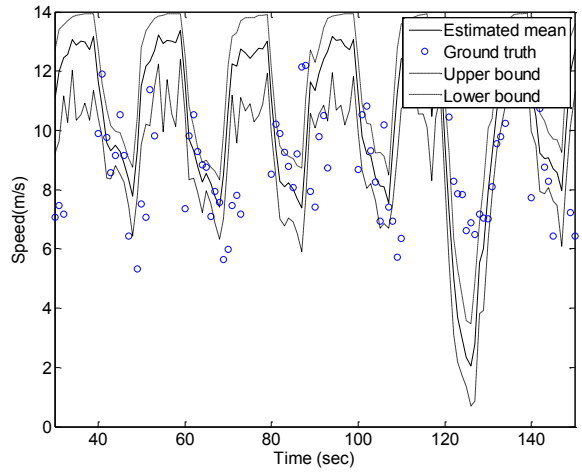
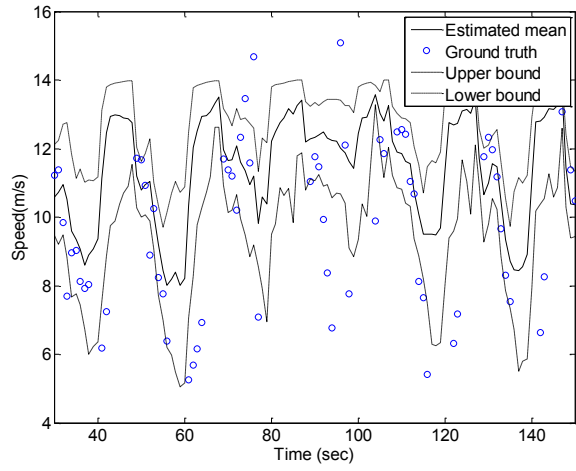
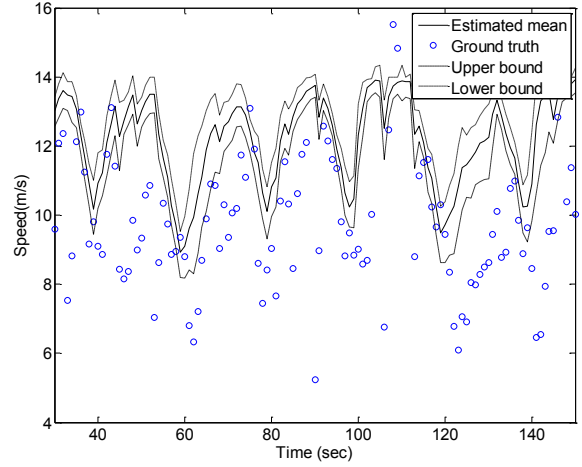


4:00 to 4:15 Peachtree street queue estimation using detector data

Northbound



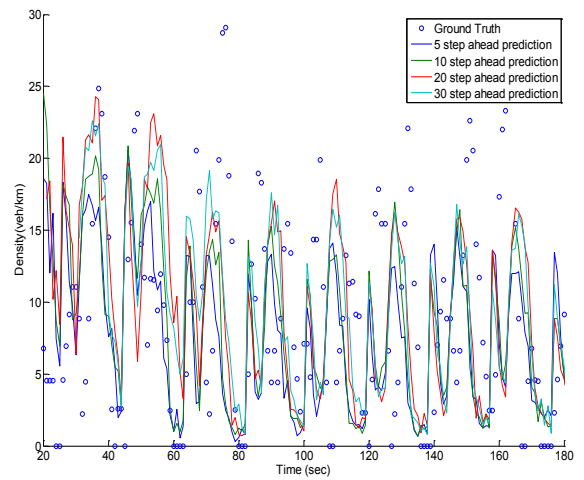
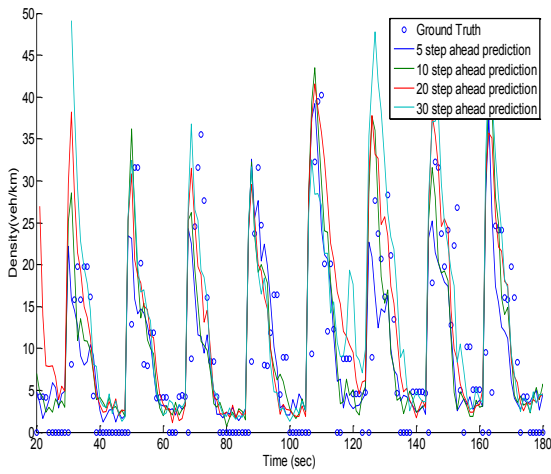
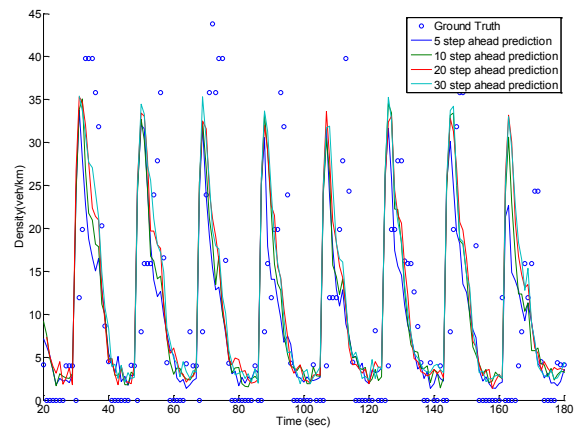
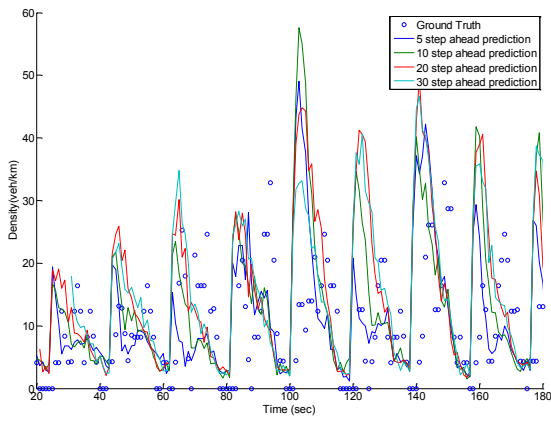
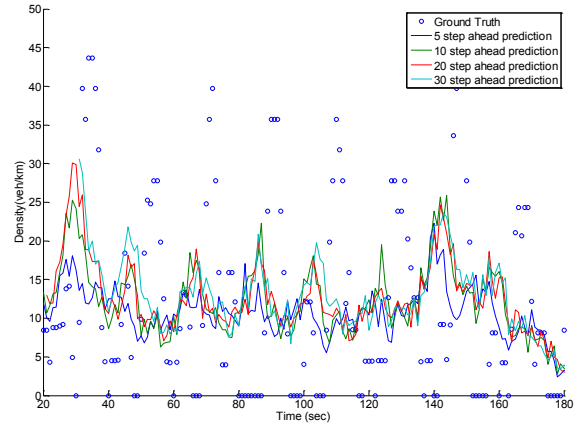
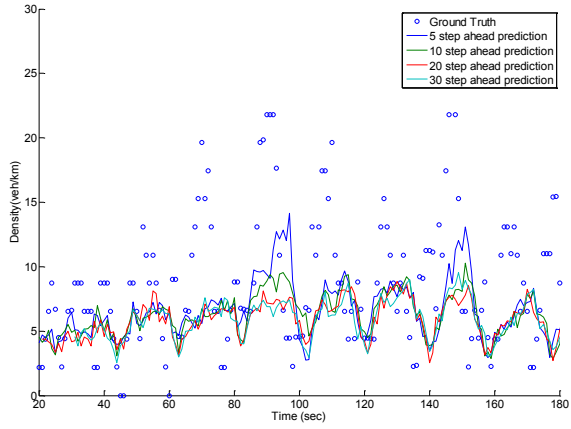
Southbound



4:00 to 4:15 Peachtree street speed estimation using detector data

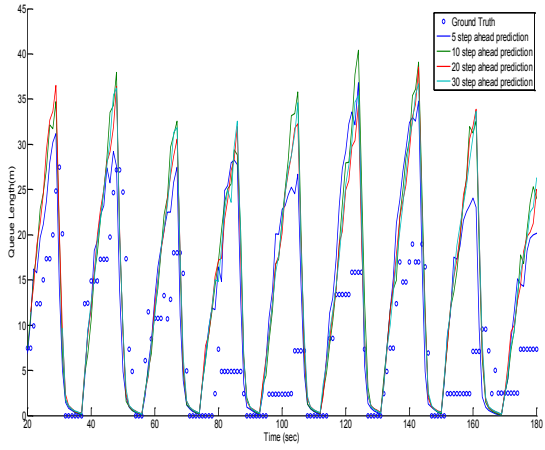
### Northbound

### Southbound

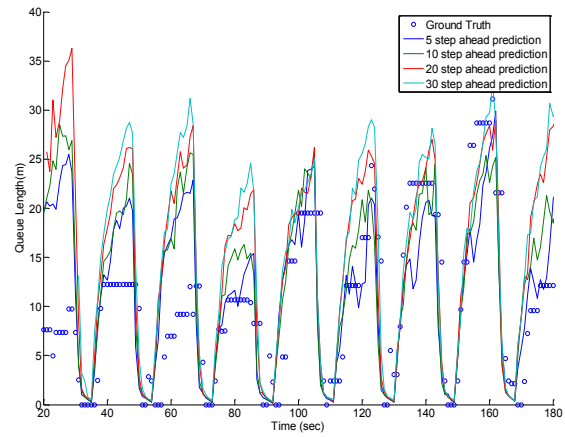
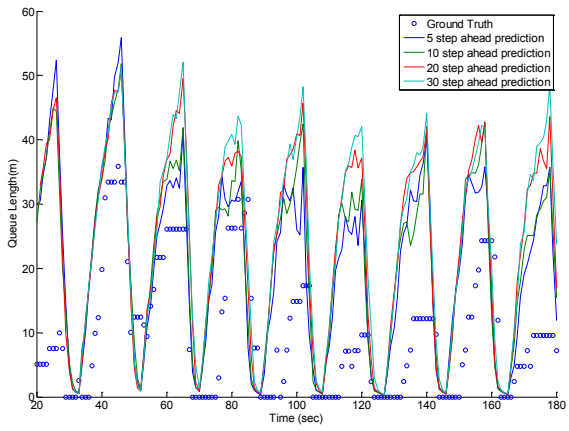
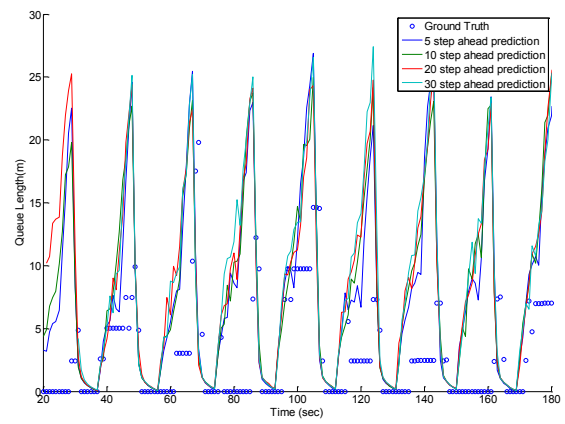
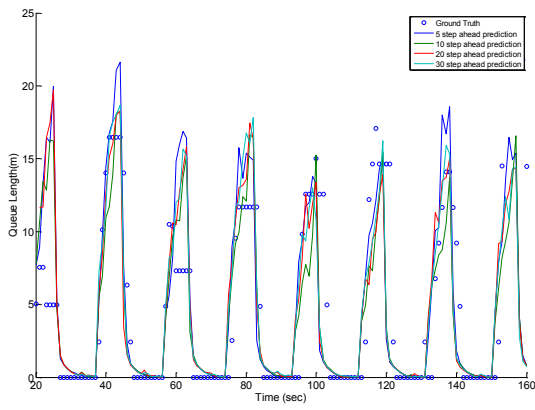
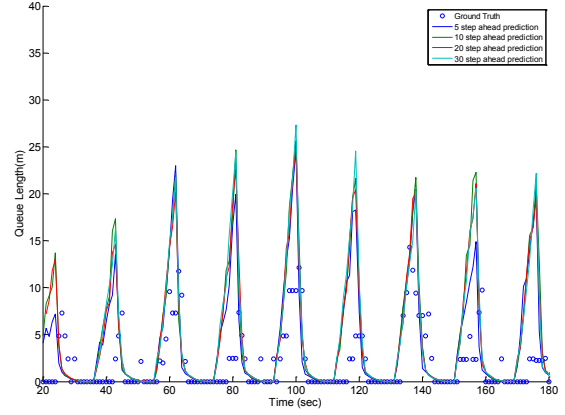


12:45 to 1:00 Peachtree street density prediction using detector data

### Northbound

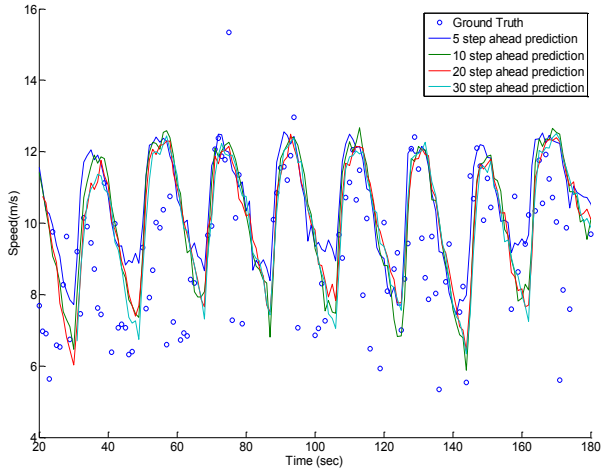


### Southbound

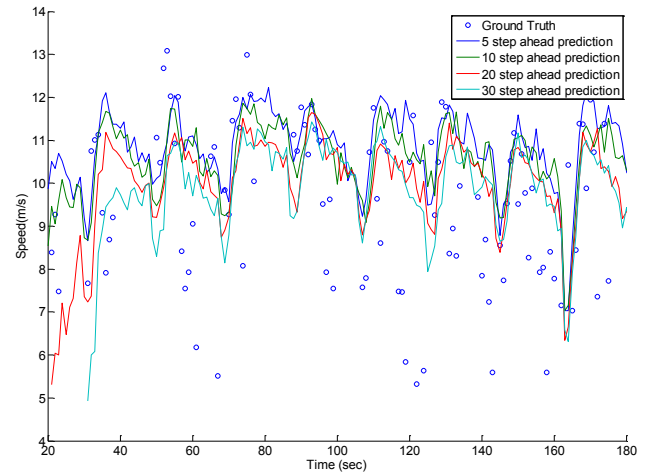
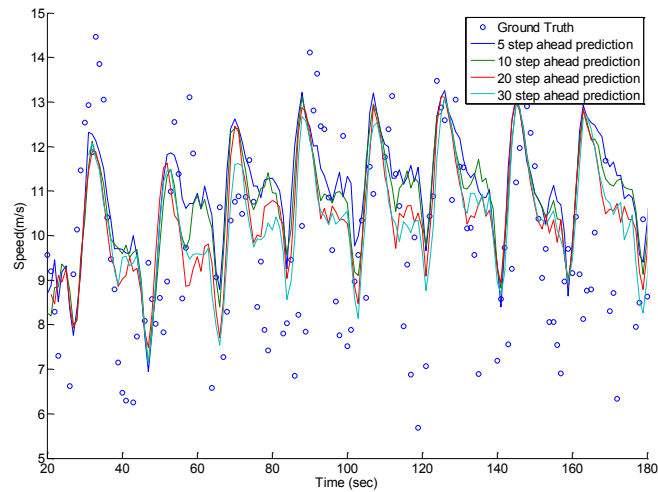
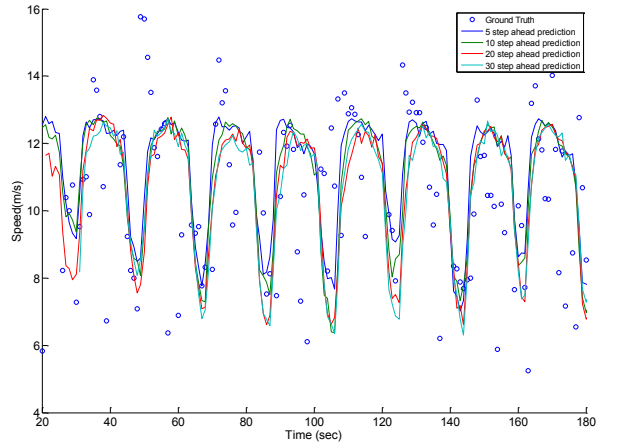
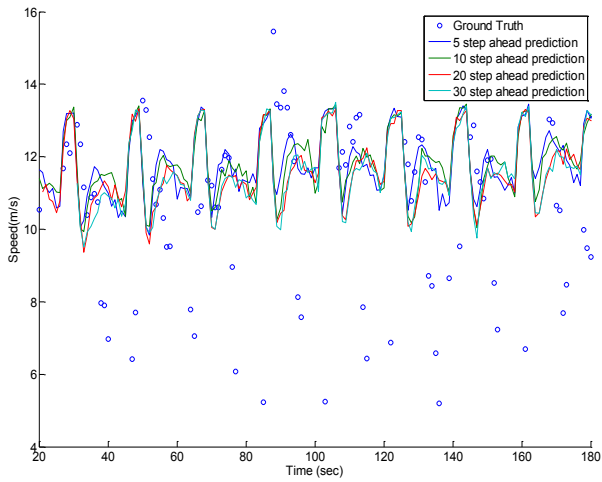
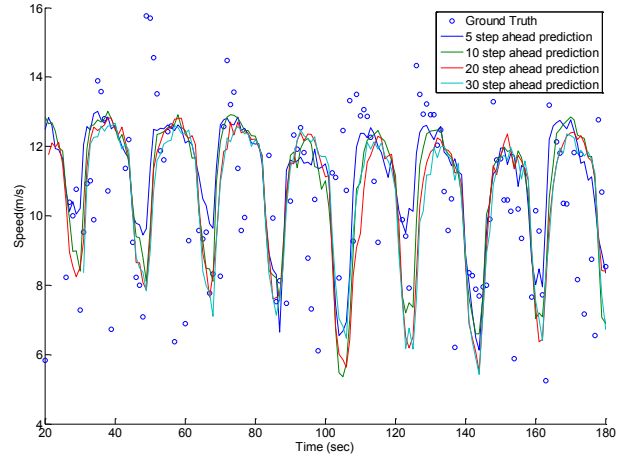


12:45 to 1:00 Peachtree street queue prediction using detector data

### Northbound

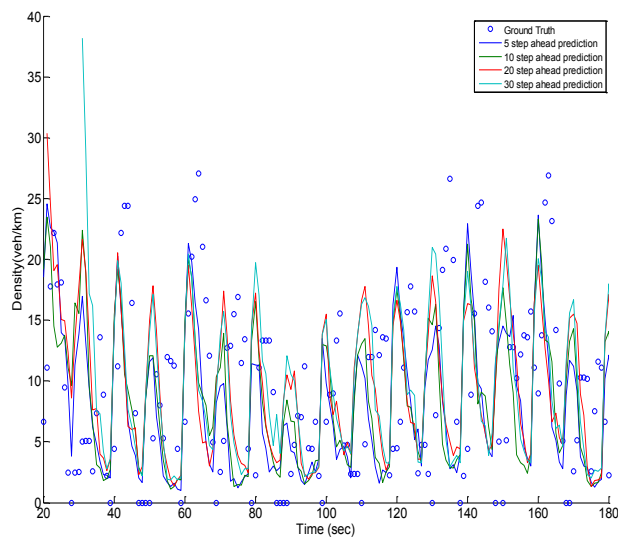
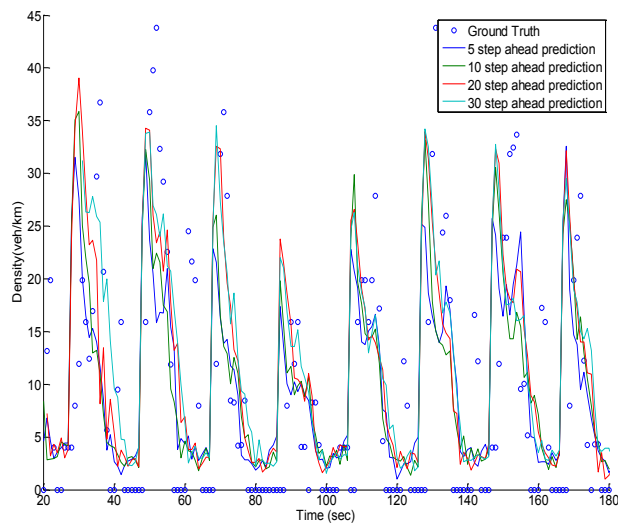
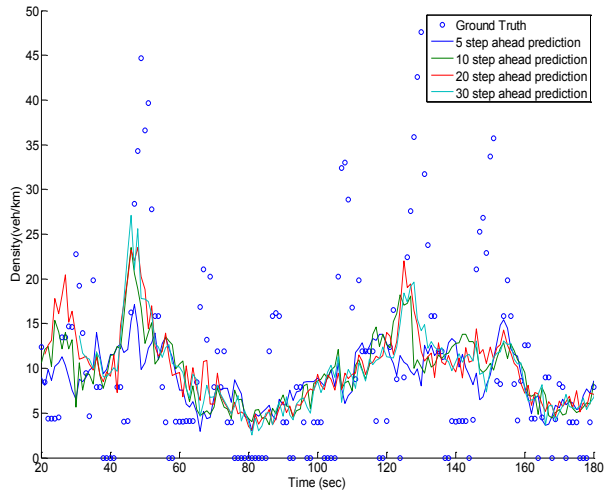


### Southbound

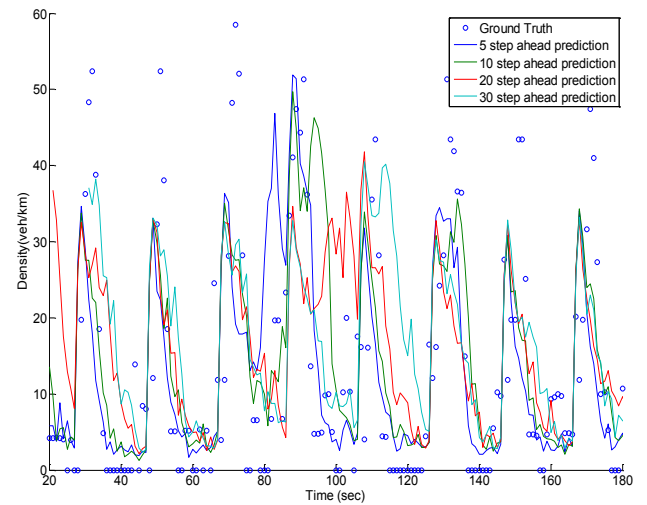
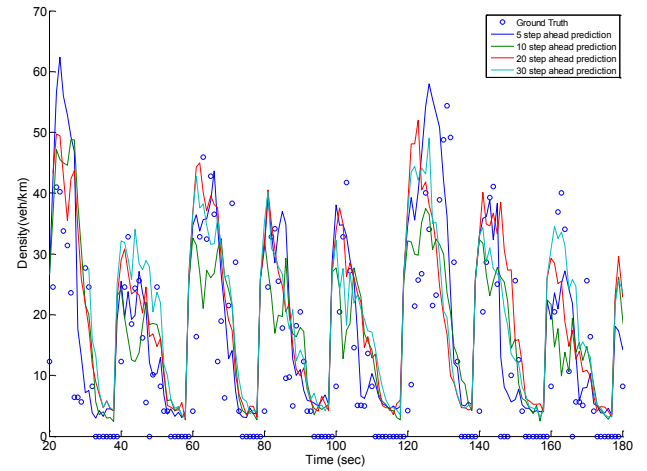
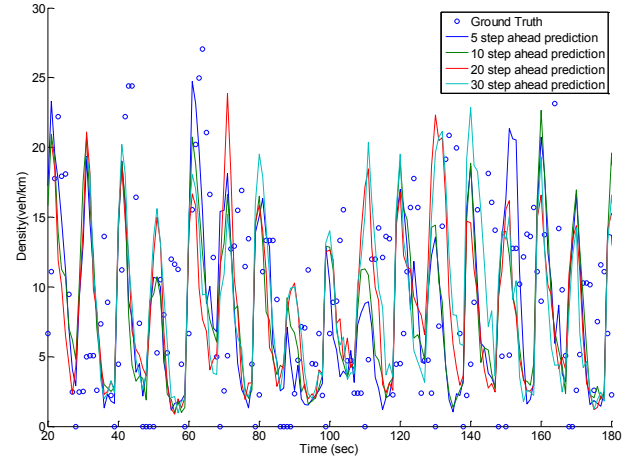


12:45 to 1:00 Peachtree street speed prediction using detector data

### Northbound

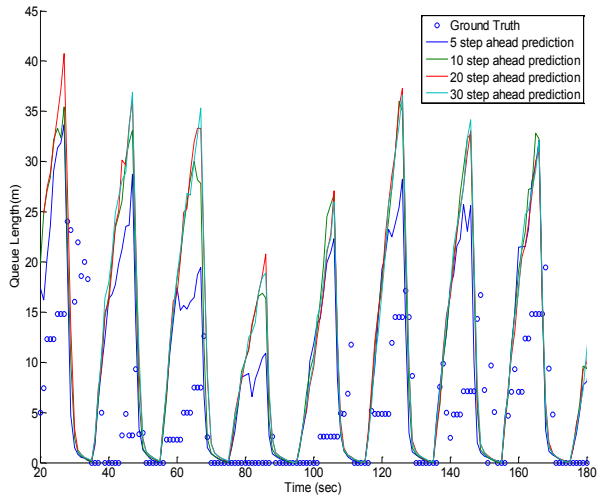


### Southbound

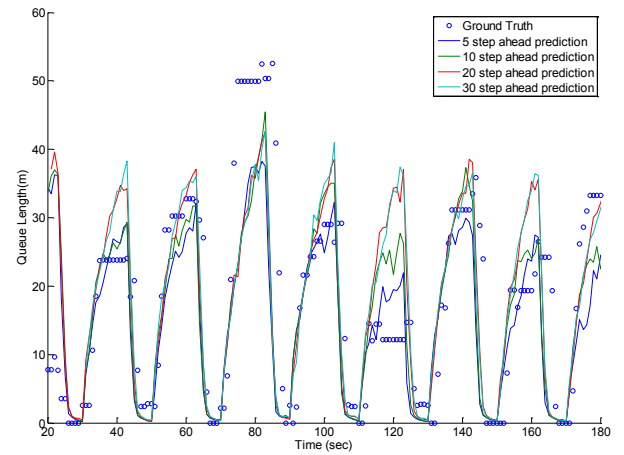
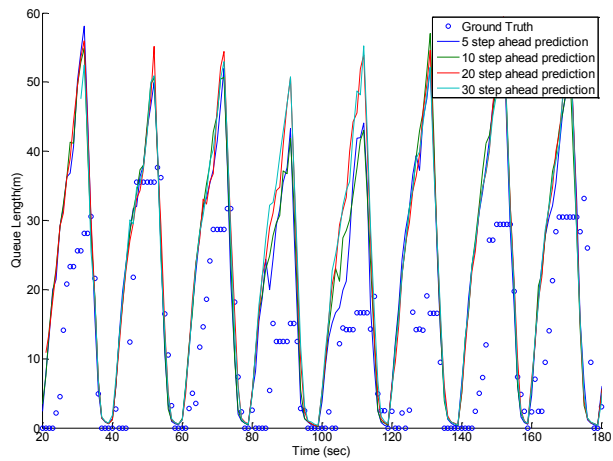
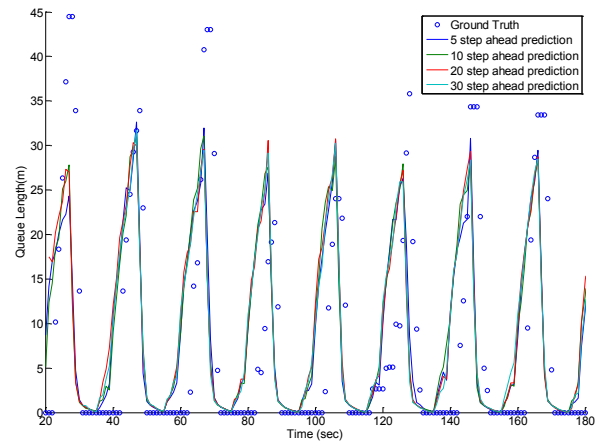
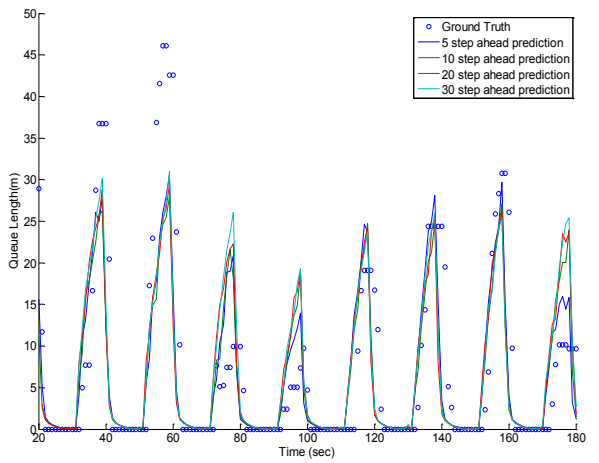
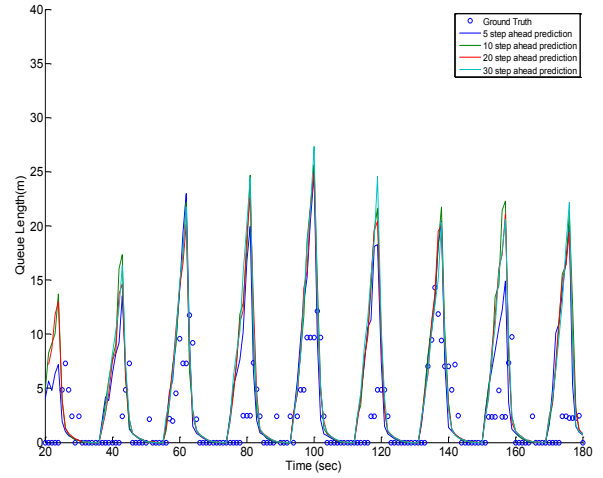


4:00 to 4:15 Peachtree street density prediction using detector data

### Northbound

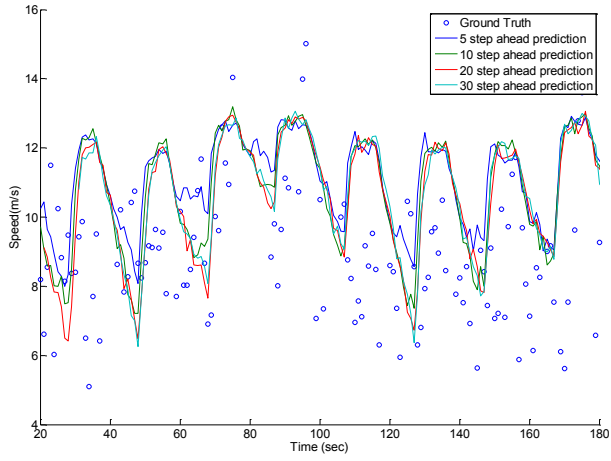


### Southbound

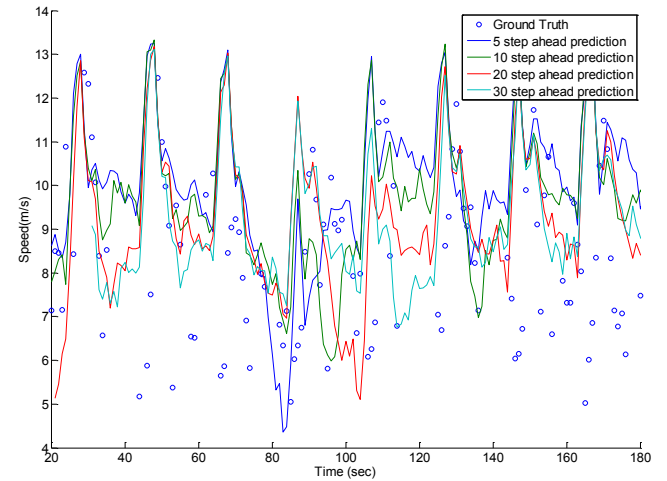
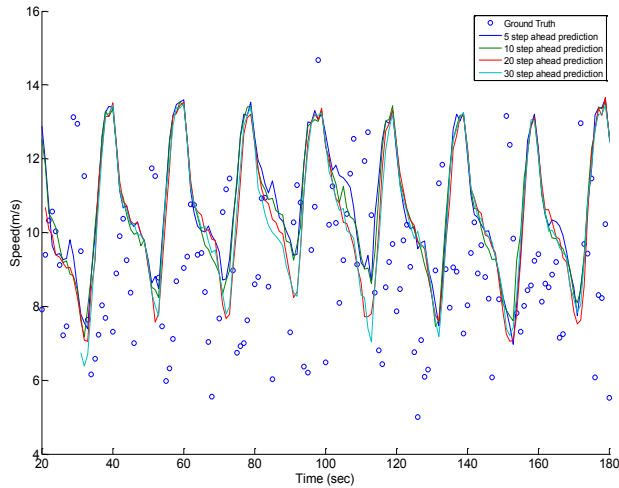
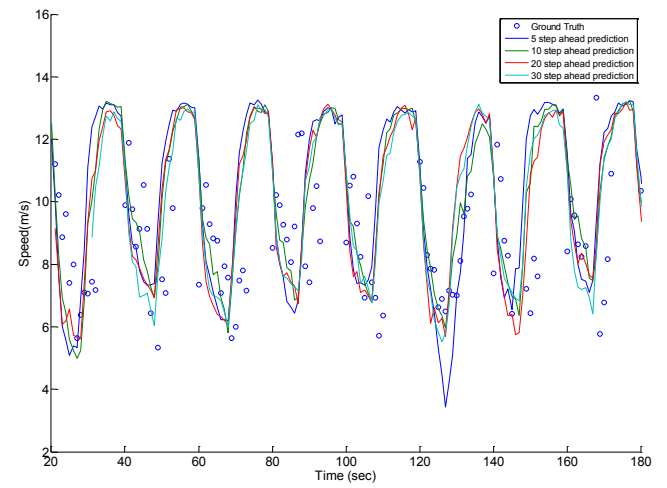
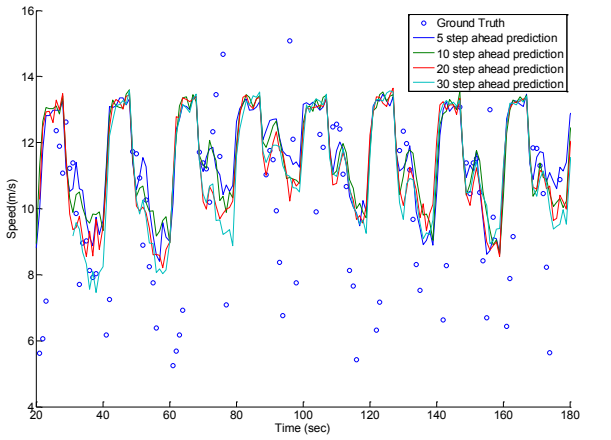
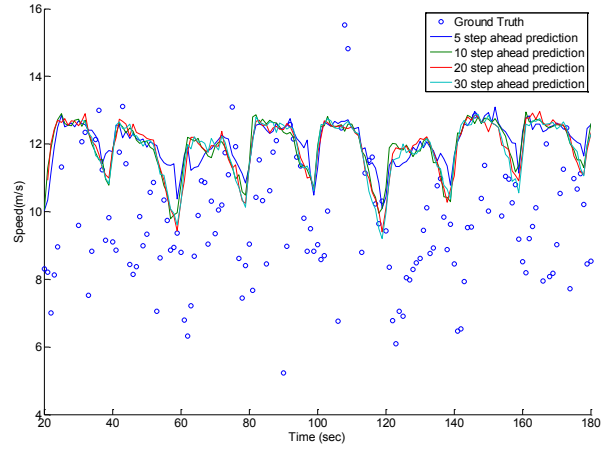


4:00 to 4:15 Peachtree street queue prediction using detector data

### Northbound

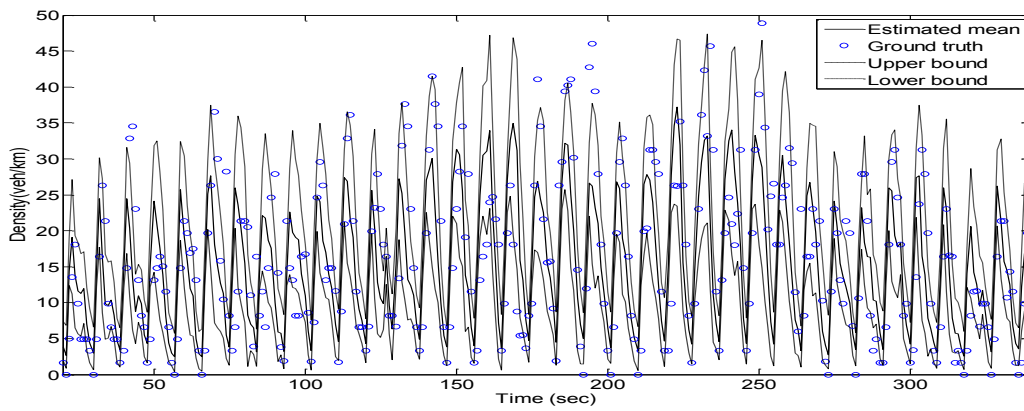
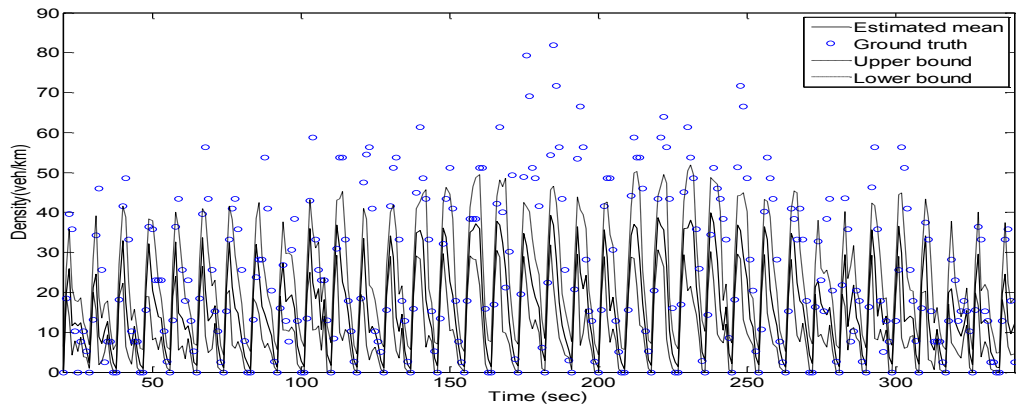
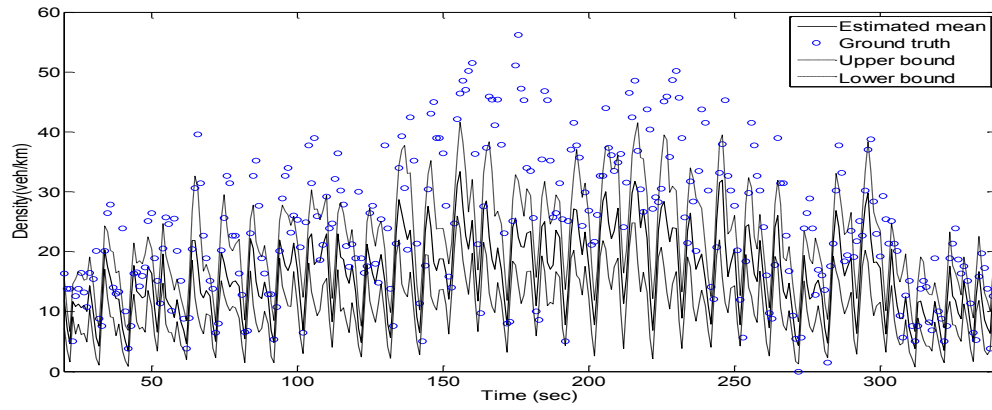
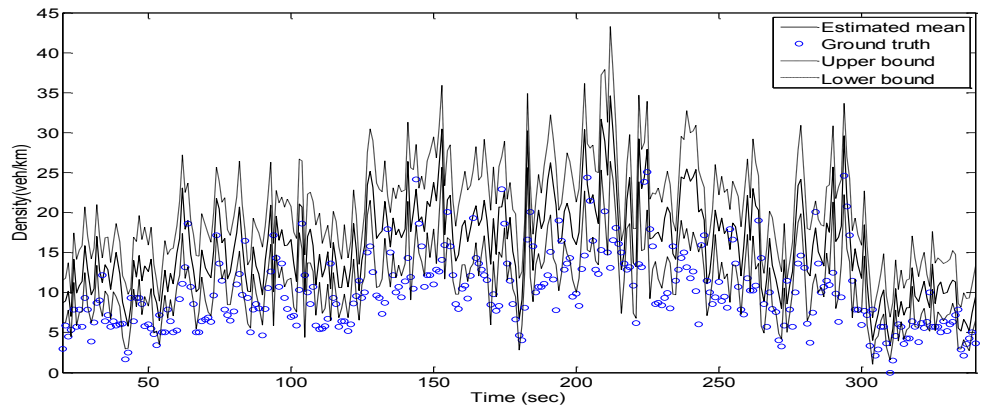


### Southbound

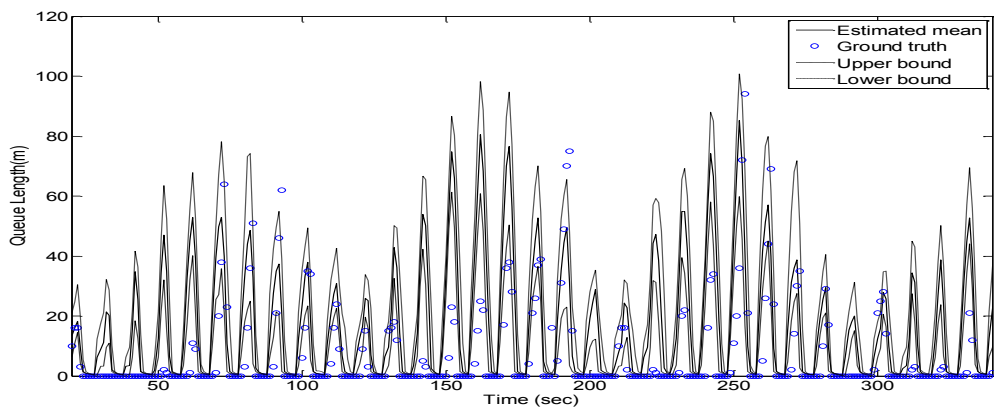
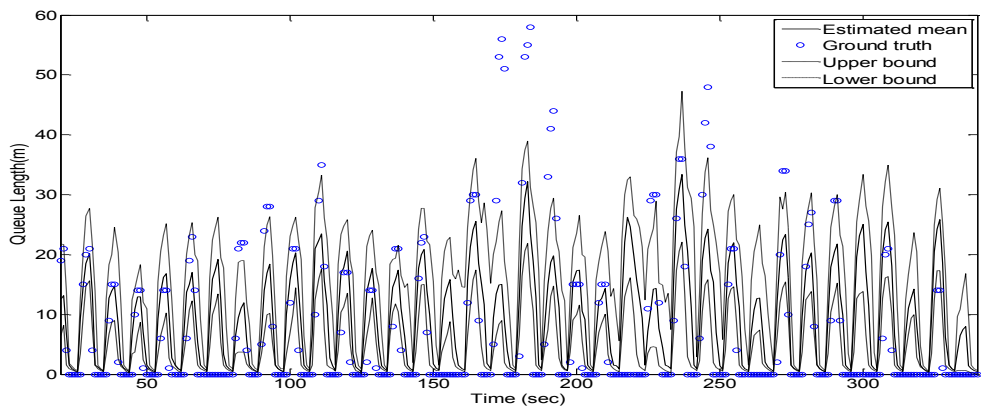
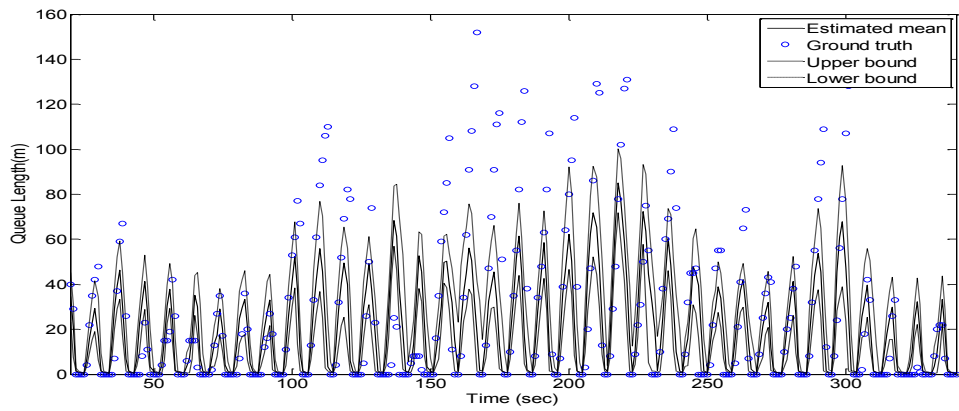
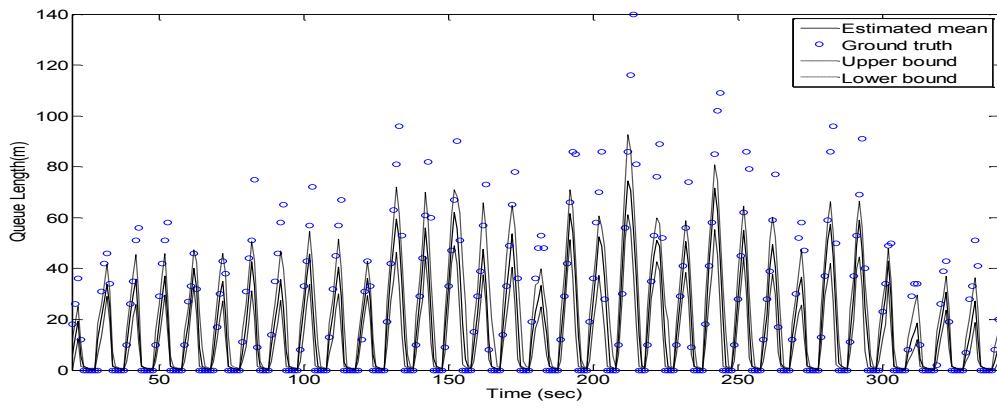


4:00 to 4:15 Peachtree street speed prediction using detector data

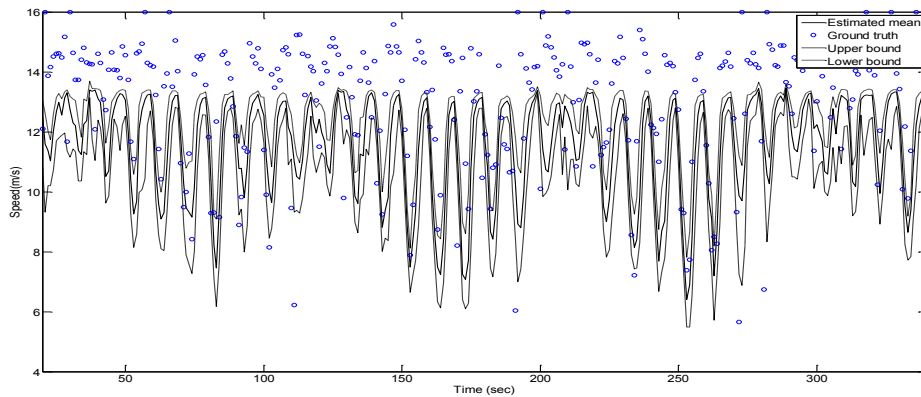
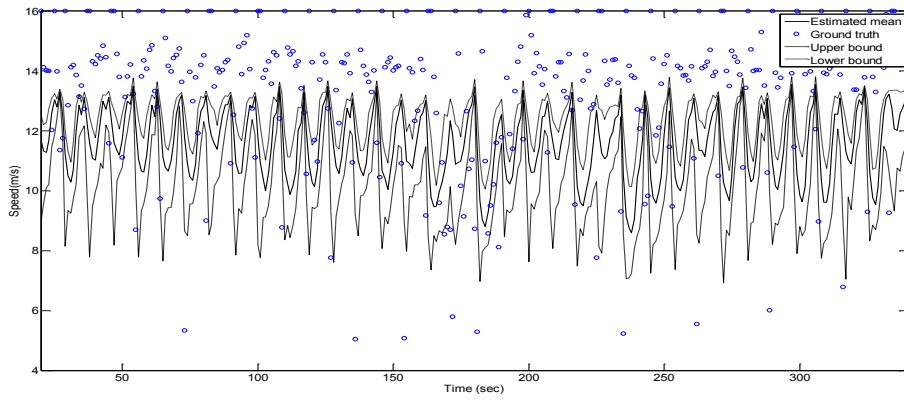
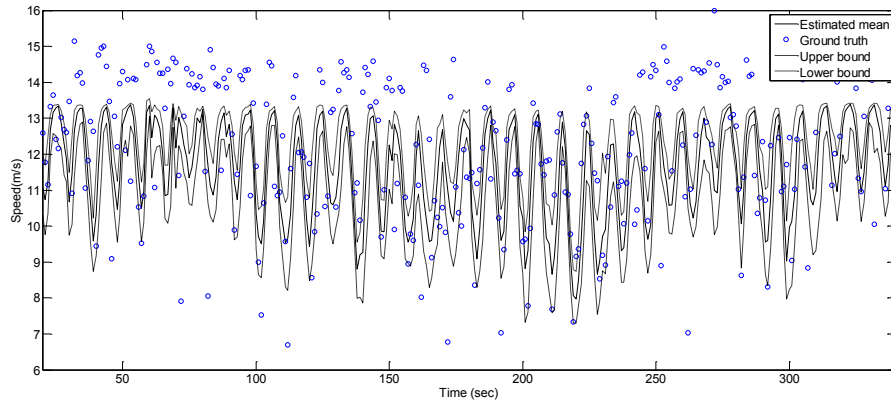
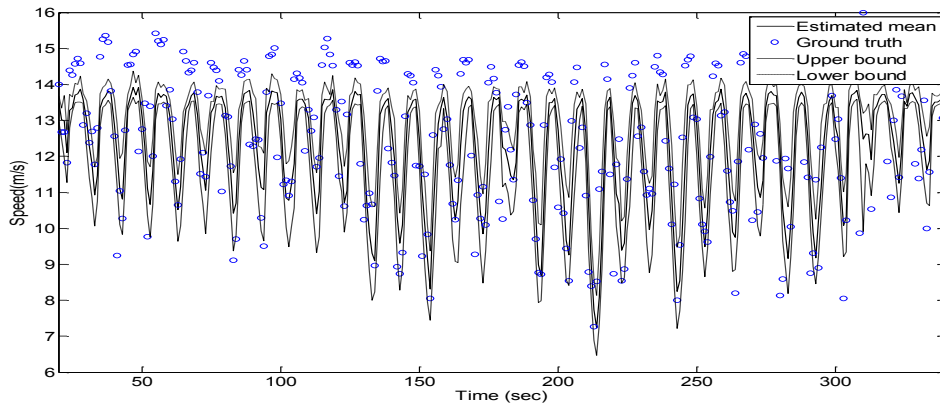
## 11. Appendix B: Computation Results of Simulation Dataset



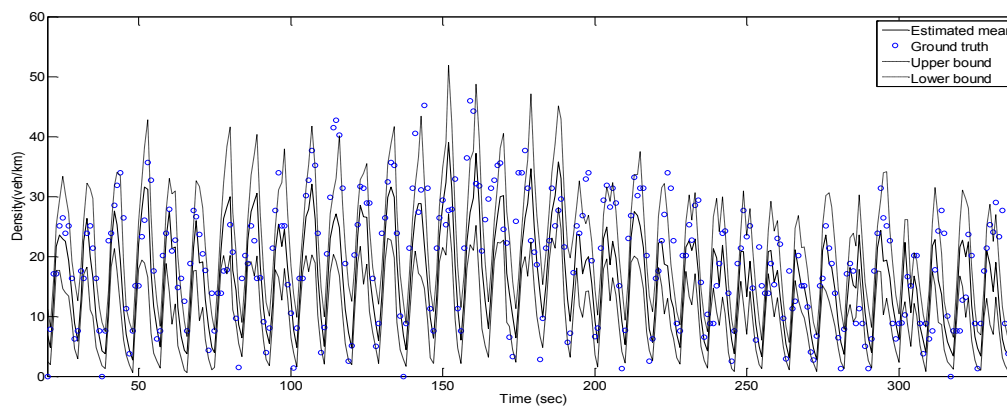
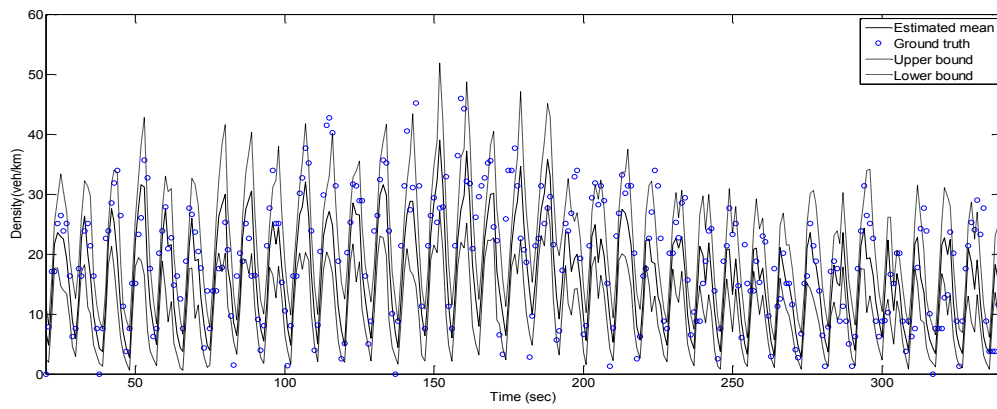
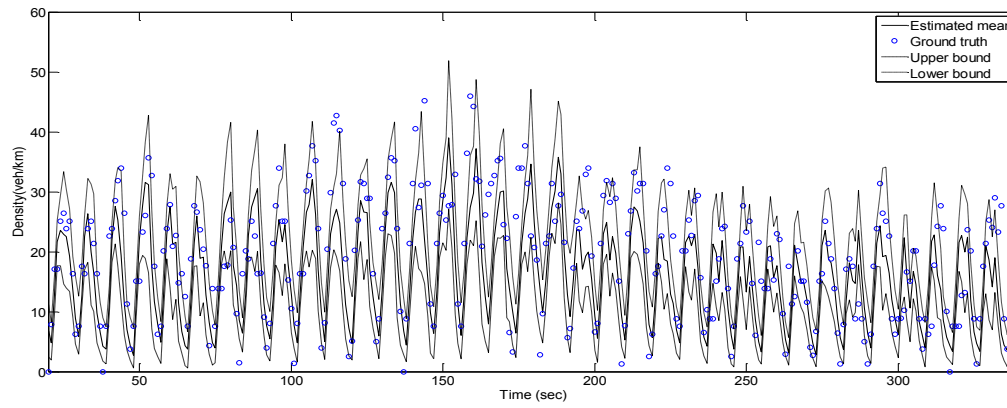
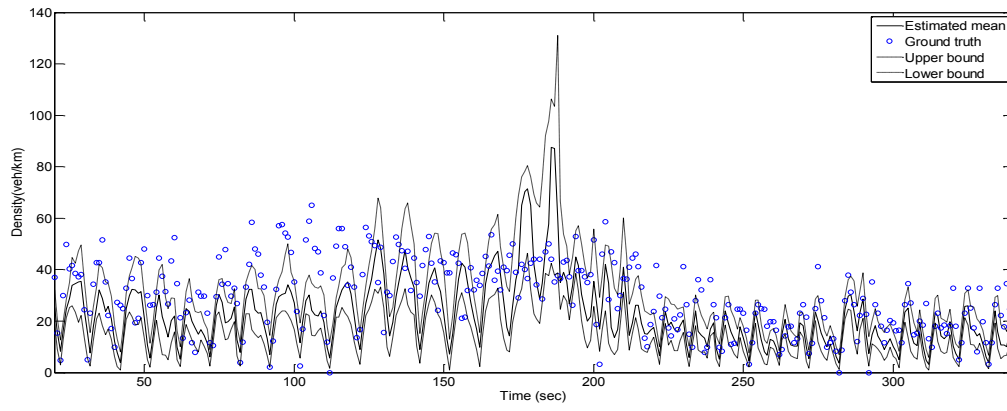
Estimated versus ground truth density of simulated dataset eastbound



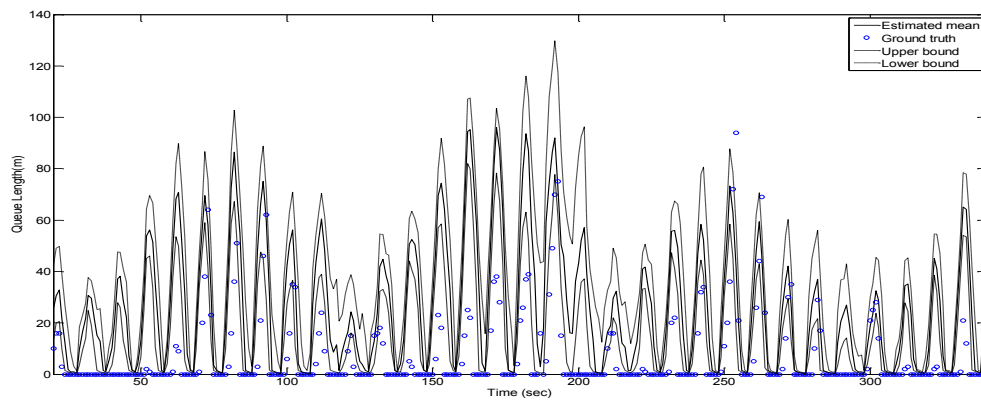
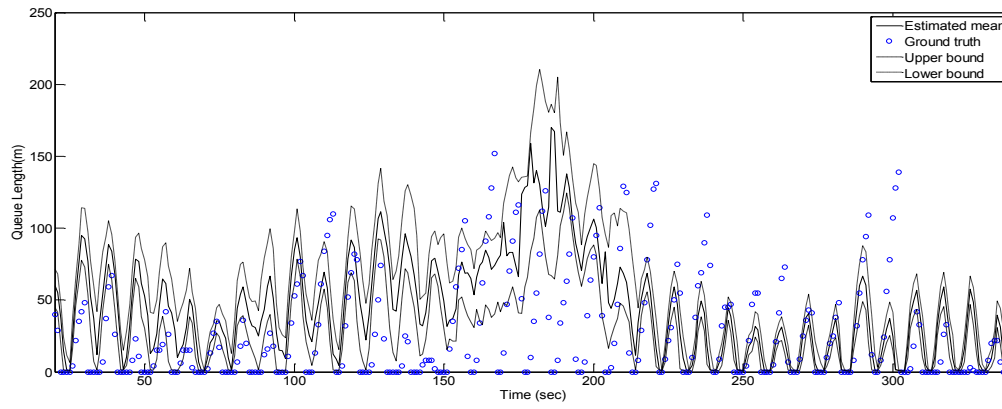
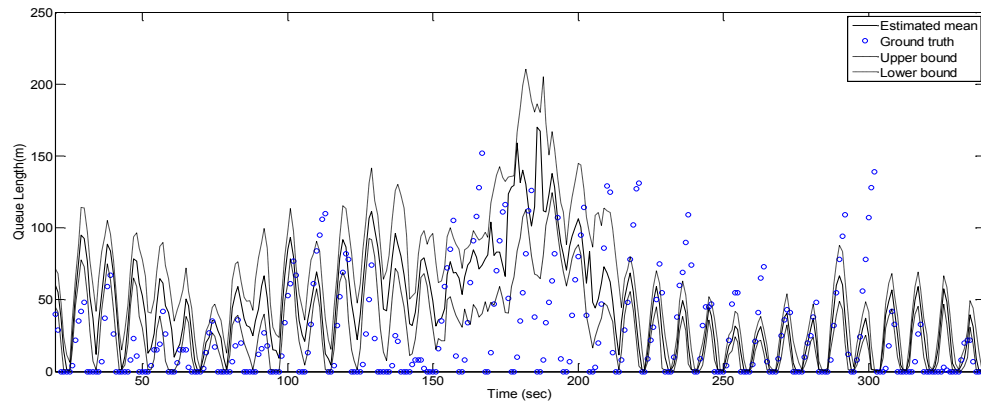
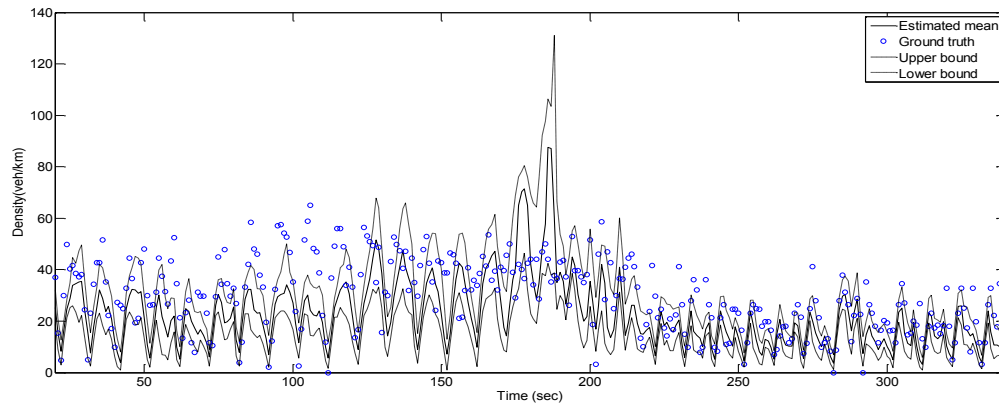
Estimated versus ground truth queue of simulated dataset eastbound



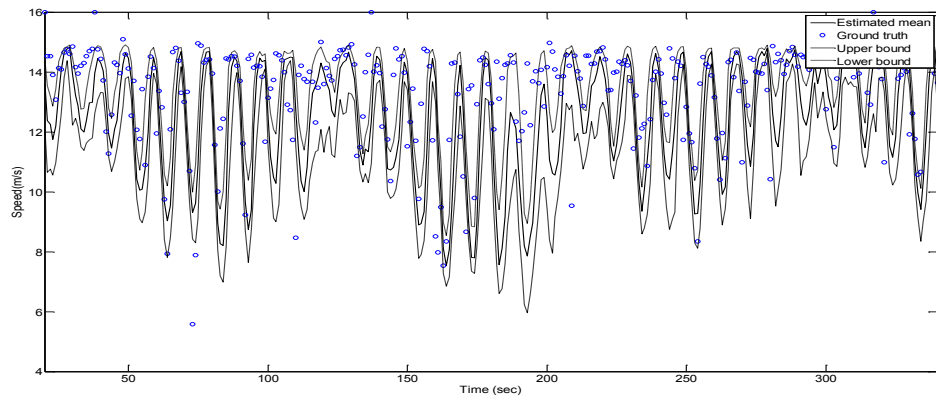
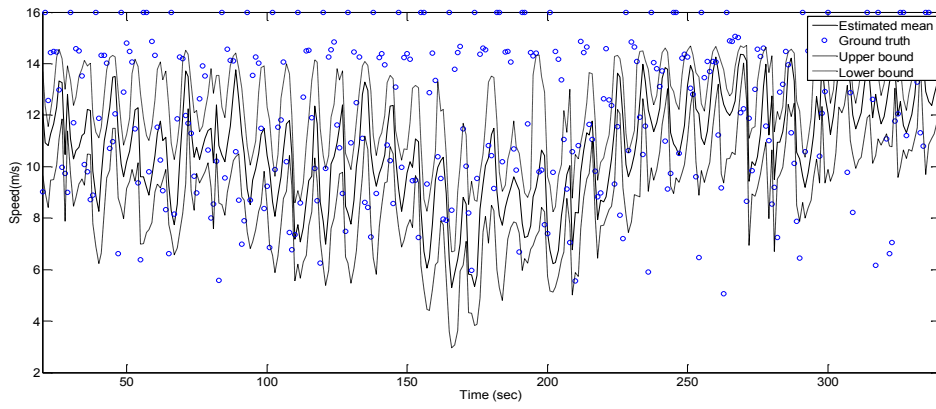
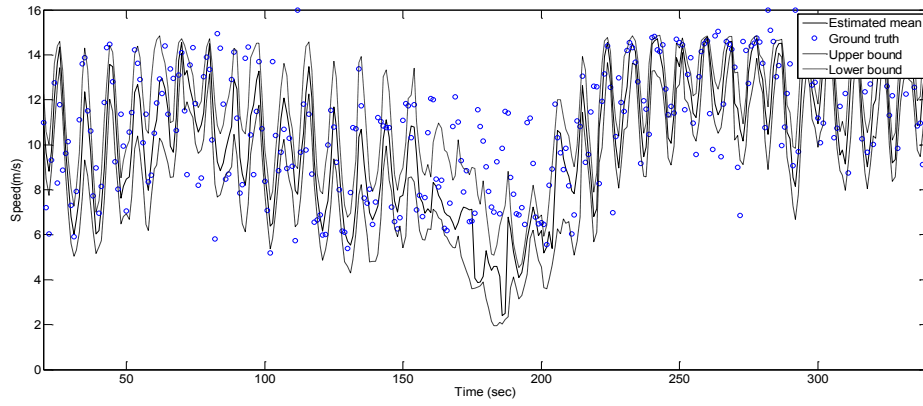
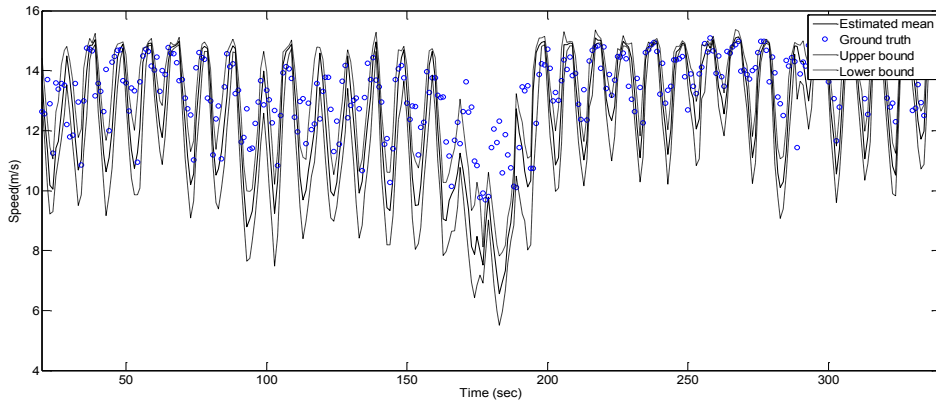
Estimated versus ground truth speed of simulated dataset eastbound



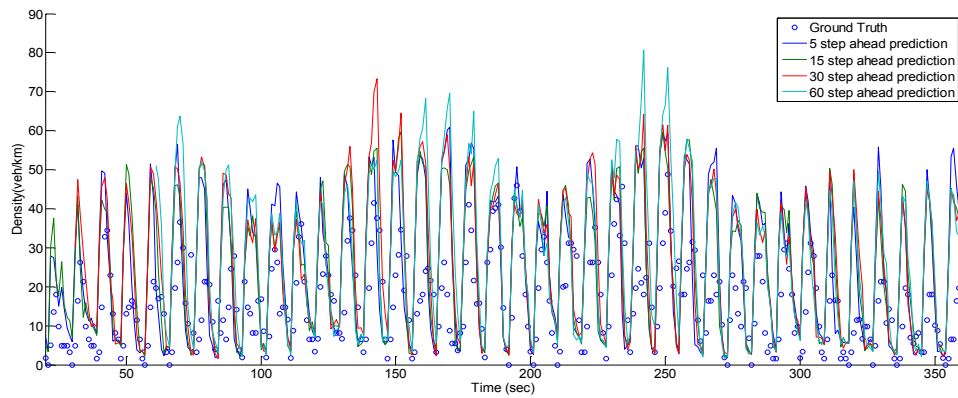
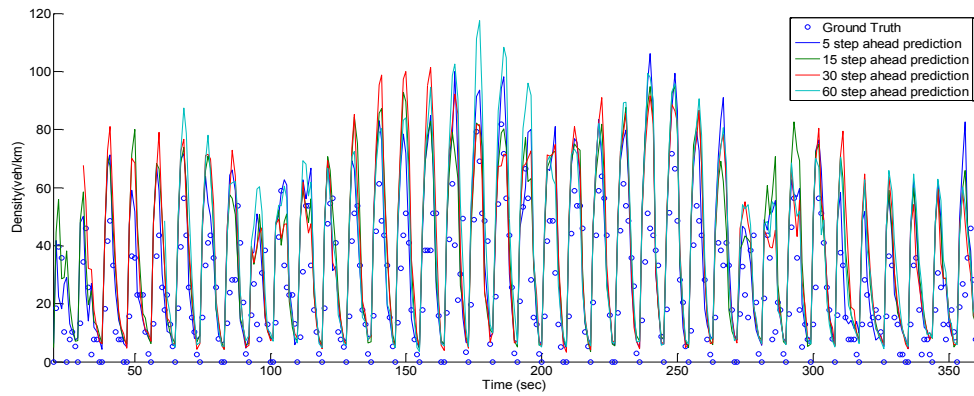
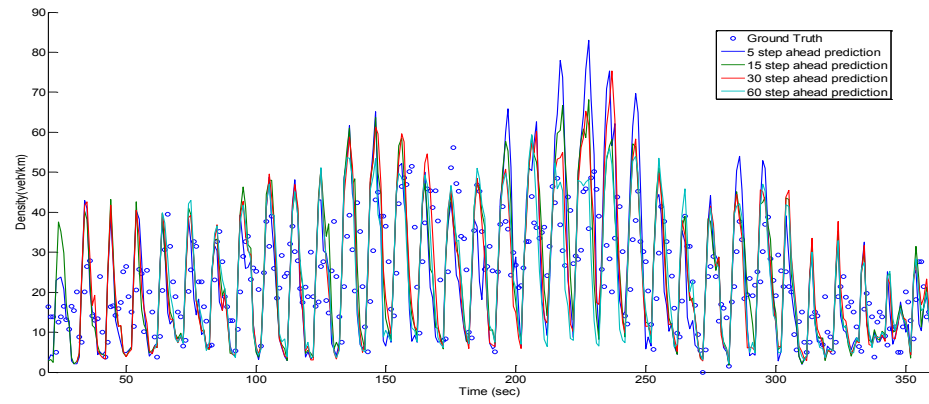
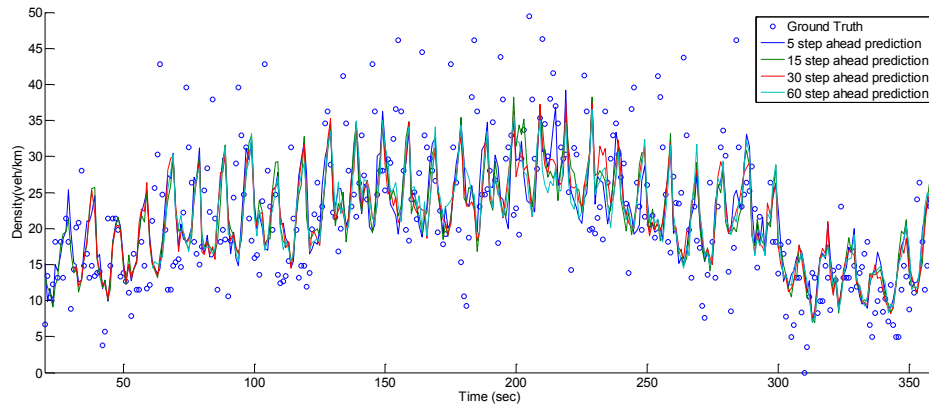
Estimated versus ground truth density of simulated dataset westbound



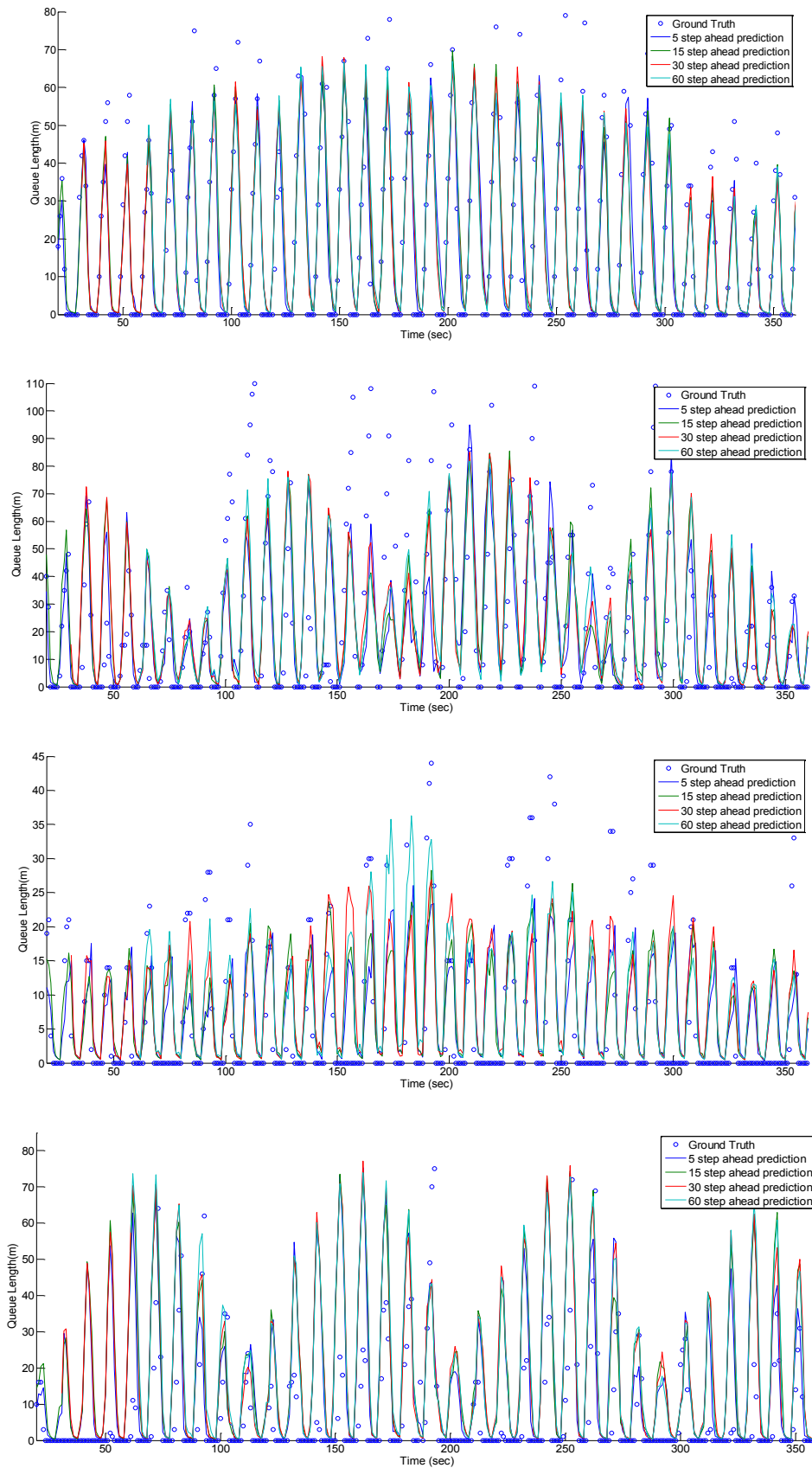
Estimated versus ground truth queue of simulated dataset westbound



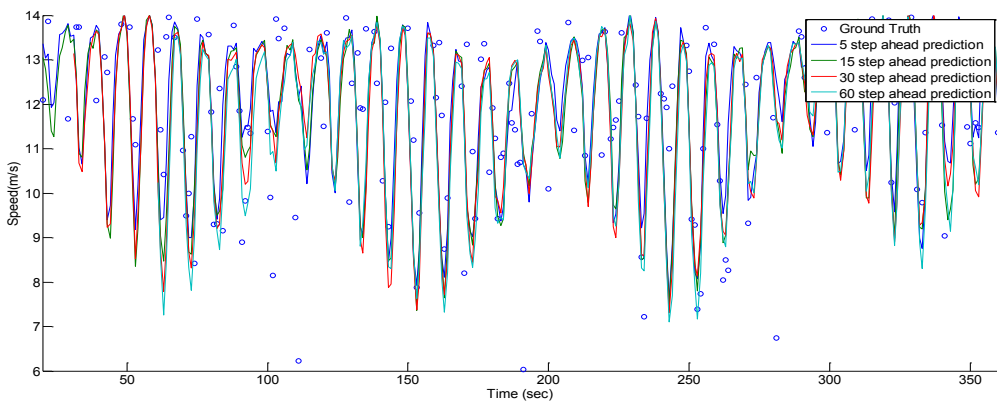
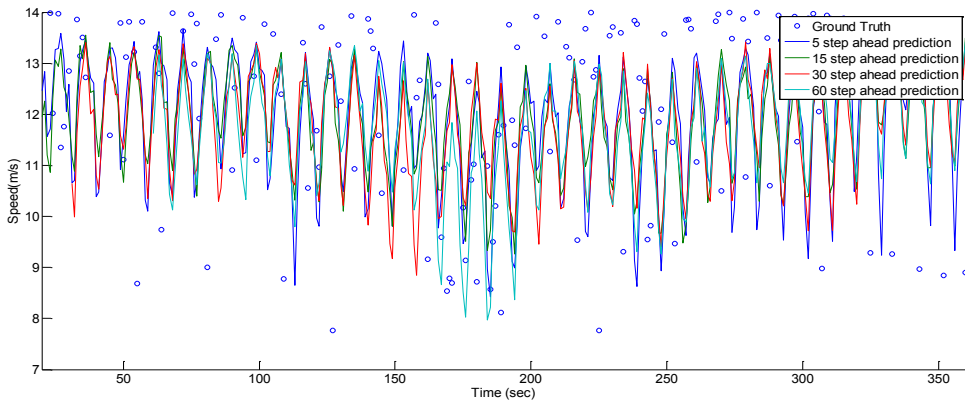
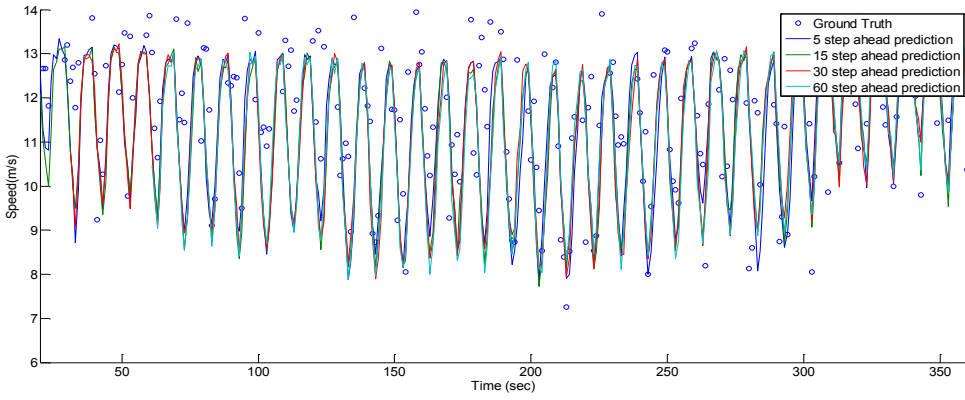
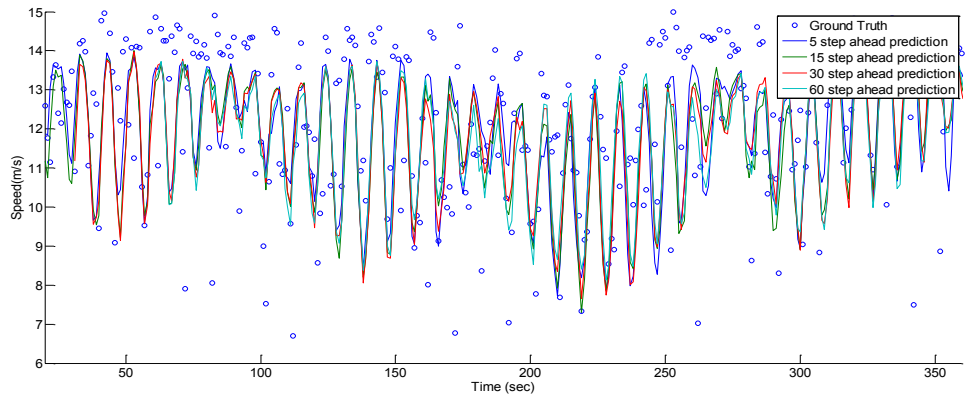
Estimated versus ground truth speed of simulated dataset westbound



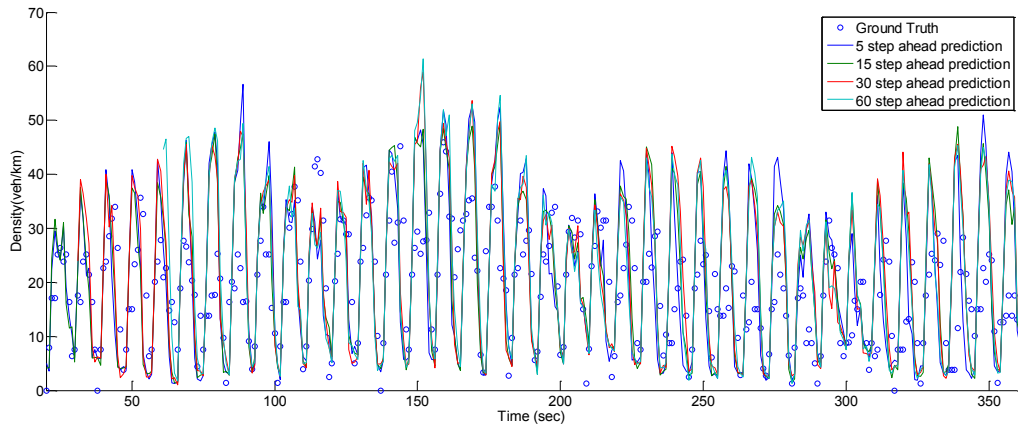
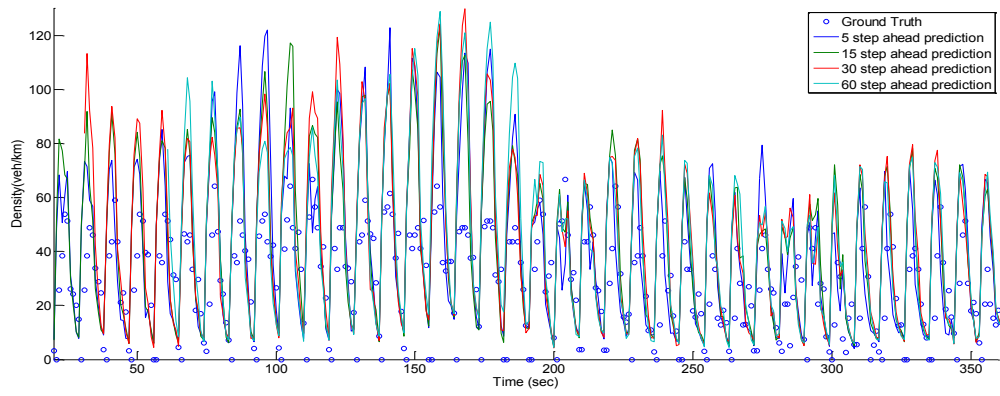
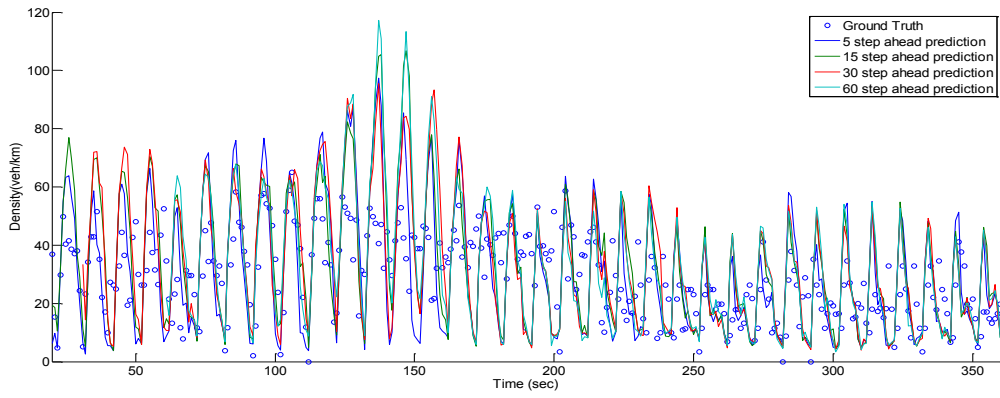
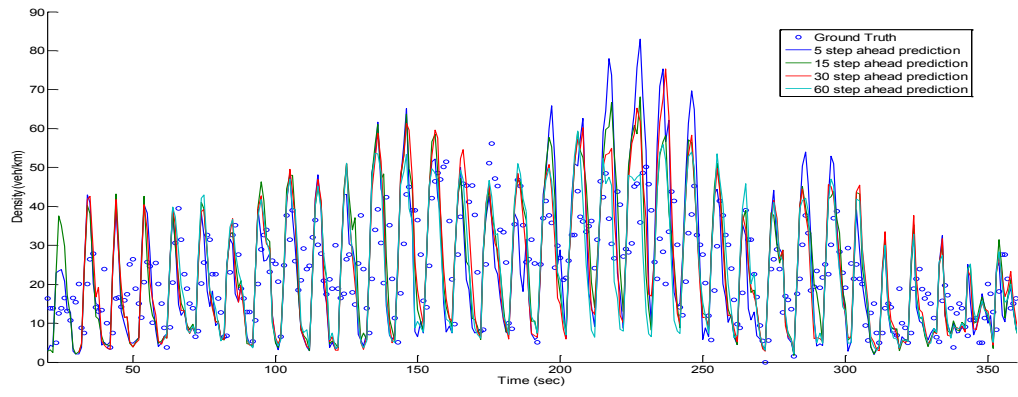
Predicted versus ground truth density of simulated dataset eastbound



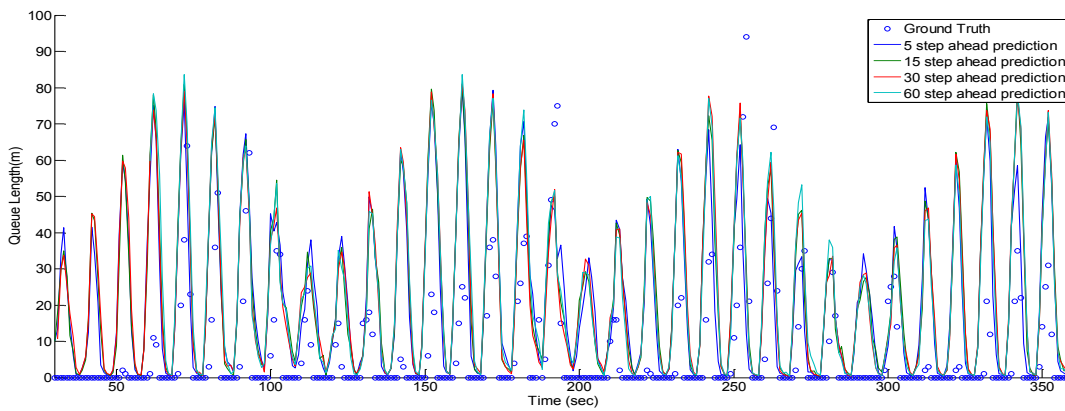
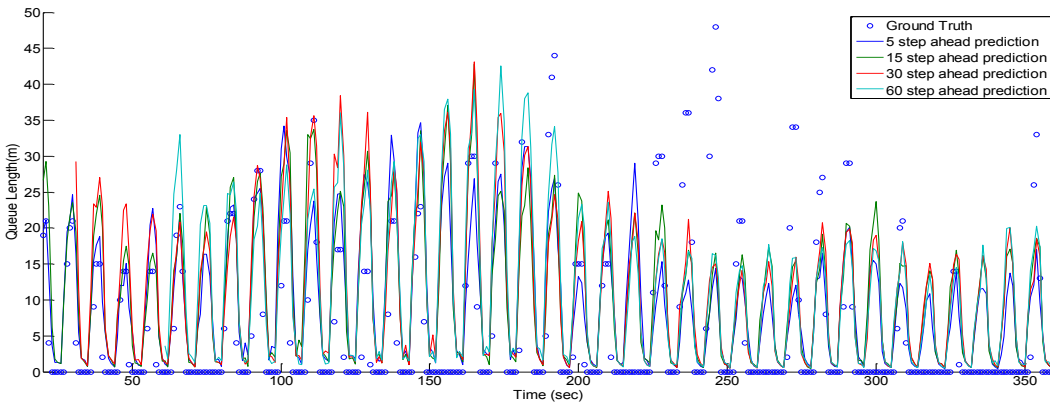
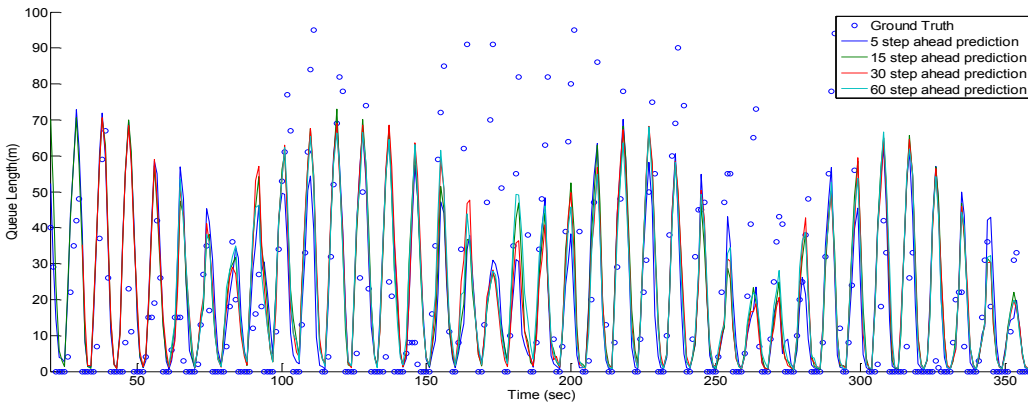
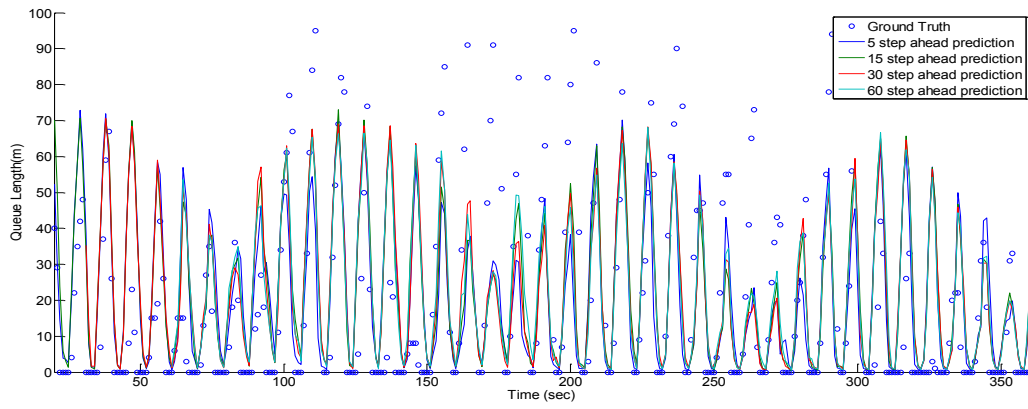
Predicted versus ground truth queue of simulated dataset eastbound



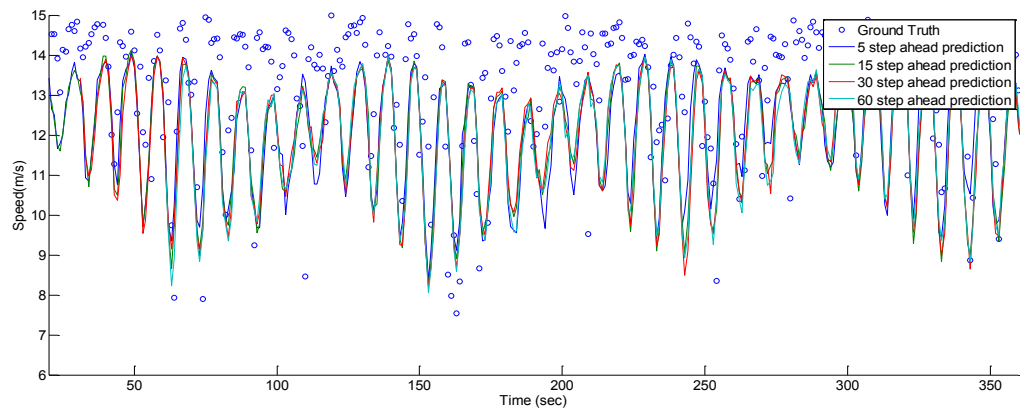
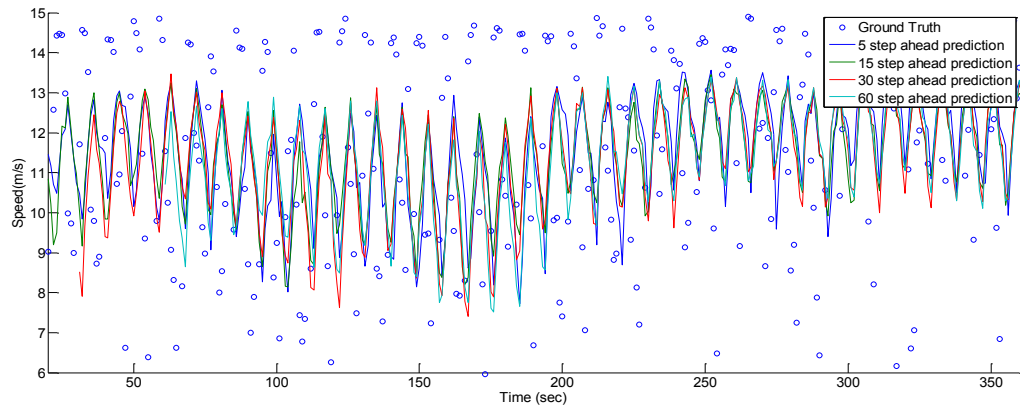
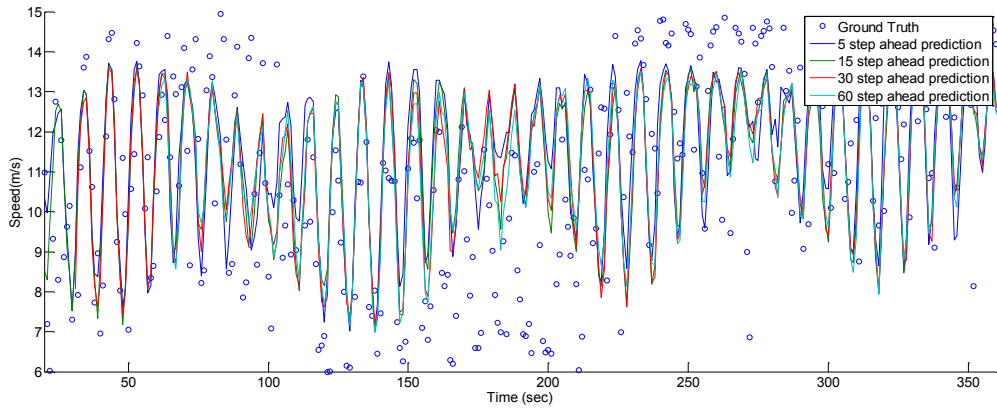
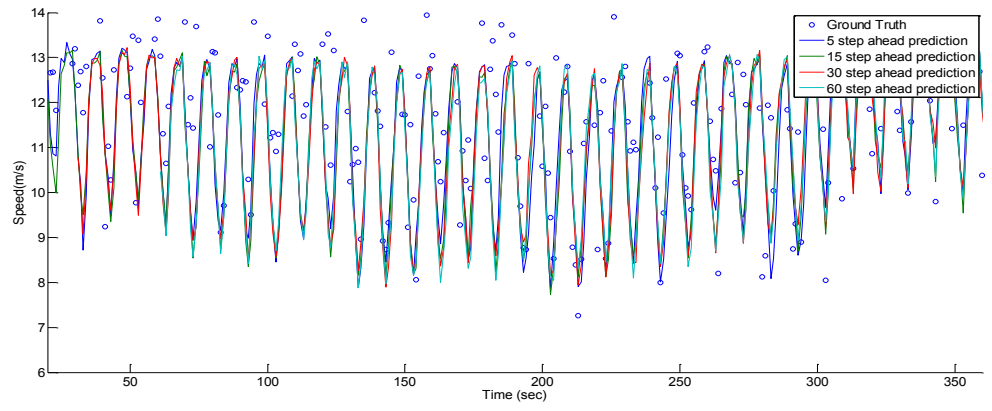
Predicted versus ground truth speed of simulated dataset eastbound



Predicted versus ground truth density of simulated dataset westbound



Predicted versus ground truth queue of simulated dataset westbound



Predicted versus ground truth speed of simulated dataset westbound

## 12. References

- [1] Abishai, P. (1979). "A study of travel time and reliability on arterial routes." *Transportation*, 8, 141-151.
- [2] Akcelik, R. (1980). "Time-dependent expressions for delay, stop rate and queue length at traffic signals." *Internal report AIR 367-1 Australian Road Research Board*.
- [3] Akcelik, R. (1988). "The highway capacity manual delay formula for signalized intersections." *ITE Journal*, 58 (3), 23-28.
- [4] Akçelik, R., and Roupail, N. M. (1994). "Overflow queues and delays with random and platooned arrivals at signalized intersections." *Journal of Advanced Transportation*, 28(3), 227-251.
- [5] Aliari, Y., and Haghani, A. (2012). "Using Bluetooth Sensors for Ground-Truth Testing of Travel Time Data." *TRB 91st Annual Meeting Compendium of Papers*.
- [6] Benjamin, C. (2002). "Estimating travel times and vehicle trajectories on freeways using dual loop detectors." *Transportation Research Part A: Policy and Practice*, 36(4), 351-364.
- [7] Berkow, M., Monsere, C., Koonce, P., Bertini, R., and Wolfe, M. (2009). "Prototype for Data Fusion Using Stationary and Mobile Data." *Transportation Research Record: Journal of the Transportation Research Board*, 2099, 102-112.
- [8] Bhaskar, A., Chung, E., and Dumont, A. G. (2009). "Estimation of Travel Time on Urban Networks with Midlink Sources and Sinks." *Transportation Research Record: Journal of the Transportation Research Board*, 2121, 41-54.
- [9] Bin, G., and Coifman, B. "Vehicle identification and GPS error detection from a LIDAR equipped probe vehicle." *Proc., Intelligent Transportation Systems Conference, 2006. ITSC '06. IEEE*, 1537-1542.
- [10] Boel, R., and Mihaylova, L. (2006). "A compositional stochastic model for real time freeway traffic simulation." *Transportation Research Part B: Methodological*, 40(4), 319-334.
- [11] Carlos, D., and Nikolas, G. (2008). "An analytical approximation for the macroscopic fundamental diagram of urban traffic." *Transportation Research Part B*, 42, 771-781.
- [12] Carpenter, J., Clifford, P., and Fearnhead, P. (1999). "Improved particle filter for nonlinear problems." *Radar, Sonar and Navigation, IEE Proceedings -*, 146(1), 2-7.
- [13] Cetin, M., and Comert, G. (2006). "Short-Term Traffic Flow Prediction with Regime Switching Models." *Transportation Research Record: Journal of the Transportation Research Board*, 1965(-1), 23-31.
- [14] Cetin, M., List, G., and Zhou, Y. (2005). "Factors Affecting Minimum Number of Probes Required for Reliable Estimation of Travel Time." *Transportation Research Record: Journal of the Transportation Research Board*, 1917(-1), 37-44.
- [15] Chaudhuri, P., Stevanovic, A., and Martin, P. (2011). "Assessing the accuracy and reliability of freeway traffic monitoring stations using GPS probe vehicle speed data." *World Review of Intermodal Transportation Research*, 3(4), 338-352.

- [16] Chen, H., and Grant-Muller, S. (2001). "Use of sequential learning for short-term traffic flow forecasting." *Transportation Research Part C: Emerging Technologies*, 9(5), 319-336.
- [17] Chen, H., Grant-Muller, S., Mussone, L., and Montgomery, F. (2001). "A Study of Hybrid Neural Network Approaches and the Effects of Missing Data on Traffic Forecasting." *Neural Computing & Applications*, 10(3), 277-286.
- [18] Chen, M., and Chien, S. (2000). "Determining the Number of Probe Vehicles for Freeway Travel Time Estimation by Microscopic Simulation." *Transportation Research Record: Journal of the Transportation Research Board*, 1719(-1), 61-68.
- [19] Chen, R., and Liu, J. S. (1996). "Predictive Updating Methods with Application to Bayesian Classification." *Journal of the Royal Statistical Society. Series B (Methodological)*, 58(2), 397-415.
- [20] Choi, K., and Chung, Y. (2002). "A Data Fusion Algorithm for Estimating Link Travel Time." *Journal of Intelligent Transportation Systems*, 7(3-4), 235-260.
- [21] Comert, G., and Cetin, M. (2009). "Queue length estimation from probe vehicle location and the impacts of sample size." *European Journal of Operational Research*, 197(1), 196-202.
- [22] Darroch, J. N. (1964). "On the Traffic light Queue." *Ann. Math. Statist.*, 35(1), 380-388.
- [23] David, S. (2008). *Urban Mobility Report (2004)*, DIANE Publishing.
- [24] Davis, G., and Nihan, N. (1991). "Nonparametric Regression and Short-Term Freeway Traffic Forecasting." *Journal of Transportation Engineering*, 117(2), 178-188.
- [25] Davis, G. A., and Kang, J. G. (1994). "Estimating destination-specific traffic density on urban freeways for advanced traffic management." *Transportation Research Record*, 1457, 143-148.
- [26] Demers, A., List, G., Wallace, W., Lee, E., and Wojtowicz, J. (2006). "Probes as Path Seekers: A New Paradigm." *Transportation Research Record: Journal of the Transportation Research Board*, 1944(-1), 107-114.
- [27] Di, X., Liu, H., and Davis, G. (2010). "Hybrid Extended Kalman Filtering Approach for Traffic Density Estimation Along Signalized Arterials." *Transportation Research Record: Journal of the Transportation Research Board*, 2188(-1), 165-173.
- [28] Dia, H. (2001). "An object-oriented neural network approach to short-term traffic forecasting." *European Journal of Operational Research*, 131(2), 253-261.
- [29] Dimitriou, L., Tsekeris, T., and Stathopoulos, A. (2008). "Adaptive hybrid fuzzy rule-based system approach for modeling and predicting urban traffic flow." *Transportation Research Part C: Emerging Technologies*, 16(5), 554-573.
- [30] Dion, F., Rakha, H., and Kang, Y.-S. (2004). "Comparison of delay estimates at under-saturated and over-saturated pre-timed signalized intersections." *Transportation Research Part B: Methodological*, 38(2), 99-122.
- [31] Dirk, H. (1991). "Queue length and waiting-time distributions at priority intersections." *Transportation Research Part B: Methodological*, 25(4), 163-174.
- [32] Dirk, H. (1994). "Queue length and delay distributions at traffic signals." *Transportation Research Part B: Methodological*, 28(5), 377-389.

- [33] Doucet, A., Godsill, S., and Andrieu, C. (2000). "On sequential Monte Carlo sampling methods for Bayesian filtering." *Statistics and Computing*, 10(3), 197-208.
- [34] Du, L., Peeta, S., and Kim, Y. H. (2012). "An adaptive information fusion model to predict the short-term link travel time distribution in dynamic traffic networks." *Transportation Research Part B: Methodological*, 46(1), 235-252.
- [35] Federal Highway Administration (2007) "NGSIM Peachtree (Atlanta) Data Analysis (4:00 p.m. to 4:15 p.m.)", *project report*, prepared by Cambridge Systematics, Inc.
- [36] Federal Highway Administration (2007) "NGSIM Peachtree (Atlanta) Data Analysis (12:45 p.m. to 1:00 p.m.)", *project report*, prepared by Cambridge Systematics, Inc.
- [37] Fei, X., Lu, C.C., and Liu, K. (2011). "A bayesian dynamic linear model approach for real-time short-term freeway travel time prediction." *Transportation Research Part C: Emerging Technologies*, 19(6), 1306-1318.
- [38] Ferman, M. A., Blumenfeld, D. E., and Dai, X. (2005). "An Analytical Evaluation of a Real-Time Traffic Information System Using Probe Vehicles." *Journal of Intelligent Transportation Systems*, 9(1), 23-34.
- [39] Gazis, D., and Liu, C. (2003). "Kalman filtering estimation of traffic counts for two network links in tandem." *Transportation Research Part B: Methodological*, 37(8), 737-745.
- [40] Gazis, D. C., and Knapp, C. H. (1971). "On-Line Estimation of Traffic Densities from Time-Series of Flow and Speed Data." *Transportation Science*, 5(3), 283-301.
- [41] Geroliminis, N., and Skabardonis, A. (2005). "Prediction of Arrival Profiles and Queue Lengths Along Signalized Arterials by Using a Markov Decision Process." *Transportation Research Record: Journal of the Transportation Research Board*, 1934(-1), 116-124.
- [42] Gordon, N. J., Salmond, D. J., and Smith, A. F. M. (1993). "Novel approach to nonlinear/non-Gaussian Bayesian state estimation." *Radar and Signal Processing, IEE Proceedings F*, 140(2), 107-113.
- [43] Greenberg, H. (1959). "An Analysis of Traffic Flow." *Operations Research*, 7(1), 79-85.
- [44] Haghani, A., Hamed, M., Sadabadi, K., Young, S., and Tarnoff, P. (2010). "Data Collection of Freeway Travel Time Ground Truth with Bluetooth Sensors." *Transportation Research Record: Journal of the Transportation Research Board*, 2160, 60-68.
- [45] Hamed, M., Al-Masaeid, H., and Said, Z. (1995). "Short-Term Prediction of Traffic Volume in Urban Arterials." *Journal of Transportation Engineering*, 121(3), 249-254.
- [46] Hellenga, B. R., and Fu, L. (2002). "Reducing bias in probe-based arterial link travel time estimates." *Transportation Research Part C: Emerging Technologies*, 10(4), 257-273.
- [47] Herrera, J. C., and Bayen, A. M. (2010). "Incorporation of Lagrangian measurements in freeway traffic state estimation." *Transportation Research Part B: Methodological*, 44(4), 460-481.
- [48] Hesham, R., Ihab, E.-S., Mazen, A., and Dion, F. "Estimating Path Travel-Time Reliability." *Proc., Intelligent Transportation Systems Conference, 2006. ITSC '06. IEEE*, 236-241.
- [49] Hollander, Y., and Liu, R. (2008). "Estimation of the distribution of travel times by repeated simulation." *Transportation Research Part C: Emerging Technologies*, 16(2), 212-231.

- [50] Jabari, S. E., and Liu, H. X. (2012). "A stochastic model of traffic flow: Theoretical foundations." *Transportation Research Part B: Methodological*, 46(1), 156-174.
- [51] Jiang, X., and Adeli, H. (2005). "Dynamic Wavelet Neural Network Model for Traffic Flow Forecasting." *Journal of Transportation Engineering*, 131(10), 771-779.
- [52] Kalman, R. E. (1960). "A New Approach to Linear Filtering and Prediction Problems." *Transactions of the ASME-Journal of Basic Engineering*, 82, 35-45.
- [53] Kamarianakis, Y., and Prastacos, P. (2003). "Forecasting Traffic Flow Conditions in an Urban Network: Comparison of Multivariate and Univariate Approaches." *Transportation Research Record: Journal of the Transportation Research Board*, 1857(-1), 74-84.
- [54] Kimber, R. M., and Hollis, E. M. (1978). "Peak period traffic delay at road junctions and other bottlenecks." *Traffic Engineering and Control*, 19(120), pp. 442-446.
- [55] Kiselev, A. B., Kokoreva, A. V., Nikitin, V. F., and Smirnov, N. N. (2004). "Mathematical modelling of traffic flows on controlled roads." *Journal of Applied Mathematics and Mechanics*, 68(6), 933-939.
- [56] Kurzhanskiy, A., and Varaiya, P. (2012). "Guaranteed prediction and estimation of the state of a road network." *Transportation Research Part C: Emerging Technologies*, 21(1), 163-180.
- [57] Kwon, J., and Petty, K. (2005). "Travel Time Prediction Algorithm Scalable to Freeway Networks with Many Nodes with Arbitrary Travel Routes." *Transportation Research Record: Journal of the Transportation Research Board*, 1935(-1), 147-153.
- [58] Kwong, K., Kavalier, R., Rajagopal, R., and Varaiya, P. (2009). "Arterial travel time estimation based on vehicle re-identification using wireless magnetic sensors." *Transportation Research Part C: Emerging Technologies*, 17(6), 586-606.
- [59] Lan, C.-J., and Davis, G. (1997). "Empirical Assessment of a Markovian Traffic Flow Model." *Transportation Research Record: Journal of the Transportation Research Board*, 1591(-1), 31-37.
- [60] Lighthill, M., and Whitham, G. (1955). "On Kinematic Waves. II. A Theory of Traffic Flow on Long Crowded Roads." *Proceedings of the Royal Society of London. Series A. Mathematical and Physical Sciences*, 229(1178), 317-345.
- [61] Liu, H., Van Zuylen, H., Van Lint, H., and Salomons, M. (2005). "Urban Arterial Travel Time Prediction with State-Space Neural Networks and Kalman Filters." *Transportation Research Record*.
- [62] Liu, H. X., and Ma, W. (2009). "A virtual vehicle probe model for time-dependent travel time estimation on signalized arterials." *Transportation Research Part C: Emerging Technologies*, 17(1), 11-26.
- [63] Liu, H. X., Wu, X., Ma, W., and Hu, H. (2009). "Real-time queue length estimation for congested signalized intersections." *Transportation Research Part C: Emerging Technologies*, 17(4), 412-427.
- [64] Long Cheu, R., Xie, C., and Lee, D.-H. (2002). "Probe Vehicle Population and Sample Size for Arterial Speed Estimation." *Computer-Aided Civil and Infrastructure Engineering*, 17(1), 53-60.

- [65] M.J., C., L.H., I., and Tampere (2007). "An Extended Kalman Filter Application for Traffic State Estimation Using CTM with Implicit Mode Switching and Dynamic Parameters." *Proceedings of the 2007 IEEE Intelligent Transportation Systems Conference*.
- [66] McNeil, D. R. (1968). "A Solution to the Fixed-Cycle Traffic Light Problem for Compound Poisson Arrivals." *Journal of Applied Probability*, 5(3), 624-635.
- [67] Mehran, B., Kuwahara, M., and Naznin, F. (2012). "Implementing kinematic wave theory to reconstruct vehicle trajectories from fixed and probe sensor data." *Transportation Research Part C: Emerging Technologies*, 20(1), 144-163.
- [68] Mihaylova, L., and Boel, R. "A particle filter for freeway traffic estimation." *Proc., Decision and Control, 2004. CDC. 43rd IEEE Conference on*, 2106-2111 Vol.2102.
- [69] Mihaylova, L., Boel, R., and Hegyi, A. (2007). "Freeway traffic estimation within particle filtering framework." *Automatica*, 43(2), 290-300.
- [70] Miller, A. J. (1963). "Settings for Fixed-Cycle Traffic Signals." *OR*, 14(4), 373-386.
- [71] Min, W., and Wynter, L. (2011). "Real-time road traffic prediction with spatio-temporal correlations." *Transportation Research Part C: Emerging Technologies*, 19(4), 606-616.
- [72] Munoz, L., Xiaotian, S., Horowitz, R., and Alvarez, L. "Traffic density estimation with the cell transmission model." *Proc., American Control Conference, 2003. Proceedings of the 2003*, 3750-3755 vol.3755.
- [73] Nahi, N. E., and Trivedi, A. N. (1973). "Recursive Estimation of Traffic Variables: Section Density and Average Speed." *Transportation Science*, 7(3), 269-286.
- [74] Newell, G. F. (1965). "Approximation Methods for Queues with Application to the Fixed-Cycle traffic Light." *SIAM Review*, 7(2), 223-240.
- [75] Ohno, K. (1978). "Computational Algorithm for a Fixed Cycle Traffic Signal and New Approximate Expressions for Average Delay." *Transportation Science*, 12(1), 29-47.
- [76] Okutani, I., and Stephanedes, Y. J. (1984). "Dynamic prediction of traffic volume through Kalman filtering theory." *Transportation Research Part B: Methodological*, 18(1), 1-11.
- [77] Park, D., and Rilett, L. (1998). "Forecasting Multiple-Period Freeway Link Travel Times Using Modular Neural Networks." *Transportation Research Record: Journal of the Transportation Research Board*, 1617(-1), 163-170.
- [78] Park, D., Rilett, L., and Han, G. (1999). "Spectral Basis Neural Networks for Real-Time Travel Time Forecasting." *Journal of Transportation Engineering*, 125(6), 515-523.
- [79] Paul, Z., and Howard, M. (2005). *Fundamentals Of Kalman Filtering: A Practical Approach*.
- [80] Pipes, L. A. (1964). "Hydrodynamics approaches Part I - An Introduction of Traffic Flow Theory." *Sepecial report 79, highway research board*.
- [81] Pipes, L. A. (1967). "CAR FOLLOWING MODELS AND THE FUNDAMENTAL DIAGRAM OF ROAD TRAFFIC." *Transportation Research Record*, Vol 1, 21-29.
- [82] Pipes, L. A. (1968). "Vehicle acceleration in the hydrodynamic theory of traffic flow." *Transportation Research Record*, 2(2), 143-149.

- [83] Prigogine, I., and Herman, R. (1971). "KINETIC THEORY OF VEHICULAR TRAFFIC." *Elsevier Publishing Company, Incorporated*, 17-54.
- [84] Pushkar, A., Hall, F. L., and Acha-Daza, J. A. (1994). "Estimation of speeds from single-loop freeway flow and occupancy data using cusp catastrophe theory model" *Transportation Research Record*, 1457.
- [85] Qiao, W., Haghani, A., and Hamed, M. (2012). "A Non-Parametric Model for Short-Term Travel Time Prediction Using Bluetooth Data." *Journal of Intelligent Transportation Systems*.
- [86] Qiao, W., Haghani, A., and Hamed, M. "Short-Term Travel Time Prediction Considering Weather Impact." *Proc., Transportation Research Board 91st Annual Meeting*.
- [87] Qing, Y., Szeto, W. Y., and Wong, S. C. (2012). "Short-Term Traffic Speed Forecasting Based on Data Recorded at Irregular Intervals." *Intelligent Transportation Systems, IEEE Transactions on*, 13(4), 1727-1737.
- [88] Qiu, T., Lu, X.Y., Chow, A., and Shladover, S. (2010). "Estimation of Freeway Traffic Density with Loop Detector and Probe Vehicle Data." *Transportation Research Record: Journal of the Transportation Research Board*, 2178(-1), 21-29.
- [89] Qiu, Z.J., Cheng, P., and Ran, B. (2007). "Investigate the feasibility of traffic speed estimation using cell phones as probes." *International Journal of Services Operations and Informatics*, 2(1), 53-64.
- [90] Rice, J., and van Zwet, E. (2004). "A simple and effective method for predicting travel times on freeways." *Intelligent Transportation Systems, IEEE Transactions on*, 5(3), 200-207.
- [91] Richards, P. I. (1956). "Shock Waves on the Highway." *Operations Research*, 4(1), 42-51.
- [92] Schrank, D., Eisele, B., and Lomax, T. (2012) "Urban mobility report 2012", Annual report, *Texas A&M Transportation Institute*.
- [93] Sethi, V., Bhandari, N., S. Koppelman, F., and L. Schofer, J. (1995). "Arterial incident detection using fixed detector and probe vehicle data." *Transportation Research Part C: Emerging Technologies*, 3(2), 99-112.
- [94] Sharma, A., Bullock, D., and Bonneson, J. (2007). "Input-Output and Hybrid Techniques for Real-Time Prediction of Delay and Maximum Queue Length at Signalized Intersections." *Transportation Research Record: Journal of the Transportation Research Board*, 2035, 69-80.
- [95] Smith, B. L., and Demetsky, M. J. "Short-term traffic flow prediction models-a comparison of neural network and nonparametric regression approaches." *Proc., Systems, Man, and Cybernetics, 1994. Humans, Information and Technology., 1994 IEEE International Conference on*, 1706-1709 vol.1702.
- [96] Smith, B. L., Williams, B. M., and Keith Oswald, R. (2002). "Comparison of parametric and nonparametric models for traffic flow forecasting." *Transportation Research Part C: Emerging Technologies*, 10(4), 303-321.
- [97] Stathopoulos, A., and Karlaftis, M. G. (2003). "A multivariate state space approach for urban traffic flow modeling and prediction." *Transportation Research Part C: Emerging Technologies*, 11(2), 121-135.
- [98] Sumalee, A., Zhong, R. X., Pan, T. L., and Szeto, W. Y. (2011). "Stochastic cell transmission model (SCTM): A stochastic dynamic traffic model for traffic state surveillance and assignment." *Transportation Research Part B: Methodological*, 45(3), 507-533.

- [99] Sun, C., Arr, G., and Ramachandran, R. (2003). "Vehicle Reidentification as Method for Deriving Travel Time and Travel Time Distributions: Investigation." *Transportation Research Record: Journal of the Transportation Research Board*, 1826(-1), 25-30.
- [100] Szeto, M. W., and Gazis, D. C. (1972). "Application of Kalman Filtering to the Surveillance and Control of Traffic Systems." *Transportation Science*, 6(4), 419-439.
- [101] Tampere, C. M. J., and Immers, L. H. "An Extended Kalman Filter Application for Traffic State Estimation Using CTM with Implicit Mode Switching and Dynamic Parameters." *Proc., Intelligent Transportation Systems Conference, 2007. ITSC 2007. IEEE*, 209-216.
- [102] Van Lint, J. W. C. (2006). "Reliable Real-Time Framework for Short-Term Freeway Travel Time Prediction." *Journal of Transportation Engineering*, 132(12), 921-932.
- [103] Viti, F., and van Zuylen, H. J. (2010). "Probabilistic models for queues at fixed control signals." *Transportation Research Part B: Methodological*, 44(1), 120-135.
- [104] Vlahogianni, E. I., Golias, J. C., and Karlaftis, M. G. (2004). "Short-term traffic forecasting: Overview of objectives and methods." *Transport Reviews*, 24(5), 533-557.
- [105] Vlahogianni, E. I., Karlaftis, M. G., and Golias, J. C. (2005). "Optimized and meta-optimized neural networks for short-term traffic flow prediction: A genetic approach." *Transportation Research Part C: Emerging Technologies*, 13(3), 211-234.
- [106] Wang, Y., and Papageorgiou, M. (2005). "Real-time freeway traffic state estimation based on extended Kalman filter: a general approach." *Transportation Research Part B: Methodological*, 39(2), 141-167.
- [107] Wang, Y., Papageorgiou, M., and Messmer, A. (2007). "Real-Time Freeway Traffic State Estimation Based on Extended Kalman Filter: A Case Study." *Transportation Science*, 41(2), 167-181.
- [108] Webster, F. V. (1958). "TRAFFIC SIGNAL SETTINGS." *Road Research Lab Tech Papers, UK, No 39*.
- [109] Williams, B., Durvasula, P., and Brown, D. (1998). "Urban Freeway Traffic Flow Prediction: Application of Seasonal Autoregressive Integrated Moving Average and Exponential Smoothing Models." *Transportation Research Record: Journal of the Transportation Research Board*, 1644, 132-141.
- [110] Williams, B., and Hoel, L. (2003). "Modeling and Forecasting Vehicular Traffic Flow as a Seasonal ARIMA Process: Theoretical Basis and Empirical Results." *Journal of Transportation Engineering*, 129(6), 664-672.
- [111] Work, D. B., and Bayen, A. M. (2008). "An Ensemble Kalman Filtering Approach to Highway Traffic Estimation Using GPS Enabled Mobile Devices." *Proceedings of the 47th IEEE Conference on Decision and Control*.
- [112] Xiaotian, S., Munoz, L., and Horowitz, R. "Highway traffic state estimation using improved mixture Kalman filters for effective ramp metering control." *Proc., Decision and Control, 2003. Proceedings. 42nd IEEE Conference on*, 6333-6338 Vol.6336.
- [113] Xiaowen, D., Ferman, M. A., and Roesser, R. P. "A simulation evaluation of a real-time traffic information system using probe vehicles." *Proc., Intelligent Transportation Systems, 2003. Proceedings. 2003 IEEE*, 475-480 vol.471.

- [114] Yang, F., Yin, Z., Liu, H., and Ran, B. (2004). "Online Recursive Algorithm for Short-Term Traffic Prediction." *Transportation Research Record: Journal of the Transportation Research Board*, 1879(-1), 1-8.
- Zhang, N., Zhang, Y., and Lu, H. (2011). "Seasonal Autoregressive Integrated Moving Average and Support Vector Machine Models." *Transportation Research Record: Journal of the Transportation Research Board*, 2215(-1), 85-92.